

**ABSTRACTS FROM THE
ISSX/MDO 2022 MEETING**

**September 11-14, 2022
Seattle, Washington, USA**



ISSX/MDO 2022 Meeting September 11-14, 2022

Seattle, Washington, USA

Contents

Sunday, September 11, 2022

Short Course 1: Fundamentals of Bioanalysis for Proteins, Cell and Gene Therapy, Organized by the Bioanalysis in ADME Science Focus Group.....	3
Abstracts: SC1.1 - SC1.4	
Short Course 2: Addressing ADME Models and Challenges of New Candidates to Better Translate <i>in vitro</i> to <i>in vivo</i> : (a) investigating low clearance drugs, (b) defining the role of the gut microbiome and (c) normalizing the use of microfluidic systems for biotransformation and toxicity.....	4
Abstracts: S2.1 - SC2.4	
Short Course 3: State of Science of PBPK 2022: Beyond P450s.....	5
Abstracts: SC3.1 - SC3.4	
Short Course 4: Transporter Phenotyping: from Qualitative Characterization to Quantitative Prediction.....	6
Abstracts: SC4.1 - SC4.4	
Opening Keynote Event: Perspectives on Long-held Clearance Concepts.....	7
Abstracts: K1 and K2	

Monday, September 12, 2022

Plenary Lecture 1: Cytochrome P450/Redox Partner Interactions.....	8
Abstract: PL1	
Parallel Symposium 1: Advances in <i>in silico</i> ADME and Structure-based Modeling Prediction.....	8
Abstracts: S1.1 - S1.4	
Parallel Symposium 2: Organization of P450 System and Related Proteins in Biological Membranes.....	10
Abstracts: S2.1 - S2.4	
Pre-doctoral/Graduate and Postdoctoral Poster Awards Finalist Poster Presentations.....	30
Abstracts: A1 - A12	
Parallel Symposium 3: Cryo-EM to Advance Functional and Mechanistic Insights of Enzymes and Transporters.....	11
Abstracts: S3.1 - S3.3	
Parallel Symposium 4: 3-D culture, Organ-on-chip, and Microphysical Systems in ADME Studies.....	12
Abstracts: S4.1 - S4.4	

Tuesday, September 13, 2022

Plenary Lecture 2: What Drugs Do to Our Bugs.....	14
Abstract: PL2	
Parallel Symposium 5: Clinical Development Impact Stories of Microdosing and Microtracer Studies.....	14
Abstracts: S5.1 - S5.4	
Parallel Symposium 6: Role of Non-coding RNAs in Xenobiotic Metabolism and Regulation.....	15
Abstracts: S6.1 - S6.4	
Poster Presentation Session 1.....	38
Abstracts: P1 - P103	
Plenary Session 1: Advancement and Influencers in the Prediction of Drug Interactions and Human Exposure.....	17
Abstracts: PS1.1 - PS1.3	

Wednesday, September 14, 2022

Plenary Lecture 3: Structure-Metabolism-Toxicity Evaluation of Protein Kinase Inhibitors.....	17
Abstract: PL3	

Plenary Session 2: Clinical Importance of Drug Transporters	17
Abstracts: PS2.1 - PS2.4	
Poster Presentation Session 2	97
Abstracts: P104 - P196	
Plenary Session 3: Drug Discovery from the Trenches	19
Abstracts: PS3.1 - PS3.4	
Poster Details	21
Finalists for the Pre-doctoral/Graduate Poster Awards Competition (Monday, September 12 - Wednesday, September 14, 2022)	30
Abstracts: A1 - A6	
Finalists for the Postdoctoral Poster Awards Competition (Monday, September 12 - Wednesday, September 14, 2022)	33
Abstracts: A7 - A12	
Poster Presentations (Monday, September 12 - Wednesday, September 14, 2022)	38
Abstracts: P1 - P196	
Author Index	145
Keyword Index	150

SC1.1 - FUNDAMENTALS OF PCR INCLUDING DIGITAL DROPLET TECHNIQUES**Matthew Albertolle***Takeda Pharmaceuticals, United States*

As oligonucleotide therapies and cellular therapies have advanced at a rapid pace in recent years, new challenges and bottlenecks have been identified in bioanalysis of these new modalities. While there are several methods to quantify oligonucleotides for bioanalysis (LC-MS/MS, Fluorescence-HPLC, hybrid ELISA), qPCR provides the most sensitivity, but forfeits some selectivity. Making this method ideal for early stage discovery of assets. This course will cover aspects of design and execution of qPCR-based methods for oligonucleotide bioanalysis including stem-loop and ddPCR. qPCR-based bioanalysis of cellular therapies is an important aspect of quantifying circulating and persisting cellular drug products. Design of a reliable and robust assay is crucial for success. This course will discuss requirements for robust assay design and execution.

SC1.2 - FUNDAMENTALS AND APPLICATIONS OF LC/MS AND CE/MS FOR LARGE MOLECULES BIOANALYSIS**Mei Han***Amgen, Inc., United States*

With the advancement of protein engineering, the innovative next generation biologics (NGBs) such as antibody drug conjugates, bioconjugates, bispecific/multi-specific biologics, nanobodies, antibody fragments, and antibody-like proteins have emerged. Those NGBs may be more specific than traditional monoclonal antibodies, achieving desired clinical efficacy and increased drug delivery efficiency with appropriate safety profile. The complex structure of NGBs brought new analytical challenges for purity assays, formulation development, as well as their pharmacological characteristics *in vitro* and *in vivo* in the context of ADME properties during drug development. Therefore, developing sensitive, selective, and robust bioanalytical methods becomes critical for comprehensive analysis of protein therapeutics.

In this short course, we aim to cover the fundamental of large molecule bioanalysis using LC/MS and CE/MS. Topics include the following aspects: 1) overview of the industry landscape of large molecule bioanalysis; 2) sample preparation method development for analyzing protein therapeutics from biologic matrices; 3) LC/MS and CE/MS technique introduction; 4) bottom-up and intact level analysis approaches; 5) intact protein mass spectrometry for protein therapeutics quantitation and biotransformation analyses; 6) case studies.

SC1.3 - IMPACT OF NOVEL LIGAND BINDING ASSAY TECHNOLOGIES ON BIOANALYSIS**Sally Fischer***Genentech, United States*

Ligand binding assays (LBAs) are critical and widely accepted tools in research and development of protein therapeutics. They are often used in measurement of pharmacokinetic (PK) and toxicokinetic (TK), biomarkers and immunogenicity or anti-drug antibodies (ADA) during preclinical and clinical development. Enzyme-linked immunosorbent assay (ELISA) has been the gold standard for LBAs, and although ELISAs are still widely used, they pose a number of challenges. ELISA assays can be time and reagent intensive, have limited dynamic range, and often lack appropriate sensitivity. In addition, matrix tolerance can be especially challenging requiring optimization of the assay for individual matrix.

During the past couple of decades, there has been emergence of a number of novel platform technologies. Technologies with higher sensitivity, lower volume needs and multiplexing capabilities. These technologies have huge potential in enabling more informed drug development decisions. However, no one technology has been able to address all the needed elements in one platform. Some of the factors that need to be considered include; Sensitivity requirements, volume availability, multiplexing, platform accessibility, ease of development, outsourcing strategy, and throughput needs. It is also important to consider availability of off-the-shelf kits or custom kits by the vendor as well as ability to develop home brew assays. Therefore, it is essential to understand what is being measured and what attributes are needed for a particular measurement, to determine which platform would be most appropriate for the particular application. This talk will provide several case studies to illustrate the capabilities of these promising technologies.

SC1.4 - FUNDAMENTALS OF IMMUNOGENICITY**Marina Li***Merck, United States*

Biotherapeutic products are the fastest growing medicines in the pharmaceutical markets. The immunogenicity of these products is a high-profile concern for the industry and the regulatory authorities. Biotherapeutics often elicit unwanted immune response that produce non-neutralizing and/or neutralizing anti-drug antibodies (ADAs) with a wide variety of clinical consequences. Detection of ADAs is a regulatory requirement of drug development to assess how ADA may impact pharmacokinetics, pharmacodynamics, patient safety, and efficacy. A variety of ADA detection platforms and

formats have been explored and the bridging electrochemiluminescence (ECL)-based approach is the industry standard, especially for monoclonal antibody therapeutics. Historically, ADA assays have been purely qualitative, with a positive or negative result reported based on statistically derived assay cut points. Testing for ADA requires deep understanding of the biologic conditions and assay conditions to know what is being measured. In this presentation, we aim to provide an overview of immunogenicity and ADA assays.

SC2.1 - LOW CLEARANCE AND UNIQUE METABOLIC PATHWAYS: A NEW CHALLENGE IN THE BIOTRANSFORMATION STUDIES OF DRUG CANDIDATES

Deepak Dalvie

Crinetics Pharmaceuticals, United States

Drug metabolism plays a defining role in the disposition of drugs and has therefore become an integral part of drug discovery and development. The objective of drug metabolism studies can vary depending upon the stage of the program. While preclinical drug metabolism studies play a key role in understanding clearance mechanisms, compound modulation and avoidance of metabolic liabilities and identification of any bioactivation possibilities, studies in development help in identifying key circulating metabolites (>10% of total circulating radioactivity) in definitive biotransformation studies in humans using radiolabeled compounds and complying with the MIST guidelines put forth by the FDA. Traditionally, metabolism has been studied and metabolites have been identified using subcellular fractions, like S9, cytosol and liver microsomal fractions as well as cellular systems, like the hepatocytes. Early involvement of drug metabolism scientists and education of medicinal chemists in minimizing metabolic liabilities of newly synthesized candidates has led to new challenges, including low-turnover (i.e. slowly metabolized) drug candidates and/or elimination of the drug candidates by other mechanisms, such as hepatobiliary transport or alternative metabolic pathways. One such non-CYP pathway that has gained importance is the role of gut microbiota in metabolism. This presentation will be focused on this problem that a metabolism scientist faces and will showcase examples of drugs with these challenges.

SC2.2 - IN VITRO TOOL KIT TO MEASURE METABOLIC STABILITY AND METABOLIC PROFILE OF LOW CLEARANCE DRUGS

Li Di

Pfizer, United States

Achieving low clearance is often a goal of drug discovery projects in order to reduce dose and dosing frequency. However, it is challenging to measure metabolic clearance, identify metabolites and study reaction phenotyping of low clearance compounds. This can lead to overprediction of clearance, underprediction of half-life, overestimation of dose, MIST issues and ambiguities in planning clinical victim DDI studies. A number of recent advances in the low clearance field allows researchers to explore the low clearance space, including hepatocyte relay, HepatoPac and Hurel coculture systems and spheroids. Hepatocyte relay method is a natural extension of the standard suspension hepatocyte assay. The assay has a lower limit of intrinsic clearance (CL_{int}) of 0.36 mL/min/kg using 2 million cells/mL with 5 relays and an accumulative incubation time of 20 hours. HepatoPac and Hurel are coculture systems with mouse fibroblasts. These coculture systems tend to have higher UGT and AKR activities and lower CYP2D6, AO and FMO activities. The lower limit of CL_{int} for HepatoPac is 1.2 mL/min/kg (7-day incubation at 0.07 million cells/mL) and for Hurel is 0.67 mL/min/kg (3-day incubation at 0.30 million cells/mL). Spheroids currently demonstrate lower enzyme activity when compared to the other systems. Scaling factors are typically needed to establish *in vitro* - *in vivo* correlations for these 3D hepatocyte systems. These low clearance methods have been applied to determine CL_{int}, profile metabolites and reaction phenotyping of low clearance compounds. Examples and case studies on applications of the various approaches will be discussed.

SC2.3 - THE ROLE OF THE GUT MICROBIOME IN METABOLISM OF DRUGS

Aaron Wright

Baylor University, United States

Microbial proteins within the human gut are increasingly being identified as critical to drug metabolism. This metabolism can be harnessed for prodrug activation, but alternately, microbial metabolism can result in poor efficacy and/or toxicity of drugs. For instance, drug metabolism may result in enterohepatic recycling of drugs leading to prolonged patient exposure and protracted side effects. In this course we will review the mechanisms associated with microbial drug metabolism within the gut, ways to understand these mechanisms, and how understanding these mechanisms can lead to improved therapeutic care.

SC2.4 - APPLICATION OF MICROFLUIDIC SYSTEMS IN MECHANISTIC NEPHROTOXICITY STUDIES OF DRUGS & XENOBIOTICS**Edward Kelly***University of Washington, United States*

In my session, I will talk about organs on chip (OoC) aka microphysiological systems (MPS) which are 3D microfluidic "avatars" of human organs. The current paradigm of drug development results in 90+% failure rates in clinical trials. Moving a drug into human clinical trials is predicated on preclinical animal safety data. The high clinical trial failure rate calls into question the predictability of animal studies. It is the hope that these revolutionary OoC/MPS models will bridge this gap in preclinical and clinical testing.

I will present results from three different studies where we applied our human kidney proximal tubule MPS model to understand the mechanism(s) of nephrotoxicity for two different xenobiotics (aristolochic acid & Ochratoxin A) and an FDA-approved antibiotic (polymyxin B). Attendees will come away with a better understanding of the potential for this technology in human safety assessment as well as the limitations.

SC3.1 - ABSORPTION PREDICTIONS: CURRENT CAPABILITIES AND KNOWING THE GAPS**Viera Lukacova***Simulations Plus, Inc., United States*

For orally administered drug products, the rate and the extent of drug absorption are results of complex interplay between different processes affecting the formulation and the drug itself. These processes include dissolution, precipitation, passive paracellular and transcellular permeability, and carrier-mediated uptake and efflux. For accurate absorption predictions, the models need to capture these processes, their interplay, and also their regional differences caused by changing physiology along the gastrointestinal tract. This presentation will discuss the role of physiologically based modeling in absorption predictions. Examples will be used to demonstrate the influence of different processes on the predicted intestinal drug absorption.

SC3.2 - UNDERSTANDING PHYSIOLOGY AND SYSTEMS PARAMETERS IN SPECIAL POPULATION MODELS**Oliver Hatley***Certara, United Kingdom*

Physiologically-based pharmacokinetics (PBPK) modeling and simulation is utilized to describe absorption, distribution, metabolism and elimination (ADME) processes for candidate drugs. The key element of this approach is the separation of information on the system (i.e., physiological parameters) from that of the drug (e.g. physicochemical characteristics determining permeability through membranes, partitioning to tissues, binding to plasma proteins or affinities toward certain enzymes and transporter proteins) and the study design (e.g. dose, route and frequency of administration, concomitant drugs and food). Changes in several physiological covariate factors can contribute to the pharmacokinetic (PK) variability between individuals and impact extrapolation between different populations. The importance of understanding of correlations between covariates in populations, with a focus on special populations (e.g. organ impairment) will be covered.

SC3.3 - CURRENT CAPABILITIES IN MODELING TRANSPORTER-MEDIATED DDIS**Bridget Morse***Eli Lilly, United States*

Predicting and interpreting clinical transporter-mediated drug-drug interactions (DDIs) have specific challenges, including inconsistencies in *in vitro*-to-*in vivo* extrapolation, lack of index substrates/inhibitors, and lack of knowledge of drug concentrations/driving forces at the site of transport, among others. Pharmacokinetic modeling, particularly physiologically-based pharmacokinetic modeling, can be invaluable for mechanistic understanding of pharmacokinetic processes involving drug transporters. However, as with all modeling applications, uncertainties still remain that need to be addressed during model building and verification to understand the role of drug transporters. These uncertainties may be specific to modeling purpose (bottom-up vs. top-down), physiologic site of the transporter/interaction (intestine vs. liver vs. kidney) and class of transporter. For example, prediction of DDIs involving the hepatic organic anion transporters (OATPs) traditionally have not been well-predicted using *in vitro* inhibition values (bottom-up). Recent advances including identification of selective *in vitro* inhibitors and selective *in vivo* biomarkers have helped evolve our modeling strategies for predicting these DDIs. Again, for hepatic transporter-mediated DDIs, just interpreting the role of transporters in observed DDIs (top-down) is challenging, as the disposition of our clinical transporter substrates is complex. Therefore, generally a wealth of *in vitro* and clinical drug interaction data, as well as a well-defined modeling strategy, are needed to tease out the role of enzymes/transporters in these drug interactions.

Conversely, in the kidney, when active renal secretion is rate-limited by basolateral uptake transporters, such as that for organic anion transporters (OATs), drug interactions are generally predicted well, using both static and PBPK models. However, understanding the role of efflux transporters in the kidney remains a challenge, as does predicting DDIs involving cationic transporters.

With discussion through such examples, this presentation will outline the current state-of-the science for modeling transporter-mediated drug interactions.

SC3.4 - OVERVIEW AND ADVANCEMENTS IN MODELING NON-CYP METABOLISM AND ASSOCIATED DDIs

Xinyuan Zhang

Daiichi Sankyo, Inc., United States

Non-CYP enzymes are responsible for drug metabolism although the number of drugs that are metabolized by non-CYP enzymes is smaller compared to that metabolized by CYP enzymes. Non-CYP enzymes include but are not limited to flavin monooxygenases (FMOs), carboxylesterases (CES), carbonyl reductase, aldehyde oxidase (AO), xanthine oxidase (XO), monoamine oxidase (MAO), UDP-glucuronosyltransferases (UGTs), etc. Quantitative prediction of non-CYP enzyme-mediated metabolism and drug-drug interactions (DDIs) is challenging because of the extra-hepatic expression, polymorphisms, and lack of relevant probe substrates and modulators. In this presentation, we will discuss some recent examples where modeling has been used to evaluate non-CYP enzyme-mediated metabolism and DDIs. We will also discuss the gaps in the modeling analyses and appropriate utilization of the models.

SC4.1 - APPLICATION OF EXTENDED CLEARANCE CONCEPT AND EXTENDED CLEARANCE CLASSIFICATION SYSTEM (ECCS) TO PREDICT CLEARANCE MECHANISM IN DRUG DISCOVERY

Manthana Varma

Pfizer, United States

Translation of transporter-mediated disposition is of interest in medicine design as it is certain now that the membrane transporters play a significant role in the ADME of drugs. Understanding the concept of transporter-enzyme interplay is critical in evaluating the clinical relevance of transporter mechanisms in clinical pharmacokinetics. Based on the accumulated knowledge, the Extended Clearance Classification System (ECCS) framework suggests significant OATP1B involvement in the pharmacokinetics of high-MW acids/zwitterions irrespective of their passive permeability obtained from the *in vitro* screens (i.e., ECCS class 1B and 3B drugs). Metabolism is a major driver for class 2 drugs, while OATs and OCT2/MATEs contribute to the renal clearance in class 3 and 4. This presentation will focus on the multitude of clinical and preclinical evidence supporting extended clearance and ECCS framework and discuss decision-trees to project transporter substrate activity based on preclinical information.

SC4.2 - *IN VITRO* ASSAYS TO STUDY TRANSPORTER PHENOTYPING: CONSIDERATIONS ON STUDY DESIGN AND MECHANISTIC MODELING

Sibylle Neuhoff

Certara UK Limited, United Kingdom

The presentation will cover general *in vitro* substrate assay methods, and how to design *in vitro* kinetic studies for transporter substrates, and what are key factors to consider. I will present some examples of mechanistic modeling of *in vitro* transport data that were successfully extrapolate to the *in vivo* situation in humans. Some basic concept and models for transporters will be discussed, in addition to advanced methods and the latest progress. Finally, I will highlight current limitations of these models and possible solutions to overcome such challenges.

SC4.3 - RELATIVE EXPRESSION AND ACTIVITY FACTORS-BASED APPROACHES TO PREDICT THE CONTRIBUTION OF TRANSPORTERS TO DRUG DISPOSITION

Per Artursson

Uppsala University, Sweden

In contrast to animal models, *in vitro* absorption, distribution, metabolism and elimination (ADME) assays offers the opportunity to investigate each individual step that influence drug disposition and exposure in isolation. Further, the *in vitro* models are often developed from human tissues or cells, potentially eliminating the need for extrapolation of species differences, e.g. with regard to transporter specificity. To realize the full potential of the human *in vitro* systems, the information they provide must be reproducible for reliable determination of relative expression and activity factors that are scalable to the *in vivo* situation. The reproducibility problem partly stems from that the assays generally are developed in academic environments as proof of concept studies. For instance, relatively small differences in cell culture conditions for 3D cultured human hepatocytes can influence transporter expression and function and subsequent IVIVE. Limited

success in parameter scaling from the *in vitro* to the *in vivo* situation has forced PBK-modelers to introduce arbitrary scaling factors that vary from one investigated compound to another. Transporter protein concentrations *in vitro* as compared to *in vivo*, and local tissue, cellular and subcellular compound concentrations (that better explain local exposure) are increasingly used in IVIVE to reduce or replace the arbitrary scaling with knowledge-based scaling factors. Tissue cellularity is considered in scaling of hepatic transport, but not to the same extent in other tissues. The reproducibility and scaling issues of new, more advanced (but also more complex) *in vitro* systems such as 3D spheroid models derived from primary cells and stem cells are addressed, these systems will be more rapidly adopted by the IVIVE-PBK modelling community. In this presentation, the importance of providing reproducible cell models will first be discussed, then the application of relative (protein) expression and activity factors will follow. Finally, a new deconvolution method of proteomics data for determination of tissue cellularity will be presented.

SC4.4 - ENDOGENOUS BIOMARKER-INFORMED APPROACH TO EVALUATE CLINICAL IMPLICATIONS OF TRANSPORTER-MEDIATED PK AND DDIs

Aleksandra Galetin

The University of Manchester, United Kingdom

In recent years, significant progress has been made in the identification and validation of endogenous substrates of clinically relevant drug transporters. Such biomarkers can provide an early indication of transporter-mediated drug-drug interactions (DDI) and inform the need for subsequent studies with clinical transporter probes. In addition to their application to de-risk perpetrator transporter-mediated DDIs, these biomarkers have the potential to be used as *in vivo* probes to investigate changes in transporter function in disease states. This short course will illustrate role of modelling and simulation to support qualification of endogenous biomarkers, focusing on coproporphyrin I (CPI), 4-pyridoxic acid and creatinine as examples. Stepwise model development and use of clinical interaction and/or pharmacogenetic data to delineate complex interplay between biomarker synthesis and transporter-mediated elimination will be shown. The presentation will illustrate application of endogenous biomarker models to investigate untested clinical scenarios and to facilitate the design of prospective clinical interaction studies for transporters of interest.

K1 - THE MODEL INDEPENDENT CLEARANCE/INTRINSIC CLEARANCE EQUATION

Leslie Z. Benet

UCSF School of Pharmacy, United States

For the past 50 years our field has believed that different models of organ elimination define the clearance relationship of drug elimination, with the well-stirred model (WSM), a generally recognized unphysiologic representation of organ disposition shown to best describe the experimental data. We have proposed that all published human and animal clearance values are arterial clearances and that no model of organ elimination is necessary to describe organ elimination. We show today that the equation the field has believed to be the WSM is, in fact, an organ of elimination model independent relationship. We recognize that no scientist wants to believe what they have done for the past 50 years is invalid and argue vigorously and honestly for the relevance of the WSM versus the parallel tube model (PTM) and the infinite number of possible dispersion models (DM) between the WSM/PTM boundary conditions. In this presentation we enumerate the positions one must continue to support when maintaining that organ models of elimination are relevant to define organ clearance. 1. The organ steady-state clearance (CL) relationship with organ blood flow (Q_{organ}) and extraction ratio (ER), $CL_{organ} = Q_{organ} \cdot ER$, can also be written as *Rate of Elimination* = $CL_{organ} \cdot C_{in}$ where C_{in} is the steady-state concentration coming into the organ, the arterial concentration. But one must believe that C_{in} is not driving the elimination and is only a reference concentration. 2. Although there are no steady-state isolated perfused rat liver (IPRL) studies consistent with the PTM and DM models, and the few studies previously supporting these models can be shown to be experimentally flawed, one must continue to believe that the PTM and DM are valid interpretations of the IPRL studies. 3. Although the relationship previously thought to be the WSM clearance equation, $CL_{organ} = Q_{organ} \cdot \frac{f_{uB} \cdot CL_{int}}{Q_{organ} + f_{uB} \cdot CL_{int}}$, where f_{uB} is the unbound fraction in blood and CL_{int} is the intrinsic clearance, can be simply derived independent of any mechanistic model of organ elimination, one must continue to believe that the equation only represents the WSM. 4. Although it is universally agreed that the area under the intra-organ concentration-time curves for the WSM, PTM and DM models differ, and it is recognized that clearance is a function of the amount eliminated divided by the concentration driving that elimination, one must believe that that intraorgan concentration differences are not relevant in determining organ clearance and that the clearance for the WSM, PTM and DM are the same for a given C_{in} and C_{out} at steady-state. We also demonstrate that the generally accepted WSM equation when basolateral hepatic influx and efflux transporters are clinically relevant, the Extended Clearance Concept (ECC) Equation, requires illogical suppositions and that this equation is not valid. We derive the correct ECC Equation. Finally, we cannot identify any useful advance in understanding measured clearance values and defining drug disposition that results from utilization of the WSM, PTM and DM models.

K2 - DEMYSTIFYING MODEL-INDEPENDENT AND MODEL-DEPENDENT CLEARANCE CONCEPTS AND EQUATIONS**K. Sandy Pang***University of Toronto, Canada*

Clearance concepts are widely applied in pharmaceutical research not only during the phases of drug development and discovery but throughout the life-span and existence of drug. Hepatic clearance (CL_{H,b}) describes the efficiency with which the liver removes a drug in the incoming circulation, defined as the rate of elimination or product of flow (QH) and the difference in input (C_{in}) and output (C_{out}) concentration at steady state QH(C_{in} - C_{out}), normalized to the incoming concentration, an observable and quantifiable entity. This model independent equation, based on Fick's law of perfusion, reflects the rate of elimination from within the liver, given by the product of the intrinsic clearance (CL_{int,H}) and the "overall unbound substrate concentration" (C_{u,H,cell}) regardless of whether transporters or membrane barriers are involved in drug distribution in liver. Models of hepatic clearance have evolved to describe events taking place within the liver. The well-stirred model (WSM) and parallel tube model (PTM) represent two extreme conditions of mixing due to bulk flow and plug flow, respectively. The more physiologic model is the dispersion model (DM) where there is dispersive flow and some degree of mixing. Each of the theoretical models differs in its designated unbound substrate concentration, and hence, the implied CL_{int,H} and model predictions on *in vivo* CL_{H,b} when given *in vitro* parameters are used together with alterations of flow, protein binding (denoted as unbound fraction) and/or CL_{int,H}. The WSM is most often used in pharmacokinetics due to its simple mathematical presentation, although incurring errors when the extraction ratio is very high. Recently, confusion is generated in terms of the clearance equation, the basic assumptions, and misquotes of the literature. There is the need for clarification of this important concept in pharmacokinetics.

PL1 - CYTOCHROME P450/REDOX PARTNER INTERACTIONS**Emily Scott***University of Michigan, United States*

Most cytochrome P450 enzymes require the input of two electrons for catalysis to occur. Microsomal P450 enzymes receive those electrons from NADPH-cytochrome P450 reductase, while mitochondrial P450 enzymes are reduced by adrenodoxin/ferrodoxin. However, interactions of these redox proteins with P450 enzymes can also have effects on other aspects of cytochrome P450 function, notably ligand binding. These allosteric effects vary by cytochrome P450 and by ligand. This not only suggests sophisticated communication between the proximal redox partner binding site and the ligand binding on the opposite side of the heme where the active site is located, but raises the possibility of differences in P450/redox partner interactions that could potentially be selectively targeted by small molecules to provide an orthogonal avenue to inhibition of specific P450 enzymes.

S1.1- COMPARISON OF MECHANISTIC AND MACHINE LEARNING BASED HUMAN PK PREDICTION**Christopher Keefer***Pfizer, United States*

The prediction of human PK remains one of the key tasks performed by DMPK scientists in drug discovery projects. This is routinely performed using mechanistic models. In recent years, machine learning (ML), with its ability to harness patterns from previous outcomes to predict future events, has gained increased popularity in application to ADME sciences. This presentation will compare the performance of mechanistic and machine learning (ML) models of human *in vivo* IV clearance for a large (~600) set of diverse compounds with literature human IV PK data and in-house measured *in vitro* endpoints. For mechanistic modeling, the well-stirred and parallel-tube approach will be compared. For the machine learning models, several different approaches were analyzed - using *in vitro* (measured) parameters only, *in silico* (QSAR model predictions) parameters only; calculated physical properties and structural descriptors; and mixed *in vitro*/physical properties and structural descriptors. Comparison of mechanistic with these different ML models will be presented. The results will show that machine learning models are as good as or better than their mechanistic counterparts.

S1.2 - A HYBRID *IN SILICO* – *IN VITRO* STRATEGY FOR GUIDING COMPOUND DESIGN AND PRIORITIZATION FOR COVALENT SCAFFOLDS INVOLVING SIGNIFICANT EXTRA-HEPATIC CLEARANCE MEDIATED BY GST**Prashant Desai***Genentech, United States*

Targeted covalent inhibitors (TCI) have gained renewed interest in recent times given their potential to inhibit targets that may otherwise be difficult to drug combined with an extended pharmacodynamic effect due to irreversible nature of their binding. At the same time such TCI pose an additional challenge with regards to estimating *in vivo* clearance during preclinical to clinical translation. This is mainly due to their potential to be cleared by extra-hepatic pathways, especially

through direct or glutathione-S-transferase (multiple isoforms expressed ubiquitously throughout the body) mediated conjugation with glutathione. To address this challenge, we have employed a hybrid approach combining mechanistic extrapolation of *in vitro* hepatic intrinsic clearance with a correlation-based scaling of *in vitro* blood intrinsic clearance to estimate *in vivo* clearance in multiple species, including its translation to human. Once the scaling factors are established based on preliminary *in vivo* data in rodents, this approach can be used to guide drug discovery programs toward improving human clearance simply based on human *in vitro* measurements for early estimation for TCI. *In silico* models to predict the key *in vitro* parameters required for human clearance prediction have been developed. These models have enabled early prioritization for synthesis by virtual assessment of clearance for a large set of compounds designed toward optimizing human PK performance. An integrated and iterative approach involving *in silico*, *in vivo* and *in vivo* models to expedite the discovery of optimized TCI will be presented.

S1.3 - *IN VITRO* AND *IN SILICO* BASED OPTIMIZATION OF DRUG HALF-LIFE

Fabio Brocatelli

Bristol Meyers Squibb, United States

The optimization of drug half-life is often a crucial objective during medicinal chemistry campaigns. This involves the concomitant optimization of volume of distribution and clearance. While tuning drug lipophilicity is often an effective strategy to optimize volume of distribution and clearance in isolation, this strategy is frequently ineffective when drug half-life is the target. This presentation will review 1) advancements in the understanding of the interplay between physiochemical and PK parameters, 2) advancements in PK *in silico* and *in vitro* to *in vivo* correlations, 3) how to leverage these technologies towards the optimization of drug half-life.

S1.4/P28 - STRUCTURE OF CYP8B1 WITH A RATIONALLY DESIGNED CYP8B1 INHIBITOR: PROVIDING DIRECTIONS FOR INHIBITOR OPTIMIZATIONS

Jinghan Liu¹, Emily Scott¹, Francis Yoshimoto², and Samuel Offei²

¹*University of Michigan, United States* and ²*University of Texas, San Antonio, United States*

Human cytochrome P450 8B1 (CYP8B1) is involved in the conversion of cholesterol to bile acids. CYP8B1 hydroxylates the steroid ring at C12 en route to production of the bile acid, cholic acid(1). Thus, this enzyme controls the ratio of cholic acid to another bile acid, chenodeoxycholic acid. The ratio of these two bile acids controls the overall hydrophobicity of the bile pool and bile acid signaling(2). Knockout studies implicated CYP8B1 as a good drug target for nonalcoholic fatty liver disease(3) and type 2 diabetes(4). However, the roles of CYP8B1 in both normal physiology and disease states are still poorly understood and no selective inhibitors have yet been developed. Herein, three rationally designed inhibitors for CYP8B1 were synthesized through incorporation of a pyridine at C12 of the C ring of the steroid, anticipating interaction between the active site heme iron of CYP8B1 and the pyridine nitrogen of the inhibitor. However, when changes in CYP8B1 heme absorbance were used to probe inhibitor binding, no spectral shifts occurred, suggesting no direct heme binding. Despite inhibitor 1 treatment showing attenuation of obesity-associated glucose intolerance in mice(5), none of the inhibitors significantly inhibited CYP8B1 metabolism of its normal substrate. A 2.65 Å X-ray structure of CYP8B1 revealed that inhibitor 2 binds in an access channel between the protein surface and active site between F, B' and A helices, rather than in the active site proper. Structural analysis suggested that a tryptophan (W281) in the active site located directly over the heme iron (Fe-Trp 8.2 Å) may prevent active site binding by sterically restricting inhibitor access and orientation for Fe binding. This hypothesis was confirmed in that all three inhibitors bound to the CYP8B1 W281F mutant with type II spectral shifts indicative of pyridine nitrogen-Fe interaction. These results are redirecting the design of new inhibitors intended to promote better understanding of the role of CYP8B1 inhibition in normal physiology and serve as the basis for future treatments for nonalcoholic fatty liver disease and type 2 diabetes.

References:

1. Staels, B. & Fonseca, V. A. Bile acids and metabolic regulation: mechanisms and clinical responses to bile acid sequestration. *Diabetes Care* 32 Suppl 2, S237-245, doi:10.2337/dc09-S355 (2009).
2. Chiang, J. Y. Recent advances in understanding bile acid homeostasis. *F1000Res* 6, 2029-2029, doi:10.12688/f1000research.12449.1 (2017).
3. Chevre, R. et al. Therapeutic modulation of the bile acid pool by Cyp8b1 knockdown protects against nonalcoholic fatty liver disease in mice. *FASEB J* 32, 3792-3802, doi:10.1096/fj.201701084RR (2018).
4. Kaur, A. et al. Loss of *Cyp8b1* Improves Glucose Homeostasis by Increasing GLP-1. *Diabetes* 64, 1168-1179, doi:10.2337/db14-0716 (2015).
5. Chung, E. et al. A synthesis of a rationally designed inhibitor of cytochrome P450 8B1, a therapeutic target to treat obesity. *Steroids* 178, 108952, doi:10.1016/j.steroids.2021.108952 (2022).

S2.1 - FUNCTIONAL INTERACTIONS BETWEEN CYP3A4 AND UDP-GLUCURONOSYLTRANSFERASES: A CRUCIAL ROLE OF LUMINAL DOMAIN OF UGT**Yuji Ishii***Kyushu University, Japan*

Cytochromes P450 (P450s, CYPs) and UDP-glucuronosyltransferases (UGTs) are enzyme families capable of catalyzing oxidation and glucuronidation. These are membrane-bound proteins located in the endoplasmic reticulum, with their predicted topologies being different. Therefore, these enzymes have been considered to work independently. Protein-protein interactions between P450 and UGT have been observed by means of affinity column chromatography, co-immunoprecipitation, and cross-linking. Their functional interactions have also been shown. UGT in P450-UGT complex is catalytically active. CYP3A4 modulates the catalytic properties of UGT isoforms, such as UGT2B7, 1A1, 1A6, and 1A7. CYP3A4 is involved in the metabolism of 50% of the drugs; however, its catalytic property *in vivo* is not completely understood by hepatic expression. Along with the modulation of UGT activity by P450, we examined whether UGT, in turn, modulates P450 activity. A baculovirus–insect cell expression system to co-express CYP3A4, NADPH-P450 reductase, and UGT1A9/UGT2B7, the major human UGT isoforms was set up. CYP3A4 activity in the presence or absence of co-expressed UGT1A9/UGT2B7 was evaluated. UGT2B7 and UGT1A9 attenuated the activity of CYP3A4. Kinetic studies showed that both UGTs diminished the V_{max} of CYP3A4. The C-terminal-truncated mutants of UGT2B7 and UGT1A9 retained the suppressive capacity as well. The changes in the kinetic parameters suggest that protein-protein interaction of UGT1A9 and CYP3A4 suppresses CYP3A4 function in a manner similar to that of UGT2B7. The luminal domain of the UGTs contain suppressive interaction site(s), whereas the C-terminal domain may contribute to the UGT isoform-specific modulation. The CYP3A4–UGT interaction may help to better understand the reason for the inter/intra-individual differences in CYP3A4 activity.

References:

1. Miyauchi Y, Nagata K, Yamazoe Y, Mackenzie PI, Yamada H, Ishii Y. Suppression of Cytochrome P450 3A4 Function by UDP-Glucuronosyltransferase 2B7 through a Protein-Protein Interaction: Cooperative Roles of the Cytosolic Carboxyl-Terminal Domain and the Luminal Anchoring Region. *Mol. Pharmacol.* 88: 800-812 (2015).
2. Miyauchi Y, Tanaka Y, Nagata K, Yamazoe Y, Mackenzie PI, Yamada H, Ishii Y. UDP-Glucuronosyltransferase (UGT)-mediated attenuations of cytochrome P450 3A4 activity: UGT isoform-dependent mechanism of suppression. *Br. J. Pharmacol.* 177: 1077-1089 (2020).

S2.2 - HEME OXYGENASE-1 AFFECTS CYTOCHROME P450 FUNCTION THROUGH THE FORMATION OF PROTEIN-PROTEIN COMPLEXES**Wayne Backes¹**, J. Patrick Connick¹, Aratrika Saha¹, and James R. Reed¹¹*Louisiana State University Health Sciences Center, United States*

Introduction: The P450 system does not function alone, but requires interactions with their redox partners, NADPH-cytochrome P450 reductase (POR) and cytochrome b5. Interactions among P450s and other P450 system proteins not directly involved in electron transfer have been identified. These include the formation of both homomeric and heteromeric P450•P450 complexes. Interestingly, formation of these complexes affect their catalytic characteristics, which can cause either synergism or inhibition depending on the P450 proteins being examined. More recently, our lab has shown that P450s also can form complexes with heme oxygenase-1 (HO-1), another interaction that can affect both P450 and HO-1 function.

Aims: The goal of this study is to examine the ability of HO-1 to interact with different CYP1 family enzymes, and to compare the differential effects on P450-mediated metabolism.

Methods: Physical complex formation was measured using bioluminescence resonance energy transfer (BRET). In this method, GFP- and Renilla luciferase (Rluc-) labeled proteins were co-transfected into HEK293T/17 cells. Addition of coelenterazine 400A causes luminescence of the Rluc-protein; however, whenever the GFP-labeled protein is complexed with the Rluc-labeled protein, energy transfer to the GFP ensues, leading to GFP fluorescence at 510 nm. The ratio of the GFP fluorescence to Rluc luminescence is measured as the BRET signal. Enzyme activities were also examined using reconstituted systems containing POR, the P450, and different concentrations of HO-1.

Results: HO-1 was shown to form a physical complex with each of the CYP1 family proteins, and as expected, differential effects on activities were observed. CYP1A1 activity was dramatically inhibited in the presence of HO-1; however, HO-1 had only a modest effect on CYP1B1 activity. Interestingly, HO-1 caused stimulation in CYP1A2 activity at subsaturating [POR], whereas the activity was inhibited at higher POR levels.

Discussion: As HO-1 and CYP1 enzymes co-exist in the endoplasmic reticulum, the potential for HO-1 to interact with P450s adds an additional layer of complexity to catalysis by both enzyme systems. With HO-1 levels being inducible by chemical and oxidative stress, its induction could lead not only to competition between HO-1 and the P450s for limiting amounts of POR, but also to alterations in monooxygenase activities due to formation HO-1•P450 complexes.

Consequently, conditions that induce HO-1 may have a significant influence on CYP1-mediated metabolism, with the

effect being dependent on the specific P450 involved in complex formation.

Conclusion: HO-1 has differential effects on each of the CYP1 proteins causing minor inhibition of CYP1B1, dramatic inhibition of CYP1A1, and an effect on CYP1A2 that is dependent on the relative POR concentration. These effects are mediated not only by competition of the P450s for POR, but also by the formation of physical HO-1•P450 complexes (supported by R01 GM123253 & ES013648).

S2.3 - ASSEMBLING THE P450 PUZZLE: IMPACT OF P450-P450 INTERACTIONS ON THE PATHWAYS OF DRUG METABOLISM

Dmitri Davydov

Washington State University, United States

Despite its seeming obviousness, the widely accepted premise that the cumulative properties of the human drug-metabolizing ensemble represent a simple aggregate of the properties of the constituting enzymes appears to be a severe oversimplification. Recent advances in studying the functional effects of hetero-association of multiple cytochrome P450 species and their interactions with other metabolically related enzymes reveal a tight integration in the human drug-metabolizing ensemble. According to modern concepts, the sources of vast interindividual variability in drug metabolism can be elucidated only when considering this ensemble as a multienzyme system whose functional parameters are determined by interactions between its constituents. In this presentation, I overview the most recent findings on the mutual effects of microsomal drug-metabolizing enzymes and propose a conceptual model suggesting their mechanistic explanation and providing a clue to further understanding the non-additive behavior of the human drug-metabolizing ensemble.

S2.4 - PROTEIN/PROTEIN INTERACTION IN THE HUMAN CYTOCHROME P450 SYSTEM

Sarah D. Burris-Hiday

University of Michigan, United States

A major superfamily of heme containing monooxygenases, cytochrome P450 enzymes metabolize a wide variety of substrates including xenobiotics, steroids, fatty acids, and vitamins. These membrane-bound enzymes require electrons for catalysis, and for 48 of the 57 human P450 enzymes, these electrons are delivered by the redox partner protein NADPH-cytochrome P450 reductase. The reductase FMN-containing domain directly binds the P450 enzyme proximal face, but little is known about the details of this transient protein-protein interaction. Studies herein utilize artificial fusions of the reductase FMN domain with either xenobiotic or steroidogenic P450 enzymes. These fusion enzymes favor a stable protein-protein interaction. The effect of the FMN domain localization with the P450 was measured for substrate and inhibitor binding and catalysis in the P450 active site. This active site is approximately 15-20 Å away from the protein-protein interaction site. Experiments were performed with the fusion enzymes alongside the respective isolated P450 isoform in order to assess the effects of the FMN domain on P450 function. These studies revealed that fusion of the FMN domain does not change the ligand binding mode. However, in the case of xenobiotic P450 enzymes, it does alter both the percent of the P450 population that binds ligand and the affinity for ligand binding, and it does so in an isoform and ligand dependent manner. Interestingly these effects were not significant for steroidogenic P450 enzymes. Furthermore, catalytic studies are being performed to probe the effects of FMN domain on substrate metabolism. Overall, these results demonstrate that the effect of the FMN domain on the P450 is both dependent on the P450 isoform and the ligand. This reveals intricate communication between the P450 active site and the surface of the P450 where the reductase FMN domain binds. This suggests that different P450 isoforms interact with the same reductase in unique ways. If this is the case, specific P450/reductase interactions could potentially be selectively disrupted to modulate the function of individual P450 isoforms in the treatment of disease.

S3.1 - CRYO-EM STRUCTURES OF ATP- AND SUBSTRATE-BOUND STATES OF MRP4

Deanna Kroetz

University of California San Francisco, United States

The multidrug resistance associated protein 4 (MRP4) is a member of the ATP binding cassette (ABC) family of transporters and effluxes diverse endogenous and exogenous molecules from cells. While implicated in both response to drugs and disease, the mechanisms driving its substrate selectivity and membrane transport are poorly understood. Structures of bovine MRP4 were determined in a nucleotide-free, substrate-bound, and an ATP-bound state at near-atomic resolutions by cryo-electron microscopy. The ATP-bound structure represents a novel outward occluded state within the MRP subfamily. ATPase activity of purified MRP4 was stimulated by adding putative substrates, prostaglandins and a sulfated steroid, but not by the previously suggested physiological substrates, including leukotriene C4 (LTC4) or cyclic nucleotides. These structures were used to distinguish the substrate selectivity between MRP4 and the related

MRP1 transporter, and to assess the impact of genetic variants of MRP4 on transport function. These findings support therapeutic targeting of MRP4 to regulate prostaglandin and steroid signaling in multiple diseases.

S3.2 - CRYO-EM STRUCTURE OF A FUNCTIONAL TETRAMERIC COMPLEX OF FULL-LENGTH CYP2B4 AND NADPH-CYTOCHROME P450 REDUCTASE

Haoming Zhang

The University of Michigan Medical School, United States

Microsomal P450 system consisting of cytochromes P450 (P450s), NADPH-cytochrome P450 oxidoreductase (POR) and cytochrome b5 (cyt b5) catalyzes oxidative transformation of ~75% of pharmaceutical drugs, playing a major role in Phase I drug metabolism. Historically P450-catalyzed reactions are recapitulated in reconstituted phospholipid liposomes since the seminal work of Drs. Anthony Lu and Minor J. Coon. Availability of this reconstituted system has greatly accelerated studies to understand the chemistry and kinetics of P450-catalyzed reactions. However, structural analysis of interactions of P450s with POR and cyt b5 in this reconstituted system has been challenging due to high heterogeneity in oligomeric states. Reconstitution of microsomal P450 system in Nanodiscs affords more homogenous preparations, but structural analysis remains challenging. The objective of our work is to develop an alternative system that is amenable to both functional and structural analysis of microsomal P450 system so that we can provide both functional and structural insights about the mechanism of action for P450-catalyzed reactions. Herein we report a tetrameric complex of [2B4]₂:[POR]₂ in amphipols. The complex is homogenous and fully functional in N-demethylation of benzphetamine compared with phospholipid reconstituted counterpart. The tetrameric complex is stoichiometrically similar to CYP102A1 homodimer. Using cryo-EM, we have determined the structures of full-length CYP102A1 homodimer as well as a delta12 variant enzyme at intermediate resolutions of 6.7-8.5Å. These structures reveal critical conformational changes required for electron transfer from FMN to the heme. Using negative stain EM, we have determined the architecture of the tetrameric complex of [2B4]₂:[POR]₂, which suggests a similar mechanism for electron transfer from POR to 2B4. Availability of a homogenous multi-unit complex amenable to both functional and structural analysis may accelerate studies to elucidate the roles of protein-protein interactions in P450-catalyzed reactions and facilitate construction of a work model for drug metabolism by microsomal P450 system.

Acknowledgement: This work was supported by the National Institutes of Health Grants GM077430 and ES030791.

S3.3 - STRUCTURAL AND FUNCTIONAL INSIGHTS INTO A PEROXISOMAL FATTY-ACID TRANSPORTER

Meghna Gupta

University of California San Francisco, United States

Peroxisomes are ubiquitous eukaryotic organelles that form a focal point for multiple metabolic pathways. Lipid metabolism, and in particular, fatty acid transport related to it, depend heavily on peroxisomal membrane proteins that have specifically evolved for such purposes. The ATP-dependent cassette (ABC) transporters of 'D' subfamily reside in the peroxisomal membrane and are responsible for fatty acid import into the peroxisomes, defects in which process are related to various metabolic disorders. Mutations in ABCD1 cause X-linked adrenoleukodystrophy (X-ALD) which manifests as mild to severe central nervous system (CNS) demyelination. Dysfunction of ABCD3 and/or peroxisome biogenesis factors (PEXs) may cause Zellweger syndrome (ZS), a heterogeneous group of peroxisome assembly disorders. In addition to inherited diseases, reduced peroxisomal function is associated with aging and pathogenesis of age-related acquired diseases like diabetes, neurodegenerative disorders. Key gaps in understanding the function of ABCDs in metabolism and disease are due to lack of structural details, particularly of their conformational plasticity during substrate transport, and how this is compromised during metabolic disorders, aging and disease.

Using CryoEM, we determined first high-resolution structures of any human peroxisomal ABC transporters (ABCD3). We show that the purified protein in the detergent is active *in vitro*. With the help of the structures and biochemical assays, we propose a mechanism of fatty-acid transport through these transporters and identify a potentially new substrate. We are also exploring interaction among peroxins and PMPs (peroxisomal membrane proteins) and have noteworthy results which help us comprehend PMP recruitment on peroxisomal membranes and peroxisome biogenesis.

S4.1 - NEXT GENERATION *IN VITRO* MODELS FOR ADME: DO MORE COMPLEX MPS MODELS MORE ACCURATELY PREDICT *IN VIVO* OUTCOME?

Tom Chan

Boehringer Ingelheim Pharmaceuticals, United States

The evolution of *in vitro* cell systems for ADME applications has progressed alongside significant advances in materials engineering, biology, and physiology. The most advanced models that are commercially available incorporate

physiological aspects of flow and mechanical stimuli. This talk provides a perspective on where we are evaluating and adapting new models into our ADME workflows, including both functional and practical considerations.

S4.2 - THE USE OF AN *IN VIVO* 3D HUMAN LIVER SPHEROID SYSTEM FOR PREDICTION OF DRUG-INDUCED ENZYME EXPRESSION, DRUG PHARMACOKINETICS AND DRUG HEPATOTOXICITY

Magnus Ingelman-Sundberg

Karolinska Institute, Sweden

Much effort is devoted to the generation of phenotypically appropriate *in vitro* systems for studying hepatic drug metabolism and clearance, drug hepatotoxicity, and liver disease. Of specific importance among liver diseases is NASH which is becoming the leading hepatic disease in the world. The lecture will be focused on a 3D spheroid liver system based on monocultures or co-cultures of PHH and NPCs, where toxicity, clearance and metabolism of drugs can be predicted. Furthermore, in this system it is possible to i) elucidate mechanisms behind chronic drug hepatotoxicity, ii) mimic liver diseases like steatosis and fibrosis, and iii) study genetic, mechanistic, and environmental factors of importance for NASH and pharmacological treatment. By choosing different genetically defined donors and siRNA-based gene silencing, the contribution of different polymorphic genes and gene products of importance for developing the diseases can be studied.

S4.3 - MICROPHYSICAL SYSTEMS IN DRUG DEVELOPMENT AND PRECISION MEDICINE

Tomoki Imaoka

Daiichi Sankyo, Co., Ltd., Japan

Opioid overdose, dependence, and addiction are a major public health crisis. Patients with chronic kidney disease (CKD) are at high risk of opioid overdose, therefore novel methods that provide accurate prediction of renal clearance (CL_r) and systemic disposition of opioids in CKD patients can facilitate the optimization of therapeutic regimens. Our recent studies aimed to predict renal clearance and systemic disposition of morphine and its active metabolite morphine-6-glucuronide (M6G) in CKD patients using a vascularized human proximal tubule microphysiological system (VPT-MPS) coupled with a parent-metabolite full body physiologically-based pharmacokinetic (PBPK) model.

The VPT-MPS, populated with a human umbilical vein endothelial cell (HUVEC) channel and an adjacent human primary proximal tubular epithelial cells (PTEC) channel, successfully demonstrated secretory transport of morphine and M6G from the HUVEC channel into the PTEC channel in a time-dependent manner; transporter inhibitors decreased translocation by 74.3% and 63.6%, respectively. The *in vitro* data generated by VPT-MPS were further incorporated into a mechanistic kidney model and parent-metabolite full body PBPK model to predict CL_r and systemic disposition of morphine and M6G. The model successfully predicted CL_r within 1.5-fold, and the plasma concentration-time profiles of morphine and M6G in both healthy subjects and CKD patients, with absolute average fold error (AAFE) values <1.5. Collectively, we have presented a novel translational strategy that couples a VPT-MPS with mechanistic PBPK modeling for quantitative prediction of the kidney disposition of drugs. The VPT-MPS recapitulates critical aspects of kidney physiological function *in vivo* and allows evaluation of active secretory clearance of morphine and M6G with sustained maintenance of transporter protein expression. The mechanistic kidney model and the parent-metabolite PBPK model successfully incorporated the VPT-MPS data and accurately predicted renal clearance and plasma concentration-time profiles of morphine and M6G in both healthy subjects and CKD patients, indicating that the *in vitro* results obtained from VPT-MPS can be translated to *in vivo* parameters, via an appropriate *in silico* framework. Taken together, we have shown that the bottom-up approach can predict opioid disposition in CKD patients and potentially mitigate the risk of overdose in those sensitive populations. We contend that this approach can be further extrapolated to a variety of drugs and investigational compounds to a priori understand kidney and systemic disposition in vulnerable patient populations.

S4.4 - THE DEVELOPMENT OF NOVEL *IN VITRO* SYSTEMS OF THE HUMAN INTESTINE TO PREDICT ORAL DRUG DISPOSITION

Christopher Arian

University of Washington, United States

The intestine functions as an important gatekeeping organ that can profoundly impact the disposition of orally administered drugs. However, limitations of currently used *in vitro* systems of the human intestine impedes their ability to predict the fate of such medications. The use of novel *in vitro* systems, such as intestinal organoids (enteroids) and the intestinal microphysiological system (MPS), may lead to improved predictions of oral drug bioavailability and associated drug-drug or natural product-drug interactions.

PL2 - WHAT DRUGS DO TO OUR BUGS**Kiran Patil**

University of Cambridge, Cambridge, United Kingdom

An adult typically harbours circa 0.5 kg of bacteria in their GI tract. These microbes outnumber the human somatic cells and feature 100 times more genes than the host. This gut microbiota contributes to various host functions, including food digestion, detoxification, neurological signalling, immune modulation, and pathogen defence. Recent studies have brought forward the critical role of microbiota in drug efficacy, mode of action, and toxicity. I will present latest research from my lab on this front, highlighting the extensive impact of host-targeted drugs on gut bacteria and discuss its mechanistic underpinnings. I will further discuss biotransformation and bioaccumulation of drugs by gut bacteria and the overall implications for drug development and safety.

S5.1 - MICROTRACER AND AMS-ENABLED STUDY DESIGNS IN CLINICAL DEVELOPMENT: APPLICATIONS, CHALLENGES AND OPPORTUNITIES**Marie Croft**

Pharmaron ABS, Inc., United States

The microtracer approach has become widely accepted in clinical development. There are two broad categories of microtracer study design. The first involves administration of a tracer amount of ^{14}C (typically 1 μCi) combined with a therapeutic ^{12}C dose. This approach allows generation of human absorption, distribution, metabolism and elimination (ADME) data from a therapeutically relevant dose, but with a much reduced ^{14}C dose than conventional used. The second approach involves the administration of an intravenous (IV) dose of ^{14}C -drug, concomitantly with a therapeutic dose of drug administered by the intended dose route (typically oral). This approach allows generation of IV pharmacokinetic data.

Microtracer designs are enabled by ultra-sensitive technology, primarily Accelerator Mass Spectrometry (AMS). AMS is a highly sensitive technique, which allows quantification of the ^{14}C concentration of a given sample by counting ^{14}C , ^{13}C , and ^{12}C atoms. The technology itself, in terms of the instrumentation and sample preparation is continuously evolving, and likewise the applications of AMS have evolved over the last 20 years

Microtracers and AMS enabled study designs are able to routinely generate data for candidate drugs, which would otherwise be much more challenging, even impossible, via traditional study designs or conventional analytical techniques. In addition, the microtracer approach can provide data at a much earlier stage of clinical development, reducing the overall drug development time.

S5.2 - THE AMS-ENABLED HUMAN ABSORPTION, DISTRIBUTION, METABOLISM & EXCRETION (HADME) STUDY: A TECHNOLOGICAL AND STRATEGIC PARADIGM SHIFT**Douglas Spracklin**

Pfizer, United States

The human radiolabeled ADME study provides a comprehensive picture of the disposition of a drug, with the data being used to inform the strategy for safety and clinical pharmacology studies. The standard ADME study design has been in place for some time; however, the application of accelerator mass spectrometry (AMS) as the detection method for carbon-14 in replacement of radioactivity measurements offers new advantages and potential.

In this talk, we will describe our experience with a new ADME study design, termed the AMS-Enabled Human ADME study. In this design, both oral and intravenous routes of administration are assessed in a single clinical study yielding the standard ADME study end points as well as additional fundamental pharmacokinetic parameters.

S5.3 - MICRODOSING AND MICROTRACER STUDIES IN PEDIATRICS: AN INNOVATIVE APPROACH TO STUDY DRUG DISPOSITION IN THIS VULNERABLE POPULATION**Bianca van Groen**

Roche, Switzerland

The disposition of drugs in children may be different from those in adults if a certain pathway is underdeveloped. This could lead to unsafe drug therapy when not accounted for. Interestingly, [^{14}C]microtracer studies permit studying drug disposition with a radioactivity exposure of even less than 0.1 μCi . Analytical advances such as these allow us to overcome ethical and analytical challenges with regard to radioactivity exposure in paediatrics. This approach is promising for first-in-child studies to delineate age-related variation in drug disposition.

S5.4 - PARADIGM SHIFT(S) TO THE HUMAN ADME STRATEGY, ENABLED BY AMS - OUTPUT FROM A CROSS-INDUSTRY CONSORTIA**Graeme Young***GSK, United Kingdom*

An EFPIA DMPK Network sponsored team representing 16 pharmaceutical companies, formed in late 2020, have been discussing the merits of moving towards a new paradigm in the design and conduct of the radiolabelled human ADME study for small molecules. The advent of the use of Accelerator Mass Spectrometry (AMS) technology in the pharmaceutical industry has facilitated the opportunity to rethink drug development in terms of DMPK science and the Clinical Pharmacology studies package. Each company is on a different part of the journey in terms of experience with AMS, its move from niche to routine adoption, inclusion of the ¹⁴C-microtracer* (IV and/or EV) design and drive or desire to conduct the historically late stage human ADME study, in early clinical development.

The team has recognised this inconsistency amongst the companies represented, but is also embracing the opportunities to seek changes where better drug development decisions can be made, based upon greater understanding of the ADME properties of assets potentially earlier than has generally been the case in the past. The microtracer approach has been accepted as a viable option through interactions related to new drug submissions with Regulatory authorities and the way appears open that may ultimately lead to a truly significant shift in the overall human ADME paradigm. Indeed, a series of incremental steps on the journey towards such a significant change in the paradigm may occur, depending on the experience and current practices for each pharmaceutical company.

* ¹⁴C-microtracer usually defined as a dose of ≤ 1 μ Ci of radioactivity.

S6.1 - WIDESPREAD DYSREGULATION OF LNCRNAs IN XENOBIOTIC-EXPOSED LIVER: SINGLE CELL APPROACHES TO ELUCIDATE LNCRNA FUNCTION**David J. Waxman** and Kritika Karri*Boston University, United States*

Long non-coding RNAs (lncRNAs) comprise a heterogeneous class of highly tissue and cell-type specific RNAs whose low expression limits detection in minor cell subpopulations and whose functions in both homeostatic liver and disease phenotypes is poorly understood. We previously established that hundreds of liver-expressed lncRNA genes are responsive to xenobiotic exposure in both rat and mouse models (Refs #1-3). Here, we developed an integrative approach to assemble the non-coding murine liver transcriptome and identify ~48,000 liver-expressed lncRNA genes based on >2,000 public liver RNA-seq samples. These lncRNA gene and isoform structures served as a reference for characterizing changes in single cell transcriptomic profiles for three mouse models of liver disease, respectively induced by exposure to: 1) TCDD, a chlorinated aromatic hydrocarbon and Ah receptor agonist; 2) the hepatotoxicant carbon tetrachloride; and 3) a high fat diet. Hepatic lipid accumulation and inflammation (non-alcoholic steatohepatitis, NASH) and liver fibrosis associated with excessive deposition of collagen and other extracellular matrix proteins are key features of these disease models. We applied trajectory inference algorithms to uncover exposure-induced changes in lncRNA and protein coding gene zonation across the liver lobule in each major hepatic cell population, including NASH-associated macrophages, a hallmark of disease progression, and collagen-producing myofibroblasts, a key source of the fibrous scar in fibrotic liver. Analysis of changes in cell-cell communication patterns induced by TCDD revealed marked decreases in EGF signaling from hepatocytes to non-parenchymal cells and increases in extracellular matrix-receptor interactions central to liver fibrosis. Finally, we implemented gene regulatory network analysis to directly link individual xenobiotic-regulated or high fat diet-responsive lncRNA genes to key biological pathways and functions, and thereby identify lncRNAs with essential regulatory functions in NASH and liver fibrosis based on network centrality metrics. These findings highlight the power of single cell transcriptomics to discover liver disease-relevant roles for poorly characterized lncRNA genes in both hepatocytes and non-parenchymal cells, and to elucidate novel aspects of foreign chemical-induced hepatotoxicity, including dysregulation of intercellular communication within the liver lobule. Supported in part by NIH grant ES024421 (to DJW).

References:

1. Lodato NJ, Melia T, Rampersaud A, Waxman DJ. Sex-differential responses of tumor promotion-associated genes and dysregulation of novel long noncoding RNAs in Constitutive Androstane Receptor-activated mouse liver. (2017) *Toxicol Sci.* 159:25-41. PMID: 28903501
2. Karri K, Waxman DJ. Widespread dysregulation of long noncoding genes associated with fatty acid metabolism, cell division, and immune response gene networks in xenobiotic-exposed rat liver. (2020) *Toxicol Sci.* 174:291-310. PMID: 31926019

3. Goldfarb CN, Waxman DJ. Global analysis of expression, maturation and subcellular localization of mouse liver transcriptome identifies novel sex-biased and TCPOBOP-responsive long non-coding RNAs. (2021) BMC Genomics. 22:212. PMID: 33761883

S6.2 - LNCRNAS HNF1A-AS1 AND HNF4A-AS1 IN DRUG METABOLISM AND DRUG-INDUCED TOXICITY

Lirong Zhang

Zhengzhou University, China

Cytochrome P450 enzymes (CYPs) are the predominant phase I enzymes in human liver, and metabolizes more than 70% of clinical drugs. CYPs expression can be induced or inhibited by endogenous or exogenous substances, which is an important factor leading to differential expression and drug-drug interaction. HNF1A-AS1 and HNF4A-AS1 are antisense lncRNAs located in the neighborhood regions of the transcription factor genes HNF1A and HNF4A, respectively. In the liver, HNF1A-AS1 and HNF4A-AS1 regulate the expression and function of several CYPs. HNF1A-AS1 positively regulates the expression of PXR and CYPs in hepatocytes. On the one hand, HNF1A-AS1 binds to PRMT1 protein, affects the subcellular localization of PRMT1, mediates the interaction between PRMT1 and PXR, and affects the histone modification status in CYP3A4 promoter region, thus regulating the expression of CYP3A4. On the other hand, HNF1A-AS1 increases HNF1A protein stability by inhibiting HNF1A ubiquitination. Conversely, HNF4A-AS1 negatively regulates the expression of PXR and CYPs in hepatocytes. Mechanistically, HNF4A-AS1 mediates the interaction between HNRNPC and HNF4A, affects the stability of HNF4A, then affects the expression of PXR as well as the enrichment of PXR and the histone modification status in the CYP3A4 promoter, thus regulating CYP3A4 expression. Importantly, HNF1A-AS1 and HNF4A-AS1 are involved in ritonavir-induced hepatotoxicity. They are also the factors contributed to the altered susceptibility to ritonavir-induced hepatotoxicity caused by rifampicin exposure. Overall, our research data indicate that HNF1A-AS1 and HNF4A-AS1 regulate the expression and function of several CYPs and play crucial roles in drug-induced liver injury.

S6.3 - NR2E3 IS A KEY COMPONENT IN P53 ACTIVATION BY REGULATING A LONG NONCODING RNA DINO IN ACUTE LIVER INJURIES

Kyounghyun Kim

University of Arkansas Medical Sciences, United States

Damage-induced long noncoding RNA (DINO) is a long noncoding RNA that directly interacts with p53 and thereby enhances p53 stability and activity in response to various cellular stresses. Here, we demonstrate that nuclear receptor subfamily 2 group E member 3 (NR2E3) plays a crucial role in maintaining active DINO epigenetic status for its proper induction and subsequent p53 activation. In acetaminophen (APAP)- or carbon tetrachloride-induced acute liver injuries, NR2E3 knockout (KO) mice exhibited far more severe liver injuries due to impaired DINO induction and p53 activation. Mechanistically, NR2E3 loss both *in vivo* and *in vitro* induced epigenetic DINO repression accompanied by reduced DINO chromatin accessibility. Furthermore, compared with the efficient reversal by a typical antidote N-acetylcysteine (NAC) treatment of APAP-induced liver injury in wild-type mice, the liver injury of NR2E3 KO mice was not effectively reversed, indicating that an intact NR2E3-DINO-p53–signaling axis is essential for NAC-mediated recovery against APAP-induced hepatotoxicity. These findings establish that NR2E3 is a critical component in p53 activation and a novel susceptibility factor to drug- or toxicant-induced acute liver injuries.

S6.4 - RNA ADVENTURES IN METABOLIC CONTROL

Tamer Sallam

University of California, United States

Long noncoding RNAs (lncRNAs) have emerged as key regulators of diverse biologic processes including metabolic regulation. The development of unbiased chromatin affinity assays has been instrumental in elucidating the function and molecular activities of lncRNAs. For example, applying RNA-centric genome wide mapping techniques revealed the molecular mode of action of the lncRNA Xist and galvanized new approaches investigating mechanisms of gene repression in physiology and disease. Despite providing novel insights into a lncRNA's "interactome" these assays have been sparingly used in metabolic applications. Here we apply a slightly modified version of Chromatin Isolation by RNA Purification (ChIRP) to systemically map the binding sites of metabolically active lncRNAs. These studies reveal new roles and mechanisms of lncRNAs in metabolic regulation.

PS1.1 - THERAPEUTIC PROTEIN DDI AND IT'S CLINICAL RELEVANCE**Qin Sun***FDA, United States*

The presentation will address the following topics related to drug-drug interaction (DDI) assessment for therapeutic proteins (TPs) mechanisms related to proinflammatory cytokine, TP is a proinflammatory cytokine, TP is a proinflammatory cytokine modulator, mechanisms unrelated to proinflammatory cytokine, DDI assessments for antibody-drug conjugates, and additional considerations for TP DDI assessments.

PS1.2 - GENE-DRUG INTERACTIONS AND VARIATION IN INDIGENOUS POPULATIONS**Katrina Claw***University of Colorado, United States*

Abstract not available.

PS1.3 - SIRNA MEDIATED DDI: CHALLENGES AND OPPORTUNITIES**Armina Abbasi***Amgen, Inc., United States*

Since 2018, five FDA approved siRNA therapeutics have entered the market with many more in late phases of clinical trials. siRNA therapeutics can silence target gene expression by taking advantage of the RNA interference (RNAi) machinery that acts as our body's natural defense mechanism against exogenous gene invasion. siRNA therapeutics deviate from small molecules and protein-based therapeutics in mechanism of action, physicochemical properties, and most ADME properties. However, due to a lack of guidance from regulatory agencies, most preclinical studies and drug applications for this modality follow a hybrid of small molecules and biologics ADME protocols. Investigating drug-drug interaction (DDI) liability is a routine and well-studied part of drug development processes. While in the case of small molecule drugs, DDIs are mostly caused by direct inhibition and/or induction interactions with cytochrome P450 and transporters, studies on triantennary N-acetylgalactosamine (GalNAc)-conjugated siRNAs over the past ten years demonstrates that such interactions are unlikely to cause these types of DDIs at clinically relevant doses. It is therefore recommended to assess siRNA DDI potential by the following three categories: 1) Direct inhibition or induction of drug metabolizing enzymes, transporters, or siRNA-related proteins (such as Argonaute 2 (Ago 2)) for siRNA containing any novel chemical modifications, ligands, or excipients, 2) Indirect drug disease interactions, and 3) Indirect mechanism-based interactions, such as any upstream or downstream effects of target degradation.

PL3 - STRUCTURE-METABOLISM-TOXICITY EVALUATION OF PROTEIN KINASE INHIBITORS**Klarissa Jackson***University of North Carolina at Chapel Hill, United States*

Tyrosine kinase inhibitors are a rapidly growing class of targeted agents that have therapeutic benefit in treating various types of cancers; however, these drugs have also been associated with potentially severe idiosyncratic hepatotoxicity. Metabolic activation by cytochrome P450 enzymes is proposed to play a key role in the idiosyncratic hepatotoxicity associated with several tyrosine kinase inhibitors through the formation of chemically reactive, potentially toxic metabolites. Research in the Jackson laboratory has investigated the contributions of individual P450 enzymes to the metabolic activation of tyrosine kinase inhibitors to elucidate the mechanisms of and risk factors for drug-induced hepatotoxicity. We have used hepatotoxic kinase inhibitors as model compounds to study how interindividual variations in P450 enzymes, due to genetic and non-genetic factors, affect the extent of drug metabolic activation. Using complementary *in vitro* reaction phenotyping approaches, we have determined the relative enzyme contributions to the metabolism and bioactivation of clinically relevant kinase inhibitors. Detection of reactive metabolite adducts through nucleophilic trapping studies and LC-MS/MS analysis provided evidence of reactive metabolite formation. Further, we have evaluated interindividual variation in kinase inhibitor metabolic activation using cytochrome P450 genotyped and phenotyped human liver microsomes and hepatocytes. This lecture will highlight the structure-metabolism evaluation of selected kinase inhibitors and the implications for drug-induced hepatotoxicity.

PS2.1 - PLACENTAL EFFLUX TRANSPORTERS IN HEALTH AND DISEASE**Lauren Aleksunes***Rutgers University, United States*

The placenta is a critical organ for fetal nutrition and growth. Transporters in the placenta play roles in the delivery of nutrients and medications to the fetus, restriction of toxicants from gaining access to the fetal circulation, and maintenance

of placental functions. This presentation will explore relationships between placental transporter proteomics and genetics in the UPSIDE epidemiological cohort of 290 mother-child dyads (Rochester, NY) and pregnancy hormones, demographics, and as well as birth outcomes. Particular attention will be placed on the intersection of environmental chemical exposure, transporter genetics, and fetoplacental growth and health.

PS2.2 - DRUG TRANSPORTERS IN CHEMOTHERAPY-INDUCED PERIPHERAL NEUROPATHY

Tore B. Stage

University of Southern Denmark, Denmark

Chemotherapy-induced peripheral neuropathy (CIPN) is a common and dose-limiting toxicity to widely used chemotherapeutics. Although the exact molecular mechanism of chemotherapy-induced peripheral neuropathy remains elusive, there is consensus that it is caused by damage to the peripheral nervous system leading to sensory symptoms. There is currently no objective biomarker of CIPN, which leads to subjective and highly variable clinician-based scoring of symptoms both clinically and in research. Recently, it has become evident that drug transporters are expressed in the peripheral nervous system. In this talk, I explore the role for drug transporters in regulating neuronal accumulation of chemotherapeutics and evidence for impact in CIPN. Furthermore, recent advances have highlighted objective biomarkers for CIPN that may improve research and clinical evaluation. This is also covered in my talk.

PS2.3 - ROLES OF TRANSPORTERS IN DISPOSITION, TUMOR TARGETING, AND TISSUE TOXICITY OF META-IODOBENZYLGUANIDINE

Joanne Wang

University of Washington, United States

Transporters on the plasma membrane of tumor cells are promising molecular “Trojan horses” to deliver drugs and imaging agents into cancer cells. Radioiodine-labeled meta-iodobenzylguanidine (mIBG), a diagnostic agent and a targeted radiotherapy for neuroendocrine cancers, enters cancer cells through the norepinephrine transporter (NET) that is highly expressed in neuroendocrine cancer cells. mIBG is eliminated by the kidney and accumulates in several normal tissues associated with radiation toxicities. Compared to cancer cells, very little is known about the transport mechanisms governing mIBG disposition in normal tissues and its elimination by the kidney. Emerging evidences suggest that the polyspecific organic cation transporters play important roles in systemic disposition and tissue-specific uptake of mIBG. This presentation focuses on the differential roles of NET, OCT and MATE transporters in mIBG disposition, response and toxicity. Understanding the molecular mechanisms governing mIBG transport in cancer and normal cells is critical for developing strategies to optimize the efficacy of ¹³¹I-mIBG while minimizing its toxicity to normal tissues.

PS2.4 - DRUG INTERACTIONS WITH MDR TRANSPORTERS

Arthur Roberts

University of Georgia, United States

P-glycoprotein (P-gp) transporter is part of the ATP Binding Cassette (ABC) transporter superfamily and effluxes a diverse range of drugs and substrates from the cytosol to the extracellular space through ATP hydrolysis and conformational changes. The transporter serves as a gatekeeper across the blood-brain barrier (BBB), plays a key role in anti-cancer drug resistance, and contributes to adverse drug reactions (ADRs) of cardiovascular drugs. The transport process is complex and has several steps, including drug binding, ATP hydrolysis, and drug-induced conformational changes. To gain better insight into the general transport mechanism of P-gp, we studied a chemically diverse range of drugs, including anthracyclines, camptothecins, and HIV protease inhibitors. The functional groups involved in molecular recognition of the transporter were investigated by saturation transfer double difference (STDD) NMR, and their affinity was ascertained by quenching of P-gp fluorescence. Several drugs induced distinct activation and inhibition phases in the P-gp-mediated ATPase kinetics and were modeled using the COMplex PATHway Simulator (COPASI), suggesting multiple drug binding to P-gp. Acrylamide quenching of P-gp fluorescence suggests that the drugs shift P-gp’s conformation between the inward-open and the outward-open conformations. The shifts observed in the acrylamide quenching experiments correlated well to their effects on the conformational distribution and dynamics of P-gp determined by atomic force microscopy (AFM). Combined with P-gp transport rates, these results allowed us to build a robust and detailed model of the P-gp transport process. The broader translation implications of P-gp transport with these drugs will also be discussed.

PS3.1 - VIRTUAL CLINICAL TRIAL SIMULATION FOR A KRASG12 COVALENT INHIBITOR USING A MECHANISTIC PHARMACOKINETIC MODEL COMBINED WITH QUANTITATIVE SYSTEMS PHARMACOLOGY APPROACH**Hiroyuki Sayama***Astellas Pharma Inc., Applied Research & Operation, Japan*

Quantitative systems pharmacology (QSP) is a novel mathematical modeling approach increasingly being applied to pharmaceutical drug discovery and development. In this presentation, a case example of the application of a mechanistic pharmacokinetic model combined with QSP approach to inform development of a small molecule, KRASG12C covalent binder, will be provided. The QSP model was constructed by integrating available *in vitro* and *in vivo* animal data as well as clinical information for a competitor, translated to human, and used to perform virtual clinical trial. The virtual clinical trial simulation was conducted to compare anti-tumor efficacy in non-small cell lung cancer patients between developing candidate and the competitor, supporting potential differentiation strategy. This presentation will highlight practical application of QSP approach for translational purpose in pharmaceutical industries.

PS3.2 - DEVELOPING A ROBUST QSP MODEL OF AAV-BASED GENE THERAPY FOR CLINICAL APPLICATIONS**Nessy Tania***Pfizer, United States*

Gene therapy provides a breakthrough approach to alter genetic mutations and directly correct underlying disease etiology. Recently, advances in genetic engineering and vector developments have allowed new gene therapies to progress successfully through the clinical drug development process. Established model-informed drug discovery (MIDD) approaches such as PK/PD fall short for estimating exposure-responses in adeno associate virus (AAV) gene therapy. To address this gap, we have developed a Quantitative Systems Pharmacology (QSP) model that incorporates the following mechanistic steps: viral vector distribution to target tissue, receptor binding and internalization, endosomal escape, nuclear translocation, capsid uncoating and transgene expression. This baseline model was calibrated to a compilation of data for AAV8 from literature and from previously published pre-clinical data on AAV8-based liver-targeted gene therapy treatments. In this presentation, we will focus on the application of the baseline model to clinical programs. Initial clinical translation of the model by accounting for physiological and biodistribution parameter changes could not fully capture the dynamics observed in individual patient data (published Phase1/2a clinical trial of rAAV-Spark100-hFIX-Padua, PF-06838435). To address this gap, we explored several mechanisms such as allometric scaling of AAV-processing kinetics or slower secretion of Factor IX from hepatocytes. Finally, we will discuss the calibration of the baseline model to published AAV5 and AAV6 mouse data, in order to eventually translate the model for Hemophilia A clinical applications. We analyzed several underlying model assumptions and incorporated different mechanistic hypotheses in order to obtain consistent agreements with observed clinical data. Thus, we present a methodology of developing and calibrating mechanistic models of AAV gene therapy that can be used to aid clinical trial design.

PS3.3 - MODEL INFORMED DEVELOPMENT FOR MRNA VACCINES**Stephen Greene***Moderna Inc., United States*

Model informed drug development (MIDD) can have an immense impact on the overall decision making and progress of mRNA therapeutic development. Case examples of MIDD will be presented across pre-clinical and clinical scenarios.

PS3.4 - M&S FOR POMPE ENZYME REPLACEMENT TREATMENT DEVELOPMENT**John Mondick***Metrum Research Group, United States*

Pompe disease is a rare autosomal recessive genetic disorder caused by variants in the gene that encodes the enzyme acid-glucosidase (GAA). These variants may result in complete absence or partial loss of endogenous GAA activity, which is responsible for the breakdown of lysosomal glycogen. The enzyme deficiency results in accumulation of intracellular glycogen leading to progressive disruption of muscle function. Cipaglucosidase alfa/miglustat is a novel first-in-class, two-component therapy in development for the treatment of adult and pediatric patients with Pompe disease. Cipaglucosidase alfa is a recombinant human GAA (rhGAA), administered intravenously that is engineered for optimal targeting to the intracellular lysosomal compartment of muscles. Miglustat is an enzyme stabilizer of cipaglucosidase alfa that is administered orally one hour prior to enzyme infusion to protect the enzyme from denaturation while in systemic circulation, designed to enhance the delivery of cipaglucosidase alfa to muscles. Given the obstacles associated with drug development for a rare disease, the Pompe program has relied heavily on model-informed drug development (MIDD) principles to guide decision making. Since numerous questions have been explored throughout the development process,

it was necessary to construct a variety of population pharmacokinetic (PK) models to guide decision making. The model structure and complexity has been dictated by: (1) the amount of clinical data available for model development and (2) the nature of the question to be addressed. For ciplagucosidase alfa/miglustat, the PK results of a small phase 1 clinical study (n = 17) were initially used for model development. Simple population PK models were developed for both drugs separately, the effects of miglustat on ciplagucosidase alfa exposures described by a simple covariate model, and the individual models were applied as simulation tools to guide drug development. Following the addition of a larger PK study (n = 114), a semi-mechanistic model was developed to describe the binding interaction between ciplagucosidase alfa and miglustat, with prevention of inactivation in blood following infusion. Two examples will be presented to demonstrate model utility. A simulation/estimation analysis for the successful design of a pediatric PK study under the FDA quality standard was performed using the simple models, and a simulation study was undertaken using the semi-mechanistic model to describe the effects of renal function on miglustat disposition and subsequent effects on ciplagucosidase exposures. The two examples will focus on the need for MIDD in rare disease applications, appropriateness of the various models to address the drug development questions, and the clinical utility of the simple versus semi-mechanistic models.

PRE-DOCTORAL/GRADUATE POSTER FINALISTS

(A1 – A6)

A1 - FLEXIBILITY OF THE F-F' LOOP, CRUCIAL FOR SUBSTRATE ACCESS TO THE CYP3A4 ACTIVE SITE, IS REDUCED UPON ALLOSTERIC INHIBITION: A NOVEL MECHANISM TO RATIONALIZE PROBE SUBSTRATE DEPENDENCIES IN KI*Lloyd Wei Tat Tang, National University of Singapore, Singapore, Singapore***A2 - INFLAMMATION AND PREGNANCY ALTER ORGANIC ANION TRANSPORTERS 1/3 ACTIVITY EMPLOYING THE PROBE DRUG FUROSEMIDE IN WOMEN***Jhohann Benzi, University of Sao Paulo, Ribeirão Preto, São Paulo, Brazil***A3 - FLUCLOXACILLIN IS A WEAK INDUCER OF CYP3A4***Ditte Bork Iversen, University of Southern Denmark, Odense, Denmark***A4 - DICLOXACILLIN CAUSES DRUG-DRUG INTERACTIONS – TRANSLATING REAL-WORLD DATA TO BASIC PHARMACOLOGY***Ann-Cathrine Dalgård Dunvald, University of Southern Denmark, Odense, Denmark***A5 - USING TARGETED MASS SPECTROMETRY-BASED PROTEOMICS TO IDENTIFY DRUG METABOLIZING ENZYMES IN THE BRAIN***Abigail Wheeler, Johns Hopkins University, Baltimore, Maryland, United States***A6 - QUANTIFICATION OF ABSOLUTE COMPOSITIONS AND TOTAL ABUNDANCE OF HOMOLOGOUS PROTEINS IN HUMAN TISSUES USING CONSERVED-PLUS-SURROGATE PEPTIDE (CPSP) APPROACH: APPLICATION IN THE QUANTIFICATION OF UDP GLUCURONOSYLTRANSFERASES***Deepak Ahire, Washington State University, Spokane, Washington, United States***POSTDOCTORAL POSTER FINALISTS (A7 – A12)****A7 - IN VIVO EVALUATION OF CYTOCHROME P450-MEDIATED CANNABINOID-DRUG INTERACTIONS IN HEALTHY ADULT PARTICIPANTS***Sumit Bansal, University of Washington, Seattle, Washington, United States***A8 - STRUCTURAL AND MECHANISTIC INVESTIGATIONS OF COVALENTLY MODIFIED CYP ENZYMES VIA MASS SPECTROMETRIC ANALYSIS***Yuanyuan Shi, University of Washington, Seattle, Washington, United States***A9 - INDUCTION OF CYTOCHROME P450 ENZYMES AND DRUG TRANSPORTERS IN 3D SPHEROID CULTURE OF PRIMARY HUMAN HEPATOCYTES***Erkka Järvinen, University of Southern Denmark, Odense, Denmark***A10 - IBRUTINIB METABOLISM IN VITRO IS CORRELATED WITH INDIVIDUAL HEPATIC CYP3A ACTIVITY AND PROTEIN EXPRESSION AND PLASMA 4B-HYDROXYCHOLESTEROL/CHOLESTEROL RATIO***Jonghwa Lee, University of North Carolina at Chapel Hill, Chapel Hill, North Carolina, United States***A11 - ONTOGENY OF HUMAN ALDEHYDE OXIDASE (AO)***Sandhya Subash, Washington State University, Spokane, Washington, United States***A12 - IMPLEMENTATION OF A PHYSIOLOGICALLY BASED PHARMACOKINETIC MODELING APPROACH TO PREDICT DISEASE-RELATED CHANGES IN DRUG PHARMACOKINETICS IN PATIENTS WITH NONALCOHOLIC FATTY LIVER DISEASE***Jeffry Adiwidjaja, The University of North Carolina at Chapel Hill, Carrboro, North Carolina, United States***ADVERSE EFFECTS (P1)****P1 - NEUROFILAMENT LIGHT CHAIN AS A BIOMARKER OF AXONAL DAMAGE IN SENSORY NEURONS AND PACLITAXEL-INDUCED PERIPHERAL NEUROPATHY IN OVARIAN CANCER PATIENTS***Christina Mortensen, University of Southern Denmark, Odense, Denmark***ANALYTICAL (P2)****P2 - VALIDATION OF A MFLC-MS/MS ASSAY FOR THE QUANTITATIVE ANALYSIS OF A NOVEL PEPTIDE, AT-01, EXTRACTED FROM K2EDTA PLASMA***Tara O'Brien, Alturas Analytics, Inc., Moscow, Idaho, United States***ANIMAL MODELS FOR PBPK (P3)****P3 - CONDITIONAL KNOCKOUT OF THE CYTOCHROME P450 OXIDOREDUCTASE GENE HIGHLIGHTS HUMAN DRUG METABOLISM IN HUMANIZED LIVER TK-NOG MICE***Hiroshi Suemizu, Central Institute for Experimental Animals, Kawasaki, Japan***ARYL HYDROCARBON RECEPTOR (P4)****P4 - EPIGENETIC REGULATION OF THE ARYL HYDROCARBON RECEPTOR (AHR) IN NORMAL AGING***Sara Abudahab, Virginia Commonwealth University, Richmond, Virginia, United States***BIOAVAILABILITY (P5-P6)****P5 - CONSIDERATIONS IN CLINICAL EVALUATION FOR PHARMACOKINETIC CHANGES OF ORALLY ABSORBED DRUGS BY BARIATRIC SURGERY***Sungyeun Bae, Seoul National University College of Medicine and Hospital, Seoul, South Korea***P6 - INTER- AND INTRA-SUBJECT ANALYSIS OF GENE EXPRESSION AND PROTEIN ABUNDANCE OF MINOR DRUG METABOLIZING ENZYMES IN HEALTHY HUMAN INTESTINE AND LIVER.***Christoph Wenzel, University Medicine Greifswald, Greifswald, Mecklenburg-Vorpommern, Germany***BIODISTRIBUTION (P7)****P7 - HEAD-TO-HEAD COMPARISON OF AAV BIODISTRIBUTION AND TRANSGENE EXPRESSION LEVELS AMONG RAAV SEROTYPES***Yosuke Yamanaka, Astellas Pharma Inc., Tsukuba-shi, Ibaraki, Japan***BIOMARKERS (P8)****P8 - QUANTIFYING PROTEIN BIOMARKERS FOR DRUG-INDUCED ORGAN INJURY ACROSS THE SPECIES BARRIER BY IMMUNOAFFINITY-LC-MASS SPECTROMETRY***Oliver Poetz, SIGNATOPE GmbH, Reutlingen, Germany*

CLEARANCE PREDICTION (P10-P12)**P10 - ADAPTATION OF *IN VITRO* METHODS TO DETERMINE UNBOUND CELL TO MEDIUM PARTITION COEFFICIENT, *K_p*, *U_u***

Virag Bujdosó-Szekely, SOLVO Biotechnology, A Charles River Company, Budapest, Hungary

P11 - INVESTIGATION OF THE UNDER PREDICTION OF *IN VIVO* CLEARANCE FROM METABOLIC INTRINSIC CLEARANCE IN THE RAT: GASTROINTESTINAL EXSORPTION AS AN IMPORTANT ELIMINATION PATHWAY IN DRUG DISCOVERY

Dermot McGinnity, AstraZeneca, Cambridge, Cambridgeshire, United Kingdom

P12 - HEPATOCYTE UPTAKE AND LOSS ASSAY (HUPLA), A NOVEL ALL-IN-ONE SYSTEM FOR OBTAINING UPTAKE, EFFLUX AND INTRINSIC CLEARANCE FOR COMPOUNDS WITH CHALLENGING PHYSICO-CHEMICAL PROPERTIES AND LOW METABOLIC TURNOVER.

Julia Schulz, AbbVie Inc., North Chicago, Illinois, United States

CONJUGATION REACTIONS AND ENZYMES (P13-P17)**P13 - REACTIVITY ASSESSMENT OF CARBOXYLIC ACID DRUGS BY USING ACYL MIGRATION RATE AND HALF-LIFE DETERMINATION OF ACYL-GLUCURONIDES**

Barry Jones, Pharmaron, Rushden, Northamptonshire, United Kingdom

P14 - CANAGLIFLOZIN-2'-O-GLUCURONIDE FORMATION IS A SELECTIVE UGT2B4 REACTION USED TO IDENTIFY CLOTRIMAZOLE AS A POTENT UGT2B4 INHIBITOR

Kimberly Lapham, Pfizer, Inc, Groton, Connecticut, United States

P15 - INTER- AND INTRA-SPECIES SEMI-QUANTITATIVE COMPARATIVE DIFFERENTIATION OF REACTIVE METABOLITES VIA COMPETITIVE TRAPPING APPROACH

Igor Mezine, Absorption, Exton, Pennsylvania, United States

P16 - METTL7A AND METTL7B ARE XENOBIOTIC ALKYL THIOL METHYLTRANSFERASE ENZYMES

Drake Russell, University of Washington, Seattle, Washington, United States

P17 - STRUCTURAL AND BIOCHEMICAL CHARACTERIZATION OF THE THIOL METHYL TRANSFERASES METTL7A AND METTL7B

Drake Russell, University of Washington, Seattle, Washington, United States

CYTOCHROME P450 (P18-P32)**P18 - GENERATION AND CHARACTERIZATION OF CYP2E1-OVEREXPRESSED HEPG2 CELLS**

Nouf Alwadei, Chapman University, Irvine, California, United States

P19 - NEW MECHANISM OF THE LIVER CYTOCHROME P450 REGULATION VIA NMDA RECEPTOR

Ewa Bromek, Maj Institute of Pharmacology PAS, Krakow, Poland

P20 - PROTEIN/PROTEIN INTERACTIONS IN THE HUMAN CYTOCHROME P450 SYSTEM

Sarah Burris-Hiday, University of Michigan, Ann Arbor, Michigan, United States

P21 - APPLYING MECHANISTIC UNDERSTANDING TO DESIGN AWAY FROM CYP3A TIME-DEPENDENT INACTIVATION: ASSAY DEVELOPMENT, VALIDATION AND**IMPLEMENTATION**

Matthew Cerny, Pfizer, Groton, Connecticut, United States

P22 - IMPACT OF CASTRATION ON THE RENAL PROXIMAL TUBULAR VACUOLIZATION IN MALE MICE WITH DECREASED EXPRESSION OF THE NADPH-CYTOCHROME P450 REDUCTASE

Xinxin Ding, University of Arizona, Tucson, Arizona, United States

P23 - STRATEGIES AND CONSIDERATIONS FOR EVALUATING THE CONTRIBUTION OF CYTOCHROME P450 1A1 TO METABOLISM OF A THERAPEUTIC CANDIDATE

Sarah Glass, Janssen Research & Development, San Diego, California, United States

P24 - HOW ABSORPTION, METABOLISM, DISTRIBUTION, AND EXCRETION CHARACTERISTICS OF ACT-1004-1239 GUIDE INVESTIGATION OF ITS DRUG-DRUG INTERACTION POTENTIAL

Christine Huynh, Idorsia Pharmaceuticals Ltd, Basel, Allschwil, Switzerland

P25 - A NOVEL PROTEOMICS PIPELINE FOR ADDUCT DISCOVERY FINDS RALOXIFENE EXPOSURE CAUSES NUMEROUS DRUG-PROTEIN ADDUCTS IN HUMAN P450S AND OTHER PROTEINS.

Nina Isoherranen, University of Washington, Seattle, Washington, United States

P27 - EVALUATING THE EFFECTS OF SCELETIUM TORTUOSUM EXTRACT ON CYP 2C9 IN LIVER MICROSOMES OF FLINDERS LINE SENSITIVE RATS

Makhotso Lekhoo, North West University, Potchefstroom, North West, South Africa

P28 - STRUCTURE OF CYP8B1 WITH A RATIONALLY DESIGNED CYP8B1 INHIBITOR: PROVIDING DIRECTIONS FOR INHIBITOR OPTIMIZATIONS

Jinghan Liu, University of Michigan, Ann Arbor, Michigan, United States

P29 - ASSAY VALIDATION OF A TARGETED IMMUNOAFFINITY PROTEOMICS ASSAY FOR ROUTINE ASSESSMENT OF DRUG METABOLIZING ENZYMES FOR THE ANALYSIS OF *IN VITRO* ENZYME INDUCTION

Oliver Poetz, SIGNATOPE GmbH, Reutlingen, Germany

P31 - GLOBAL VERSUS TARGETED PROTEOMICS FOR QUANTIFICATION OF DMET PROTEINS IN HUMAN LIVER, KIDNEY, AND INTESTINE

Dilip Kumar Singh, Washington State University, Spokane, Washington, United States

P32 - CHARACTERIZATION OF DRUG-METABOLIZING ENZYMIC ACTIVITIES IN THE HEPATOCYTES ISOLATED FROM THE CHIMERIC TK-NOG MICE WITH HUMANIZED LIVERS

Shotaro Uehara, Central Institute for Experimental Animals, Kawasaki, Japan

DIFFERENCES IN METABOLISM (SPECIES, GENDER, AGE, DISEASES) (P34)**P34 - A MECHANISM OF GDC-0919 IN RATS AND DOGS: UNEXPECTED CYANIDE RELEASE FROM IMIDAZO[1,5-A]ISOINDOLE AND SPECIES DIFFERENCES IN GLUCURONIDATION**

Shuai Wang, Genentech, South San Francisco, California, United States

DISPOSITION (P35-P41)**P35 - GENERATION OF A CREATINE KINASE BRAIN-TYPE KNOCKOUT MOUSE MODEL TO STUDY TENOFOVIR BIOACTIVATION**

Colten Eberhard, Johns Hopkins University School of Medicine, Baltimore, Maryland, United States

P36 - EVALUATION OF FRACTION UNBOUND VALUES OVER VARYING CONCENTRATIONS OF CNS COMPOUNDS IN BRAIN, BLOOD, AND PLASMA PROTEIN BINDING

Richard Grater, Biogen, Cambridge, Massachusetts, United States

P37 - INVESTIGATING THE IMPACT OF BLOOD COLLECTION METHODS AND ETHNICITY ON HUMAN PLASMA PROTEIN BINDING

Barry Jones, Pharmaron, Rushden, Northamptonshire, United Kingdom

P38 - BIODISTRIBUTION OF TOPOTECAN-LOADED POLYMERIC NANOPARTICLES FOR THE LACTONE AND TOTAL TOPOTECAN FORMS

YONG-BOK LEE, College of Pharmacy, Chonnam National University, Gwangju, South Korea

P39 - AMS-ENABLED HUMAN ADME STUDY OF THE FGFR INHIBITOR DERAZANTINIB

Karine Litherland, Basilea Pharmaceutica International Ltd, Allschwil, Switzerland

P40 - A DECADE OF HUMAN ADME AT QUOTIENT: REVIEWING KEY STUDY DESIGN VARIABLES AND OUTCOMES

Iain Shaw, Quotient Sciences, Nottingham, United Kingdom

P41 - UNDERSTANDING THE ABSORPTION, METABOLISM AND EXCRETION OF MASITINIB IN HEALTHY MALE SUBJECTS

Iain Shaw, Quotient Sciences, Nottingham, United Kingdom

DRUG DISCOVERY AND DEVELOPMENT (P42-P49)**P42 - OPTIMIZATION OF MDCK PERMEABILITY ASSAY TO ENABLE SEMI-HIGH THROUGHPUT SCREENING AND EXPLOITATION OF *IN SILICO* AND MODELLING TOOLS TO SUPPORT DISCOVERY PROJECTS**

Karpagam Aravindhan, GSK, Collegeville, Pennsylvania, United States

P43 - A COMPARISON OF THE EFFECTIVENESS OF EQUILIBRIUM DIALYSIS AND ULTRACENTRIFUGATION IN DETERMINING THE PLASMA PROTEIN BINDING OF HIGH BINDING INVESTIGATIONAL DRUGS

Vicky Birks, Pharmaron UK, Rushden, Northamptonshire, United Kingdom

P44 - PRECLINICAL AND CLINICAL ADME PROFILE OF ETC-159, AN ORAL PORCUPINE INHIBITOR, FOR THE TREATMENT OF PATIENTS WITH ADVANCED SOLID TUMOURS

Vishal Pendharkar, Experimental Drug Development Centre, Singapore, Singapore, Singapore

P45 - UNIQUE DATA OBSERVATIONS AND FINDINGS FROM VARIED INCUBATION TIMES ON PLASMA PROTEIN BINDING

Charles Rotter, Takeda California Global DMPK, San Diego, California, United States

P46 - THE DEVELOPMENT AND VALIDATION OF A COMPUTATIONAL MODEL TO PREDICT HUMAN LIVER**MICROSOME STABILITY**

Pranav Shah, NCATS/NIH, Rockville, Maryland, United States

P47 - A MEGA-ANALYSIS ON ADME AND TOXICITY OF INOTERSEN, PATISIRAN, AND VUTRISIRAN FOR THE TREATMENT OF HEREDITARY TRANSTHYRETIN-MEDIATED AMYLOIDOSIS

Sherouk Tawfik, University of Connecticut, Storrs, Connecticut, United States

P48 - INVESTIGATION OF CLINICAL ADME AND PHARMACOKINETICS OF THE HIV-1 MATURATION INHIBITOR GSK3640254 USING AN INTRAVENOUS MICROTRACER COMBINED WITH THE ENTEROTRACKER® BILIARY SAMPLING

Bo Wen, GlaxoSmithKline, Collegeville, Pennsylvania, United States

P49 - SELECTION OF ANALYTICAL PLATFORMS FOR BIOMARKER AND BIOANALYTICAL QUANTIFICATION IN PRECLINICAL RESEARCH WITH CASE STUDIES

Faizan Zubair, Takeda Pharmaceuticals, San Diego, California, United States

DRUG INTERACTION (P50-P57)**P50 - CHARACTERIZATION OF THE PHARMACODYNAMICS OF ORAL DRONABINOL BEFORE AND AFTER ONE-WEEK OF HYDROCORTISONE OR ESTRADIOL TREATMENT IN HEALTHY, PREMENOPAUSAL WOMEN**

Aurora Authement, University of Washington, Seattle, Washington, United States

P51 - DURATION OF THE EFFECT OF COBICISTAT ON SIMVASTATIN PHARMACOKINETICS AND MIDAZOLAM SYSTEMIC CLEARANCE: ESTIMATING THE TURNOVER HALF-LIVES OF INTESTINAL AND HEPATIC CYP3A4

Janne Backman, Univ Helsinki, Helsinki, Finland

P52 - MODULATION OF NICOTINE METABOLISM IN MICE BY ORALLY AND INTRAPERITONEALLY ADMINISTERED TRANS-CINNAMALDEHYDE AND TRANS-2-METHOXYCINNAMALDEHYDE

Uyen-Vy Navarro, Pacific University Oregon, Hillsboro, Oregon, United States

P53 - INFLUENCE OF FOOD, SEX, AND BCRP INHIBITION ON FUROSEMIDE ORAL PHARMACOKINETICS IN RATS

Vijaya Saradhi Mettu, Washington State University, Spokane, Washington, United States

P54 - USE OF *IN VITRO* DATA TOWARDS CLINICAL PREDICTION OF DRUG-DRUG INTERACTION RISK DUE TO TIME-DEPENDENT INHIBITION OF CYTOCHROME P450 1A2, 2C8, 2C9, 2C19, AND 2D6

Elaine Tseng, Pfizer Inc, Groton, Connecticut, United States

P55 - PHYSIOLOGICALLY BASED PHARMACOKINETIC (PBPK) MODELING OF PYROTINIB TO UNDERSTAND THE IMPACT OF INTERPLAY BETWEEN CYP3A4 AND P-GP ON ITS DDIS WITH CYP3A4 INHIBITORS/INDUCERS

Tarang Vora, Simulations Plus, Inc., Lancaster, California, United States

P56 - ENZYME- AND TRANSPORTER-MEDIATED CLINICAL DRUG INTERACTIONS WITH DRUGS APPROVED BY THE U.S. FOOD AND DRUG ADMINISTRATION IN 2021: WHAT CAN BE LEARNED FROM NEW DRUG APPLICATION REVIEWS?

Jingjing Yu, UW Drug Interaction Solutions, Seattle, Washington, United States

P57 - *IN VITRO* EVALUATION OF PROTAC® DEGRADER ARV-110 (BAVDEGALUTAMIDE) FOR CYTOCHROME P450- AND TRANSPORTER-MEDIATED DRUG-DRUG INTERACTION

George Zhang, Arvinas Inc., New Haven, Connecticut, United States

ENZYME INDUCTION (P58-P64)**P58 - ALTERNATIVE CYP3A4 INDUCERS FOR RIFAMPIN**

Kuan-Fu Chen, Simcyp Limited (Division of Certara), Bellevue, Washington, United States

P59 - CHARACTERIZATION OF JNJ-2482272 [4-(4-METHYL-2-(4-(TRIFLUOROMETHYL)PHENYL)THIAZOLE-5-YL)PYRIMIDINE-2-AMINE] AS A STRONG AHR ACTIVATOR IN RAT AND HUMAN

Kevin Coe, Janssen Research & Development, San Diego, California, United States

P60 - FIVE DONORS, THREE ENDPOINTS, ONE WELL; EVALUATION OF A STREAMLINED POPULATION APPROACH TO DETERMINE INDUCTION POTENTIAL OF NEW CHEMICAL ENTITIES.

Cody Fullenwider, Takeda Pharmaceuticals, San Diego, California, United States

P61 - EXPRESSION DYNAMICS OF GENES INVOLVED IN XENOBIOTICS METABOLISM AFTER EXPOSURE TO NUCLEAR RECEPTOR LIGANDS OF NR1I SUBFAMILY IN 3D PRIMARY HUMAN HEPATOCYTE SPHEROIDS

Petr Pavek, Charles University, Faculty of Pharmacy in Hradec Kralove, Hradec Kralove, Czech Republic

P62 - DEVELOPMENT OF A STRATEGY TO IDENTIFY AND EVALUATE LIGAND AND INDIRECT ACTIVATORS OF RAT CAR

Takumi Sato, University of Shizuoka, Shizuoka-shi, Shizuoka-ken, Japan

P63 - REVISITING THE IMPACT OF ST. JOHN'S WORT ON CYP3A METABOLISM IN RATS – A COMPARATIVE STUDY

Anima Schäfer, University of Basel, Basel, Switzerland

P64 - STRUCTURAL CHARACTERIZATION OF CONSTITUTIVE TRANSCRIPTIONAL ACTIVITY OF THE NUCLEAR RECEPTOR PXR AND THE GENERATION OF LIGAND-SENSITIVE PXR MUTANTS.

Ryota Shizu, University of Shizuoka, Shizuoka, Japan

ENZYME INHIBITION/INACTIVATION (P65-P67)**P65 - 1-AMINOBENZOTRIAZOLE (ABT) IS NOT AN IDEAL PAN-CYP INHIBITOR FOR REACTION PHENOTYPING OF LOW CLEARANCE COMPOUNDS IN LONG-TERM CELL CULTURE MODELS**

Krishna Aluri, AstraZeneca, Waltham, Massachusetts, United States

P66 - FOUR STEPS TO ACCURATELY SELECT ENZYME INHIBITION MODELS AND DETERMINE INHIBITION CONSTANT (KI) VALUES FOR CYP INHIBITION BY MRTX COMPOUND A, A PROTOTYPICAL SOS1 INHIBITOR

Natalie Nguyen, Mirati Therapeutics, Inc., San Diego, California, United States

P67 - LOCALIZATION OF ADDUCTS FORMED BY REACTIVE METABOLITES IN CYP2C9 IMPACTS PRESENCE OF TIME DEPENDENT INHIBITION

Ellen Riddle, University of Washington, Seattle, Washington, United States

EXTRAHEPATIC METABOLISM (P68-P70)**P68 - ENTERIC VERSUS HEPATIC URIDINE 5'-DIPHOSPHO (UDP)-GLUCURONOSYLTRANSFERASE (UGT) ACTIVITY: A COMPARISON OF CRYOPRESERVED HUMAN INTESTINAL MUCOSA (CHIM) AND CRYOPRESERVED HUMAN HEPATOCYTES (CHH) IN THE ENZYME KINETICS OF B-ESTRADIOL, CHENODEOXYCHOLIC ACID,**

Albert Li, Discovery Life Sciences, Columbia, Maryland, United States

P69 - CONVERSION OF DRUG METABOLITES BACK TO PARENT DRUGS BY HUMAN GUT MICROBIOTA IN AN EX VIVO FERMENTATION SCREENING PLATFORM

Evita van de Steeg, TNO, Zeist, Netherlands

P70 - UPDATED STATUS ON THE COLOR DEVELOPERS CURRENTLY USED IN THERMAL PAPERS ON THE FRENCH MARKET, RELATED HAZARDS AND HUMAN EXPOSURE RISKS

Daniel Zalko, INRAE, Toulouse, France

HEPATIC UPTAKE (P71)**P71 - TRANSPORTER KINETICS AND MODULATION OF THE ORGANIC CATION TRANSPORTER OCT1 (SLC22A1) IN 3D CULTURED PRIMARY HUMAN HEPATOCYTES**

Alina Meyer, Uppsala University, Uppsala, Sweden

HEPATOCYTES (P72-P79)**P72 - PROTEOME DECONVOLUTION OF LIVER BIOPSIES REVEALS HEPATIC CELL COMPOSITION AS AN IMPORTANT MARKER OF CELL SPECIFIC RESPONSES**

Rebekkah Hammar, Uppsala University, Uppsala, Sweden

P73 - AN *IN VITRO* INVESTIGATION OF CANNABIDIOL METABOLISM AND HEPATOTOXICITY USING THREE-DIMENSIONAL HUMAN HEPATOCYTE SPHEROIDS

Jessica Beers, University of North Carolina at Chapel Hill, Chapel Hill, North Carolina, United States

P74 - OPTIMIZATION OF HEPATOCYTE BINDING ASSAY CONDITIONS TO ADDRESS LOW COMPOUND RECOVERY ISSUES IN EARLY DRUG DISCOVERY

Megha Chandrashekhar, Amgen, South San Francisco, California, United States

P75 - ROLE OF OXIDATIVE STRESS IN HEPEXTEND SUPPLEMENT MEDIATED IMPROVEMENT IN METABOLIC AND TRANSPORTER FUNCTION OF PRIMARY HUMAN HEPATOCYTES

Rohit Jindal, Thermo Fisher Scientific, Frederick, Maryland, United States

P76 - DEVELOPMENT OF AN INTEGRATED ASSESSMENT TOOL TO CATEGORISE DILI RISK IN DISCOVERY

Barry Jones, Pharmaron, Rushden, Northamptonshire, United Kingdom

P77 - 3D SPHEROIDS USING PRIMARY HUMAN HEPATOCYTES TO PREDICT DRUG INDUCED LIVER INJURY

Barry Jones, Pharmaron, Rushden, Northamptonshire, United Kingdom

P78 - OPTIMIZING A MICROCAVITY PLATE-BASED HUMAN HEPATOCYTE SPHEROID MODEL FOR *IN VITRO* CLEARANCE STUDIES

David Kukla, AbbVie, North Chicago, Illinois, United States

P79 - HUMAN HEPATOCYTE SPHEROIDS - EVALUATION OF DRUG METABOLIZING ENZYME ACTIVITY AND CLINT

Ting Wang, Boehringer Ingelheim, Danbury, United States

IMMUNOTOXICOLOGY (P81)

P81 - THE ROLE OF MYELOPEROXIDASE IN CLOZAPINE-INDUCED INFLAMMATION: LINKING REACTIVE METABOLITE FORMATION AND IDIOSYNCRATIC DRUG-INDUCED AGRANULOCYTOSIS

Samantha Sernoskie, University of Toronto, Toronto, Ontario, Canada

IN SILICO (P82)

P82 - APPLICATIONS OF PHYSIOLOGICALLY-BASED PHARMACOKINETIC MODELS TO INVESTIGATE FOOD EFFECTS ON ORAL ABSORPTION OF IBUPROFEN SODIUM

Lisa Cheng, The University of British Columbia, Vancouver, British Columbia, Canada

IN VITRO IN VIVO EXTRAPOLATION (IVIVE) (P83-P89)

P83 - VITAMIN K1 METABOLISM - THE ROAD LESS TRAVELED: UTILITY OF NON-LINEAR MIXED EFFECT MODELS IN THE EVALUATION OF COMPLEX GENOMIC TRAITS

Nathan Alade, University of Washington, Seattle, Washington, United States

P84 - PROTEIN ABUNDANCE OF RAT P-GP AND BCRP EFFLUX TRANSPORTERS IN TRANSFECTED MDCK, MDCKII, LLC-PK1 CELL MONOLAYERS AND RAT BRAIN MICROVESSELS

Zubida Al-majdoub, The University of Manchester, Manchester, United Kingdom

P85 - ISOLATED PRIMARY ENTEROCYTES AND 3D ENTEROIDS AS INTESTINAL *IN VITRO* ADME MODELS REFLECTIVE OF NATIVE EPITHELIUM

Rebekkah Hammar, Uppsala Universitet, Uppsala, Sweden

P86 - ISOLATED PRIMARY COLONOCYTES AND 3D COLONOIDS AS INTESTINAL *IN VITRO* ADME MODELS REFLECTIVE OF NATIVE EPITHELIUM

Rebekkah Hammar, Uppsala Universitet, Uppsala, Sweden

P87 - AN ENCOUNTER WITH A NEXT GENERATION BLOOD-BRAIN BARRIER PBPK MODEL WITH ENHANCED PROTEOMIC-INFORMED TRANSPORTER IVIVE CAPABILITIES

Janita Hogan, Merck & Co Inc, West Point, Pennsylvania, United States

P88 - A COMPARISON OF THE *IN VITRO IN VIVO* CORRELATION OF SMALL MOLECULE METABOLISM IN THREE LONG-TERM PRIMARY HUMAN HEPATOCYTE CULTURE MODELS

Hlaing Maw, Boehringer Ingelheim Pharmaceuticals, Inc., Ridgefield, Connecticut, United States

P89 - ESTABLISHMENT OF *IN VITRO* ASSAYS TO PREDICT THE *IN VIVO* CLEARANCE OF PEPTIDES IN RAT

Anna Vildhede, AstraZeneca, Mölndal, Sweden

IN VITRO TECHNIQUES (P90-P100)

P90 - STRATEGIES TO IMPROVE BEYOND RULE OF 5 COMPOUND RECOVERIES WITHIN *IN VITRO* ASSAYS: EFFECT OF VARIOUS EXCIPIENTS

Julius Enoru, AbbVie, South San Francisco, California, United States

P91 - A VALIDATED SOLUTION FOR SHIPPING PRIMARY HUMAN PROXIMAL TUBULE CELL MONOLAYERS BETWEEN LABORATORIES

Lucy Gentles, Newcells Biotech, Newcastle Upon Tyne, United Kingdom (+44), United Kingdom

P92 - EFFECT OF DRUGS THAT CAUSE CHOLESTATIC DRUG-INDUCED LIVER INJURY ON BILE ACID TRANSPORT AND METABOLISM

Thomas Kralj, BioIVT, Santa Clara, California, United States

P93 - CHARACTERIZATION OF XENOBIOTIC DISPOSITION POTENTIAL OF PLACENTAL CELL LINES (JEG-3, JAR, BEWO, AND HTR-8/SVNEO) AND PLACENTAL TISSUE THROUGH QUANTITATIVE GLOBAL PROTEOMICS

Laken Kruger, Washington State University, Spokane, Washington, United States

P94 - DEVELOPMENT OF A HIGH-THROUGHPUT TIME DEPENDENT INHIBITION OF CYP450 ASSAY IN CRYOPRESERVED HUMAN HEPATOCYTES

Sravani Adusumalli, Cyprotex, Watertown, Massachusetts, United States

P95 - CYTOTOXIC REACTIVE METABOLITE ASSAY WITH PERMEABILIZED CRYOPRESERVED HUMAN HEPATOCYTES FOR THE IDENTIFICATION OF DRUG CANDIDATES WITH POTENTIAL TO CAUSE IDIOSYNCRATIC DRUG-INDUCED LIVER INJURIES

Albert Li, Discovery Life Sciences, Columbia, Maryland, United States

P97 - METHODS FOR SEMI-AUTOMATING THE CYTOCHROME P450 INHIBITION CONSTANT (KI) ASSAY IN 384-FORMAT

Cody Parker, Mirati Therapeutics, San Diego, California, United States

P99 - CHARACTERIZATION OF CLEARANCE MECHANISMS IN AN ALL-HUMAN CELL BASED TRI-CULTURE SYSTEM

Mitchell Taub, Boehringer Ingelheim Pharmaceuticals, Ridgefield, Connecticut, United States

P100 - BULK AND SINGLE CELL PROTEOMICS REVEAL CONVERGENT RESPONSES TO HEPATOTOXIC DRUGS EFAVIRENZ, NEVIRAPINE, AND ACETAMINOPHEN IN HUMAN HEPATOCYTES

Yuting Yuan, Johns Hopkins University, Baltimore, Maryland, United States

KIDNEY (P101)

P101 - SYNERGISTIC EFFECTS OF OCHRATOXIN A AND HEAT STRESS IN A KIDNEY MICROPHYSIOLOGICAL SYSTEM

Jade Yang, University of Washington, Seattle, Washington, United States

METABOLISM (P104-P129)

P104 - "MIST" STUDIES: A COMPARISON OF METHODOLOGIES FOR EARLY DETECTION OF DISPROPORTIONATE HUMAN METABOLITES

Eleanor Barton, Pharmaron UK Ltd., Rushden, Northamptonshire, United Kingdom

P105 - EXAMINING THE NEPHROTOXICITY INDUCED BY BENZALKONIUM CHLORIDES IN 2D AND 3D-CULTURED HUMAN PROXIMAL TUBULE EPITHELIAL CELLS

Marie Brzoska, University of Washington, Seattle, Washington, United States

P106 - METABOLITE ELUCIDATION USING TIER ONE DATA (MET-OD)

Elias Carvalho Padilha, National Center for Advancing Translational Sciences (NCATS), North Bethesda, Maryland, United States

P107 - METABOLIC PATHWAYS OF ICLEPERTIN: CLINICAL INSIGHT FROM PRECLINICAL DATA

Tom Chan, Boehringer Ingelheim Pharmaceuticals Inc., Ridgefield, Connecticut, United States

P108 - IDENTIFICATION, SEMIQUANTITATION, STRUCTURE ELUCIDATION, AND REACTION PHENOTYPING OF A MAJOR CIRCULATING METABOLITE IN HUMANS ADMINISTERED WITH BMS-863233

Weiqi Chen, BMS, Princeton, New Jersey, United States

P109 - HEPATIC GLUCURONIDATION AND BIOACTIVATION RESISTANCE OF THE NATURAL PRODUCT QUEBECOL IN HUMAN AND RAT LIVER MICROSOMES

Gabriel Dalio Bernardes da Silva, University of Saskatchewan, Saskatoon, Saskatchewan, Canada

P110 - SALMON GILL EPITHELIAL CELL MODEL FOR XENOBIOTIC METABOLISM

Christiane Fæste, Norwegian Veterinary Institute, Norway

P111 - DETERMINATION OF ACYL-, O-, AND N-GLUCURONIDE USING CHEMICAL DERIVATIZATION COUPLED WITH LIQUID CHROMATOGRAPHY – HIGH RESOLUTION MASS SPECTROMETRY

Yukuang Guo, Takeda, Boston, Massachusetts, United States

P112 - DAPL1 AFFECTS PERINATAL MOUSE SENSITIVITY TO MATERNAL TCDD EXPOSURE: COMPARATIVE STUDY USING HOMOZYGOUS FETUSES FROM DAPL1 HETEROZYGOUS DAM

Yuji Ishii, Graduate School of Pharmaceutical Sciences, Kyushu University, Fukuoka, Japan

P113 - ASSESSING THE IMPACT OF BENZALKONIUM CHLORIDES ON GUT MICROBIOME AND LIVER METABOLISM

Vanessa Lopez, University of Washington, Seattle, Washington, United States

P114 - MECHANISTIC ANALYSIS OF OCHRATOXIN-A NEPHROTOXICITY

Anish Mahadeo, University of Washington, Seattle, Washington, United States

P115 - PREDICTING REACTIVITY TO DRUG METABOLISM: BEYOND CYP5

Mario Öeren, Optibrium, Cambridge, Cambridgeshire, United Kingdom

P116 - ADAGRASIB METABOLISM AFTER SINGLE AND MULTIPLE ORAL DOSING IN HUMANS

Lisa Rahbaek, Mirati Therapeutics, San Diego, California, United States

P117 - OXIDIZED METABOLITES AND UNUSUAL CONJUGATES OF AZD9496 BY MICROBIAL BIOTRANSFORMATION

Julia Shanu-Wilson, Hypha Discovery, Abingdon, Oxfordshire, United Kingdom

P118 - ACYL MIGRATION AND STABILITY OF THC-COOH-GLUCURONIDE IN BIOLOGICAL MATRICES

Keiann Simon, University of Washington, Seattle, Washington, United States

P119 - LC-MS METHOD FOR DETECTION OF 1ST, 2ND AND 3RD GENERATION OLIGONUCLEOTIDE THERAPEUTICS IN LIVER AND KIDNEY HOMOGENATE SAMPLES FOR METABOLISM STUDIES

Irina Slobodchikova, Alliance Pharma, Malvern, Pennsylvania, United States

P120 - ROLE OF MIR-7-5P IN MITOCHONDRIAL METABOLISM

Gavin Traber, University of California, Davis - School of Medicine, Sacramento, California, United States

P121 - NOVEL BIOENGINEERED MIR-1291 MODULATES XENOBIOTIC NUTRIENT TRANSPORTERS AND METABOLIC ENZYMES TO CONTROL CELL METABOLISM

Meijuan Tu, UC Davis, Sacramento, California, United States

P122 - METABOLITE IDENTIFICATION BY INTEGRATION OF DATA ACQUISITION, DIFFERENTIAL MASS SPECTROMETRY, AND DATA PROCESSING TECHNIQUES: APPLICATION TO GLUCAGON-LIKE PEPTIDE-1 (GLP-1) METABOLITE DETECTION AND IDENTIFICATION

Pengcheng Wang, Novartis Institutes for Biomedical Research, Inc, Cambridge, Massachusetts, United States

P123 - CHARACTERIZATION OF THE METABOLIC PATHWAYS OF DEUCRAVACITINIB (BMS-986165)

Ming Yao, Bristol-Myers Squibb Co, Princeton, New Jersey, United States

P124 - METABOLITE IDENTIFICATION, CATABOLISM AND COMPOUND DEGRADATION STUDIES FOR ANY MOLECULE SIZE AND HRMS DATA SOURCE

Ismael Zamora, Lead Molecular Design, S.L., Sant Cugat del Vallés, Barcelona, Spain

P125 - AUTOMATIC QUANTIFICATION WORKFLOW USING HIGH RESOLUTION MASS SPECTROMETRY

Ismael Zamora, Lead Molecular Design, S.L., Sant Cugat del Vallés, Barcelona, Spain

P126 - COMPARISON OF CID AND EAD FRAGMENTATION WITH AUTOMATED ASSIGNMENT FOR SMALL MOLECULE STRUCTURE ELUCIDATION

Ismael Zamora, Lead Molecular Design, S.L., Sant Cugat del Vallés, Barcelona, Spain

P127 - IN VITRO METABOLITE PROFILING COMPARISON OF RADIOACTIVE 14C-LABELED MYCLOBUTANIL, TRICYCLAZOLE, OXYFLUORFEN, PRONAMIDE, BIPHENYL, AND BUTOXYETHYLBENZOATE IN RAT LIVER MICROSOMES AND RAT LIVER METMAXTM HEPATOCYTES

Fagen Zhang, The Dow Chemical Company, Midland, Michigan, United States

P128 - COMBINING PRODUCT ION FILTERING, 2-PYRIDINE CARBOXALDEHYDE-TAGGING, AND BACKGROUND SUBTRACTION FOR STUDYING MACROCYCLIC PEPTIDE METABOLISM AND SOFTSPOTS

Haiying Zhang, Bristol-Myers Squibb, Princeton, New Jersey, United States

P129 - NOVEL N+-METHYLATION OF TASELISB (GDC-0032): STRUCTURAL CHARACTERIZATION AND REACTION PHENOTYPING

Weiping Zhao, Genentech, South San Francisco, California, United States

NON-P450 PHASE 1 ENZYMES (P131)**P131 - BLOCKING ALDEHYDE OXIDASE METABOLISM TO MITIGATE TOX FINDINGS**

Justin Ly, Genentech, South San Francisco, California, United States

OLIGONUCLEOTIDE (P132)**P132 - IN VITRO-IN VIVO METABOLITE PROFILING AND IDENTIFICATION OF OLIGONUCLEOTIDE**

Gengyao Qin, WuXi AppTec Co. Ltd., Shanghai, China

PHARMACOGENETICS (P134-P136)**P134 - FREQUENCY OF THE I/D VARIANT IN THE ACE1 GENE AMONG THE CIRCASSIAN SUBPOPULATION IN JORDAN**

Nancy Hakooz, School of Pharmacy-University of Jordan, Amman, Jordan

P135 - METABOLIC EFFECTS OF PERFLUOROCTANE SULFATE IN MULTIPLE ORGANS OF RATS USING NUCLEAR MAGNETIC RESONANCE-BASED METABOLOMICS

Ching-yu Lin, National Taiwan University, Taipei, Taiwan

P136 - CYP4F2*3 (V433M) POLYMORPHISM IMPACTS BENZALKONIUM CHLORIDE METABOLISM IN AN ALKYL CHAIN LENGTH-DEPENDENT MANNER

Linxi Zhu, University of Washington, Seattle, Washington, United States

PHARMACOKINETICS AND PHARMACODYNAMICS (P137-P144, P184)**P137 - A NOVEL THREE-DIMENSIONAL IMAGING AND ASSESSMENT OF THE NEW ZEALAND WHITE RABBIT EYE**
*Gianna Ferron, TissueVision Inc., Newton, Massachusetts, United States***P138 - NOVEL WHOLE-BRAIN SERIAL TWO-PHOTON PLUS AND MALDI-IHC IMAGING OF AMYLOID-BETA PLAQUE DYNAMICS IN PRE-CLINICAL ALZHEIMER'S DISEASE ANIMAL MODELS**

Gianna Ferron, TissueVision Inc., Newton, Massachusetts, United States

P139 - ANTIBACTERIAL EFFICACY OF THE MACROCYCLIC DEPSIPEPTIDE TEIXOBACTIN IN THE NEUTROPENIC MOUSE PK-PD MODEL OF THIGH INFECTION

Peng Hsiao, Ferring Research Institute Inc., San Diego, California, United States

P140 - EFFECT OF FOOD ON PHARMACOKINETICS AND PHARMACODYNAMICS OF HIP1601, A DUAL DELAYED-RELEASE FORMULATION OF ESOMEPRAZOLE, IN HEALTHY SUBJECTS

Sejung Hwang, Seoul National University College of Medicine, Seoul, South Korea

P141 - TOXICOKINETICS OF ORALLY MICRO-DOSED [14C]-BENZO[A]PYRENE FOLLOWING DIETARY INTERVENTION WITH BRUSSELS SPROUTS AND 3,3'-DIINDOLYLMETHANE (DIM) SUPPLEMENTS USING UPLC-ACCELERATOR MASS SPECTROMETRY (UPLC-AMS)

Monica Maier, Oregon State University, Corvallis, Oregon, United States

P142 - PROTEOMIC QUANTIFICATION OF RECEPTOR TYROSINE KINASES INVOLVED IN CANCER DEVELOPMENT AND PROGRESSION IN PATIENTS WITH COLORECTAL CANCER LIVER METASTASIS

Zubida Al-majdoub, The University of Manchester, Manchester, United Kingdom

P143 - DEVELOPMENT OF AN IN VIVO MODEL TO STUDY ACQUISITION OF ANTIBIOTIC RESISTANCE USING A CLINICALLY RELEVANT DOSING STRATEGY AND "HUMANIZED" ANTIMICROBIAL EXPOSURES

Noelle Williams, UT Southwestern Medical Center, Dallas, Texas, United States

P144 - DETERMINING EFFECT OF ISOTRETINOIN ON CYP2D6 AND CYP3A4 ACTIVITY IN PATIENTS WITH SEVERE ACNE

Yuqian Zhao, University of Washington, Seattle, United States

P184 - CHARACTERIZATION OF NONCLINICAL DRUG METABOLISM AND PHARMACOKINETIC PROPERTIES SHOWS CONSISTENCY AMONG THREE PHOSPHORODIAMIDATE MORPHOLINO OLIGONUCLEOTIDES FDA-APPROVED FOR DUCHENNE MUSCULAR DYSTROPHY

Marie Claire Mukashyaka, Sarepta Therapeutics, Inc., Cambridge, Massachusetts, United States

PHARMACOKINETIC MODELING (P145-P148)**P145 - PARENT-METABOLITE PHARMACOKINETIC MODELING, TISSUE DISTRIBUTION, AND BIOTRANSFORMATION STUDIES OF NOVEL EDARAVONE ORAL PRODRUG**

Seok-jin Cho, CHA University, Seongnam-si, Gyeonggi-do, South Korea

P146 - NONLINEAR MIXED-EFFECTS MODELLING TO REVISIT ETHANOL PHARMACOKINETICS

Uwe Fuhr, University of Cologne, Faculty of Medicine and University Hospital Cologne, Cologne, Northrhine-Westfalia, Germany

P147 - CHARACTERIZATION OF TRANSPORTER-MEDIATED DISPOSITION OF HEPATOBILIARY IMAGING AGENTS IN ISOLATED PERFUSED RAT LIVERS USING A MULTI-COMPARTMENT PHARMACOKINETIC MODEL

Angela Jeong, University of North Carolina, Chapel Hill, Chapel Hill, North Carolina, United States

P148 - POPULATION PHARMACOKINETICS OF CEFEPIME IN CRITICALLY ILL ADULT PATIENTS WITH HOSPITAL-ACQUIRED OR VENTILATOR-ASSOCIATED PNEUMONIA

Dong-Hwan Lee, Hallym University Sacred Heart Hospital, Anyang, Gyeonggi-do, South Korea

PHARMACOKINETIC PREDICTION (P149)**P149 - THE STRATEGY FOR EFFICACY EVALUATION OF THE MESENCHYMAL STEM CELL THERAPEUTICS: PHARMACOKINETIC STUDY OF ADJUVANT CHEMOTHERAPY IN RECURRENT GLIOBLASTOMA PATIENTS**

Young Bean Hong, College of Pharmacy, CHA University, Seongnam-si, Gyeonggi-do, South Korea

PHYSIOLOGICALLY-BASED PHARMACOKINETIC (PBPK) (P150-P170)**P150 - PBPK SIMULATION-BASED EVALUATION OF ISONIAZID DISPOSITION IN PREGNANCY FOR NAT-2 FAST AND SLOW ACETYLATORS**

Ogochukwu Amaeze, University of Washington, Seattle, Washington, United States

P151 - APPLICATION OF PBPK MODELING TO ASSESS PUR1900, AN INHALED FORMULATION OF ITRACONAZOLE, AS AN INHIBITOR OF CYP3A4 METABOLISM

Mackenzie Bergagnini-Kolev, Certara, Duvall, Washington, United States

P152 - COMPARATIVE ANALYSIS OF SHORT-CHAIN AND LONG-CHAIN PER- AND POLYFLUOROALKYL SUBSTANCES USING PHYSIOLOGICALLY-BASED TOXICOKINETIC MODELLING

James Chun Yip Chan, Agency for Science, Technology and Research, Singapore, Singapore

P153 - DELINEATING THE COMPLEX INTERPLAY OF ENZYMES AND TRANSPORTERS IN GOVERNING THE ABSORPTION AND DISPOSITION OF ATORVASTATIN AND THE METABOLITES USING PHYSIOLOGICALLY BASED PHARMACOKINETIC (PBPK) MODELING

Revathi Cha, Simulations Plus, Millcreek, Pennsylvania, United States

P154 - EVALUATING THE UTILITY OF TAPE STRIPPING DATA IN THE QUANTITATIVE DERIVATION OF PARTITION COEFFICIENTS CRITICAL FOR DERMAL PBPK MODEL DEVELOPMENT

Jing Yi Eleanor Cheong, Agency for Science, Technology and Research Singapore, Singapore, Singapore

P155 - MECHANISTIC UNDERSTANDING OF TRANSPORTER-DEPENDENT DISPOSITION OF PERFLUOROCTANESULFONIC ACID USING PHYSIOLOGICALLY-BASED TOXICOKINETIC MODELLING

SHENG YUAN CHIN, Agency for Science, Technology and Research (A*STAR), Singapore, Singapore

P156 - PHYSIOLOGICALLY BASED PHARMACOKINETIC MODELLING APPROACHES FOR GENDER-SPECIFIC RISK ASSESSMENT OF N-NITROSODIMETHYLAMINE (NDMA)

Seok-jin Cho, CHA University, Seongnam-si, Gyeonggi-do, South Korea

P157 - DEVELOPMENT OF A PHYSIOLOGICALLY-BASED PHARMACOKINETIC MODEL FOR PRACINOSTAT IN GASTROPLUS

Jeff Clarine, Mirati Therapeutics Inc., San Diego, California, United States

P159 - PREDICTING DELTA-9-TETRAHYDROCANNABINOL (THC) SYSTEMIC EXPOSURE AND RESPONSE IN HUMANS FOLLOWING DIFFERENT ROUTES OF CANNABIS PRODUCTS ADMINISTRATION USING PARENT-METABOLITE PBPK/PD MODELING

Mayur K. Ladumor, University of Washington, Seattle, Washington, United States

P160 - PHYSIOLOGICALLY BASED PHARMACOKINETIC MODELING AND SIMULATION FOR FEXUPRAZAN IN HUMAN

Kyeong-Ryoon Lee, Korea Research Institute of Bioscience and Biotechnology, Cheongju-Si, Chungbuk, South Korea

P161 - THE USEFULNESS OF A PHYSIOLOGICALLY-BASED PHARMACOKINETICS (PBPK) MODEL DEVELOPED IN MONKEY IN THE PREDICTION OF HUMAN PHARMACOKINETICS IN LIVER IMPAIRMENT POPULATION AND DRUG-DRUG INTERACTIONS

Xiaomin Liang, Gilead, Foster City, California, United States

P162 - SATURABLE RENAL REABSORPTION OF PERFLUOROCTANOIC ACID PROVIDES A UNIFIED EXPLANATION FOR ITS DIVERGENT HALF-LIVES IN HIGH AND LOW EXPOSURE SETTINGS

Jieying Lin, A*STAR Skin Research Labs, Singapore, Singapore

P163 - A SATURABLE PLASMA PROTEIN BINDING MODEL FROM IN VITRO DATA CAN PREDICT NONLINEAR PHARMACOKINETICS IN A PBPK MODEL

Louis Lin, University of British Columbia, Vancouver, British Columbia, Canada

P164 - PH-DEPENDENT STABILITY OF SIMVASTATIN: PHYSIOLOGICALLY-BASED PHARMACOKINETIC MODELING OF SIMVASTATIN AND SIMVASTATIN ACID PHARMACOKINETICS, DRUG INTERACTIONS AND FOOD EFFECT

Bridget Morse, Eli Lilly, Indianapolis, Indiana, United States

P165 - ELUCIDATING MECHANISMS UNDERLYING A PHARMACOKINETIC NATURAL PRODUCT-DRUG INTERACTION USING A MODELING AND SIMULATION APPROACH

James Nguyen, Washington State University, Spokane, Washington, United States

P166 - PROTEOMIC CHARACTERIZATION OF CLINICALLY RELEVANT DRUG-METABOLIZING ENZYMES AND TRANSPORTERS IN THE LIVER AND DIFFERENT INTESTINAL SECTIONS OF SPRAGUE DAWLEY RAT FOR APPLICATIONS IN PBPK MODELING

Sheena Sharma, Washington State University, Spokane, Washington, United States

P167 - A PHYSIOLOGICALLY-BASED PHARMACOKINETIC MODEL FOR HYDROXYCHLOROQUINE AND DESETHYLHYDROXYCHLOROQUINE IN HEALTHY AND COVID-19 POPULATIONS

Claire Steinbronn, University of Washington, Seattle, Washington, United States

P168 - PREDICTING HUMAN PHARMACOKINETICS BY USING EX VIVO MODELS AND PBPK MODELING; DEMONSTRATOR STUDY USING ROSUVASTATIN AND DIGOXIN

Lianne Stevens, Leiden University Medical Center, Leiden, Netherlands

P169 - PHYSIOLOGICALLY BASED PHARMACOKINETIC MODELS FOR KRATOM, A BOTANICAL WITH OPIOID-LIKE EFFECTS, AND KRATOM-DRUG INTERACTIONS MEDIATED BY CYP3A AND CYP2D6

Rakshit Tanna, Washington State University, Spokane, Washington, United States

P170 - DEVELOPMENT OF REPRESENTATIVE SENSITIVE CYP2C8 SUBSTRATE AND MODERATE CYP2C8 INHIBITOR PBPK MODELS TO SUPPORT LABELING RECOMMENDATIONS FOR TUCATINIB

Ian Templeton, Certara UK Ltd., Simcyp Division, Seattle, Washington, United States

PROTEIN BINDING (P171)

P171 - SPECIES-DEPENDENT ALPHA 1-ACID GLYCOPROTEIN BINDING AND THE IMPACT ON PLASMA PROTEIN BINDING OF PF-07321332 (NIRMATRELVIR), AN ORALLY BIOAVAILABLE SARS-COV-2 3CL PROTEASE INHIBITOR

Heather Eng, Pfizer, Groton, Connecticut, United States

PROTEOMICS (P172)

P172 - ANALYSIS OF RETINOL BINDING PROTEIN 4 (RBP4) AND TRANSTHYRETIN (TTR) IN PLASMA BY QUANTITATIVE LC-MS/MS: INSIGHTS INTO PLASMA PROTEOMICS

Aprajita S. Yadav, University of Washington, Seattle, Washington, United States

RADIOLABEL (P173)

P173 - RADIOLABEL IS NECESSARY TO UNCOVER NONINTUITIVE METABOLITES OF BIIB104: NOVEL RELEASE OF [14C]NITRILE FROM THIOPHENE AND SUBSEQUENT FORMATION OF [14C]THIOCYANATE

Chungang (Chuck) Gu, Biogen, Cambridge, Massachusetts, United States

TOXICITY (P175)

P175 - VERIFICATION OF THE "CARBONYL STRESS" HYPOTHESIS IN A YEAST MODEL OF REACTIVE ENDOGENOUS ELECTROPHILE TOXICITY

Philip Burcham, University of Western Australia, Crawley, WA, Australia

TRANSPORTERS (P176-P196)

P176 - HEPATIC UPTAKE TRANSPORT MECHANISMS OF HIF PROLYL-HYDROXYLASE INHIBITORS (DUSTATS)

Yi-An Bi, Pfizer Inc, Groton, Connecticut, United States

P177 - STRUCTURE, SUBSTRATE RECOGNITION AND INHIBITOR BINDING OF ORGANIC CATION TRANSPORTER 1 (SLC22A1)

Tongyi Dou, NHLBI/NIH, Bethesda, Maryland, United States

P178 - PROTEIN ABUNDANCE OF DRUG TRANSPORTERS IN HUMAN HEPATITIS C LIVERS

Marek Drozdzyk, Pomeranian Medical University, Szczecin, Poland

P179 - CHARACTERIZATION OF THE TRANSPORTER-MEDIATED UPTAKE OF THE EXPERIMENTAL MALE CONTRACEPTIVE H2-GAMENDAZOLE

Raymond Hau, University of Arizona, Tucson, Arizona, United States

P180 - PREDICTION OF DRUG-INDUCED LIVER TOXICITY USING RATIO OF PLASMA CMAX TO IC50 FOR BSEP INHIBITION

Kan He, Frontage Laboratories, Inc., Princeton, New Jersey, United States

P181 - PREDICTION OF DRUG-INDUCED LIVER TOXICITY USING RATIO OF PLASMA CMAX TO MDR3 IC50

Kan He, Frontage Laboratories, Inc., Princeton, New Jersey, United States

P182 - EVALUATION OF REMDESIVIR AS A POTENTIAL SUBSTRATE OF OATP1B1, P-GP, MRP1, AND MRP2 *IN VITRO*

Jae-Gook Shin, Inje University College of Medicine, Busan, South Korea

P183 - INFLUENCE OF KNOCKOUT AND HUMANIZATION OF SLCO2B1 ON ATORVASTATIN DISPOSITION IN RATS

Jonny Kinzi, University of Basel, Basel, Basel-Town, Switzerland

P185 - WHY IS THE SYSTEMIC EXPOSURE OF DUAL CYP3A AND OATP SUBSTRATES GREATLY AFFECTED IN HEPATIC IMPAIRMENT? INSIGHTS FROM THE EXTENDED CLEARANCE MODEL

Mayur K. Ladumor, University of Washington, Seattle, Washington, United States

P187 - QUANTITATIVE EXPRESSION OF LIPID AND NUCLEOSIDE TRANSPORTERS IN LUNG TISSUES FROM HUMAN, RAT, DOG AND CYNOMOLGUS MONKEY

Congrong Niu, Gilead Sciences, Foster City, California, United States

P188 - PROTEIN-MEDIATED UPTAKE EFFECT ON THREE INTESTINAL UPTAKE TRANSPORTERS SHOWS SUBSTRATE AND PH-DEPENDENT INTERACTIONS

Md Masud Parvez, Abbvie Biotherapeutics, South San Francisco, California, United States

P189 - EVIDENCE OF ALBUMIN-MEDIATED UPTAKE PHENOMENON WITH RENAL ORGANIC ANION TRANSPORTER 1

Shawn Pei Feng Tan, University of Manchester, Manchester, England, United Kingdom

P190 - RAT AS A MODEL FOR PREDICTING HUMAN RENAL ORGANIC ANION TRANSPORTER-MEDIATED DRUG-DRUG INTERACTIONS

Aarzo Thakur, Washington State University, Spokane, Washington, United States

P191 - IDENTIFICATION OF PUTATIVE ORGANIC ANION TRANSPORTER 2 INHIBITORS: SCREENING, STRUCTURE-BASED ANALYSIS AND CLINICAL DRUG INTERACTION RISK ASSESSMENT

Manthena Varma, Pfizer, Groton, Connecticut, United States

P192 - EVALUATION OF THE TRANSWELL SYSTEM AS A NEW TOOL TO PREDICT ORGANIC CATION TRANSPORTER 2 (OCT2) AND MULTIDRUG AND TOXIN EXTRUSION PROTEINS (MATES) MEDIATED RENAL DDI

Leticia S. Vieira, University of Washington, Seattle, Washington, United States

P193 - DRUG-DRUG INTERACTION POTENTIAL OF PHARMACEUTICAL EXCIPIENTS ON UPTAKE AND EFFLUX TRANSPORTERS

Mark Warren, BioIVT, Santa Clara, California, United States

P194 - BIOENGINEERING MICRORNAs TO MODULATE SOLUTE CARRIER TRANSPORTERS AND XENOBIOTIC TRANSPORT

Colleen Yi, UC Davis, Sacramento, California, United States

P195 - IS THE PROTEIN-MEDIATED UPTAKE OF STATINS BY HEPATOCYTES AN EXPERIMENTAL ARTIFACT?

Mengyue Yin, University of Washington, Seattle, Washington, United States

A1 - FLEXIBILITY OF THE F-F' LOOP, CRUCIAL FOR SUBSTRATE ACCESS TO THE CYP3A4 ACTIVE SITE, IS REDUCED UPON ALLOSTERIC INHIBITION: A NOVEL MECHANISM TO RATIONALIZE PROBE SUBSTRATE DEPENDENCIES IN K_i**Lloyd Wei Tat Tang**¹, Wan Wei², J. Ravi Kumar Verma², Hao Fan², and Eric Chun Yong Chan¹¹National University of Singapore, Singapore and ²Bioinformatics Institute, Singapore

In vitro cytochrome P450 (P450) drug inhibition assays typically rely on a P450 isoform-selective probe substrate for the quantitative determination of its inhibition kinetic constant (K_i). While these kinetic constants were classically regarded as intrinsic features of the inhibitor and were thought to be independent of the surrogate probe substrate utilized, there is now growing consensus that such reductionistic assumptions are only valid when both the probe substrate and inhibitor are competing for access to the same binding site on the P450 enzyme. Beyond this, the exact biochemical basis for probe substrate-dependencies in K_i remain largely obfuscated. Consequently, the purpose of our study was to elucidate plausible structural determinants underpinning these atypical observations. *In vitro* steady-state enzymatic inhibition assays conducted using human recombinant CYP3A4 enzymes and the FDA-recommended probe testosterone revealed that the fibroblast growth factor receptors (FGFR) inhibitors erdafitinib and pemigatinib noncompetitively inhibited CYP3A4 with apparent K_i values of 10.2 ± 1.1 μM and 3.3 ± 0.9 μM respectively. Remarkably, when rivaroxaban was adopted as the probe substrate in these assays there was a 2.0- and 3.2-fold decrease in its apparent K_i values to 5.1 ± 0.5 μM and 1.0 ± 0.1 μM respectively, thereby suggesting that the noncompetitive inhibition of CYP3A4 by both FGFR inhibitors exhibited probe substrate-dependency. In order to glean mechanistic insights into this observed phenomenon, erdafitinib and pemigatinib were first docked to the allosteric site in CYP3A4. Following which, molecular dynamics (MD) simulations of apo- and holo (erdafitinib- and pemigatinib-bound) CYP3A4 were conducted to investigate the structural changes induced. Comparative structural analyses of representative MD frames extracted by hierarchical clustering revealed that the allosteric inhibition of CYP3A4 by erdafitinib and pemigatinib did not substantially modulate its active site characteristics (i.e., cavity volume and shape). In contrast, we discovered that allosteric binding of the FGFR inhibitors reduces the structural flexibility of the F-F' loop region. As the F-F' loop is oriented directly above the active site and functions as an important gating mechanism to regulate substrate access to the catalytic heme, we surmised that the increased rigidity of the F-F' loop engenders a more constrained entrance to the CYP3A4 active site, which in turn impedes access of the larger rivaroxaban molecule to a greater extent than testosterone and culminates in more potent inhibition of its CYP3A4-mediated metabolism. In conclusion, our findings provide a potentially novel mechanism to rationalize probe substrate-dependencies in K_i arising from the allosteric noncompetitive inhibition of CYP3A4. From a broader clinical perspective, our study also reiterates the importance of using a clinically relevant probe for pharmacokinetic drug-drug interaction studies due to probe substrate-dependent differences in K_i.

A2 - INFLAMMATION AND PREGNANCY ALTER ORGANIC ANION TRANSPORTERS 1/3 ACTIVITY EMPLOYING THE PROBE DRUG FUROSEMIDE IN WOMEN**Jhohann Richard Benzi**, Adriana Rocha, Matheus De Lucca Thomaz, Julia Colombari, Patricia Melli, Geraldo Duarte, and Vera Lanchote

University of Sao Paulo, Brazil

Even though the effect of inflammatory cytokines on CYP enzymes has been investigated *in vivo*, little is known about the impact of inflammation on drug transporter activity, especially during pregnancy. This study aimed to investigate the impact of inflammation (using pyelonephritis, a renal bacterial infection, as a model) in pregnant patients before and after treatment with antibiotics, as well as non-pregnant healthy volunteers employing furosemide (FUR), a loop diuretic probe drug for the OAT 1/3 activity *in vivo*. Pregnant patients diagnosed with pyelonephritis (n = 10 – phase 1) received a single oral dose of FUR 40 mg and were treated with intravenous doses of antibiotic cefuroxime. After at least one week after hospital discharge, pregnant patients (n = 7 – phase 2) were considered healthy and received another single oral dose of FUR 40 mg. Healthy non-pregnant women (n = 12) were recruited and received a single oral dose of FUR 40 mg. Blood and urine samples were collected up to 12h after FUR administration in all groups. A panel of 11 proinflammatory cytokines was evaluated in plasma samples. FUR and its major metabolite glucuronide were quantified in plasma and urine. PK analysis was accessed by non-compartmental analysis and expressed as a median. Phase 1 pregnant patients presented higher cytokines plasma concentration when compared to phase 2 pregnant patients for IL-6 (20.4 vs 0.21 pg/mL), IFN-γ (5.60 vs 0.92 pg/mL), IL-8 (5.01 vs 0.28 pg/mL) and CRP (18.7 vs 1.69 ng/mL). FUR PK parameters were similar in both phase 1 and phase 2 for AUC_{0-∞} (1255.76 vs 1110 ng*h/mL), C_{max} (315 vs 504 ng/mL), CL/F (32.0 vs 36.0 L/h), V_d/F (133 vs 215 L), F_u (0.96 vs 0.78 %). However, phase 1 pregnant women presented higher values of T_{max} (1.88 vs 1.00 h) and lower values of CL_r (5.32 vs 12.1 L/h), CL_{secretion} (5.26 vs 8.02 L/h), and a marginal difference on CL_{formation} (0.87 vs 2.57 L/h p-value = 0.07). Healthy non-pregnant women presented lower values of CL/F (19.7 L/h), V_d/F (55.9 L), F_u (0.18%) and CL_r (6.13 L/h) and higher values of AUC_{0-∞} (2025 ng*h/mL). Although the low number of individuals investigated, these results indicate that inflammation reduces OAT1/3 or UGT1A9 and UGT1A1 activities, whereas the pregnancy enhances these transporters' activity.

A3 - FLUCLOXACILLIN IS A WEAK INDUCER OF CYP3A4

Bitte Bork Iversen¹, Ann-Cathrine Dunvald¹, Erkka Järvinen¹, Daniel Jespersen², Flemming Nielsen¹, Kim Brøsen¹, Per Damkier³, Helen Hammer⁴, Oliver Pötz⁴, and Tore B. Stage¹

¹University of Southern Denmark, Denmark, ²Otterup Pharmacy, Denmark, ³Odense University Hospital, Denmark, and ⁴SignaTope GmbH, Germany

Flucloxacillin is a well-known, narrow spectrum, antibiotic used against *Staphylococcus aureus* (1). It is an agonist to Pregnane X Receptor (PXR), a nuclear receptor that regulates the expression of Cytochrome P450 (CYP) 3A4, CYP2C9, CYP2C19, and CYP2B6 (2,3). We performed an *in vitro* and an *in vivo* study, to assess if flucloxacillin induces CYP3A4, CYP2C9, CYP2C19, CYP2B6, CYP2D6, and CYP1A2. We conducted a randomized, two-phase, cross-over, clinical pharmacokinetic cocktail study. We included 14 healthy subjects and measured the impact of 10 and 28 days of flucloxacillin treatment on the pharmacokinetics of drugs from the previously validated Basel Cocktail to determine CYP enzyme activity (4). Additionally, we performed an *in vitro* study with 3D spheroids of primary human hepatocytes in two donors. We exposed hepatocytes to flucloxacillin for 4 days and measured the mRNA-expression using quantitative polymerase chain reaction (qPCR) and protein abundance using quantitative immunoaffinity Liquid Chromatography with Tandem Mass Spectrometry (LC-MS/MS).

Flucloxacillin reduced the area under the plasma concentration time-curve (AUC) from 0-72 h for midazolam (CYP3A4) after 10 days {geometric mean ratio [GMR] [95% confidence interval (CI)]: 0.70 [0.53-0.92]} and 28 days [GMR (95% CI): 0.73 (0.61-0.88)]. A similar trend was observed for the metabolic ratio of midazolam 2 hours after administration, [GMR 10 days (95% CI): 2.01 (1.11-3.65) and GMR 28 days (95% CI): 2.08 (1.02-4.25)]. Neither CYP2C9, CYP2C19, CYP2D6, CYP2B6, or CYP1A2 were induced after 10 or 28 days of treatment. Supporting the clinical study results, *in vitro* data show that flucloxacillin causes a dose-dependent induction of CYP3A4 mRNA- and protein expression with a maximal induction of 4- and 2.7-fold respectively within the tested concentration range (0-15-250 µM). This translational study demonstrates that flucloxacillin can be categorized as a weak/mild inducer of CYP3A4 according to the Food and Drug Administration (FDA) (5) and European Medicine Agency (EMA) (6). Caution should be taken when prescribing flucloxacillin for 10 and 28 days, especially for drugs with a narrow therapeutic interval.

References

1. Rayner C, Munckhof WJ. Antibiotics currently used in the treatment of infections caused by *Staphylococcus aureus*. *Intern Med J*. 2005 Dec;35 Suppl 2:S3-16.
2. Stage TB, Graff M, Wong S, Rasmussen LL, Nielsen F, Pottegård A, et al. Dicloxacillin induces CYP2C19, CYP2C9 and CYP3A4 *in vivo* and *in vitro*. *Br J Clin Pharmacol*. 2018;84(3):510–9.
3. Brewer CT, Chen T. PXR variants: the impact on drug metabolism and therapeutic responses. *Acta Pharm Sin B*. 2016 Sep;6(5):441–9.
4. Donzelli M, Derungs A, Serratore MG, Noppen C, Nezcic L, Krahenbuhl S, et al. The basel cocktail for simultaneous phenotyping of human cytochrome P450 isoforms in plasma, saliva and dried blood spots. *Clin Pharmacokinet*. 2014 Mar;53(3):271–82.
5. Clinical Drug Interaction Studies — Cytochrome P450 Enzyme- and Transporter-Mediated Drug Interactions. Guidance for Industry [Internet]. [cited 2022 Jun 15]. Available from: <https://www.fda.gov/media/134581/download>
6. Guideline on the investigation of drug interactions [Internet]. [cited 2022 Jun 15]. Available from: https://www.ema.europa.eu/en/documents/scientific-guideline/guideline-investigation-drug-interactions-revision-1_en.pdf

A4 - DICLOXACILLIN CAUSES DRUG-DRUG INTERACTIONS – TRANSLATING REAL-WORLD DATA TO BASIC PHARMACOLOGY

Ann-Cathrine Dalgård Dunvald¹, Erkka Järvinen¹, Helen Hammer², Oliver Pötz², Anton Pottegård¹, and Tore B. Stage¹

¹University of Southern Denmark, Denmark and ²SignaTope GmbH, Germany

Dicloxacillin is an inducer of CYP enzymes that causes drug-drug interactions (DDIs). This study aims to highlight the clinical importance of this DDI using a translational approach.

We conducted a self-controlled register-based cohort study using data from The Copenhagen Primary Care Laboratory Database (CopLab) from 2000 to 2015. The cohort included current warfarin users with two or more measures of International Normalized Ratio (INR) and a filled prescription for dicloxacillin. Warfarin is metabolized by CYP2C9 and CYP3A4, has a narrow therapeutic range, and is monitored frequently with INR, making it useful when assessing DDIs. We used active comparison with other antibiotics. To quantify the magnitude of the DDI, we conducted comprehensive *in vitro* studies using 3D spheroid primary human hepatocytes from two donors. We incubated cells with increasing doses of dicloxacillin and assessed mRNA expression and protein abundance of CYP3A4, CYP2C9, CYP2C8, CYP2C19, and CYP2B6 using quantitative Polymerase Chain Reaction (qPCR) and Liquid Chromatography with Tandem Mass Spectrometry (LC-MS/MS).

We identified 671 individuals receiving concomitant treatment with warfarin and dicloxacillin. Mean INR levels dropped from 2.50 to 1.84 within 1 to 3 weeks of initiating dicloxacillin, a mean decrease of -0.67 (95% CI -0.75; -0.59). In addition, two out of three individuals experienced INR levels below the therapeutic range (<2.0) within 1 to 3 weeks after initiating dicloxacillin, compared to 26% during a similar interval before dicloxacillin treatment ($p < 0.01$). Flucloxacillin, another isoxazolyl penicillin, caused a minor decrease in INR (mean INR difference -0.37 (95% CI -0.60; -0.14), while amoxicillin and phenoxymethylpenicillin showed no clinically relevant change in INR (mean INR difference 0.21 (95% CI 0.09; 0.32) and 0.07 (95% CI 0.00; 0.14), respectively). *In vitro* studies showed CYP enzyme induction by dicloxacillin in a dose-dependent manner. CYP2C9 and CYP3A4 mRNA expression increased by 1.7-fold and 5.1-fold compared to baseline. CYP2C9 and CYP3A4 protein expression increased by 1.3-fold and 3.0-fold, respectively. We conclude that treatment with dicloxacillin causes a clinically relevant decrease in INR among current warfarin users. This DDI is seemingly explained *in vitro* by induction of drug metabolism through an increased expression of CYP2C9 and CYP3A4 involved in warfarin metabolism. This translational approach highlights dicloxacillin as a potential perpetrator in CYP-mediated drug-drug interactions.

A5 - USING TARGETED MASS SPECTROMETRY-BASED PROTEOMICS TO IDENTIFY DRUG METABOLIZING ENZYMES IN THE BRAIN

Abigail Wheeler, Benjamin Orsburn, and Namandjé Bumpus
Johns Hopkins University, United States

UDP-glucuronosyltransferases (UGTs) are a family of drug metabolizing enzymes that add glucuronic acid to xenobiotics to make them more readily excretable. This reaction is the second most common in drug metabolism, with oxidation via cytochromes P450 (P450s) being the first. While UGTs are well characterized in the liver, there is far less known about the expression and activity of these enzymes in the brain. We used brain microsomes isolated from humans, cynomolgus macaques, and mice to test for glucuronidation of efavirenz, a non-nucleoside reverse transcriptase inhibitor used to treat HIV, and P450 dependent metabolites of EFV. This study showed the glucuronidation of metabolites 8-hydroxyefavirenz and 8,14-dihydroxyefavirenz in all three species. However, direct glucuronidation of EFV was noted only in the cynomolgus macaque brain microsomes, indicating that there may be species differences in UGT expression and activity in the brain. We hypothesized that we would be able to elucidate these differences by employing a targeted mass spectrometry-based proteomics approach to identify drug metabolizing enzymes, particularly UGTs, in brain microsomes. First, brain and liver microsomes from all three species were prepared via lysis, reduction, alkylation, and acidification. Proteins were linearized and subjected to suspension trapping to remove all other biomolecules. Peptides were obtained by tryptic digestion of the suspended proteins. To obtain the highest possible sample depth, the resulting peptides from the brain microsomes were separated into 8 fractions by high pH reversed phase chromatography. A targeted UGT detection method was developed by first running a data-dependent analysis on liver microsomes, which were also used as a positive control due to their high concentrations of drug metabolizing enzymes. For LCMS analysis, we used a state-of-the-art ZenoTOF 7600 instrument with zeno-trapping capabilities which can improve sensitivity up to 20-fold over traditional time-of-flight systems. From the untargeted data-dependent analysis, we identified unique peptides corresponding to UGT enzymes to create a target peptide list. Liver microsomes were then analyzed using these target peptide lists with and without scheduled ionization. Once the target list was iteratively narrowed to approximately 100 of the most LCMS compliant peptides, brain microsomes were analyzed. The UGTs identified in the brain microsomes were as follows: humans – UGT1A1, UGT1A4, UGT1A5, UGT1A6, UGT1A8, UGT1A9, UGT2A1, UGT2A2, UGT2B4, UGT2B17, and UGT2B28; cynomolgus macaques – UGT1A2, UGT1A7, UGT1A9, UGT1A10, UGT2A2, UGT2B9, and UGT2B20; and mice – Ugt1a9, Ugt2a3, Ugt2b17, Ugt3a1, and Ugt3a2. Interestingly, several peptides demonstrated higher intensities in the brain microsomes than in the liver microsomes. In the human microsomes, peptides corresponding to UGTs 1A5, 1A6, 2A2, and 2B17 were observed at higher concentrations in the brain than liver. For macaques, the more abundant peptides in the brain corresponded to UGTs 1A7 and 1A10. The only peptide noted to be more abundant in the mouse brain microsomes was derived from Ugtab17. The identification of these UGTs not only informs us on the potential glucuronidation of EFV in the brain, but is relevant to study of any brain-penetrant drugs that undergo UGT-mediated metabolism.

A6 - QUANTIFICATION OF ABSOLUTE COMPOSITIONS AND TOTAL ABUNDANCE OF HOMOLOGOUS PROTEINS IN HUMAN TISSUES USING CONSERVED-PLUS-SURROGATE PEPTIDE (CPSP) APPROACH: APPLICATION IN THE QUANTIFICATION OF UDP GLUCURONOSYLTRANSFERASES

Deepak Ahire¹, Mitesh Patel², Sujal Deshmukh², and Bhagwat Prasad¹

¹Washington State University, United States and ²Novartis Institutes for BioMedical Research, United States

Selective quantification of drug-metabolizing enzymes and transporter proteins (DMETs) using liquid chromatography-tandem mass spectrometry (LC-MS/MS)-based quantitative proteomics has been extensively utilized for mechanistic and translational studies during drug discovery and development. Targeted proteomics has emerged as an important technique for the quantification of drug-metabolizing enzymes and transporters in complex tissues and cells.

Characterization of absolute compositions and total abundance of homologous proteins, such as UDP glucuronosyltransferases (UGTs), is important for predicting the fractional contribution of individual isoforms (fm) involved in the metabolism of drug substrates as well as for applications in physiologically based pharmacokinetic (PBPK) modeling. Conventional targeted proteomics that utilizes surrogate peptides often results in high technical and inter-laboratory variability due to peptide-specific digestion efficiency leading to data inconsistencies. To address these issues, we developed a universal conserved plus surrogate peptide (CPSP) approach to determine the absolute compositions (relative distributions) of homologous DMETs and applied it to obtain absolute profiles of UGT1As and UGT2Bs in human liver microsomes (HLM), human intestinal microsomes (HIM), human kidney microsomes (HKM), and human liver S9 (HLS9) fractions. At first, we identified peptides that were conserved in multiple isoforms of UGT1As (IPQTVLWR) and UGT2Bs (VLWR). Then, the conserved peptides of UGT1s and UGT2Bs were used as calibrators for quantifying UGT protein abundance in the recombinant UGT systems (rUGT) samples. Finally, the standardized individual rUGTs were used as calibrators to determine UGT levels using surrogate peptides in the pooled HLM, HIM, HKM, and HLS9 fractions, which were then used to quantify the % abundance of individual UGT1As and UGT2Bs in each tissue. We determined that the % composition of UGT1A1:1A3:1A4:1A6:1A8:1A9 was 35:5:36:11:13, whereas UGT2B4:2B7:2B10:2B15:2B17 was 20:32:22:21:5 in the human liver. Similarly, the human kidney and intestine show unique compositions of UGT1As and UGT2Bs. The method was validated by assessing correlations of UGT compositions between HLM and HLS9 samples ($R^2 > 0.98$). The analysis of conserved peptides also provided the total abundance (pmol/mg protein) of UGT1As and UGT2Bs, i.e., 268.0 and 341.7 (HLM), 20.64 and 92.37 (HIM), 138.17 and 98.86 (HKM), which was comparable to the sum of individual UGT proteins quantified by surrogate peptide approach. In summary, the absolute compositions and total abundance data generated by the CPSP approach were successfully applied for the physiologically-based pharmacokinetic (PBPK) modeling of diclofenac in adults and children. The CPSP method developed for the quantification of UGT1As and UGT2Bs could be extended as a universal and cost-effective approach for quantification of absolute composition and total abundance of other clinically relevant DMETs.

A7 - *IN VIVO* EVALUATION OF CYTOCHROME P450-MEDIATED CANNABINOID-DRUG INTERACTIONS IN HEALTHY ADULT PARTICIPANTS

Sumit Bansal¹, C. Austin Zamarripa², Tory R. Spindle², Elise Weerts², Ryan Vandrey², Mary F. Paine³, and Jashvant D. Unadkat¹

¹University of Washington, United States, ²Johns Hopkins University School of Medicine, United States and ³Washington State University, United States

Increasing legalization and use of cannabis products have collectively increased the risk of adverse cannabis-drug interactions. Cannabidiol (CBD) and delta-9-tetrahydrocannabinol (THC), the most abundant cannabinoids in cannabis, are potent inhibitors of several cytochrome P450 (CYP) and UDP-glucuronosyltransferase (UGT) enzymes. Based on *in vitro-in vivo* extrapolation, oral CBD (700 mg) was predicted to precipitate pharmacokinetic interactions with drugs primarily metabolized by CYP1A2, CYP2C9, CYP2C19, CYP2D6, CYP3A, UGT1A9, UGT2B4, and UGT2B7. In contrast, oral THC (20 mg) was predicted to precipitate pharmacokinetic interactions with only drugs primarily metabolized by CYP2C9 and CYP3A. These predictions were evaluated in the current work by conducting an *in vivo* pharmacokinetic interaction study involving cannabis extracts containing THC or CBD+THC and five CYP probe drugs. Healthy adult participants (n=18) completed 3 experimental test sessions, in a randomized order, where they were administered a brownie containing 1) no cannabis (placebo), 2) cannabis extract with 20 mg THC but no CBD (THC) or 3) cannabis extract with 20 mg THC + 640 mg CBD (THC+CBD), each separated by at least one week. Thirty minutes after consuming the brownie, participants were administered an oral CYP probe drug cocktail consisting of caffeine (100 mg; CYP1A2), losartan (25 mg; CYP2C9), omeprazole (20 mg; CYP2C19), dextromethorphan (30 mg; CYP2D6), and midazolam (2 mg; CYP3A). Plasma and urine were collected to 24 hours after the cocktail administration. Probe drugs, THC, and their metabolites were quantified in plasma using UPLC-MS/MS. Plasma AUC was determined using noncompartmental analysis. Compared to THC, THC+CBD increased the geometric mean AUC ratio (AUCGMR) of THC and 11-OH-THC/THC AUCGMR by 2.7- and 3.8-fold, respectively and decreased the 11-COOH-THC glucuronide/11-COOH THC AUCGMR by 38% likely due to inhibition of CYP2C9-mediated THC metabolism to 11-OH-THC and sequential UGT-mediated metabolism of 11-OH-THC and 11-COOH THC. Consequently, as compared to THC alone, THC+CBD significantly increased the pharmacodynamic effects of THC (self-reported ratings of anxiety and sedation, heart rate, and impairment on a battery of cognitive performance tests). THC+CBD significantly inhibited CYP1A2, 2C9, and 2C19 activities, as evidenced by the increase in AUCGMR of caffeine, losartan, and omeprazole and a corresponding decrease in AUCGMR of paraxanthine/caffeine, losartan carboxylic acid/losartan, and 5-OH omeprazole/omeprazole (Table 1). THC+CBD modestly inhibited CYP3A activity (1.6-fold increase in midazolam AUCGMR). Unexpectedly, THC+CBD increased the AUCGMR of 1'-OH midazolam/midazolam by 1.8-fold (Table 1) and decreased 1'-OH midazolam glucuronide/1'-OH midazolam AUCGMR by 49%, likely due to inhibition of sequential UGT-mediated metabolism of 1'-OH midazolam. In contrast, THC had no effect on any of the CYP activities (except CYP2C9), and THC+CBD had no effect on CYP2D6 activity but appeared to inhibit the sequential metabolism of dextromethorphan, the metabolite of dextromethorphan. Urine samples will be analyzed to confirm these cannabinoid-mediated CYP- and UGT-

inhibition data by determining the formation clearances of the metabolites. These results can be used to guide dose adjustment of drugs co-consumed with cannabis products.

Table 1. Geometric mean ratio (GMR) of CYP probe drug plasma AUC or metabolite/probe drug plasma AUC in healthy adult participants (n=18) administered a brownie containing THC (20 mg) or THC+CBD (20 mg+640 mg) relative to a placebo brownie.				
CYP	Probe Drug	Endpoint	GMR (90% CI)	
			THC	THC+CBD
1A2	Caffeine	Caffeine AUC _{0-t} (ng.h/mL) ^a	0.98 (0.91–1.05)	1.27 (1.13–1.43)
		Paraxanthine/Caffeine AUC _{0-t} ratio ^a	0.97 (0.91–1.04)	0.60 (0.50–0.73)
2C9	Losartan	Losartan AUC _{0-t} (ng.h/mL) ^a	1.13 (1.02–1.25)	1.75 (1.58–1.94)
		Losartan carboxylic acid/Losartan AUC _{0-t} ratio ^a	1.02 (0.92–1.12)	0.70 (0.64–0.76)
2C19	Omeprazole	Omeprazole AUC _{0-t} (ng.h/mL) ^b	1.00 (0.71–1.42)	2.99 (2.16–4.14)
		5-Hydroxy omeprazole/Omeprazole AUC _{0-t} ratio ^b	0.97 (0.87–1.08)	0.47 (0.41–0.53)
2D6	Dextromethorphan	Dextromethorphan AUC _{0-t} (ng.h/mL)	1.22 (0.94–1.57)	1.22 (0.94–1.58)
		Dextrophan/Dextromethorphan AUC _{0-t} ratio	0.74 (0.62–0.88)	1.42 (1.15–1.76)
3A	Midazolam	Midazolam AUC _{0-t} (ng.h/mL) ^c	1.06 (0.96–1.16)	1.58 (1.39–1.78)
		1'-Hydroxymidazolam/Midazolam AUC _{0-t} ratio ^c	0.93 (0.81–1.07)	1.79 (1.57–2.04)

Bold values indicate significantly different from placebo brownie (90% CI does not include 1.00). AUC_{0-t}, area under the plasma concentration vs. time curve from time zero to 24 h except where samples fell below LLOQ, ^at=12 h (n=3); ^bt=12 h (n=12); ^ct=8 h (n=4); ^ct=12 h (n=5).

Supported by NIH grants U54 AT008909, P01 DA032507, and T32 DA007209.

A8 - STRUCTURAL AND MECHANISTIC INVESTIGATIONS OF COVALENTLY MODIFIED CYP ENZYMES VIA MASS SPECTROMETRIC ANALYSIS

Yuanyuan Shi¹, Matthew Cerny², and Rheem Totah¹

¹University of Washington, United States and ²Pfizer Inc, United States

Background: Due to their prominence in drug metabolism, cytochrome P450 (CYP) mediated drug-drug interactions are of primary concern. Currently employed approaches are limited to empirical screening of analogs in high/moderate throughput CYP inactivation assays with the aim of identifying analogs with reduced or insignificant inactivation potential. Such tactics are labor intensive, often unsuccessful, and provide at best kinetic data for inactivation. Failure to eliminate CYP inactivation can, in part, be explained by an incomplete understanding of the mechanistic underpinnings of CYPs inactivation. Therefore, we propose an approach to eliminate inactivation via mechanistic and structural understanding of CYP time-dependent inactivation using mass spectrometric (MS) analysis of adducted peptides of inactivated CYPs. Methods: Using reported inactivators eight CYPs (CYP2B6, CYP2C8, CYP2C9, CYP2C19, CYP2D6, CYP3A4, CYP3A5 and CYP2J2) were evaluated to identify adducted peptides. Following quenching of incubation mixtures and trypsin digestion, the resulting peptides were analyzed by an untargeted proteomics approach using nano liquid chromatography tandem mass spectrometry (nano LC-MS/MS). Various search algorithms software coupled with optimized criteria were applied to screen and identify the adducted proteolytic peptides. Results and Conclusions: We established a liquid chromatography-coupled with optimized mass spectrometry assays for proteolytic peptides for the eight CYPs. Using this approach, we consistently capture literature reported adducts as well as novel adducts. For example, with CYP3A4, 14 unique adducted protein sites were identified after screening 15 different known inactivators. Applying the same incubation conditions and LC-MS/MS method used for CYP3A4, we consistently identified adducted peptides that were reported in the literature for the remaining seven CYPs mentioned above in addition to several novel adducts. Structural insights drawn from the adducted peptides can provide medicinal chemists actionable data regarding the enzyme inactivation mechanisms, the nature of the peptide-bound adduct, and may provide avenues to enable more rapid implementation of avoidance strategies for time-dependent inactivators.

A9 - INDUCTION OF CYTOCHROME P450 ENZYMES AND DRUG TRANSPORTERS IN 3D SPHEROID CULTURE OF PRIMARY HUMAN HEPATOCYTES**Erkka Järvinen**¹, Helen Hammer², Oliver Pötz², Magnus Ingelman-Sundberg³, and Tore B. Stage¹¹University of Southern Denmark, Denmark, ²SIGNATOPE GmbH, Germany and ³Karolinska Institutet, Sweden

Primary human hepatocytes (PHH) are the gold standard *in vitro* tool to study regulation of drug metabolizing enzymes and transporters. PHHs are typically cultured as monolayer cultures, however, this culture format leads to dedifferentiation of hepatocytes and loss of hepatocyte phenotype within days. More advanced culture formats of PHHs, such as the 3D spheroid culture, have been shown to retain the hepatic phenotype for weeks. Importantly, the expression of drug-metabolizing cytochrome P450 enzymes (CYPs) and drug transporters are stable in the spheroid culture of PHHs for multiple weeks. In this work, we evaluated induction of important drug-metabolizing CYPs and drug transporters in three different donors of spheroid PHHs after four days treatment with various inducers. The evaluated enzymes and transporters included CYP1A2, CYP2B6, CYP2C8, CYP2C9, CYP2C19, CYP3A4, ABCB1, ABCC2 and SLCO1B1. Induction was measured at mRNA and protein levels by employing real-time polymerase chain reaction and quantitative liquid chromatography-mass spectrometry proteomics. Rifampicin increased expression of CYP3A4 mRNA by 5 to 7-fold and CYP3A4 protein by 4-fold. The mRNA of CYP2B6 was highly induced by rifampicin and phenobarbital and was 9-fold higher than in non-treated spheroids, while both compounds induced the protein expression of CYP2B6 by 2-fold at maximum. CYP1A2 was only induced by omeprazole and beta-naphthoflavone. Rifampicin induced ABCB1 and ABCC2 by 2-fold at mRNA levels, while protein levels were increased 2- and 1.3-fold for ABCB1 and ABCC2. None of the probe inducers induced mRNA levels of SLCO1B1. In conclusion, 3D spheroid culture of PHHs is suitable for studying induction of CYPs and drug transporters.

A10 - IBRUTINIB METABOLISM *IN VITRO* IS CORRELATED WITH INDIVIDUAL HEPATIC CYP3A ACTIVITY AND PROTEIN EXPRESSION AND PLASMA 4 β -HYDROXYCHOLESTEROL/CHOLESTEROL RATIO**Jonghwa Lee**, John Fallon, Phil Smith, and Klarissa Jackson

University of North Carolina at Chapel Hill, United States

Ibrutinib (1-[(3R)-3-[4-amin-3-(4-phenoxyphenyl)-1H-pyrazolo [3,4-d]pyrimidin-1-y1]-1-piperidinyl]-2-propen-1-one) is an orally administered Bruton's tyrosine kinase inhibitor approved for the treatment of various B-cell malignancies, including chronic lymphocytic leukemia and mantle cell lymphoma [1]. Ibrutinib is metabolized primarily by oxidation via CYP3A4/5 to M37 (the primary active metabolite), M34, and M25 [2]. Although ibrutinib is effective in treating patients, significant interindividual variability in pharmacokinetics and response has been reported, and managing ibrutinib treatment-associated toxicities remains an important clinical challenge [3]. Plasma concentrations of the circulating CYP3A-mediated cholesterol metabolite 4 β -hydroxycholesterol (4 β -HC), or the normalized 4 β -HC to total cholesterol ratio (plasma 4 β -HC/cholesterol ratio) have been suggested as possible endogenous biomarkers of CYP3A activity in clinical settings [4]. We hypothesized that plasma 4 β -HC/cholesterol ratio may be used to predict individual CYP3A activity and hepatic ibrutinib metabolism *in vitro*. The objectives of this study were to 1) assess the relationship between ibrutinib metabolite formation, CYP3A protein concentration, and CYP3A activity in single-donor primary human hepatocytes, and 2) evaluate the utility of plasma 4 β -HC/cholesterol ratio to predict individual ibrutinib metabolism in matched donors. Ibrutinib (5 μ M) was incubated with primary human hepatocytes from 15 individual donors (ages 1-63 years). Ibrutinib metabolites were measured by LC-MS/MS analysis. Formation of metabolites (M37, M34, and M25) varied widely between the donors. M37 and M25 formation was highly correlated with individual CYP3A activity (measured by midazolam 1'-hydroxylation) and CYP3A4 protein concentration (measured by quantitative targeted absolute proteomics). We also measured 4 β -HC and cholesterol concentrations in plasma samples from the same donors. M37, M34, and M25 formation in hepatocytes was significantly correlated with plasma 4 β -HC/cholesterol ratio in adult donors (Spearman correlation coefficients (r) for M37, M34, and M25 were 0.80, 0.78, and 0.83, respectively) when pediatric donors were excluded from the analysis. Collectively, these data indicate that ibrutinib metabolism is highly correlated with individual hepatic CYP3A activity and protein concentration in primary human hepatocytes as well as plasma 4 β -HC/cholesterol ratio from the same matched donors. To our knowledge, this is the first study to demonstrate a significant relationship between this endogenous CYP3A biomarker and CYP3A-mediated drug metabolism *in vitro*.

References:

1. Winer, E.S., R.R. Ingham, and J.J. Castillo, PCI-32765: a novel Bruton's tyrosine kinase inhibitor for the treatment of lymphoid malignancies. *Expert Opin Investig Drugs*, 2012. 21(3): p. 355-61.
2. Scheers, E., et al., Absorption, metabolism, and excretion of oral (1)(4)C radiolabeled ibrutinib: an open-label, phase I, single-dose study in healthy men. *Drug Metab Dispos*, 2015. 43(2): p. 289-97.
3. Eisenmann, E.D., et al., Intentional Modulation of Ibrutinib Pharmacokinetics through CYP3A Inhibition. *Cancer Res Commun*, 2021. 1(2): p. 79-89.

4. Mao, J., et al., Perspective: 4beta-hydroxycholesterol as an emerging endogenous biomarker of hepatic CYP3A. *Drug Metab Rev*, 2017. 49(1): p. 18-34.

A11 - ONTOGENY OF HUMAN ALDEHYDE OXIDASE (AO)

Sandhya Subash¹, Deepak Ahire¹, Michael Zientek², Priyanka Kulkarni², Cyrus Khojasteh³, Robert Jones³, Bernard Murray⁴, Bill Smith⁵, Steven Leeder⁶, Scott Heyward⁷, and Bhagwat Prasad¹

¹Washington State University, United States, ²Takeda Pharmaceuticals, United States, ³Genentech Inc., United States, ⁴Gilead Sciences, United States, ⁵Terminal Phase Consulting LLC, United States, ⁶Children's Mercy Hospital, United States, and ⁷BioIVT Inc., United States

Aldehyde oxidase (AO) has emerged as an important enzyme in drug metabolism over the past decade; however, unlike the cytochromes P450 and UDP-glucuronosyltransferases, the ontogeny of AO is not well characterized. The objective of our study was to characterize the age-dependent hepatic AO abundance and activity (carbazeran oxidation). These data were measured in pediatric human liver cytosols (n=119) and human hepatocytes (n=51). The samples and calibrator (purified AO protein) were digested using trypsin, and the protein abundance was measured by quantifying the surrogate peptides (LVNELTEFAK and MIQVVSR) by LC-MS/MS. The formation of 4-oxo carbazeran was monitored by incubating the cytosols (0.2 mg/ml) or hepatocytes (0.2 million cells per incubation) with 25 μ M carbazeran at 37 °C for 5 min (cytosol) or 10 and 30 min (hepatocytes). The mean cytosolic abundance of AO (pmol/mg protein) in neonatal (0-28 days), infant (29 days - 1 Yr), early childhood (>1 - 6 Yr), middle childhood (>6 - 12 Yr), and early adolescence groups (>12 - 18 Yr) was 1.7 ± 1.9 , 13.8 ± 12.3 , 38.2 ± 20.8 , 37.2 ± 21.5 , and 33.2 ± 17.1 , respectively, whereas AO abundance in the pooled adult liver cytosol was 30.9 ± 4.59 pmol/mg protein. Thus, the mean AO abundance increased by 20-fold from the neonatal levels, reaching adult levels by middle childhood (>6 - 12 Yr). The AO abundance when fitted to a non-linear model showed an age50 of 1.2 years. The mean activity of AO in neonatal, infant, early childhood, middle childhood, and adolescence groups was 0.8 ± 1 , 5.3 ± 11.2 , 23.8 ± 29.9 , 24.8 ± 28.7 , and 14.5 ± 26.9 pmol/min/mg protein respectively, whereas the activity in the pooled adult liver cytosol was 79.7 ± 8.73 pmol/min/mg protein. The AO activity showed large inter-individual variability and poor correlation with the abundance values, which was likely due to the loss of activity in storage. This suggests that quantitative proteomics is useful as a better alternate for characterizing ontogeny for enzymes such as AO that are prone to activity loss in storage. The mean activity for the different age groups showed a trend similar to that seen in the abundance values. AO abundance and activity did not show any association with sex. Preliminary analysis of human hepatocyte data shows a similar trend. In summary, we performed a comprehensive characterization of ontogeny of human AO. The AO ontogeny data can potentially be applied towards developing physiologically based pharmacokinetic (PBPK) models in accordance with ICH E11A guideline for predicting pediatric drug disposition.

A12 - IMPLEMENTATION OF A PHYSIOLOGICALLY BASED PHARMACOKINETIC MODELING APPROACH TO PREDICT DISEASE-RELATED CHANGES IN DRUG PHARMACOKINETICS IN PATIENTS WITH NONALCOHOLIC FATTY LIVER DISEASE

Jeffry Adiwidjaja¹, Jessica Spire², and Kim Brouwer¹

¹The University of North Carolina at Chapel Hill, United States and ²Simulations Plus, Inc., United States

Introduction. Understanding disease-related changes in the pharmacokinetics of drugs in patients with nonalcoholic fatty liver disease (NAFLD) is of clinical importance to guide optimal dosing regimens for this patient population. Methods. A virtual NAFLD patient population, stratified into simple steatosis and the more advanced stage, nonalcoholic steatohepatitis (NASH) was developed using GastroPlus v.9.8.2 (Simulations Plus, Inc.) to support the implementation of a physiologically based pharmacokinetic (PBPK) modeling approach. The model accounts for (patho)physiological changes associated with the disease and alterations in protein levels of metabolizing enzymes and transporters pertinent to drug disposition [1]. The virtual NAFLD population model was verified using previously published clinical pharmacokinetic data for pioglitazone, rosuvastatin and metformin as illustrative examples of drugs commonly used by patients with NAFLD. Results. PBPK model predictions of pioglitazone and rosuvastatin plasma concentrations, and hepatic radioactivity levels (represented by standardized uptake values [SUV]) of ¹¹C-metformin were in good agreement with the clinically-observed data. Importantly, the PBPK simulations provided reliable estimates of the extent of changes in key pharmacokinetic parameters for the diseased population compared with the non-NAFLD control group, consistent with the reported changes in the corresponding clinical studies. Clinically-reported vs PBPK model predicted ratios (NASH patients divided by healthy individuals) for trough concentrations (C_{ss,min}) of pioglitazone were 1.46 vs 1.42, respectively. The corresponding ratios for the active metabolite of pioglitazone, hydroxy-pioglitazone, that is formed predominantly through a CYP2C8-mediated pathway were 0.68 and 0.66, respectively. This was in concordance with the proteomics-informed reduction in CYP2C8 abundance by ~34% that was implemented in the virtual NASH patient population. The clinically-reported vs PBPK model predicted ratios for the systemic exposure (AUC_{0-inf}) of rosuvastatin in obese NASH patients compared to non-NAFLD lean individuals were 0.83 and 0.80, respectively, corresponding to a prediction fold-difference that was close to unity. The PBPK simulation highlighted that decreased OATP1B1 abundance, increased

protein levels of BCRP, and differences in body weight and liver size may all contribute to the slight net reduction in systemic exposure of rosuvastatin observed in NASH patients compared to the non-NAFLD cohort. Meanwhile, simple steatosis and NASH appeared to have minimal impact on peak hepatic SUV of ^{11}C -metformin, with observed and model predicted ratios to that of healthy individuals of 1.10 vs 0.95 for simple steatosis and 0.92 vs 0.77 for NASH, respectively. Conclusion. A virtual population model within the PBPK framework representing patients with NAFLD was successfully developed with a good predictive capability of estimating disease-related changes in drug pharmacokinetics. This supports the use of a PBPK modeling approach for prediction of the pharmacokinetics of new investigational or repurposed drugs for potential treatment of NAFLD, and may help inform dose adjustment of drugs commonly used to treat comorbidities in this patient population.

Funding. The financial support of Simulations Plus, Inc. is gratefully acknowledged.

Reference:

1. Murphy WA, et al. Considerations for Physiologically Based Modeling in Liver Disease: From Nonalcoholic Fatty Liver (NAFL) to Nonalcoholic Steatohepatitis (NASH). Clin Pharmacol Ther 2022, doi: 10.1002/cpt.2614

P1 - NEUROFILAMENT LIGHT CHAIN AS A BIOMARKER OF AXONAL DAMAGE IN SENSORY NEURONS AND PACLITAXEL-INDUCED PERIPHERAL NEUROPATHY IN OVARIAN CANCER PATIENTS

Christina Mortensen¹, Karina Dahl Steffensen², Emma Simonsen¹, Kamille Herskind¹, Jonna Skov Madsen², Ditte Bork Iversen¹, Troels Korshøj Bergmann¹, Anton Pottegård¹, and Tore Bjerregaard Stage¹

¹University of Southern Denmark, Denmark and ²Lillebaelt University Hospital of Southern Denmark, Denmark

Paclitaxel-induced peripheral neuropathy (PIPN) is a barrier to effective cancer treatment and impacts short- and long-term quality of life among cancer patients. PIPN predominantly consists of sensory symptoms ranging from tingling to neuropathic pain in hands and feet. PIPN represents a major challenge in oncology due to lack of an objective biomarker or validated method to grade PIPN severity and to predict patients at risk of PIPN. We used a translational approach to assess the utility of neurofilament light chain (NFL) as a biomarker of PIPN in a human cell model and in ovarian cancer patients. We measured NFL in medium from human induced pluripotent stem-cell derived sensory neurons (iPSC-SNs) treated with paclitaxel using single-molecule array (Simoa) technology. iPSC-SNs were exposed to paclitaxel concentrations of 0.1, 1, and 10 μM for 48 hours. Serum NFL (sNFL) levels were quantified in 190 ovarian cancer patients receiving paclitaxel/carboplatin chemotherapy at baseline and after each of the following 2 or 6 cycles. PIPN-related adverse outcomes were obtained from medical records and from a research database with gradings of PIPN severity. Cox regression model was performed with different sNFL cut-offs after first cycle to determine its utility to predict risk of PIPN-related adverse outcomes. The apparent elimination half-life of sNFL was estimated in patients that discontinued paclitaxel. Paclitaxel neurotoxicity in iPSC-SNs was accompanied by NFL release in a concentration-dependent manner ($P < 0.001$, analysis of variance). sNFL levels increased substantially in patients during paclitaxel/carboplatin chemotherapy with considerable interindividual variability. Patients with sNFL > 150 pg/mL after first cycle had increased risk to discontinue paclitaxel early (unadjusted HR: 2.47 (95% CI 1.16-5.22), adjusted HR: 2.25 (95% CI: 0.88-5.79)). Similar trends were shown for risk of severe PIPN and paclitaxel dose reduction due to PIPN. The median elimination half-life of sNFL was 43 days (IQR 27-82 days). NFL constitutes an objective biomarker of neurotoxicity in iPSC-SNs and in ovarian cancer patients with high sNFL predicting PIPN-related adverse outcomes. If prospectively validated, sNFL can be utilized to study PIPN and may guide clinical decision making and personalize treatment with paclitaxel.

P2 - VALIDATION OF A MFLC-MS/MS ASSAY FOR THE QUANTITATIVE ANALYSIS OF A NOVEL PEPTIDE, AT-01, EXTRACTED FROM K2EDTA PLASMA

Tara O'Brien¹, Chad Christianson¹, Daniel Kim², Sangeetha Bollini², and Andrew Vick²

¹Alturas Analytics, Inc, United States and ²Attralus, United States

Since the synthesis of the first therapeutic peptide, insulin, in 1921, our understanding of the therapeutic potential of proteins and peptides has increased significantly. As our understanding expands, targeted biopharmaceutical candidates are being identified and explored at an increasing rate. As these treatments become more mainstream and effective, the need for robust, GLP-compliant quantitative assays is growing. Previously, the majority of analysis has been done utilizing ELISA assays or similarly intensive, expensive methods. While robust, these methods do not offer the ease and high throughput potential that can be achieved with a MFLC (micro flow)-MS/MS method. Additionally, many of these existing methods require a high sample volume, which can be limiting when it comes to regulated analysis. In support of two GLP studies featuring AT-01, a novel, synthetic amyloid-targeting peptide designed for imaging systemic amyloid deposits, GLP-compliant methods were developed in both rat and dog K2EDTA plasma utilizing a straightforward MFLC-MS/MS method. Here AT-01 was extracted from plasma using a Phenomenex Strata XPro micro-elution plate and analyzed by MFLC-MS/MS. AT-01 was spiked into plasma and a 25 μL aliquot was plated in a LOW-bind 96 well plate. Internal standard was added, and the sample was acidified with a 4% phosphoric acid solution. The total volume was loaded onto a pre-conditioned Strata XPro micro-elution plate, rinsed with water, and then eluted into a clean 96 well LOW Bind plate with two volumes of 1:74:25 trifluoroacetic acid/acetonitrile/water. A final dilution was done with water + 0.1% formic acid. The extract was analyzed on an API-6500 mass spectrometer equipped with an Optiflow source, operating in positive ESI mode. The MFLC system was a Waters M Class set to run a binary gradient method with a flow rate of 40 $\mu\text{L}/\text{min}$. Chromatographic separation was achieved using a Kinetics Biphenyl column (1.7 μm , 50 x 1.0mm) from Phenomenex. The methods were linear from 30.0 – 5000 ng/mL with an R-value of 0.9961 for rat and 0.9936 for dog. Matrix effects from six individual lots of plasma in each species were examined and found to be within $\pm 5.8\%$ of nominal across the LQC and HQC for rat, and within -9.6 and +6.8% of nominal across the LQC and HQC for dog. Blanks were also examined using six individual lots of plasma for each species. In both cases, the assay was found to be selective across all lots. The methods were validated according to FDA guidance and met a priori acceptance criteria. These low sample volume methods were found to provide a selective and accurate quantification of this innovative peptide.

P3 - CONDITIONAL KNOCKOUT OF THE CYTOCHROME P450 OXIDOREDUCTASE GENE HIGHLIGHTS HUMAN DRUG METABOLISM IN HUMANIZED LIVER TK-NOG MICE

Hiroshi Suemizu¹, Yuichi Iida², Miyuki Ida-Tanaka¹, Kenji Kawai¹, Yuichiro Higuchi¹, Satoshi Ito³, Hidetaka Kamimura¹, Mamoru Ito¹, Hiroshi Yamazaki⁴, Mitsuo Oshimura⁵, Yasuhiro Kazuki⁵, and Shotaro Uehara¹

¹Central Institute for Experimental Animals, Japan, ²Shimane University Faculty of Medicine, Japan, ³Sekisui Medical Co., Ltd., Japan, ⁴Showa Pharmaceutical University, Japan, and ⁵Tottori University, Japan

Chimeric TK-NOG mice with a humanized liver (Hu-liver) are a unique animal model for predicting drug metabolism in humans. However, residual mouse hepatocytes occasionally prevent precise evaluation of human drug metabolism. P450 oxidoreductase (POR) is a diflavin enzyme responsible for electron donation to a large number of P450 enzymes; therefore, functional deletion of POR results in loss or low activities for most P450 enzymes. We developed a liver-specific POR conditional knockout (POR cKO) humanized liver TK-NOG mouse by two-step homologous recombination in embryonic stem cells (NOG-ES) from NOG mouse. Expression of POR protein and mRNA, and enzymatic activity in the liver and small intestine of POR cKO mice were examined by immunoblot analysis, quantitative RT-PCR, and enzymatic assays, respectively. POR cKO mice with the fl/null genotype, in which one floxed allele is pre-deleted, exhibited nearly complete loss of POR function due to low POR protein and gene expression. NADPH-cytochrome c reductase and cytochrome P450 (P450)-mediated drug oxidation activities in liver microsomes from POR cKO fl/null mice were negligible. Immunohistochemical analysis was used to determine if POR protein-expressing hepatocytes were still present. A remarkable reduction in the number of POR-expressing cells was found in the livers of the POR cKO fl/null mice. We prepared humanized liver mice based on the POR cKO strain by transplantation of human hepatocytes (POR cKO Hu-liver). The liver of POR cKO Hu-liver mice was filled with human hepatocytes that stained with an anti-human mitochondria antibody. Drug-metabolizing activities of phenacetin O-deethylation, diclofenac 4'-hydroxylation, omeprazole 5-hydroxylation, metoprolol O-demethylation, and midazolam 1'-hydroxylation in liver microsomes from POR cKO Hu-liver mice were comparable to those in normal Hu-liver mice. The circulating and urinary levels of S-4'-hydroxywarfarin (a major warfarin metabolite in mice) in the original Hu-liver mice were about 21 to 28% of the total metabolites examined, despite the high chimeric ratio. In contrast, in Por cKO Hu-liver mice, which have a similar chimeric ratio to the original Hu-liver mice, the S-4'-hydroxywarfarin ratio was reduced to only 1.2 to 2.5% of the total metabolites examined. The minimal interference of drug-metabolizing activity in residual mouse hepatocytes represents a major advantage of this novel model over the normal humanized liver model. Overall, the POR cKO Hu-liver mouse is likely to become the preferred platform for the study of human drug metabolism and pharmacokinetics.

P4 - EPIGENETIC REGULATION OF THE ARL HYDROCARBON RECEPTOR (AHR) IN NORMAL AGING

Sara Abudahab

Virginia Commonwealth University, United States

Purpose: Older adults are vulnerable to adverse drug reactions, and we believe that changes in epigenetics could result in impaired drug metabolism. We are investigating the AhR, a ligand dependent transcription factor that regulates xenobiotic metabolism and has been associated with the process of aging itself. We hypothesize that 1) DNAm and gene expression of AhR change with age 2) genes regulated by AhR are affected by epigenetic aging 3) many of these AhR age-differentially methylated genes are involved in drug metabolism.

Methods: We obtained liver tissues of C57Bl/6 mice from the National Institute on Aging (NIA) for 4, 18, 24, and 32 months, n=12 per group. We measured DNAm levels using high resolution melt on a QuantStudio3 (Applied Biosystems). Reverse transcription of RNAs was performed using the iScript cDNA Synthesis Kit (Bio-Rad) and TaqMan (ThermoFisher) and qPCR was performed. For the data integration, we used liver AhR chromatin immunoprecipitation data from Fader et al., 2017 and liver Methyl-CpG-Binding Domain sequencing of age-differentially methylated regions generated by Sandoval-Sierra et al., 2020. We used Fisher's exact test to test for enrichment using all mouse RefSeq as well as liver DNase hypersensitivity (GSE60430) as background-sets.

Results: The average DNAm levels of 4, 18, 24 and 32 months were 100%, 83.9%, 92.2% and 92.9%, respectively and the ANOVA test showed a significant change in DNAm (p=0.00024). AhR expression did not change with age, and we hypothesize that this because AhR was not activated by a ligand in the NIA livers. Fisher's exact test showed a significant enrichment with a p-value < 2.2x10⁻¹⁶, OR= 4.8. Using just genes active in the liver, the results were also significant (p= 1.381x10⁻⁰⁸, OR= 3.1). The pathway analyses of the AhR differentially methylated genes using PANTHER as well as DAVID identified "cellular response to chemicals" as an enriched pathway with 1.93-fold (p= 3.172 x 10⁻⁵, FDR= 4.982 x 10⁻²) and 1.54-fold (p= 4.3 x 10⁻³, FDR= 0.2), respectively.

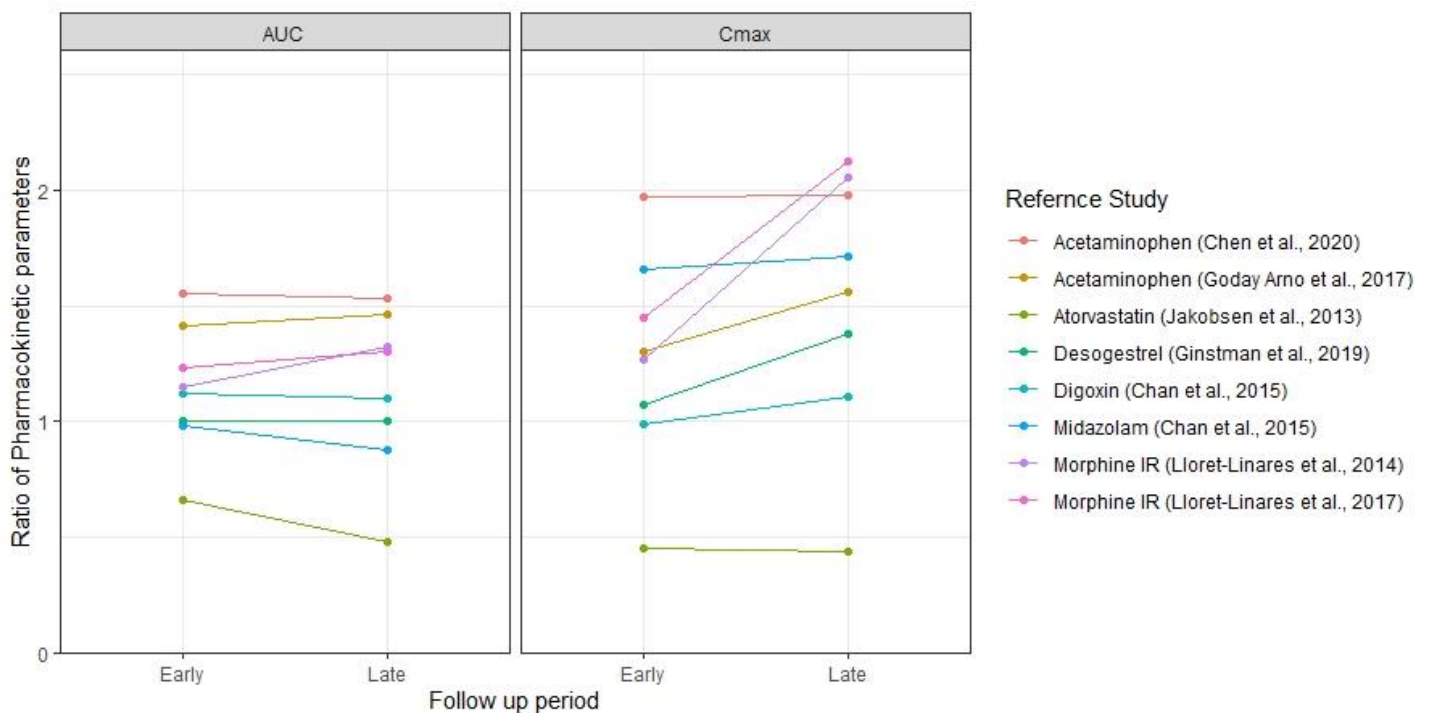
Conclusions: The variability in drug metabolism is a major issue in pharmacotherapy, especially in the elderly. Our results show that DNAm change with age at the AhR promoter and that AhR target genes are also affected with aging.

P5 - CONSIDERATIONS IN CLINICAL EVALUATION FOR PHARMACOKINETIC CHANGES OF ORALLY ABSORBED DRUGS BY BARIATRIC SURGERY

Sungyeun Bae and SeungHwan Lee

Seoul National University College of Medicine and Hospital, South Korea

Obesity has been a growing worldwide concern and surgical intervention including bariatric surgery is considered as one of the options for the treatment. However, the change in pharmacokinetics (PKs) of drugs after surgery is still on debate. To investigate the potential covariates that can influence area under the curve (AUC) and the maximum plasma concentration (C_{max}), the study design of previous reports screened by the pre-determined eligibility criteria were reviewed. Ratios of AUC and C_{max} after surgery to before were calculated in each study. Whether the time after surgery or the type of control group affects the changes in PK parameters was investigated. Ratio of AUC calculated in the early and late follow-up period with 6 months as the cutoff value was similar after Roux-en-Y gastric bypass surgery. Whether the control is the pre-surgical condition of the same patients or the matched healthy subjects did not affect the PK parameters but certain type can be preferred in special occasions. This is the first article exploring the appropriate methodology in designing clinical studies for changes in PK characteristics of orally administered drugs in patients with bariatric surgery.



P6 - INTER- AND INTRA-SUBJECT ANALYSIS OF GENE EXPRESSION AND PROTEIN ABUNDANCE OF MINOR DRUG METABOLIZING ENZYMES IN HEALTHY HUMAN INTESTINE AND LIVER.

Christoph Wenzel¹, Joanna Lapczuk-Romanska², Marek Ostrowski², Marek Drozdziak², and Stefan Oswald³

¹University Medicine Greifswald, Germany, ²Pomeranian Medical University, Poland, and ³University Medical Center Rostock, Germany

First pass metabolism by phase I and phase II-enzymes is a major determinant of the oral bioavailability of various drugs. In the past, the liver was assumed as the organ where the first pass metabolism mainly takes place. However, there is convincing evidence that first pass metabolism occurs partly already in intestinal epithelia and can have a strong impact on oral drug absorption. In this regard, the protein abundance of several intestinal drug-metabolizing enzymes (DMEs, e. g. CYP3A4) was found to be comparable to the liver. However, contrary to available data on major DMEs, there is a lack of data on several other enzymes involved in drug metabolism, i.e. "minor" DMEs. Interestingly, many drugs with narrow therapeutic indexes, such as anti-cancer drugs or directly acting oral anticoagulants (DOACs) are substrates of those enzymes. To fill this gap in knowledge, we successfully developed and validated a mass spectrometry-based targeted proteomics method for the quantification of 24 clinically relevant carboxylesterases (CES), UDP-glucuronosyltransferases (UGT) and cytochrome P450 (CYP)-enzymes. We applied our method to jejunal and liver tissue specimens of 11 healthy organ donors (8 males, 11 females, age: 19-60 y). This gives us the opportunity to get insights into the intra-subject data for a direct comparison of liver and gut in the same individuals. Our analysis was performed in whole tissue lysate that

underwent the filter aided sample preparation procedure (FASP), which includes a tryptic digest. In addition, the respective mRNA-levels of the encoding genes were determined by quantitative real-time PCR. We found several enzymes to be of higher (e.g. CES2, UGT2B17, CYP 2J2) or similar (e.g. CYP2C18, CYP2C19) abundance in the jejunum compared to the liver. On the contrary, most of the investigated enzymes were of high abundance in liver tissue (e.g. CYP4F2, CYP2E1). Moreover, our results showed a notable high variation between the individuals. Our findings on protein level were mostly reflected in the gene expression data. Precise data on protein abundance can be used for PBPK-based modelling and prediction like the proteomics-informed relative expression factor approach. This can be used for optimized dosing regimens and may help to improve efficacy and safety of drug therapy.

P7 - HEAD-TO-HEAD COMPARISON OF AAV BIODISTRIBUTION AND TRANSGENE EXPRESSION LEVELS AMONG RAAV SEROTYPES

Yosuke Yamanaka, Akihiro Matsumoto, and Yoshiteru Kamiyama
Astellas Pharma Inc., Japan

Recombinant adeno-associated virus (rAAV) is expected as one of the most promising gene delivery vector for a wide range of gene therapy applications. As each rAAV serotype has different tissue tropism and persistence of transgene expression, it is important to understand the biodistribution properties of each rAAV serotype and choose the suitable rAAV serotype against the target indication for drug development. The biodistribution of rAAV has been extensively studied in various experimental conditions in different laboratories. However, integrating the data from different laboratories may not be feasible if the analytical conditions are different. Thus, in order to accurately understand the different biodistribution properties of each rAAV serotype, we have conducted head-to-head quantitative comparison of AAV2, AAV8, and AAV9 biodistribution after single intravenous administration to mice. Using rAAV carrying the identical viral genome sequence encoding cytomegalovirus (CMV)-enhanced Green Fluorescent Protein (EGFP), the time-course of viral DNA copy number and transgene expression in each animal was evaluated throughout the experiment duration (4 h – day 28 post dosing). The EGFP cDNA coding region of the AAV viral DNA was detected by qPCR to evaluate the AAV viral DNA distribution. The EGFP protein was measured by ELISA to evaluate the transgene expression. In blood, the viral DNA concentration of AAV9 showed the highest among AAV2, AAV8 and AAV9 at all the evaluated timepoints. Although the viral DNA concentration of AAV2, and AAV8 showed comparable up to 48 h post dosing, AAV2 viral DNA decreased more rapidly from the blood than AAV8 after 7 days post dosing. In tissues except blood, the viral DNA concentration of AAV2, AAV8 and AAV9 showed the highest at 4 h post dosing (the earliest time point). Subsequently, the viral DNA concentration of AAV2, AAV8 and AAV9 rapidly decreased up to 1 week post dosing, followed by relatively slower decrease or little change between 1 week and 4 weeks post dosing. The EGFP protein expression increased time-dependently and then reached plateau after 1 week post dosing. Comparing the tissue tropism of AAV2, AAV8 and AAV9, AAV2 showed lower viral DNA and transgene expression in all the tested tissues except spleen. AAV9 had the highest viral DNA and transgene expression in all the dissected tissues except liver. In the liver, AAV8 viral DNA and transgene expression was comparable to those of AAV9. These results showed the different biodistribution of AAVs and that AAVs have distinct tissue tropism in each serotype, under the same experimental conditions.

P8 - QUANTIFYING PROTEIN BIOMARKERS FOR DRUG-INDUCED ORGAN INJURY ACROSS THE SPECIES BARRIER BY IMMUNOAFFINITY-LC-MASS SPECTROMETRY

Andreas Steinhilber, Hannah Haag, Viktoria In thai Anselm, Wael Naboulsi, Hannes Planatscher, and **Oliver Poetz**
SIGNATOPE GmbH, Germany

There is an unmet need for reliable assays to detect drug-induced organ toxicity, as organ toxicity remains one of the major causes of drug development failure. During the drug development process, mandatory tests must be performed on various animal species such as rodents, dogs and non-human primates to rule out organ toxicity. So far, such studies are dominated by time-consuming and non-quantitative histological analyses.

Therefore, potential protein biomarkers from body fluids for the detection of drug-induced liver (DILI), kidney (DIKI) and vascular injury (DIVI) were investigated by academic-industrial consortia - the Safer and Faster Evidence-based Translation Consortium (SAFE-T) and the Predictive Safety Testing Consortium (PSTC). Potential protein and microRNA biomarkers were analyzed in retrospective and prospective studies. The results were recognized by the FDA and the EMA and led to letters of support recommending a selection of these biomarkers for further investigation. The qualification process is currently being continued by the TransBioline consortium, which is supported by the EU's Innovative Medicine Initiative program.

We have established a protein assay platform for the analysis of renal, vascular and liver injury biomarkers in urine, serum or plasma for preclinical species and humans. First, proteins are enzymatically fragmented with trypsin. Peptides derived from the biomarkers are enriched by the use of multi-specific antibodies (TXP antibodies) targeting common C-terminal amino acid motifs present in the sequences of the biomarkers, regardless of species. The immunaffinity enriched peptides are detected and quantified by nano-liquid chromatography coupled to mass spectrometry (IA-LC-MS/MS) with reference to synthetic isotope-encoded standards. The necessary technological developments for the robust and sensitive

detection of these proteins will be outlined. Examples of biomarker analyses in preclinical and clinical safety studies provided by PSTC and TransBioline members will be discussed.

The application of immunoprecipitation with group-specific TXP antibodies in combination with mass spectrometric detection enables the quantification of biomarkers in urine, serum or plasma of all common animal models. The results strongly support the validation of translational drug-induced organ injury protein biomarkers.

P9 - ABSTRACT WITHDRAWN

P10 - ADAPTATION OF *IN VITRO* METHODS TO DETERMINE UNBOUND CELL TO MEDIUM PARTITION COEFFICIENT, $K_{p,uu}$

Virag Bujdosó-Szekely, Katalin Jemnitz, Johanna Pacsuta, and Zsuzsanna Gaborik
SOLVO Biotechnology, A Charles River Company, Hungary

Hepatic overall clearance is the outcome of the complex interplay between ADME processes (sinusoidal uptake, metabolism, canalicular secretion, sinusoidal efflux) [1]. Extended Clearance Model (ECM) serves as a reference to classify drugs based on their *in vitro* determined clearance mechanisms [1]. This model groups compounds into four classes by which the rate determining step of their elimination can be predicted. For transport proteins and metabolic enzymes only unbound drugs are available, the concentration of which determines efficacy, toxicity, pharmacokinetics, and pharmacodynamics. ECM not only serves as a classification system but also provides indirect estimates of unbound intrahepatic drug concentration i.e., unbound liver-to-blood partition coefficient ($K_{p,uu}$) [2]. If transport is the rate determining step in drug disposition, concentrations in plasma and liver might be asymmetric ($K_{p,uu} \neq 1$) that determines the rate of intracellular processes. $K_{p,uu}$ can be calculated based on K_p : hepatocellular drug accumulation and hepatic unbound fraction (f_u). The latter parameter can be measured by 3 approaches (homogenization/temperature/logD7.4 method), of which the temperature method resulted in best approach compared to calculation based on the ECM [2]. Our aim was to adapt and validate the method for f_u and $K_{p,uu}$ determination for compounds with different plasma-binding from distinct classes of ECM groups using radioactive and bioanalytical methods. Using the temperature method [2] active/passive uptake were determined at steady state for 30/60/90 minutes, at 37°C/4°C using plated human hepatocytes. Rosuvastatin, pitavastatin, atorvastatin, fluvastatin, pravastatin, verapamil and ketoconazole were used as substrates. f_u values were determined at 4°C. K_p was evaluated based on the media and intracellular concentrations, and $K_{p,uu}$ was calculated as follows: $K_{p,uu} = K_p \times f_u$. The order of f_u values is $FLV \approx PTV < ATV < RSV < PRV$ which correlate well to literature data, together with our $K_{p,uu}$ parameters. Results of radiolabelled versus unlabelled substrate measurements are also corresponding. Interestingly, in the literature these values vary in a broad scale possibly due to different hepatocyte lots. However, our data fits into this range of parameters. $K_{p,uu}$ and unbound intracellular concentration are parameters of growing interest in drug discovery, especially for class 3 and 4 drugs, which are cleared mostly by active and passive uptake and efflux processes [1]. Thus, intracellular unbound concentration is probably unequal to the one applied extracellularly in *in vitro* experiments. To generate reliable *in vitro* data for *in vivo* hepatic clearance prediction, $K_{p,uu}$ should be taken into account.

References:

1. Camenisch G, Riede J, Kunze A, Huwyler J, Poller B, Umehara K. The extended clearance model and its use for the interpretation of hepatobiliary elimination data. *ADMET & DMPK* 3(1) (2015) 1-14
2. Riede J, Camenisch G, Huwyler J, Poller B. Current *In Vitro* Methods to Determine Hepatic $K_{p,uu}$: A Comparison of Their Usefulness and Limitations. *Journal of Pharmaceutical Sciences* 106 (2017) 2805-2814

P11 - INVESTIGATION OF THE UNDER PREDICTION OF *IN VIVO* CLEARANCE FROM METABOLIC INTRINSIC CLEARANCE IN THE RAT: GASTROINTESTINAL EXSORPTION AS AN IMPORTANT ELIMINATION PATHWAY IN DRUG DISCOVERY

Dermot McGinnity, Aaron Smith, Joanne Wilson, Graeme Scarfe, and Andy Pike
AstraZeneca, United Kingdom

Prediction of *in vivo* clearance from hepatocyte intrinsic clearance (CL_{int}) is a well-established methodology, however, it is not uncommon to see some level of under prediction due to omission of the contribution non-metabolic processes. During the development of series of novel A2a receptor antagonists we determined *in vivo* clearance in rats was moderate to high, despite negligible hepatocyte CL_{int} , and typically under predicted by 3-10 fold. As the series were moderately lipophilic neutral molecules with high passive permeability, significant non-metabolic clearance was not anticipated, nonetheless, this was investigated in a bile duct cannulated rat study for a representative compound (AZ-X). A high renal clearance of 15 mL/min/kg, accounting for approximately half the total clearance and equivalent to 14x $GFR \times f_u$, was observed and subsequent studies showed similar data for analogues. However, despite the high renal clearance

component, and some biliary excretion, a persistent tendency to under predict the residual fraction of the total clearance from *in vitro* metabolic CL_{int} was still observed. We therefore decided to investigate the potential for excretion of the compounds into the gut lumen from the circulation (gastrointestinal “exsorption”) following intravenous dosing to bile duct cannulated wild type and P-gp/BCRP knockout rats for AZ-X. These studies showed that in wild type animals 34% of the dose was recovered unchanged in faeces compared with 7% of the clearance which was attributable to metabolism. These data supported the hypothesis that exsorption accounted for the majority of residual total clearance, consistent with the low hepatocyte CL_{int}. In contrast, in P-gp/BCRP knockout rats only 3% of the dose was recovered in the faeces suggesting active efflux by P-gp and/or BCRP is the primary mechanism driving exsorption mediated clearance for these compounds. This work demonstrates that exsorption into the gastrointestinal tract can account for a significant fraction of total clearance in the rat and may contribute to the underprediction of hepatic clearance from *in vitro* experiments. Furthermore, it demonstrates a key role for efflux transporters in exsorption and highlights the need to consider this elimination pathway in drug discovery and development in conjunction with, metabolic, biliary and renal CL in animals and humans.

P12 - HEPATOCYTE UPTAKE AND LOSS ASSAY (HUPLA), A NOVEL ALL-IN-ONE SYSTEM FOR OBTAINING UPTAKE, EFFLUX AND INTRINSIC CLEARANCE FOR COMPOUNDS WITH CHALLENGING PHYSICOCHEMICAL PROPERTIES AND LOW METABOLIC TURNOVER.

Julia Schulz, David Stresser, and John Cory Kalvass

AbbVie Inc., United States

Underprediction of hepatic clearance is a significant contributor to uncertainty in advancing compounds to the clinic.^[1] The extended clearance concept has helped to address this issue by expanding from metabolic clearance (CL_{met}) alone to include drug distribution processes into the liver, including active uptake clearance (PS_{influx}), active efflux clearance (PS_{efflux}), and passive diffusion (PS_{pd}).^[2] However, these parameters are measured in assays and test systems that require distinct scaling factors, introducing significant variability and decreasing prediction confidence. Measuring these four intrinsic kinetic parameters driving hepatic clearance within a single assay system would ostensibly alleviate some of these concerns.

To this end, we designed the Hepatocyte Uptake and Loss Assay (HUpLA) as an “all-in-one” two-step hepatocyte assay to determine CL_{met}, PS_{influx}, PS_{efflux}, and PS_{pd} in parallel. In step 1, we equilibrate primary human hepatocytes with drugs and measure hepatic uptake under different conditions to distinguish PS_{influx} and PS_{pd}. Once the system reaches steady state, determined by $K_{\text{equilibration}} = \text{CL}_{\text{met}} + \text{PS}_{\text{efflux}} + \text{PS}_{\text{pd}}$, we rapidly exchange the drug-containing medium with drug-free medium. During the second step, we determined egress clearance (PS_{efflux} + PS_{pd}) from the appearance of drug in the medium. Additionally, CL_{met} can be estimated from drug loss from the entire incubation (cells + medium). However, since compound loss is directly measured from pre-loaded hepatocytes only rather than from the summed combination of drug-containing cells and drug-containing media, this assay could increase sensitivity for very low turnover compounds. The four kinetic parameters can be obtained by simultaneously fitting the extended clearance model to all data from steps 1 and 2. In addition, auxiliary parameters can be determined from the data, including the unbound media-to-cell ratio (K_{p,uu,cell}), a measure of cellular distribution as well as the unbound fraction in hepatocytes (f_{u,hep}) and the incubation (f_{u,inc}). Furthermore, in a variation of the assay, addition of plasma may improve the apparent solubility and reduce non-specific binding, improving clearance determination of challenging compounds, many with poor physicochemical properties. Here, we outline the method development and challenges in optimizing the HUpLA. The main issue we are experiencing is changing the medium rapidly. Rapid medium exchange is necessary to enable quantitation of drug efflux into drug-free medium in the critical early period of this portion of the experiment (first 0-5 minutes). After unsuccessful attempts using centrifugation (not fast enough) and filtration (clogging), we focus our efforts on using plateable hepatocytes on collagen-coated 96-well plates. However, further optimization of efflux measurements is necessary.

Based on our initial experiments, we determined the following clearance parameters for pitavastatin: CL_{met}=0.22±0.08 l/min/106 cells, PS_{influx}=5.97±2.01 l/min/106 cells, PS_{efflux}=0.03±0.01 l/min/106 cells, and PS_{pd}=4.27±0.53 l/min/106 cells. Together, these parameters contribute to an average CL_{int} of 489 ml/min/106 cells, comparable to previously published results.^[3]

To summarize, the four kinetic parameters driving hepatic clearance can be estimated from HUpLA results via simultaneous fitting. After further optimization, we plan to evaluate clearance prediction accuracy across a wide array of compounds with challenging physicochemical properties.

References:

1. Bi, Y.A., et al., *Effect of Human Plasma on Hepatic Uptake of Organic Anion-Transporting Polypeptide 1B Substrates: Studies Using Transfected Cells and Primary Human Hepatocytes*. Drug Metab Dispos, 2021. 49(1): p. 72-83.
2. Varma, M.V., et al., *Predicting Clearance Mechanism in Drug Discovery: Extended Clearance Classification System (ECCS)*. Pharm Res, 2015, 32(12) p. 3785-802.

3. Riede, J., et al, *New IVIVE method for the prediction of total human clearance and relative elimination pathway contributions from in vitro hepatocyte and microsome data*. Eur J Pharm Sci, 2016. 86: p. 96-102.

P13 - REACTIVITY ASSESSMENT OF CARBOXYLIC ACID DRUGS BY USING ACYL MIGRATION RATE AND HALF-LIFE DETERMINATION OF ACYL-GLUCURONIDES

Barry Jones¹ and Jennifer Vance²

¹Pharmaron, United Kingdom and ²Pharmaron, United States

Acyl glucuronides (AGs) formed by conjugation of carboxylic acids with glucuronic acid, is one of the potential reactive metabolites which could lead to idiosyncratic drug toxicity. Since the patient-related susceptibilities leading to idiosyncratic toxicity are not sufficiently understood, the best strategy is to minimize drug-related risk factors such as potential acyl glucuronide formation. Here, we describe a rapid *in vitro* assay for the assessment of the reactivity of acyl glucuronides. This assay employs human liver microsomes as matrix with UDPGA as the cofactor. β -glucuronidase was used to distinguish 1-O position of the glucuronic acid from their migrated isomers. The sample analysis was performed using Thermo Q Exactive high resolution mass spectrometer coupled with Dionex UltiMate 3000 UHPLC. For migration rates, 7 warning/withdrawn drugs and 6 safe drugs were investigated. In most cases, data were comparable with published data and cutoff values: migration rates >20% indicating higher risk of reactivity and <10% low/no risk. Based on the migration rate data, 2 warning/withdrawn drugs and 2 safe drugs were selected for further validation for migration rate and half-life of AGs. These data are also comparable with literature values and shows good reproducibility. So, any pair (one warning/withdrawn drug and safe drug) could be used as control compounds for this assay. Our approach relying on the acyl glucuronide migration rate and half-life determination of an acyl glucuronide to evaluate reactivity of 1-O- β -acyl glucuronide can be used to support the selection of low-risk drug candidates in the drug discovery stage.

P14 - CANAGLIFLOZIN-2'-O-GLUCURONIDE FORMATION IS A SELECTIVE UGT2B4 REACTION USED TO IDENTIFY CLOTRIMAZOLE AS A POTENT UGT2B4 INHIBITOR

Kimberly Lapham, Nicholas Ferguson, Mark Niosi, Christine Orozco, and Theunis Goosen

Pfizer, Inc, United States

UGT2B4 is a drug metabolizing enzyme expressed in the liver at levels comparable to other major hepatic UGTs, but reagents to quantitatively assess its contribution to drug metabolism (i.e., chemical inhibitor or relative activity factors) are not available. Canagliflozin-2'-O-glucuronide (C2OG) formation, a minor metabolic route, was reported to be UGT2B4 selective(1). In a previous study, we confirmed C2OG selectivity, presented C2OG formation kinetics in rhUGT2B4, and demonstrated 16 α -phenyllongifolol, 16 β -phenyllongifolol, and clotrimazole are potentially potent inhibitors of rhUGT2B4 catalytic activity(2). The studies presented herein describe C2OG formation kinetics in HLM and the characterization of 16 α -phenyllongifolol, 16 β -phenyllongifolol, and clotrimazole potency and selectivity towards UGT2B4 inhibition. In HLM, C2OG formation presented with severe substrate inhibition kinetics confounding estimations of K_m , V_{max} and K_i . Incorporation of a Hill coefficient (n) was required to obtain kinetic fits and parameter estimates. In HLM with BSA, C2OG $S_{50,u}$, V_{max} , $K_{i,u}$, and n was 30.4 μ M, 540 pmol/min/mg, 34.3 μ M and 2.88, respectively. Without BSA, C2OG $S_{50,u}$, V_{max} , $K_{i,u}$, and n was 1188 μ M, 3104 pmol/min/mg, 25.3 μ M and 1.31, respectively. Clotrimazole, 16 α -phenyllongifolol, and 16 β -phenyllongifolol presented with HLM $IC_{50,u}$ values of 0.035, 0.041, and 0.037 μ M in the presence of BSA and 0.011, 0.031, and 0.020 μ M in the absence of BSA, respectively. 16 α -Phenyllongifolol and 16 β -phenyllongifolol were nearly equipotent inhibitors of UGT2B4 and UGT2B7 in HLM negating previous assumptions of selectivity for UGT2B7 since UGT2B4 was not studied until now. However, with the discovery that clotrimazole is >100-fold more selective for UGT2B4 inhibition compared to all other UGT isoforms investigated (UGTs 1A1, 1A3, 1A4, 1A6, 1A9, 2B7, 2B15, and 2B17), clotrimazole and the phenyllongifolols can be used in concert to quantitatively differentiate UGT2B4 and UGT2B7 contribution to metabolism. Applying this approach to zidovudine, a commonly used UGT2B7 probe substrate, the fraction of metabolism catalyzed by UGT2B4 and UGT2B7 was estimated at 0.20 and 0.77, respectively. These studies confirm selective inhibition of UGT2B4 by clotrimazole and should prove useful in routine *in vitro* phenotyping assessments of potential new drug candidates metabolized by UGT2B4.

References:

1. Francke S, Mamidi RN, Solanki B, Scheers E, Jadwin A, Favis R, Devineni D. *In vitro* metabolism of canagliflozin in human liver, kidney, intestine microsomes, and recombinant uridine diphosphate glucuronosyltransferases (UGT) and the effect of genetic variability of UGT enzymes on the pharmacokinetics of canagliflozin in humans. J Clin Pharmacol. 2015 Sep;55(9):1061-72.
2. Lapham K, Ferguson N, Niosi M, Novak JJ, Orozco CC, and Goosen TC. *In vitro* evaluation of UDP-glucuronosyltransferase (UGT) 1A3 and UGT2B4 inhibition. (P100) Poster presented at 12th International ISSX Conference; 2019 July 28-31; Portland, Oregon.

P15 - INTER- AND INTRA-SPECIES SEMI-QUANTITATIVE COMPARATIVE DIFFERENTIATION OF REACTIVE METABOLITES VIA COMPETITIVE TRAPPING APPROACH

Igor Mezzine, Chris Bode, Sid Bhoopathy, and Ismael Hidalgo
Absorption Systems, United States

We hypothesized that glutathione transferases (GST) could differ in specificity towards trapping of reactive metabolites (RM). To investigate this hypothesis, reactive metabolites (RM) of three model compounds (acetaminophen (APA), clozapine (CLZ), and nefazodone (NFZ)) were generated in human liver microsomes (HLM) as well as monkey (MkLM), rat (RLM), and mouse (MsLM) liver microsomes. The RM were trapped via GSH conjugation with (+) or without (-) the competitive chemical trapping agent N-acetyl cysteine (NAC). For each compound, the corresponding stable isotope-labeled (SIL) GSH conjugates (GC) were generated in HLM in the presence of SIL-GSH and were used as internal standards for the purpose of semi-quantification. The samples were analyzed by LC-HRMS and the levels of GC were established relative to those in a (-) NAC HLM incubation sample. The enzymatic trapping efficiency (ETE) in HLM, defined as the ratio of GC in (-) NAC/(+) NAC samples, was highly RM dependent, and it is suggested that poorly trapped RM (lower ETE) could be of higher toxicological concern. Graphical representation of normalized relative yields (NRY) of GC and normalized ETE (NETE) in animal matrices vs. HLM assigns animal RM to one of four zones (NRY/NETE) 1) Low/High; 2) Low/ Low 3) High/Low, and 4) High/High. It is suggested that the presence of RM in zone 1 could point to preclinical tox species in which achieving adequate exposure to a particular RM would be more challenging

P16 - METTL7A AND METTL7B ARE XENOBIOTIC ALKYL THIOL METHYLTRANSFERASE ENZYMES

Rheem Totah, **Drake Russell**, and Marvin Chau
University of Washington, United States

Thiol methyltransferase (TMT) is a membrane-associated enzyme that catalyzes the S-methylation of exogenous aliphatic and phenolic thiols. TMT is one of two S-methyltransferases, with thiopurine methyltransferase (TPMT), a well-characterized cytosolic enzyme that selectively methylates thiopurines being the second. Thiols are reactive nucleophiles that can form damaging covalent bonds with essential biomolecules, and their metabolism is often unpredictable. S-methylation is a major metabolic pathway for many thiol-containing therapeutics and can dramatically alter drug activity and toxicity. TMT has a broad substrate specificity, with potential substrates including 7 α -thiospironolactone (TSL), mertansine, the active metabolites of prasugrel and clopidogrel, ziprasidone, and captopril. Despite TMT's role in the S-methylation of many clinically relevant compounds, little is known about the enzyme(s) responsible for this activity. Previously, TMT activity was attributed to a 28 kDa protein by partial purification, but the protein was not identified. Our lab has recently identified putative methyltransferase-like protein 7B (METTL7B) as a thiol methyltransferase. METTL7B is a 28 kDa microsome-associated protein with a similar tissue distribution and a similar substrate specificity to TMT. Although there is no specific inhibitor for TMT, 2,3-dichloro-a-methylbenzylamine (DCMB) potently inhibits TMT and has been used to distinguish suspected TMT activity in liver microsomes. Interestingly, despite its similarities to TMT, METTL7B was not inhibited by DCMB, and because of this, we hypothesized that more than one enzyme is involved in TMT activity. Putative methyltransferase-like protein 7A (METTL7A) is an uncharacterized protein in the same protein family as METTL7B. METTL7A is suspected to be a membrane-associated methyltransferase and shares 75% sequence homology with METTL7B, but little is known about its endogenous function. In this work, we report that METTL7A is an S-methyltransferase with many similarities to TMT, including potent inhibition by DCMB. Using quantitative proteomics on individual human liver microsome samples and gene modulation experiments in HepG2 and HeLa cells, we determined that TMT activity correlates well with METTL7A protein levels and expression levels. Furthermore, the purification of a His-GST-tagged recombinant protein and extensive biochemical characterization established that METTL7A can methylate a wide variety of thiol-containing substrates, including TSL, dithiothreitol (DTT), 4-chlorothiophenol, and mertansine. From this work, we conclude that both METTL7A and METTL7B methylate aliphatic and phenolic thiols.

P17 - STRUCTURAL AND BIOCHEMICAL CHARACTERIZATION OF THE THIOL METHYL TRANSFERASES METTL7A AND METTL7B

Drake Russell¹, Rheem Totah¹ and Taeyoon Jung²

¹University of Washington, United States and ²University of Washington, South Korea

Methyl transferase-like proteins-7A and -7B (METTL7A and METTL7B) have recently been identified as microsomal associated phase II methyl transferases that transfer a methyl group from S-adenosyl methionine to exogenous alkyl and phenyl thiols including 7 α -thiospironolactone (TSL), dithiothreitol (DTT), 4-chlorothiophenol, captopril, and mertansine. Both enzymes consist of 244 residues and share 60% sequence identity and 75% sequence homology. METTL7A and METTL7B each possess a 28-residue long hydrophobic signaling sequence at their N-terminus, which helps target the proteins into lipid droplets. This hydrophobic region is thought to form a hairpin loop and imbed in the phospholipid monolayer surrounding lipid droplets. METTL7 enzymes are proposed to be involved in lipid droplet formation, but their precise endogenous function remains unknown. Like other microsomal drug-metabolizing enzymes, the lipid environment

surrounding METTL7 enzymes is important for their activity. Recombinant METTL7A and METTL7B's methylation activity is highly enhanced in the presence of 1,2-Dimyristoyl-sn-glycero-3-phosphoglycerol (DMPG), a phospholipid used to stabilize other lipid droplet associated proteins. In this project, we developed an expression construct that utilizes an N-terminal His-SUMO- tag, which allows efficient solubilization of the enzymes from bacterial membrane. This His-SUMO N-terminal tagged construct yielded METTL7A and METTL7B proteins that were 15-fold more active than the GST-tagged proteins we previously developed. The SUMO-tagged METTL7 construct is used to probe the relationship between enzyme activity and N-terminal interaction with different lipid environments, as well as differences in structure and activity between METTL7A and METTL7B. METTL7A is potently inhibited by the historical microsomal thiol methyltransferase (TMT) inhibitor 2,3-dichloro-alpha-methylbenzylamine (DCMB), while the methylation activity of METTL7B is not affected despite the high sequence homology and similar substrate specificity. In this work, we utilize AlphaFold generated models, binding site analysis software, and *in silico* small molecule binding prediction approaches to identify several key unique residues in the active site of METTL7A that can explain its sensitivity to DCMB inhibition. We also use the His-SUMO-tag construct to generate single point mutations in the active site of METTL7A that will determine which residues are important for DCMB inhibition. This work is important to identify key differences in the active sites of METTL7A and METTL7B and will be utilized in the development of novel probe inhibitors that will be useful for identifying endogenous functions of these thiol methyltransferases.

P18 - GENERATION AND CHARACTERIZATION OF CYP2E1-OVEREXPRESSED HEPG2 CELLS

Nouf Alwadei, Mamunur Rashid, Devaraj Venkatapura Chandrashekar, Simin Rahighi, Ajay Sharma, and Reza Mehvar
Chapman University, United States

Purpose: Ischemia/reperfusion (IR) injury is the major cause of graft dysfunction and failure in vascular occlusion both during liver transplantation and liver surgery. The mechanisms of hepatic IR injury are not very well understood. Our aim was to generate and characterize a CYP2E1-overexpressed HepG2 cells to be used for *in vitro* investigations of the potential role of CYP2E1 in liver IR.

Methods: GFP-tagged CYP2E1 and empty vector (EV) plasmids were used for transfection of CYP2E1 and Control cells, respectively. Briefly, 50 to 70% confluent HepG2 cells (70 x10⁴ cells/well) were transfected with the plasmids using lipofectamine at a ratio of 2 µg:5 µl/well (DNA:Lipofectamine). Subsequently, the overexpressed clones were selected by the addition of G418 (1400 µg/ml). Overall, 6 clones from each group were isolated and grown separately. To confirm the integration of CYP2E1 and EV plasmids into HepG2 genome, the clones were characterized by the following methods: 1. The clone images were captured by fluorescence microscopy to calculate the percentage of transfected cells. 2. Real time PCR (RT-PCR) was conducted to detect CYP2E1 and GFP gene expression levels, which were normalized against the reference gene beta actin. 3. Western blot analysis was carried out to determine CYP2E1 and GFP protein contents in the microsomal fraction of these clones. 4. GFP ELISA assay was done using the total cell lysate protein of each clone to measure the GFP protein. 5. The CYP2E1 enzymatic activities of the clones were tested in the microsomal fractions, with chlorzoxazone as a substrate using Liquid Chromatography-tandem mass spectrometry (LC-MS/MS).

Results: Stable CYP2E1- and EV-overexpressed HepG2 cells were successfully developed. The average percentage of transfection in both groups was ~80%. After normalizing the data with beta-actin, RT-PCR showed that clones no. 3 and 6 in the EV group had the highest GFP gene expression level (Δ ct= -0.77 and -1.59, respectively), where the wild-type CYP2E1 gene expression level was low (Δ ct= 13.7 and 14.165, respectively). For CYP2E1 clones, clone no. 5 had the highest CYP2E1 and GFP gene expression levels (Δ ct= 2.83 & 2.67, respectively). Western blot analysis using anti-CYP2E1 antibody indicated that only CYP2E1 clone no.5 produced a significant GFP-tagged CYP2E1 protein band with a molecular weight (MW) of ~75 kD. The presence of CYP2E1-GFP band in clone no. 5 was also confirmed by anti-GFP antibody. Furthermore, EV clones no. 3 and 6 produced a GFP protein band with a MW of 27 kD. GFP ELISA indicated that GFP in EV clones was 10-folds higher than CYP2E1 clones. Microsomes from CYP2E1 clone no. 5 were catalytically active with chlorzoxazone as a substrate, whereas little or no activity was found with EV clones no. 6 and no. 3, respectively. The metabolite formation rate of CYP2E1 clone no. 5 was 150-fold higher (75 pmol/min/mg) than EV no. 6 (0.5 pmol/min/mg). **Conclusions:** CYP2E1- and GFP-overexpressed HepG2 cells were successfully generated and characterized. The CYP2E1 cells expressed CYP2E1-GFP, which was catalytically active. The developed cells will be used as a cellular model for *in vitro* hypoxia reoxygenation injury.

P19 - NEW MECHANISM OF THE LIVER CYTOCHROME P450 REGULATION VIA NMDA RECEPTOR

Ewa Bromek, Renata Puklo, Anna Haduch, Agnieszka Basińska-Ziobroń, and Władysława Daniel
Maj Institute of Pharmacology, Polish Academy of Sciences, Poland

Introduction: Cytochrome P450 (CYP) enzymes are members of the superfamily of heme-containing monooxygenases that play an important role in the oxidative metabolism of endogenous and exogenous compounds (drugs, toxins). Knowledge of the regulation of cytochrome P450 in the liver by drugs and toxic substances at the level of the hepatocyte is already broad, however, physiological regulation of CYP expression via the central nervous system has been investigated only in the last years. Our previous studies showed an important role of brain monoaminergic systems

(dopaminergic, noradrenergic and serotonergic) in the neuroendocrine regulation of liver cytochrome P450 expression. Recent results performed after repeated intraperitoneal administration of the antagonist of GluN2B subunit of NMDA receptor, the compound CP-101,606 with antidepressant properties, showed the decreased activity and expression of most liver CYP enzymes tested, which correlated with changes in serum hormone concentrations [1].

In order to distinguish between central and peripheral mechanisms of cytochrome P450 regulation by CP-101,606, in the present study we aimed at investigation whether the 5-day intracerebral treatment with the compound CP-101,606 affects liver cytochrome P450.

Methods: The experiment was carried out on male Wistar rats. Guide cannulas were implanted bilaterally into the lateral brain ventricles. The animals were given CP-101,606 (6, 15 or 30 µg) for 5 days. 2 h after the last dose, the rats were killed by decapitation. Liver microsomes were prepared including the procedure of washing. The activities of cytochrome P450 enzymes (CYP2A, 2B, 2C6, 2C11, 2D, 3A) were measured in liver microsomes, based on velocity of metabolic reactions, specific for individual CYP enzymes (HPLC with UV or fluorescence detection). Statistical significance was assessed using Student's t-test.

Results and Conclusion: The obtained results indicate that the NMDA receptor GluN2B subunit antagonist CP-101,606 given locally into the brain lateral ventricles affects the CYP activity in the liver. The 5-day treatment with CP-101,606 produced dose-dependent changes in the activity of investigated enzymes (CYP2A, CYP2D, CYP2C6, CYP2C11, CYP3A).

Thus, a new physiological mechanism of regulating liver CYP by the brain glutamatergic system has been revealed. These studies should help to predict and interpret the effect of new drugs acting via NMDA receptor on cytochrome P450. It is of great concern that apart from their targeted therapeutic effect, new drugs may affect different physiological processes including cytochrome P450 function. Therefore, different drug-drug interactions may occur in relation to cytochrome P450 regulation by NMDA receptor. Since the investigated CYP enzymes are also responsible for metabolizing endogenous substrates, new NMDA drugs may also interfere with the metabolism of physiologically important substrates (eg. steroids).

Acknowledgments: This study was financially supported by the OPUS 12 grant no 2016/23/B/NZ7/02283 (from the National Science Centre, Kraków, Poland) and by statutory funds from the Maj Institute of Pharmacology, Polish Academy of Sciences, Kraków, Poland.

References:

1. Bromek E, Haduch A, Rysz M, Jastrzębska J, Pukło R, Wójcikowska O, Danek PJ, Daniel WA. The Selective NMDA Receptor GluN2B Subunit Antagonist CP-101,606 with Antidepressant Properties Modulates Cytochrome P450 Expression in the Liver. *Pharmaceutics*. 2021;13(10):1643. doi: 10.3390/pharmaceutics13

P20 - PROTEIN/PROTEIN INTERACTIONS IN THE HUMAN CYTOCHROME P450 SYSTEM

Sarah D. Burris-Hiday and Emily Scott
University of Michigan, United States

A major superfamily of heme containing monooxygenases, cytochrome P450 enzymes metabolize a wide variety of substrates including xenobiotics, steroids, fatty acids, and vitamins. These membrane-bound enzymes require electrons for catalysis, and for 48 of the 57 human P450 enzymes, these electrons are delivered by the redox partner protein NADPH-cytochrome P450 reductase. The reductase FMN-containing domain directly binds the P450 enzyme proximal face, but little is known about the details of this transient protein-protein interaction. Studies herein utilize artificial fusions of the reductase FMN domain with either xenobiotic or steroidogenic P450 enzymes. These fusion enzymes favor a stable protein-protein interaction. The effect of the FMN domain localization with the P450 was measured for substrate and inhibitor binding and catalysis in the P450 active site. This active site is approximately 15-20 Å away from the protein-protein interaction site. Experiments were performed with the fusion enzymes alongside the respective isolated P450 isoform in order to assess the effects of the FMN domain on P450 function. These studies revealed that fusion of the FMN domain does not change the ligand binding mode. However, in the case of xenobiotic P450 enzymes, it does alter both the percent of the P450 population that binds ligand and the affinity for ligand binding, and it does so in an isoform and ligand dependent manner. Interestingly these effects were not significant for steroidogenic P450 enzymes. Furthermore, catalytic studies are being performed to probe the effects of FMN domain on substrate metabolism. Overall, these results demonstrate that the effect of the FMN domain on the P450 is both dependent on the P450 isoform and the ligand. This reveals intricate communication between the P450 active site and the surface of the P450 where the reductase FMN domain binds. This suggests that different P450 isoforms interact with the same reductase in unique ways. If this is the case, specific P450/reductase interactions could potentially be selectively disrupted to modulate the function of individual P450 isoforms in the treatment of disease.

P21 - APPLYING MECHANISTIC UNDERSTANDING TO DESIGN AWAY FROM CYP3A TIME-DEPENDENT INACTIVATION: ASSAY DEVELOPMENT, VALIDATION AND IMPLEMENTATION**Matthew Cerny**¹ and Drake Russell²¹Pfizer, United States and ²University of Washington, United States

Time-dependent inactivation (TDI) of cytochrome P450 3A (CYP3A) in early drug discovery continues to be a common occurrence. Despite its prevalence, currently available high-throughput assays do not inform on the mechanism(s) of inactivation. Additionally, lower throughput assays that do inform on mechanism(s) of inactivation are inadequate to permit rapid compound assessment. Therefore, currently employed approaches to avoid TDI are generally limited to empirical screening of analogs in high-to-moderate throughput CYP3A inactivation assays with the aim of identifying analogs with reduced or insignificant inactivation potential. Several mechanistic assays (e.g. metabolic intermediate complex, P450 loss, heme loss/heme adduct formation and protein adduct formation) are commonly utilized to identify the mechanism(s) of and structural features involved in CYP3A inactivation. The focus of this work is to develop high(er) throughput versions of the aforementioned assays to enable rapid identification of the mechanism(s) and structural features involved in inactivation. By understanding the mechanism of and structural features involved in TDI, medicinal chemists can remove or modify these features and thereby eliminate TDI. A summary of the development and validation of these assays will be presented along with an outline for their use in compound design.

P22 - IMPACT OF CASTRATION ON THE RENAL PROXIMAL TUBULAR VACUOLIZATION IN MALE MICE WITH DECREASED EXPRESSION OF THE NADPH-CYTOCHROME P450 REDUCTASEQing-Yu Zhang¹, **Xinxin Ding**², and Xiangmeng Wu¹¹University of Arizona College of Pharmacy, United States and ²University of Arizona, United States

The NADPH-cytochrome P450 reductase (CPR, or POR for P450 oxidoreductase) is the essential electron donor for microsomal P450 enzymes, which play important roles in the homeostasis of many endogenous compounds as well as in the biotransformation of xenobiotics. An age-dependent and male-specific vacuolization in the proximal tubules (PT) of the renal cortex was reported recently in Cpr-low mouse, which has substantially decreased CPR expression in all organs (Ding, L., Li, L., Liu, S., Bao, X., Dickman, K. G., Sell, S. S., Mei, C., Zhang, Q.-Y., Gu, J., and Ding, X.: Proximal tubular vacuolization and hypersensitivity to drug-induced nephrotoxicity in male mice with decreased expression of the NADPH-cytochrome P450 reductase. *Toxicol. Sci.*, 173:362–372, 2020). The Cpr-low mouse has elevated serum testosterone and progesterone levels. The aim of the present study was to test the hypothesis that the renal vacuolization in the male Cpr-low mouse was due to the elevation of circulating testosterone, but not progesterone. Castration surgery was performed in male Cpr-low mice at one month of age, to test whether the PT vacuolization can be prevented, or at four months of age, when PT vacuolization has already occurred in control Cpr-low mice, to see whether the existing PT vacuolization can be resolved; mice were examined for renal histopathology and serum hormone levels at six months of age. The results showed that castration at one month of age completely protected the kidney against PT vacuolization. Castration at four months of age also led to a large reduction of PT vacuolization, but some vacuoles were still present when observed at 6 months of age. A comparison of the extents of PT vacuolization in four-month-old Cpr-low mice and six-month-old Cpr-low mice that were castrated at four months of age showed that the castration did not remove existed PT vacuoles. Castration at either one or four months of age led to decreases in serum testosterone level from approximately 5 ng/mL to lower than 50 pg/mL when measured at 6 months of age, while not affecting serum progesterone levels, a result suggesting that the increase in testosterone, but not the increase in progesterone, was responsible for the PT vacuolization in male Cpr-low mice. These findings help us to understand the mechanisms underlying the PT vacuolization in mice with reduced CPR expression and to assess potential renal impacts of CPR deficiency in humans.

P23 - STRATEGIES AND CONSIDERATIONS FOR EVALUATING THE CONTRIBUTION OF CYTOCHROME P450 1A1 TO METABOLISM OF A THERAPEUTIC CANDIDATE**Sarah Glass**, Yuen Tam, Weixuan Chen, Kai Wang, Kevin Coe, and Laurie Volak*Janssen Research & Development, L.L.C., United States*

Cytochrome P450 (CYP) 1A1 is an aryl hydrocarbon receptor-inducible enzyme with variable expression in the liver and a range of extrahepatic tissues including the lung, skin, and gastrointestinal tract. While CYP1A1 has predominantly been associated with the metabolism of procarcinogens including polycyclic aromatic hydrocarbons, CYP1A1 has recently gained increased recognition for its potential importance in the metabolism of pharmaceutical drugs. A recent study identified 50% of compounds in a commercial drug library as CYP1A1 substrates with high clinical interindividual pharmacokinetic variability observed when CYP1A1 plays a major role in drug metabolic clearance (1). Despite the potential importance of CYP1A1 in drug discovery and development, the systems to characterize the contribution of CYP1A1 to drug metabolism are not as well defined as the major drug metabolizing CYPs (e.g., CYP3A). This present work aims to identify and validate a CYP1A1 chemical inhibitor for CYP phenotyping and to assess the application of recombinant CYPs and extrahepatic microsomes to study human and dog CYP1A1-mediated drug metabolism with

preclinical Compound A. Compound A was identified as a human CYP3A4 and CYP1A1 substrate in recombinant CYP phenotyping. To assess the contribution of CYP1A1 to hepatic metabolism, a newly developed chemical inhibition CYP phenotyping assay in human liver microsomes (HLMs) with CYP1A1 inhibitor hesperetin was utilized. Pharmacokinetic studies in beagle dogs with Compound A showed variable clearance and lower than anticipated exposure. Interindividual variability in canine liver CYP1A1 expression is reported to be high, like in human liver. We hypothesized that variability and extrahepatic CYP1A1 expression in dogs may contribute to the observed PK results. Studies with recombinant dog CYPs identified Compound A as a substrate for CYP1A1, 1A2, 1B1, and 3A12, with metabolism by CYP1A1 being very efficient (CL_{int} 14.8 μL/min/pmol). Preliminary results indicate that Compound A is also metabolized in dog intestine, lung, and kidney microsomes and human intestine microsomes. Studies with extrahepatic fractions in the presence of CYP inhibitors are in progress to confirm the involvement of CYP1A1 in this turnover. Ultimately, these studies illustrate a method to assess the contribution of CYP1A1 to drug metabolism in HLMs and highlight the remaining gaps in understanding the contribution of CYP1A1 to systemic metabolic clearance, including in pre-clinical species.

Reference:

1. Lang, D., Radtke, M., and Bairlein, M. (2019) Highly variable expression of CYP1A1 in human liver and impact on pharmacokinetics of riociguat and granisetron in humans. *Chem. Res. Toxicol.* 32, 6, 1115-1122.

P24 - HOW ABSORPTION, METABOLISM, DISTRIBUTION, AND EXCRETION CHARACTERISTICS OF ACT-1004-1239 GUIDE INVESTIGATION OF ITS DRUG-DRUG INTERACTION POTENTIAL

Christine Huynh¹, Swen Seeland¹, Carmela Gnerre¹, Henriette Meyer zu Schwabedissen², Jasper Dingemans¹ and Patricia N. Sidharta¹

¹*Idorsia Pharmaceuticals Ltd, Switzerland and* ²*University of Basel, Switzerland*

Cytochrome P450 (CYP) 3A4 is an enzyme involved in the metabolism of multiple xenobiotics and therefore is an important key player in drug-drug interactions (DDIs). ACT-1004-1239, is a potent and selective, first-in-class ACKR3/CXCR7 antagonist. To identify whether CYP3A4 is involved in the metabolism of ACT-1004-1239, CYP reaction phenotyping studies were performed *in vitro*. Moreover, a human absorption, metabolism, distribution, and excretion (ADME) study was conducted to elucidate the metabolic pathways of ACT-1004-1239. The *in vitro* studies consisted of two complementary approaches, i.e., 1) incubation with human liver microsomes in the absence and presence of CYP-specific chemical inhibitors and 2) incubation with several recombinant CYP enzymes. The human ADME study was integrated in a first-in-human study applying a microtracer approach. Six healthy male subjects were orally dosed with 1 μCi ¹⁴C-ACT-1004-1239 concomitantly with 100 mg non-radioactive ACT-1004-1239. Excreta (i.e., urine and feces) were collected up to 240 h post-dose and were analyzed for ¹⁴C-drug related material (i.e., mass balance) with accelerator mass spectrometry (AMS). Pooled excreta samples were used to construct radiochromatograms (i.e., metabolite profiling) using high-performance liquid chromatography (HPLC) together with AMS. Elucidation of metabolite structures was performed with HPLC coupled to high resolution mass spectrometry. Based on the *in vitro* studies, CYP3A4 was the main enzyme involved in the metabolism of ACT-1004-1239 to, almost exclusively, M1 accounting for 94% of total turnover. lesser extent via urine (14.5%). Metabolite profiling in feces and urine indicated that 25.1% of total excreta was eliminated as M1. Further, structure elucidation of other metabolites (with an abundance of >5% per matrix radiochromatogram) revealed the metabolites A1 (4.0%; in feces) and A2 (15.3%; in feces). Both originated from M1, indicating that the main elimination pathway of ACT-1004-1239 is catalyzed by CYP3A4. Other elimination pathways were through unchanged parent (15.3%; in urine and feces) and A3 (2.7%; in feces), while 21.6% were not assigned. Taken together, the main elimination pathway of ACT-1004-1239 in humans is via CYP3A4, emphasizing the need to conduct victim DDI studies. Since a proportion of the ACT-1004-1239 elimination pathway is unknown, a victim DDI study with a strong index inhibitor such as itraconazole can provide more insight on the actual dependency on CYP3A4.

P25 - A NOVEL PROTEOMICS PIPELINE FOR ADDUCT DISCOVERY FINDS RALOXIFENE EXPOSURE CAUSES NUMEROUS DRUG-PROTEIN ADDUCTS IN HUMAN P450S AND OTHER PROTEINS.

Alex Zelter¹, Michael Riffle¹, Michael Hoopmann², Daniel Jaschob¹, Guo Zhong¹, Robert Moritz², Michael MacCoss¹, Trisha Davis¹, and **Nina Isoherranen**¹

¹*University of Washington, United States and* ²*Institute of Systems Biology, United States*

Drug metabolism by cytochrome P450s (CYPs) in the liver can produce electrophilic metabolites that react with cellular nucleophiles including critical proteins. This can cause toxic side effects via formation of covalent protein adducts. Detection and characterization of such adducts is confounded as the mass, proteins and amino acids modified by reactive metabolites are often unknown and multiple metabolic pathways can lead to different protein adducts. Here we report the development of proteomics methods and software tools able to identify drug-protein adducts with no prior knowledge of their nature (1). We used these methods to identify numerous novel protein adducts in human liver CYPs and other

proteins resulting from the bioactivation of raloxifene by CYP enzymes. Three sets of samples were incubated with raloxifene or vehicle only control: (a) purified CYP3A4 plus rat P450 reductase; (b) insect cell microsomes expressing one CYP (either CYP3A4, CYP3A5, CYP2C8, CYP2C9 or CYP2C19) plus human P450 reductase and cytochrome b5; and (c) human liver microsomes (HLMs). Samples were analyzed via LC-MS/MS and data dependent acquisition (DDA) data were searched using our novel open search algorithm, called Magnum or using the closed search algorithm, comet. Treatment specific adducts were highlighted using adduct discovery tools built into our proteomics data visualization platform, called Limelight. Data independent acquisition (DIA) data were acquired in parallel, and transitions of interest were quantified using Skyline. Open searching of raloxifene treated versus untreated CYP3A4 was performed using Magnum. A Limelight analysis of the resulting data found 471.15 Da as the mass most enriched in treated samples. This mass agrees with previously published work. In contrast to previous publications, which report just two raloxifene-protein adducts on CYP3A4 (Cys239 and Tyr75), we identified and localized 22 new raloxifene adducts in CYP3A4 and P450 reductase. Adducted amino acids included cysteine, tryptophan and tyrosine residues. Comet searching of raloxifene treated versus untreated HLMs resulted in the discovery of numerous treatment specific protein adducts in CYPs and in many other liver proteins including important enzymes such as GSTs and ADHs. Similar experiments with insect cell microsomes expressing individual CYPs verified the presence of multiple raloxifene adducts in specific CYPs and in P450 reductase. These adducts have not been observed before and indicate a previously unsuspected abundance and diversity of raloxifene induced drug-protein adducts in human liver proteins. We analyzed the DIA data corresponding to the identified adducts and quantified raloxifene-specific signals in individual HLM and supersome samples. Our work suggests that metabolic activation of raloxifene by CYP enzymes results in adduct formation with multiple proteins in the human liver. The methods and software presented here can be used to discover and quantify xenobiotic-protein adducts with no prior knowledge of the adduct mass or the adducted peptides or proteins. (1) Riffle et al. Discovery and visualization of uncharacterized drug-protein adducts using mass spectrometry. *Anal. Chem.* 2022, 94, 8, 3501–3509.

P26 - ABSTRACT WITHDRAWN

P27 - EVALUATING THE EFFECTS OF Sceletium TORTUOSUM EXTRACT ON CYP 2C9 IN LIVER MICROSOMES OF FLINDERS LINE SENSITIVE RATS

Makhotso Lekhooa, Nicholas Mashego, and Rose Hayeshi
North West University, South Africa

Sceletium Tortuosum is a South African plant with promise in the treatment of neuropsychiatric diseases due to its multiple mechanisms of action (1). Usage of herbal medicines as adjunctive treatment has increased the risk of drug-herb interactions due to their co-administration with other drugs. However, there is no information on the effect of Sceletium Tortuosum on Cytochrome (CYP) 2C9. The CYP 2C9 is responsible for 15 - 20 % of drug (i.e., Warfarin, Phenytoin, Losartan and non-steroidal anti-inflammatory drugs etc) metabolism (2). Hence, the study aimed to evaluate the effects of oral treatment with Sceletium Tortuosum on the CYP 2C9 enzyme in male Flinders Line Sensitive (FSL) rats. Livers were obtained from a previous study, where male FSL rats were treated daily over 14 days with either saline or a 3-tier dose (10, 25 and 30 mg/kg) of Sceletium Tortuosum extract. Microsomal fractions were prepared by ultracentrifugation and protein concentration was determined by the Bradford method with bovine serum albumin as the standard (3;4). Measurement of CYP 2C9 activity was adapted from previous studies (5;6). The reaction mixture contained 0.1M sodium phosphate buffer, 0.25 mg/ml of microsomal protein, water and 7-methoxy-4-trifluoromethylcoumarin (MFC) as substrate. Pre-incubation was 10 minutes at 37 °C and the reaction was initiated by the addition of NADPH, followed by 30 minutes of incubation. Reactions were terminated with 80 % acetonitrile and 20 % 0.5M Tris solution. Fluorescence measurements (Ex = 405 nm; Em = 535 nm) were measured with a spectrophotometer (SpectraMax® Paradigm, USA). Michaelis-Menten equation was used to determine the Km of the substrates and statistical analysis was done in Graph Pad, Prism. Liver protein concentrations ranged from 17.5 to 51.7 mg/ml. The substrate km was 20 µM. CYP 2C9 was not induced after treatment with 25 and 30 mg/kg Sceletium Tortuosum in FSL rats over 14 days. In conclusion, the extract did not induce CYP 2C9 enzyme in FSL rat liver, hence there are no expected drug-herb interactions.

References:

1. Gericke J., Lekhooa M., Steyn S., Viljoen A., Harvey B. An acute dose-ranging evaluation of the antidepressant properties of Sceletium tortuosum (Zembrin®) versus escitalopram in the Flinders Sensitive Line rat. *Journal of Ethnopharmacology*; 2022; 284 (114550): 2.
2. Van Booven D, Marsh S, McLeod H, Carrillo M, Sangkuhl K, Altman R. Cytochrome P450 2C9-CYP2C9. *Pharmacogenet Genomics*; 2011; 20 (4) 277.
3. Pelkonen O, Turpeinen M, Hakkola J, Honkakoski P, Hukkanen J, Raunio H. Inhibition and induction of human cytochrome P450 enzymes: current status. *Archives of toxicology*; 2008; 82(10): 670.
4. Damre A, Mallurwar R, Behera D. Preparation and characterization of rodent intestinal microsomes: comparative assessment of two methods. *Indian journal of pharmaceutical sciences*; 2009; 71(1):75.

5. Bapiro E, Egnell C, Hasler A, Masimirembwa C. Application of higher throughput screening (HTS) inhibition assays to evaluate the interaction of antiparasitic drugs with cytochrome P450s. *Drug Metabolism and Disposition*; 2001; 29(1):30-35.
6. Hayeshi, R. H. 2004. *In vitro* interactions of natural products and antiparasitic drugs with drug metabolising enzymes and transporters. University of Zimbabwe. (Thesis – PhD)

P28/S1.4 - STRUCTURE OF CYP8B1 WITH A RATIONALLY DESIGNED CYP8B1 INHIBITOR: PROVIDING DIRECTIONS FOR INHIBITOR OPTIMIZATIONS

Jinghan Liu¹, Emily Scott¹, Francis Yoshimoto², and Samuel Offei²

¹University of Michigan, United States and ²University of Texas, San Antonio, United States

Human cytochrome P450 8B1 (CYP8B1) is involved in the conversion of cholesterol to bile acids. CYP8B1 hydroxylates the steroid ring at C12 en route to production of the bile acid, cholic acid(1). Thus, this enzyme controls the ratio of cholic acid to another bile acid, chenodeoxycholic acid. The ratio of these two bile acids controls the overall hydrophobicity of the bile pool and bile acid signaling(2). Knockout studies implicated CYP8B1 as a good drug target for nonalcoholic fatty liver disease(3) and type 2 diabetes(4). However, the roles of CYP8B1 in both normal physiology and disease states are still poorly understood and no selective inhibitors have yet been developed. Herein, three rationally designed inhibitors for CYP8B1 were synthesized through incorporation of a pyridine at C12 of the C ring of the steroid, anticipating interaction between the active site heme iron of CYP8B1 and the pyridine nitrogen of the inhibitor. However, when changes in CYP8B1 heme absorbance were used to probe inhibitor binding, no spectral shifts occurred, suggesting no direct heme binding. Despite inhibitor 1 treatment showing attenuation of obesity-associated glucose intolerance in mice(5), none of the inhibitors significantly inhibited CYP8B1 metabolism of its normal substrate. A 2.65 Å X-ray structure of CYP8B1 revealed that inhibitor 2 binds in an access channel between the protein surface and active site between F, B' and A helices, rather than in the active site proper. Structural analysis suggested that a tryptophan (W281) in the active site located directly over the heme iron (Fe-Trp 8.2 Å) may prevent active site binding by sterically restricting inhibitor access and orientation for Fe binding. This hypothesis was confirmed in that all three inhibitors bound to the CYP8B1 W281F mutant with type II spectral shifts indicative of pyridine nitrogen-Fe interaction. These results are redirecting the design of new inhibitors intended to promote better understanding of the role of CYP8B1 inhibition in normal physiology and serve as the basis for future treatments for nonalcoholic fatty liver disease and type 2 diabetes.

References:

- 1 Staels, B. & Fonseca, V. A. Bile acids and metabolic regulation: mechanisms and clinical responses to bile acid sequestration. *Diabetes Care* 32 Suppl 2, S237-245, doi:10.2337/dc09-S355 (2009).
- 2 Chiang, J. Y. Recent advances in understanding bile acid homeostasis. *F1000Res* 6, 2029-2029, doi:10.12688/f1000research.12449.1 (2017).
- 3 Chevre, R. et al. Therapeutic modulation of the bile acid pool by Cyp8b1 knockdown protects against nonalcoholic fatty liver disease in mice. *Faseb J* 32, 3792-3802, doi:10.1096/fj.201701084RR (2018).
- 4 Kaur, A. et al. Loss of *Cyp8b1* Improves Glucose Homeostasis by Increasing GLP-1. *Diabetes* 64, 1168-1179, doi:10.2337/db14-0716 (2015).
- 5 Chung, E. et al. A synthesis of a rationally designed inhibitor of cytochrome P450 8B1, a therapeutic target to treat obesity. *Steroids* 178, 108952, doi:10.1016/j.steroids.2021.108952 (2022).

P29 - ASSAY VALIDATION OF A TARGETED IMMUNOAFFINITY PROTEOMICS ASSAY FOR ROUTINE ASSESSMENT OF DRUG METABOLIZING ENZYMES FOR THE ANALYSIS OF *IN VITRO* ENZYME INDUCTION

Helen Hammer, Andreas Steinhilber, Hannes Planatscher, and **Oliver Poetz**

SIGNATOPE GmbH, Germany

In vitro analyses of cytochrome P450 induction by drug candidates are of great importance for the evaluation of drug-drug interactions. mRNA expression analyses in cultured human hepatocytes are required by regulatory authorities. However, mRNA only indirectly reflects enzyme concentration and activity. Here, we show the results of a study according to FDA's Bioanalytical Method Validation Guidance for Industry.

We have developed and validated an immunaffinity LC-MS/MS assay for the simultaneous quantification of CYP isoforms 1A2, 2B6, 2C8, 2C9, 2C19, and 3A4 in primary human hepatocytes. The cells or tissue samples are lysed and proteolytically digested. Immunaffinity enrichment (IA) of proteotypic peptides and isotopically labeled standards is then performed, followed by LC-MS analysis for protein quantification. The multiplex assay is capable of quantifying CYPs from less than 10 µg protein extract. The validation data demonstrate that quantification of cytochrome P450 (CYP) enzyme protein levels by IA-LC-MS/MS is suitable for routine assessment of enzyme induction from hepatocyte cultures on 96-well plates on protein level.

P30 - ABSTRACT WITHDRAWN**P31 - GLOBAL VERSUS TARGETED PROTEOMICS FOR QUANTIFICATION OF DMET PROTEINS IN HUMAN LIVER, KIDNEY, AND INTESTINE**

Dilip Kumar Singh, Deepak Ahire, Guihua Yue, and Bhagwat Prasan
Washington State University, United States

Accurate quantification of drug metabolizing enzyme and transporter (DMET) proteins is a prerequisite for the *in vitro* to *in vivo* extrapolation (IVIVE) of drug metabolism and transport. The conventional targeted DMET proteomics requires custom synthesis of stable isotope labeled surrogate peptides as calibrators and assumes 100% trypsin digestion efficiency [1]. Label- and standard-free total protein approach (TPA) is emerging as a better alternative for protein quantification that has a potential to address these limitations [2]. In this study, we applied TPA approach for protein quantification in human liver, kidney and intestine, and compared the abundances of DMET proteins generated by TPA approach with the previously collected targeted DMET proteomics data.

Commercially available human liver microsomes (HLM, pool of n=150), kidney microsomes (HKM, pool of n=8), and intestinal microsomes (HIM, pool of n=15) were digested by trypsin. The global proteomics data were acquired using nanoLC coupled with Q-Exactive HF mass spectrometer in the data-independent acquisition (DIA) mode and analyzed using MaxQuant. TPA data (triplicates) of DMET proteins were compared with previously collected targeted proteomics data.

Global proteomics analysis identified 3565, 3930, and 3584 DMET proteins in HLM, HKM and HIM, respectively. Out of these, a total of 2735 proteins were common in all three tissues, and 440, 385, and 163 proteins were common in HLM/HKM, HKM/HIM, and HLM/HIM, respectively. Whereas, 227, 370, and 301 proteins were uniquely detected in HLM, HKM, and HIM, respectively. Amongst the quantitative proteins (detected in all triplicates), a total of 25 cytochrome P450s (CYPs) and UDP glucuronosyltransferases (UGTs) were identified in HLM, HKM and HIM. CYP2C19, UGT1A6, UGT1A9, UGT2A3, UGT2B7, and UGT2B17 were detected in all three tissues, and CYP2B6 was detected in HLM/HKM, UGT2A1 was detected HKM/HIM, and CYP2C9, CYP3A4, CYP3A5, UGT1A1, and UGT1A4 were detected in HLM/HIM, respectively. HLM expressed the following unique enzymes: CYP1A2, CYP2A6, CYP3A7, CYP2C8, CYP2C18, CYP2D6, CYP2E1, CYP2J2, UGT1A3, UGT2B4, UGT2B10, and UGT2B15. Most of common CYPs and UGTs were higher in HLM, except UGT1A9 and UGT2A3 in HKM, and UGT2A3 and UGT2B17 in HIM. In general, the abundance values of DMET proteins were 2-4-fold higher using TPA approach as compared to the targeted proteomics data perhaps due to the limitation of trypsin digestion inefficiency in the latter. The relative rank order of different DMET proteins was comparable when analyzed using TPA versus targeted data.

We applied and validated the label-free TPA approach against the targeted proteomics data for the quantification of DMET proteins in liver, kidney, and intestine. TPA offers distinct advantages for protein quantification as it doesn't require peptide standards as calibrators and the normalization by the total MS response accounts for trypsin digestion variability. We expect that the use of this versatile label-free approach across laboratories will increase the availability of more accurate and comprehensive protein abundance information, which will enhance the IVIVE of drug metabolism and transport.

References:

1. Ahire, D. et al. (2022) *Pharmacol Rev*, 74, 769-796.
2. Wiśniewski, J. R. et al. (2014) *J Proteomics*, 109, 322-331.

P32 - CHARACTERIZATION OF DRUG-METABOLIZING ENZYMATIC ACTIVITIES IN THE HEPATOCYTES ISOLATED FROM THE CHIMERIC TK-NOG MICE WITH HUMANIZED LIVERS

Shotaro Uehara¹, Yuichiro Higuchi¹, Nao Yoneda¹, Norie Murayama², Hiroshi Yamazaki², and Hiroshi Suemizu¹
¹*Central Institute for Experimental Animals, Japan* and ²*Showa Pharmaceutical University, Japan*

The cryopreserved primary human hepatocytes (PHH) have been considered the gold standard for assessing drug metabolism and toxicity. However, the use of this model is limited due to the limited number of hepatocytes in the same donor. In this study, we isolated the hepatocytes (Hu-liver cells) from the immunodeficient TK-NOG mice transplanted with five different PHH by *in vivo* human hepatocyte repopulation technology and evaluated their drug-metabolizing competence. The Hu-liver cells from five different PHH comprised 96% pure human hepatocytes, 84% cell viability, and high cell yield (average 1.2×10^8 cells/mouse). The enzymatic activities of phase I and phase II enzymes, namely phenacetin O-deethylation (CYP1A2 activity), bupropion hydroxylation (CYP2B6 activity), diclofenac 4'-hydroxylation (CYP2C9 activity), omeprazole 5-hydroxylation (CYP2C19 activity), S-mephenytoin 4'-hydroxylation (CYP2C19 activity), metoprolol O-demethylation (CYP2D6 activity), midazolam 1'-hydroxylation (CYP3A4/5 activity), T-1032 N-oxygenation (CYP3A5 activity), 7-hydroxycoumarin-glucuronidation (Uridine 5'-diphospho-glucuronosyltransferase activity), and 7-

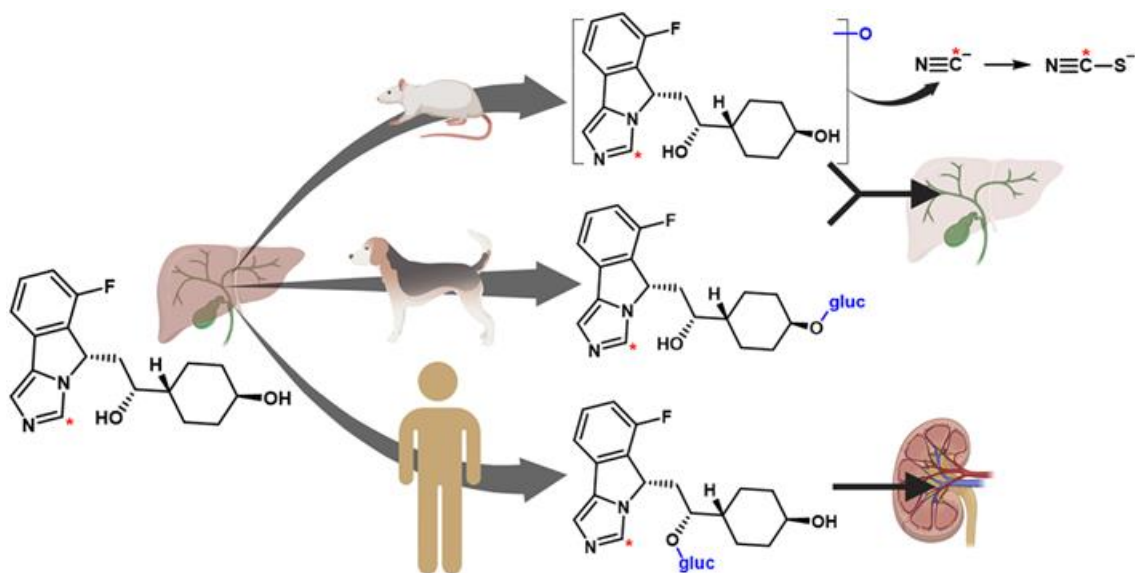
hydroxycoumarin sulfation (Sulfotransferase activity) in the Hu-liver cells were analyzed. Each enzymatic activity in the Hu-liver cells was comparable to the drug-metabolizing activities in PHH reported previously. The drug-metabolizing enzymatic activities in the Hu-liver cell suspensions showed small variability (coefficient of variation of <20%) among the intra-lot (among vials from the same mouse) and intra-batch (among vials from separate mice) from the same PHH. Notably, the Hu-liver cells from the PHH genotyped as CYP3A5*3/*3 (poor expressers) showed significantly lower T-1032 N-oxygenation rates than those from the PHH harboring the CYP3A5*1 allele (extensive expressers, $p < 0.01$). Indeed, the low expression level of CYP3A5 mRNA in the Hu-liver cells from the PHH was genotyped as CYP3A5 *3/*3. Overall, the Hu-liver cells exhibited robust and reproducible drug-metabolizing enzymatic activities based on the gene expression levels of the drug-metabolizing enzymes. These results suggest that the stable and sustainable Hu-liver cells are a valuable experimental liver cell model for studying drug metabolism.

P33 - ABSTRACT WITHDRAWN

P34 - AME OF GDC-0919 IN RATS AND DOGS: UNEXPECTED CYANIDE RELEASE FROM IMIDAZO[1,5-A]ISOINDOLE AND SPECIES DIFFERENCES IN GLUCURONIDATION

Shuai Wang, Shuguang Ma, Eugene Chen, Jing Wang, Cyrus Khojasteh, and Laurent Salphati
Genentech, United States

GDC-0919 (navoximod) is a small molecule inhibitor of indoleamine 2,3-dioxygenase 1 (IDO1) developed for alleviating T cell immunosuppression in cancer patients. This study describes the absorption, metabolism, and elimination of GDC-0919 in rats and dogs and the comparison with human results. In human, GDC-0919 was mainly cleared through glucuronidation to M28, which was the major metabolite in circulation (58%) and urine (60%). While in dogs and rats, GDC-0919 and its metabolites were mainly eliminated through biliary excretion (>65%). An unexpected cyanide release and species differences in glucuronidation were investigated and are discussed. In rats, the unexpected thiocyanate metabolite M1 was captured as the major circulating metabolite (30%). The novel cyanide release is proposed to have occurred via oxidation on the fused imidazole ring, which led to ring opening and rearrangement. A major chiral inversion metabolite M51 was also captured and was likely formed through reduction of a ketone intermediate metabolite by aldo-keto reductase. In dogs, glucuronidation was the major clearance mechanism. Interestingly, a different glucuronide M19 represented the major metabolite in circulation (52%) and excreta (78%) in dogs. The striking difference in glucuronidation can likely be explained by the species difference in UGT1A9, which was mainly responsible for M19 formation in human. The differences in the metabolism and elimination observed *in vivo* were recapitulated qualitatively with liver microsomes, suspended hepatocytes and sandwich cultured hepatocytes.



P35 - GENERATION OF A CREATINE KINASE BRAIN-TYPE KNOCKOUT MOUSE MODEL TO STUDY TENOFOVIR BIOACTIVATION**Colten Eberhard** and Namandjé Bumpus*Johns Hopkins University School of Medicine, United States*

Tenofovir-diphosphate (TFV-DP) is the pharmacologically active metabolite of tenofovir (TFV), which is formulated as a prodrug and prescribed for the treatment and prevention of HIV infection. TFV-DP is formed intracellularly by sequential phosphorylation of TFV by nucleotide kinases. Previous work in our group has identified kinases that catalyze the formation of TFV-DP in peripheral blood mononuclear cells, colon and vaginal tissues. However, tenofovir activating enzymes in other tissues have yet to be identified. Recently, we have determined that creatine kinase brain-type (CKB) can phosphorylate tenofovir-monophosphate (TFV-MP) to TFV-DP, *in vitro*, to a similar extent as creatine kinase muscle-type, a known TFV activating enzyme. With this, we investigated whether naturally occurring mutations in CKB can disrupt the formation of TFV-DP, in turn potentially improving our understanding of the interindividual variability of TFV efficacy. To do this, fifteen naturally occurring mutations were chosen and mutant proteins were recombinantly expressed. Purified proteins were incubated with phosphocreatine and TFV-MP, and resulting metabolites were detected using ultra-high performance liquid chromatography tandem mass spectrometry (uHPLC-MS). Eight mutations (C74S, R96P, S128R, R132H, R172P, R236Q, R292Q, and H296R) significantly diminished the formation of TFV-DP, *in vitro*. Subsequent kinetic analyses investigating the reverse canonical reaction (ATP dephosphorylation) showed that five of these mutations (R96P, R132H, R236Q, R292Q, and H296R) resulted in a catalytic efficiency less than 20% of WT, as a result of increases in K_m . Additionally, differential scanning fluorimetry revealed that five mutations with reduced TFV-DP formation (C74S, R96P, R132H, R172P, and R236Q) displayed double peaks or shouldering in their melting curves, suggesting mutation-induced local domain instabilities. From this, we hypothesize that mutations that decrease catalytic efficiency or disrupt thermal stability of CKB may impact the formation of TFV-DP. To determine the *in vivo* contribution of CKB in TFV-DP formation, we established a CRISPR-mediated *Ckb* knockout mouse model, on the C57BL/6J background, by introducing two deletions (55bp and 28bp) into the gene. Interestingly, while protein knockout has been confirmed by immunoblot and proteomic analyses of colon lysates, gene expression of *Ckb* is unchanged in the colon of knockout animals. At the mRNA level, Sanger sequencing of cDNA confirmed a new 3' splice site in exon 2 and an out-of-frame start codon. If this mRNA is translated, a protein of just five amino acids would be produced. The *Ckb* knockout mice are fertile, with an average litter size of 7.2, and display expected male/female frequencies. Additionally, the weight gained by knockout mice does not differ from the weight gained by wild-type mice descended from the same CRISPR founder, based on measurements through 6 months of age. These *Ckb* knockout mice that we have established will provide a unique model to investigate TFV disposition.

P36 - EVALUATION OF FRACTION UNBOUND VALUES OVER VARYING CONCENTRATIONS OF CNS COMPOUNDS IN BRAIN, BLOOD, AND PLASMA PROTEIN BINDING**Richard Grater**, Mukesh Lulla, and Parrick Trapa*Biogen, United States*

O-linked N-Acetylglucosamine (O-GlcNAc) is implicated in various diseases including cancers, diabetes, cardiac dysfunction, and neurodegenerative diseases¹. Pharmacological inhibition of O-GlcNAcase (OGA), the sole enzyme that removes O-GlcNAc, reproducibly reduces the progress of neurodegeneration in various Alzheimer's disease (AD) mouse models manifesting either tau or amyloid pathology. Independent pharmacological proof-of-biology experiments have demonstrated that chronic OGA inhibition dramatically reduced tau pathology in brain and improved functional deficits in preclinical models of tauopathy. In preclinical studies of OGA inhibitors, on-linear pharmacokinetics were observed, most noticeably the decrease in terminal half-life with increasing dose. Also noticed was the concentration dependent partition coefficient (K_p) in rodent's brains, with several fold more K_p at lower plasma concentrations. The purpose of this investigation was to determine whether changes of the concentration of the test articles (Compounds A and B) will also affect the fraction unbound (f_u) values while assessing the protein binding (brain, blood, and plasma) in the rat and human. Both test articles are CNS small molecule compounds. The concentrations of the analytes assessed in this experiment were 10, 30, 100, 300, and 1000 nM. Rapid Equilibrium Dialysis (RED) device was utilized to assess the protein binding for all matrices and incubated for 6 hours. The samples were analyzed by multiple reaction monitoring on a multiplexing LC-LX4 system (Thermo - Waltham, MA) coupled to an API-5500 mass spectrometer (Sciex - Framingham, MA). The results indicated a dramatic rise in f_u values with increasing concentration of both test articles, especially in the brain and a much lesser extent in the blood. There was not much of correlation in f_u and test article concentrations in plasma PB. This data suggests that there is much more binding to the OGA receptors in brain at lower concentrations than blood and plasma for both rat and human.

Reference:

1. Zhu Y, Shan X, Safarpour F, et al. Pharmacological Inhibition of O-GlcNAcase Enhances Autophagy in Brain through an mTOR-Independent Pathway. *ACS Chem Neurosci*. 2018;9(6):1366-1379. doi:10.1021/acscchemneuro.8b00015

P37 - INVESTIGATING THE IMPACT OF BLOOD COLLECTION METHODS AND ETHNICITY ON HUMAN PLASMA PROTEIN BINDING

Barry Jones¹ and Jennifer Vance²

¹Pharmaron, United Kingdom and ²Pharmaron, United States

Background: Plasma protein binding (PPB) plays an important role in the distribution, metabolism and pharmacokinetics (PK) of a potential drug. Binding to plasma proteins limits the unbound fraction (Fu) of drugs that can enter the tissue and be metabolized. A two-fold error in the *in vitro* Fu measurement can significantly affect the estimation of the *in vivo* metabolism of drugs. Therefore, measuring the PPB data accurately is critical for evaluating drug safety and efficacy. Blood bags and vacutainers are commonly used for blood collection and storage. However, the PPB measurements often vary between the blood bag- and vacutainer-collected human blood. This could be caused by the plasticizer in the blood bags leaching into the blood and disrupting the binding of drugs to α 1-acid glycoprotein (AAG). Another key factor that impacts the PPB values is the ethnicity of the blood donors. Studies have reported the ethnic differences in PPB results. In this study, we systematically investigated the effects of blood collection methods and ethnicity on human PPB data for drugs.

Methods: We used the equilibrium dialysis method to investigate the *in vitro* protein binding of 15 drugs in human plasma collected by BioIVT vacutainer, local vacutainer, or BioIVT blood bag from Asian or Caucasian & Melanoderm volunteers. The test drugs (1 μ M) were incubated (37°C, 5% CO₂) in plasma and dialyzed against phosphate-buffered saline (PBS) for 6 hours. The concentrations of drugs in plasma and PBS were analyzed by UPLC-MS/MS.

Results: We found that the Fu values are higher (~2 folds) in the blood bag-collected plasma than the vacutainer-collected plasma for drugs with a higher bound fraction to AAG. There is little difference in the Fu values when tested in plasma from different ethnic groups.

Conclusion: The plasticizers in plasma collected by blood bag showed a significant effect on the PPB determination of AAG-binding compounds. Blood collected using vacutainers (without plasticizers) is preferred for the collection of blood for the protein binding experiment. Ethnic differences appear, at least in this study, to have little influence on the protein binding data for most compounds.

P38 - BIODISTRIBUTION OF TOPOTECAN-LOADED POLYMERIC NANOPARTICLES FOR THE LACTONE AND TOTAL TOPOTECAN FORMS

Yong-Bok Lee, Ji-Hun Jang, and Seung-Hyun Jeong

College of Pharmacy, Chonnam National University, South Korea

Topotecan hydrochloride (TOPO HCl) is an anticancer drug that has been actively applied to the treatment of several cancer types, including ovarian cancer and lung cancer, through topoisomerase inhibition. Challenging aspects in the clinical efficacy of TOPO include limited bioavailability (approximately 20%) and conversion to the inactive (carboxylated) form by facile hydrolysis of the active site (lactone form). Therefore, in an effort to improve the clinical efficacy of TOPO, exploration of additional administration routes or formulation attempts were required. The purpose of this study was to determine the in-vivo pharmacokinetics and biodistribution characteristics of nanoformulated TOPO. To quantitatively confirm these characteristics, the lactone form and the total form reversibly converted (to lactone form) from the carboxyl form using acid were analyzed separately. In addition, we tried to improve the bioavailability and drug delivery to target tissues (brain, lungs, and lymphatic system) compared to the conventional free TOPO HCl through nanoformulation of TOPO. Preparation of nanoformulation (as TOPO-loaded nanoparticles) was performed by encapsulating TOPO in poly(lactic-co-glycolic acid) [PLGA] polymer through double emulsion solvent evaporation method. To quantitatively and qualitatively confirm the pharmacokinetics and biodistribution characteristics of TOPO-loaded nanoparticles, it was applied to animal experiments on rats. Also, quantitative analysis of lactone and total forms was performed in in-vitro release test and in-vivo experiments to confirm the stabilization of the hydrolysis of TOPO and the duration of the active form. TOPO-loaded nanoparticles showed distinctly different pharmacokinetics and biodistribution properties from free TOPO HCl. TOPO-loaded nanoparticles maintained TOPO in an active form in the body for a longer time than free TOPO HCl, and the same trend was confirmed in the in-vitro release test. Both oral and intravenous administration of TOPO-loaded nanoparticles showed 1.5 – 4 times lower active site hydrolysis than free TOPO HCl. In a quantitative assessment, the drug delivery efficiencies of TOPO-loaded nanoparticles to brain, lungs, and lymphatic tissues were approximately 2 – 10 times higher than those of free TOPO HCl. Even in qualitative imaging of in-vivo tissues, the distribution of TOPO-loaded nanoparticles to target tissues was higher than that of free drug. The results of this study strongly suggest that

nanoformulation can improve the maintenance of active form of TOPO in the body and effective delivery to target tissues compared to conventional free drug.

P39 - AMS-ENABLED HUMAN ADME STUDY OF THE FGFR INHIBITOR DERAZANTINIB

Karine Litherland¹, Elwin Verheij², Mathias Wind¹, Franziska von Siebenthal¹, Gerda Sanvee¹, Agnes Kaelin Aebi¹, Rianne de Lig², Esther van Duijn², Wouter Vaes², Marc Engelhardt¹, Ray Cooke³, and Nand Singh⁴

¹Basilea Pharmaceutica International Ltd, Allschwil, Switzerland, ²TNO Biomedical Health, Netherlands, ³Pharmaron, United Kingdom, and ⁴Quotient Sciences, United Kingdom

Background: Derazantinib is an oral FGFR inhibitor under clinical development for patients with intrahepatic cholangiocarcinoma, urothelial cancer, and gastric cancer. As part of the development program of derazantinib, an open-label, parallel group clinical study was conducted to assess the absorption and disposition of derazantinib after intravenous (IV) and oral administrations. Accelerator mass spectrometry(AMS)-enabled and LC-MS/MS analysis were performed for mass balance, routes of excretion and elimination, absolute oral bioavailability, and metabolism of derazantinib in healthy male subjects. Material/Methods: In Part 1, six subjects received a single oral dose of 300 mg derazantinib, followed 8 hours later by an IV microdose of 100 µg [14C]-derazantinib (≤9.25 kBq). In Part 2, six subjects received a single oral dose of 300 mg [14C]-derazantinib (≤1.9 MBq). Subjects were kept in the clinic until 22 days post-dose and then returned at regular intervals up to Day 49. Blood, urine, and feces samples were collected throughout the study for assessment of total radioactivity, derazantinib, its acid metabolite, and metabolite profiling. AMS was used to determine total radioactivity concentrations in plasma, urine and feces and [14C] derazantinib concentrations in plasma. For the quantification and characterization of metabolites in plasma and feces, samples were fractionated using an ultra-performance liquid chromatography (UPLC) system that was coupled to a high-resolution mass spectrometer (hrMS). Due to the low 14C levels in plasma pools from Part 1 of the study, a large volume of injection (80 µL) was required to load an adequate amount of 14C onto the column and a 2D-UPLC setup was developed to profile plasma pool sample at approximately 1 mBq total RA on column. Results: Following administration of 100 µg [14C]-derazantinib via IV infusion, an average of 97% of the radioactivity administered was recovered in excreta over 49 days. The majority of total radioactivity (90%) was recovered in feces indicating that hepatic excretion was the main route of elimination following IV administration. Following single oral administration of 300 mg [14C]-derazantinib, an average of 83% of the radioactivity administered was recovered in excreta over 49 days. The majority of total radioactivity (76.5%) was recovered in the feces as derazantinib. Only 10.8% of the fecal recovery was excreted in the first 72 h post-dose suggesting that hepatic excretion was the main route of elimination following oral dosing of derazantinib. The fraction absorbed was above 60% and the oral bioavailability of derazantinib was 56%. Unchanged derazantinib was the major circulating component in plasma after oral and IV dosing, representing at least 48% of the 14C-radiochromatogram. The acid metabolite and an oxidized glucuronide metabolite of derazantinib were the only other circulating components contributing to more than 10% of total radioactivity (approximately 11% and 12% after oral administration, respectively). Conclusion: Following a 300 mg oral dose administration, derazantinib is well absorbed with an absolute bioavailability of 56%. Hepatic excretion was the main route of elimination following IV and oral dosing of [14C]-derazantinib. A new approach combining 2D-UPLC and AMS analysis was used successfully to profile low level of 14C in plasma pool samples.

P40 - A DECADE OF HUMAN ADME AT QUOTIENT: REVIEWING KEY STUDY DESIGN VARIABLES AND OUTCOMES

Iain Shaw, Gareth Whitaker, and Katie Stuart
Quotient Sciences, United Kingdom

Introduction: With a draft FDA guidance (1) issued and under review there is considerable interest in the design and conduct of human mass balance studies. Conventional human mass balance (ADME) studies are well understood study designs which help drug companies generate data to support drug development and registration typically requiring a radioactive dose of 100µCi and the utilisation of liquid scintillation counting (LSC) and mass spectrometry (LC-MSMS). Over the last ten years study designs have evolved to address the challenges presented by new drug candidates, to benefit from new technologies and with a better understanding of how to interpret the data that can be generated from the analysis of collected samples.

Methods: This poster will describe various approaches to the conduct of human ADME studies conducted at Quotient Sciences that were driven by the characteristics of the drugs being tested:

1. Studies with long half-life molecules where it was not practical to have the volunteers resident for a sufficient time to achieve a >90% recovery.
2. Studies with potent drugs and cytotoxic molecules where the drug dose was limited such that conventional methods could not be used to fully describe the metabolite characterisation period of the study for all matrices.

3. Conventional ADME studies augmented by the integration of an IVMT period which as well as enabling a clear evaluation of absolute oral bioavailability, also enable a qualitative assessment of fraction absorbed and fraction surviving gut metabolism as well as mass balance and metabolite characterisation.
4. Studies requiring study participants with specific qualifying characteristics, considering the impact on study design and the complexities encountered when recruiting subjects from more limited populations (such as precise genotype or reproductive status).
5. Study design considerations where there is a need to consider metabolism at steady state.

Conclusion: The variety in the approaches described, that can be taken to obtain human ADME data, demonstrate the advances in technology available to the DMPK scientist to investigate and understand the disposition of drugs in development.

Reference:

1. Clinical Pharmacology Considerations for Human Radiolabeled Mass Balance Studies, FDA, May 2022

P41 - UNDERSTANDING THE ABSORPTION, METABOLISM AND EXCRETION OF MASITINIB IN HEALTHY MALE SUBJECTS

Iain Shaw¹, Francois Bellamy², Franck Pitre², Stuart Mair¹, Wouter H J Vaes³, Ray Cooke⁴, and Rianne De Ligt³
¹Quotient Sciences, United Kingdom, ²AB Science, France, ³TNO, Netherlands, and ⁴Pharmaron UK, United Kingdom

Introduction: Masitinib mesylate (AB1010) is an oral tyrosine kinase inhibitor that targets mast cells and macrophages. Because of its potent and selective activity against CSF-1R, masitinib is able to inhibit the CSF1/CSF-1R signalling pathway thereby regulating CSF-1R-dependent cells such as microglia. By merit of its activity against c-Kit, LYN and FYN, masitinib is able to inhibit mast cell activity. Masitinib is currently in development as a potential treatment in four different therapeutic areas, neurology, inflammatory diseases, oncology and viral diseases.

As part of the development programme for masitinib, an open labelled, single period radiolabelled study was performed in healthy male subjects. The study assessed the absorption and disposition of masitinib after oral administration and enabled determination of mass balance, routes of excretion and metabolism.

Materials and Methods: Each subject received a single dose of [¹⁴C] AB10104 mg/ml (free base) provided as 50 ml oral solution containing NMT 37 kBq (1000 nCi) [¹⁴C] in the fasted state.

Radiolabelled drug product manufacturing was performed in a GMP manufacturing suite that is integrated with the clinical pharmacology unit. Blood, urine and faeces samples were collected until 168h post dose and assayed for total radioactivity, parent drug and [¹⁴C] parent drug.

Results: Following a single 200 mg (50 ml of 4 ng/ml) oral dose of [¹⁴C] AB1010, a mean of 69% (range 55% to 83%) of radioactivity administered was recovered by the end of the sampling period (168h). The majority of radioactivity was recovered in faeces (up to 59% of the administered dose).

The low urinary recovery (approximately 10% of the administered dose) indicated that renal clearance was not a major contributor to elimination. Low recovery of radioactivity in the faeces over the first 24h post dose together with approximately 80% of the total radioactivity recovered in faeces collected more than 48h after dosing suggested biliary elimination of parent drug or metabolites was the most likely major route of elimination.

The geometric mean apparent terminal half-life for total radioactivity (95h) was considerably longer than that observed in parent AB1010 or quantifiable metabolites AB3280 and AB2436, which supported the rationale that covalent binding following oxidative metabolism was an explanation for the portion of the circulating radioactive dose that was not able to be characterised.

Conclusion: This study and the associated sample analysis provided an understanding of the mass balance, routes and rates of excretion and metabolism of masitinib.

P42 - OPTIMIZATION OF MDCK PERMEABILITY ASSAY TO ENABLE SEMI-HIGH THROUGHPUT SCREENING AND EXPLOITATION OF *IN SILICO* AND MODELLING TOOLS TO SUPPORT DISCOVERY PROJECTS

Karpagam Aravindhhan, Shanon Berry, Theresa Roethke, Gregory Peckham, Stephen Eisennagel, Brandon Santiago, Molly Karlinsey, Jens Sydor, Michael Reilly, and Mukesh Mahajan
GSK, United States

P-glycoprotein (P-gp) is one of the significant drug transporters expressed in different organs, including the small intestine, kidney, liver, lungs, colon, and blood-brain barrier. The safety and efficacy of drugs can be dramatically influenced by P-gp activity. So, it becomes vital to assess P-gp activity in drug discovery, which demands increased throughput. This investigation aimed to enable a 24-to-96 well format switch to increase the throughput of the MDCK permeability assay and further exploit *in silico* and modeling tools with rigorous data standards to yield accurate and

reliable data generation. The observational bias in well format was examined by monitoring two controls (amprenavir and propranolol) in 24 and 96 well formats. Control responsiveness was similar between the two assay formats. Additionally, 15 GSK compounds were investigated in 24 and 96-well formats to address response uncertainties. A high degree of correlation was observed for all three assay parameters: A-to-B permeability ($r_2 = 0.94$), B-to-A permeability ($r_2 = 0.82$), and efflux ratio ($r_2 = 0.94$). Prediction sensitivity analysis using two internal GSK *in silico* models for a total of 296 and 976 compounds (24-well and 96-well formats, respectively) suggests high sensitivity for efflux ratio (24-well format (84%) and 96-well format (85%)) and permeability (24-well format (93%) and 96-well format (97%)). Investigation of 1298 compounds revealed distinct permeability-recovery profiles for GSK-A and GSK-B. Membrane Plus 2 modeling disclosed that GSK-A had a lower cellular free fraction (12%) than GSK-B (56%). This approach provides a comprehensive assay characterization scheme to recognize the factors influencing the permeability assay and make an informed decision regarding the compound under investigation in a drug discovery setting.

P43 - A COMPARISON OF THE EFFECTIVENESS OF EQUILIBRIUM DIALYSIS AND ULTRACENTRIFUGATION IN DETERMINING THE PLASMA PROTEIN BINDING OF HIGH BINDING INVESTIGATIONAL DRUGS

Vicky Birks¹, Annabell Pitcher¹, Susan Bellaire², Line Oste², Michael Hall¹, and Astrid Capello²

¹Pharmaron UK Ltd., United Kingdom and ²Galapagos NV, Belgium

Introduction: The aim of this study was to determine the optimal approach to measure the plasma protein binding (ppb) of highly bound (>99%) investigational drugs.

Methods: The ppb of five compounds (A–E) was investigated using two different methods, equilibrium dialysis (ED) and ultracentrifugation (UC). The ppb of all five compounds was determined in human plasma; in addition, the ppb of compounds C and D was analysed in mouse, rat and dog plasma. Measurements were performed both in 10% (v/v) plasma diluted in buffer, and in undiluted plasma. For ED, buffer was placed in one half-cell, and the test compound-spiked plasma (diluted and undiluted) placed in the other half-cell of Dianorm® apparatus, and duplicate cells dialysed for 3 hours. The residual plasma and dialysate were removed from the cells and the plasma cells washed with buffer. For UC, spiked plasma was loaded into 1.5 mL centrifuge tubes. Samples were centrifuged at >200,000 x g for 20 hours in a Sorvall WX80Ultra ultracentrifuge. Aliquots of each supernatant were then removed and transferred into Eppendorf tubes. The concentration of compound in aliquots of solutions from each dialysis compartment and the buffer washes, and the concentration in each spiked plasma and ultracentrifuge supernatant sample, were analysed by LC-MS, and the analyte/internal standard response ratio determined.

Results: Unbound (% free) values for each compound are presented in the Table.

Conclusions: These results indicate that the extent of ppb was similar in 10% plasma and undiluted plasma (mouse, rat, dog and human) when determined by ED. The extent of ppb in 10% plasma was similar when determined using ED and UC. There was greater variability in measured ppb between diluted and undiluted plasma when determined by UC compared with ED. It is concluded that unbound values of less than 1% can be accurately determined using diluted plasma. The results determined using one method (ED or UC) can be confirmed by using the other, thereby increasing the reliability of the data.

Table. Unbound (% free) values for compounds A–E in undiluted and 10% plasma samples

Compound	Technique	Plasma sample	% Free			
			Human plasma	Mouse plasma	Rat plasma	Dog plasma
A	ED	Undiluted	0.960	NA	NA	NA
		10%	1.70			
	UC	Undiluted	1.09			
		10%	0.965			
B	ED	Undiluted	4.23	NA	NA	NA
		10%	5.73			
	UC	Undiluted	4.10			
		10%	2.73			
C	ED	Undiluted	0.570	0.545	0.300	1.27
		10%	0.600	0.960	0.255	1.75
	UC	Undiluted	0.410	0.565	0.630	1.48
		10%	0.310	0.275	0.130	1.00
D	ED	Undiluted	0.055	0.105	0.490	0.140
		10%	0.115	0.170	0.515	0.145
	UC	Undiluted	1.51	1.39	4.84	2.00
		10%	0.505	0.440	0.955	0.270
E	ED	Undiluted	3.16	NA	NA	NA
		10%	2.83			
	UC	Undiluted	1.14			
		10%	1.47			

ED, equilibrium dialysis; NA, not applicable; UC, ultracentrifugation

P44 - PRECLINICAL AND CLINICAL ADME PROFILE OF ETC-159, AN ORAL PORCUPINE INHIBITOR, FOR THE TREATMENT OF PATIENTS WITH ADVANCED SOLID TUMOURS

Vishal Pendharkar, Sylvia Bong Hwa Gan, Nurul Nazihah Rozaini, Stephanie Blanchard, Ranjani Nellore, Julienne Roi Cometa, Veronica Diermayr, Venkateshan Srirangam Prativadibhayankara, and Kantharaj Ethirajulu
Experimental Drug Development Centre, Singapore

ETC-159 (ETC-1922159) is a small molecule selectively inhibiting the O-acyltransferase porcupine enzyme that is required for the palmitoylation of all Wnts in the Wnt signalling pathway. ETC-159 showed moderate to high protein binding in human (92 %), dog (96 %), rat (84 %) and monkey (80 %) plasma. ETC-159 was stable in human, dog, rat, mouse and monkey liver microsomes and human hepatocytes with half-lives >60 minutes indicating it is stable towards P450 metabolism. Metabolism of ETC-159 is through N-alkylation, mono-oxygenation and dehydrogenation. The N-demethylated metabolite of ETC-159 was also seen *in vivo*, but, less than 10% of the parent compound. Chemically synthesised metabolites were used to confirm the metabolic pathways of ETC-159. The IC₅₀ values of ETC-159 for all the CYPs (CYP1A2, CYP2A6, CYP2D6, CYP2C9, CYP2C19, CYP2E1, CYP2B6 and CYP3A4) were >100 µM, indicating a low potential for a P450 drug-drug interaction. In a CYP450 induction study, ETC-159 showed no significant potential to induce CYP1A2, CYP2B6 and CYP3A4 P450 isozymes. ETC-159 is highly permeable and is not a Breast Cancer Resistance Protein (BCRP) transporter substrate. The pharmacokinetics of ETC-159 showed rapid absorption in mouse, rat and dog (T_{max} from 0.5 to 2.0 h). The oral terminal half-life was 1.5, 3.0 and 3.9 h in mouse, rat and dog, respectively. ETC-159 showed a low volume of distribution in mouse (1.51 L/kg), rat (2.9 L/kg) and dog (0.3 L/kg). The systemic clearance of ETC-159 was low in mouse (0.72 L/h/kg), rat (0.67 L/h/kg) and dog (0.05 L/h/kg) in terms of liver blood flow. Following i.v administration, terminal half-life was 1.18, 3.9 and 4.9 h, in mouse, rat and dog, respectively. The volume of distribution was 1.48, 1.0 and 0.6 L/kg and the systemic clearance 0.88, 0.27 and 0.14 L/h/kg, in mouse, rat and dog, respectively. The oral bioavailability of ETC-159 was 100 %, 39 % and 100 % in mouse, rat and dog, respectively. Clinical pharmacokinetics of ETC-159 showed slower absorption in cancer patients ranging from 2-8 h. The half-life was longer than predicted by pre-clinical data, and exposure increased in dose-related manner from 1 to 30 mg, both at Day 1 and at Day 15. The dose dependant pharmacokinetic profile of ETC-159 was similar when given in combination with pembrolizumab. The plasma concentration of the major metabolite was expectedly <10% of the parent indicating low systemic metabolism. Pharmacometric modelling suggested an exposure-response correlation with downstream PD markers in the Wnt pathway including Axin2 and β-CTX. ETC-159 is currently in Phase 1B clinical trial as a treatment for solid tumours as single agent or in combination with pembrolizumab.

P45 - UNIQUE DATA OBSERVATIONS AND FINDINGS FROM VARIED INCUBATION TIMES ON PLASMA PROTEIN BINDING

Charles Rotter, Mostafa Khan, Faizan Zubair, Cody Fullenwider, Kirk Kozminski, Kuny Mizono, and Will Tao
Takeda California Global DMPK, United States

Introduction: Mouse pharmacology studies are commonly supported and team needs to understand unbound plasma concentrations relative to compound potency. While mouse plasma protein binding (PPB) was investigated using equilibrium dialysis (HTD), large differences in fraction unbound (f_u) were observed for similar protocols at 2 sites. A unique trend (acceleration in the f_u value measured with time) was observed specific to mouse PPB and not associated with other tested species (rat or human). One might expect a leveling off of f_u value between 4-6 hours, but a large upswing in f_u after 6 hours was noted. Kinetically, as compound gets closer and closer to equilibrium, the rate of change would slow down. To further probe this, multiple control compounds were assessed in PPB time-course to understand trend across 3 species. Further, mouse plasma had proteomics analysis to understand matrix stability relative to incubation time.

Hypothesis: Degradation of plasma protein during extended incubation equilibrium dialysis assay is occurring but is species specific to mouse.

Methods: Equilibrium dialysis assay methodology (n=8 compounds, at 1 μ M, n=3 replicates). Assay performed at 37 °C, 5% CO₂ incubator, and 4, 6 and 20 hour incubations.

Proteome analysis: mouse plasma was incubated in HT dialysis block for 0, 4, and 20 hours. Incubated plasma and buffers were utilized for proteomics analysis. Post protein quant, samples were digested and analyzed using high-resolution mass spectrometry.

Results: Notable differences in percentage unbound (f_u) was observed in mouse plasma when comparing 4 vs 20 hour incubations. For example, Warfarin f_u in mouse plasma increased almost 4-fold and Imipramine f_u in mouse plasma increased almost 2.5-fold. These results align with internal compounds (TA-001), where f_u in mouse plasma increased up to 5-fold. Further, a comparison of plasma protein at different incubations indicating an increase in the number of dysregulated proteins and peptides with longer times. In total, 21 peptides were dysregulated between 4 and 20 hour time points, of which 19 peptides were decreased at 20 hour time point, indicating a potential protein degradation.

Mouse PPB (% f_u) results: Sertraline (1.1 vs 1.6), Propranolol (17.2 vs 20.4), Phenacetin (56.9 vs 67.8), Imipramine (9.34 vs 23.1), Warfarin (5.6 vs 20.2), Olanzapine (28.1 vs 35.6), Amitriptyline (5.3 vs 6.6), TA-001 (10.3 vs 50.1).

Results for rat and human plasma f_u are shown below, but were not as significantly influenced with incubation time to 20 hours. Rat PPB (% f_u) results: Sertraline (2.6 vs 2.0), Propranolol (21.7 vs 25.5), Phenacetin (55.0 vs 51.8), Imipramine (23.3 vs 23.0), Warfarin (0.7 vs 0.8) respectively. **Human PPB (% f_u) results:** Sertraline (2.0 vs 3.7), Propranolol (35.5 vs 45.9), Phenacetin (71.1 vs 72.2), Imipramine (19.2 vs 25.5), Warfarin (1.7 vs 2.2), Olanzapine (28.1 vs 35.6), Amitriptyline (10.6 vs 14.8) respectively.

Conclusions: Unique to mouse PPB (and not observed in rat or human), compound becomes unbound to the plasma over time (20 hours) and it is not an equilibration issue. Data suggests mouse protein degradation is occurring with longer incubation time and may impact the mouse plasma f_u .

P46 - THE DEVELOPMENT AND VALIDATION OF A COMPUTATIONAL MODEL TO PREDICT HUMAN LIVER MICROSOME STABILITY

Pranav Shah, Vishal Siramshetty, and Xin Xu
NCATS/NIH, United States

Hepatic metabolic stability is a key parameter in drug discovery as it impacts oral bioavailability as well as elimination of a compound. The major enzymatic system responsible for metabolism of xenobiotics is the cytochrome P450 (CYP450) isoenzyme family. CYP450s are responsible for more than 75% of drug metabolism and the major isoform amongst these enzymes is CYP3A4 which is responsible for metabolism of ~50% of known xenobiotics in humans. The current standard for preliminary estimation of the human metabolic stability of a compound at the discovery stage is the *in vitro* clearance assay using human liver microsomes (HLMs). Data from this assay is used as a rank-ordering mechanism to progress compounds further in the drug discovery process. At the National Center for Advancing Translational Sciences (NCATS), a high-throughput multi-time point HLM stability assay is employed as a Tier II assay, and ~5000 compounds from more than 40 discovery and development projects have been screened for HLM stability. To offset the rising drug development costs, *in silico* machine learning approaches have gained popularity and success. Predictive models are routinely employed in major pharmaceutical companies and results from these models are used as a rank-ordering mechanism for prioritizing compound synthesis. While other HLM stability models exist, they are usually developed using small datasets or with data sourced from literature which can induce error on account of different protocols and lab-to-lab variables. In this study, we employed traditional and advanced machine learning techniques to develop quantitative structure activity relationship models for predicting HLM stability. Additionally, the best model from our study with training and validation accuracies over 77% has been made publicly available on the NCATS ADME portal

(<https://opendata.ncats.nih.gov/adme/>). The *in silico* model developed from this dataset will serve as a powerful tool to accelerate translational research across various drug discovery institutions.

P47 - A MEGA-ANALYSIS ON ADME AND TOXICITY OF INOTERSEN, PATISIRAN, AND VUTRISIRAN FOR THE TREATMENT OF HEREDITARY TRANSTHYRETIN-MEDIATED AMYLOIDOSIS

Sherouk Tawfik, Julia Migliorati, and Xiaobo Zhong

University of Connecticut, United States

Some mutations in the transthyretin (TTR) gene can cause a severe heterogeneous multisystem disorder, known as hereditary transthyretin amyloidosis (hATTR) (Plante-Bordeneuve and Said, 2011; Adam et al., 2019). Patients eventually develop deposition of the TTR protein in many organs and body systems, which most frequently results in progressive polyneuropathy or cardiac dysfunction with many patients experiencing both (Gertz et al., 2017). TTR abnormal overaccumulation in cardiac tissue can lead to heart failure, thickening of the ventricular walls, diastolic dysfunction, and arrhythmia. Before nucleic acid-based therapeutics became available, diflunisal treatment and liver transplantation were the two therapeutic options for hATTR. However, neither option restores the damage induced by TTR deposition and both are only appropriate for relatively healthy individuals due to safety and mortality risks. Hence, direct reduction of abnormal overaccumulation of TTR should be the principle for developing drug therapeutics to treat hATTR. Nucleic acid-based therapeutics, including antisense oligonucleotide (ASO) and small interfering RNA (siRNA) drugs, have proven to be an efficient strategy to reduce mRNA and protein production in disease organs and cells. In the last four years, the US Food and Drug Administration (FDA) has approved three nucleotide acid-based drugs for the treatment of hATTR, including Ionis' inotersen (an ASO drug approved in October 2018) (Gales, 2019) and Alnylam's patisiran and vutrisiran (siRNA drugs approved in October 2018 and June 2022, respectively) (Hoy, 2018). Both ASO and siRNA drugs can reduce mRNA and protein expression, however, their pharmacological features are different in terms of therapeutic efficacy and toxicity. In this study, a systematic mega-analysis on inotersen, patisiran, and vutrisiran was performed by analyzing available information and data from PubMed publications, FDA drug labels, and clinical trial databases, such as ClinicalTrials.gov. This mega-analysis included a comprehensive comparison among inotersen, patisiran, and vutrisiran on target binding sites in the TTR mRNA; nucleotide sequence compositions; chemical modifications in nucleotides; delivery systems; principle of drug action; administration routes; body system distributions; cellular uptake by endocytosis; endosome subcellular trafficking; endosome release; excretion from target cells; preclinical studies on efficacy and cytotoxicity; outcomes of clinical trials; adverse drug reactions and toxicity; and post-market information. The mega-analysis provides a comprehensive overview on the treatment of hATTR by these ASO and siRNA drugs with an emphasis on their ADME and toxicity features.

References:

1. Adams D, Koike H, Slama M, and Coelho T. 2019. Hereditary transthyretin amyloidosis: a model of medical progress for a fatal disease. *Nat Rev Neurol*, 15(7):387-404.
2. Gales L. 2019. Tegsedi (inotersen): an antisense oligonucleotide approved for the treatment of adult patients with hereditary transthyretin amyloidosis. *Pharmaceuticals*, 12(2):78.
3. Gertz MA. 2017. Hereditary ATTR amyloidosis: burden of illness and diagnostic challenges. *Am J Manag Care*, 23(7):S107-S112.
4. Hoy SM. 2018. Patisiran: first global approval. *Drugs*, 78(15):1625-1631.
5. Plante-Bordeneuve V and Said G. 2011. Familial amyloid polyneuropathy. *Lancet Neurol*, 20(12):1086-1097.

P48 - INVESTIGATION OF CLINICAL ADME AND PHARMACOKINETICS OF THE HIV-1 MATURATION INHIBITOR GSK3640254 USING AN INTRAVENOUS MICROTRACER COMBINED WITH THE ENTEROTRACKER® BILIARY SAMPLING

Bo Wen

GlaxoSmithKline, United States

GSK3640254 is a next-generation maturation inhibitor in development for HIV-1 treatment, with pharmacokinetics (PK) supporting once-daily oral dosing in human. This open-label, non-randomized, 2-period clinical mass balance and excretion study was used to investigate the excretion balance, PK, and metabolism of GSK3640254. The combination of an intravenous ¹⁴C microtracer with duodenal bile sampling using a new device EnteroTracker® in this study enabled derivation of absorption and first-pass parameters, including fraction absorbed (Fabs), proportion escaping first-pass extraction through the gut wall and liver (Fg and Fh, respectively), hepatic extraction (Eh), and other conventional clinical pharmacokinetic parameters. Intravenous PK of GSK3640254 was characterized by low plasma clearance (1.04 L/h), moderate terminal phase half-life (21.7 hours), and low volume of distribution at steady state (28.7 L). Orally dosed GSK3640254 was absorbed (Fabs = 0.26), with a high fraction escaping gut metabolism (Fg = 0.898) and a low hepatic

extraction ratio ($E_h = 0.00544$), which is consistent with low *in vitro* intrinsic clearance in liver microsomes and hepatocytes. No major metabolites in human plasma required further qualification in animal studies. Both unchanged GSK3640254 and its oxidative and conjugative metabolites were excreted into bile, with GSK3640254 likely subject to further metabolism through enterohepatic recirculation. Renal elimination of GSK3640254 as the parent drug or its metabolites was negligible, with >94% of total recovery of oral dose and majority of the recovered radioactivity in feces (>99%). GSK3640254 was metabolized solely by CYP3A4 in incubations with human liver microsomes, whilst UGT1A4 and UGT2B7 were involved in glucuronidation of GSK3640254. Taken together, this approach identified hepatic metabolism and biliary excretion as a major elimination pathway for absorbed drug, which would be overlooked based solely on analyses of plasma, urine, and fecal matrices.

P49 - SELECTION OF ANALYTICAL PLATFORMS FOR BIOMARKER AND BIOANALYTICAL QUANTITATION IN PRECLINICAL RESEARCH WITH CASE STUDIES

Faizan Zubair, Katherine Lundeen, Ben Mayes, Mostafa Khan, and Michael Zientek
Takeda Pharmaceuticals, United States

Quantitation of biomarker is crucial for drug discovery and development. With the advances in analytical platforms, scientists have many options for bioanalytical quantitation. These advancements have also created a challenge in that bioanalytical scientists can be overwhelmed with the choices or simply choose a platform that they are most familiar with. The goal of this work is to outline a decision-making process to select an optimal platform and the sample prep approach to reproducibly quantify bioanalytes of interest.

There are two major categories of analytical platforms: liquid chromatography mass spectrometry (LCMS) and ligand-binding assays (LBA). LCMS bridges the separation ability of chromatography with the selective detection of mass spectrometry. There are many types of chromatography including reverse phase (C18 being the most popular), normal phase, mixed-mode, ionic, size-exclusion and others. Similarly, there are several mass spectrometry configurations to choose from including triple-quad, time-of-flight, orbitrap, FT-ICR, hybrid, and tribrid. While LCMS does not require custom reagents, LBA is dependent on antibodies or other binding reagents to selectively interact with the target of interest. For LBA, we have several platforms to choose from including meso-scale discovery, western blotting, Peggy Sue, Simoa, and others.

In this work, we describe three case studies demonstrating our decision-making process for selecting the analytical platform for a given application. In the first case study, our goal was to measure drug distribution in the gut tissue. Since the drug was antisense-oligonucleotide, imaging mass spectrometry approach (eg. MALDI mass spectrometry) was not ideal because of low sensitivity of this approach for these types of molecules. Instead, we utilized an in-situ hybridization technology to map the distribution of ASOs in the tissue. While this technology is more sensitive, it has limitations in terms of specificity as it cannot discriminate between the parent drug and its truncated products.

In the second case study our goal is to measure a protein biomarker in the brain tissues. Because of ease of antibody availability, we utilized ELISA and western blotting approaches in parallel. The results from the two technologies were contradictory in that ELISA was able to detect this protein biomarker in the knockout animals whereas western blot showed that protein biomarker was absent. Additional evaluation of this is ongoing to conclusively resolve the contradiction between the two approaches.

In the last case study, our goal is to quantify exosomal proteins to quantify circulating biomarkers. Here we initially used crude exosomal prep where entire exosome population from a cell culture was spun down using ultracentrifugation approach and the biomarkers were quantified using discovery proteomics approach. While this approach was able to detect our proteins of interest in *in vitro* assays, our goal is to selectively isolate exosomes from specific cell types. To achieve this goal, we are planning to purify cell specific exosomal populations using selective surface antibody markers. Thus, a combination of LBA approach for enrichment and LCMS approach for detection is chosen.

P50 - CHARACTERIZATION OF THE PHARMACODYNAMICS OF ORAL DRONABINOL BEFORE AND AFTER ONE-WEEK OF HYDROCORTISONE OR ESTRADIOL TREATMENT IN HEALTHY, PREMENOPAUSAL WOMEN

Aurora Authement, John Amory, Katya Rubinow, and Nina Isoherranen
University of Washington, United States

Women of reproductive age and pregnant women often consume cannabis recreationally or as self-medication for several conditions such as nausea, pain, and anxiety. The psychoactive compound in the cannabis plant, Δ -9-tetrahydrocannabinol (THC) is metabolized to its psychoactive metabolite 11-OH-THC predominantly by CYP2C9 with minor contributions from CYP2C19 [1]. The expression and activity of these CYPs could be altered by sex steroids [2,3]. However, little is known about the impact of altered hormone states on the pharmacokinetics or pharmacodynamics of THC. Endogenous hormones, such as estradiol and cortisol, have dynamic plasma concentrations in response to physiological changes or from administration as therapeutics. We hypothesized that increased estradiol and cortisol concentrations will decrease THC exposure via CYP2C9 induction and thus lead to a decrease in the pharmacodynamic effect of THC. In a current clinical study, the impact of one-week administration of 0.3 mg transdermal estradiol and 30 mg

oral hydrocortisone on the pharmacokinetics and pharmacodynamics of orally administered dronabinol, the FDA-approved synthetic THC, is being evaluated using a randomized crossover design with each participant taking hydrocortisone and estradiol in two separate study arms. Enrolled participants are healthy, premenopausal, and ethnically diverse women. Each study arm consists of an untreated (control) hormone study day and a subsequent study day on the seventh day of hormone treatment. On each study day, 2.5 mg of dronabinol is administered orally. Urine, plasma, serum, vital signs, and visual analogue scales (VAS) are collected at baseline (pre-dose) and for 24 hours post-dose. Pharmacodynamic effects of dronabinol are assessed using heart rate, blood pressure, and several VAS. On the control study days, heart rate increased 20-40% 4 to 8 hours after administration of dronabinol. Following treatment with hydrocortisone, heart rate increased 20-30% between 4 to 8 hours post-administration. Similarly, after one week of estradiol treatment, heart rate also increased 20-30% 4 to 8 hours post-administration. Blood pressure had similar trends between study days and post-administration of dronabinol. Over 50% of participants noted feeling high on at least one of the study days after dronabinol administration. This data will give insight into the pharmacodynamic effects of a low dose of dronabinol in the presence and absence of relevant hormones, estradiol and hydrocortisone.

References:

1. Patilea-Vrana G et al., Hepatic Enzymes Relevant to the Disposition of (-)- Δ^9 -Tetrahydrocannabinol (THC) and Its Psychoactive Metabolite, 11-OH-THC. *DMD* 2019, 47(3):249-256
2. Papageorgiou I et al., Effect of Pregnancy-Related Hormones on Hepatic CYP3A Induction. *DMD* 2013, 41(2):281-290
3. Choi S et al., Isoform-specific regulation of cytochromes P450 expression by estradiol and progesterone. *DMD* 2013, 41(2):263-269

P51 - DURATION OF THE EFFECT OF COBICISTAT ON SIMVASTATIN PHARMACOKINETICS AND MIDAZOLAM SYSTEMIC CLEARANCE: ESTIMATING THE TURNOVER HALF-LIVES OF INTESTINAL AND HEPATIC CYP3A4

Janne Backman¹, Taavi Kaartinen¹, Aleksi Tornio², Outi Lapatto-Reiniluoto³, Jasleen K. Sodhi⁴, and Mikko Niemi¹

¹University of Helsinki, Finland, ²University of Turku, Finland, ³Helsinki University Hospital, Finland, and ⁴Plexxikon, Inc, United States

Cobicistat, a very strong mechanism-based inhibitor of cytochrome P450 (CYP) 3A4 is used as a pharmacokinetic enhancer of HIV-1 protease inhibitors. It is structurally related to ritonavir but has no meaningful antiretroviral activity. The duration of its CYP3A4 inhibiting effect has not been reported, and clinical evidence concerning the turnover half-life of CYP3A4 to determine the rate of enzyme recovery in humans is inadequate.

The objective of this study was to characterize the inhibitory effect of cobicistat on CYP3A4 by using oral simvastatin and intravenous midazolam as sensitive (index) substrates of intestinal and hepatic CYP3A4, respectively. An additional objective was to estimate the time-course of recovery of CYP3A4 activity after stopping cobicistat treatment using these two index substrates.

We conducted a 5-phase fixed order pharmacokinetic study, where nine healthy volunteers were administered a 0.1-mg intravenous dose of midazolam and a 20-mg oral dose of simvastatin 1, 25, 49 and 73 hours after pretreatment with 150 mg of cobicistat once daily for 3 or 4 days. Blood samples were collected up to 23 hours postdose. Plasma concentrations and pharmacokinetic parameters of the above drugs and their metabolites were determined. A regression model was used to estimate the turnover half-life of CYP3A4 based on recovery of the oral clearance of simvastatin and systemic clearance of midazolam.

The AUC of simvastatin was increased 62-fold (90% confidence interval (CI) 31-125), 27-fold (90% CI 11-62) and 3.6-fold (90% CI 1.5-8.9) in the 1-hour, 25-hour and 49-hour phases, respectively, and while a smaller increase was still seen in the 73-hour phase, it was no longer statistically significant. The clearance of midazolam was decreased to 18% (90% CI 13-24%), 37% (90% CI 26-47%), and 67% (53-84%) in the 1-hour, 25-hour and 49-hour phases, respectively, while only a small nonsignificant decrease was seen in the 73-hour phase. The turnover half-life of CYP3A4 was estimated to be 20 hours based on intravenous midazolam and 30 hours based on oral simvastatin.

In conclusion, typical clinically used cobicistat dosing causes a very strong inhibition of CYP3A4 both in the intestinal wall and in the liver, leading to a hazardous interaction when simvastatin or intravenous midazolam is used concomitantly. Hepatic and intestinal CYP3A4 activities can be estimated to recover within about 4 days after cessation of cobicistat treatment. Based on our clinical data, the turnover half-lives of hepatic and intestinal CYP3A4 are relatively short, between 20-30 hours.

P52 - MODULATION OF NICOTINE METABOLISM IN MICE BY ORALLY AND INTRAPERITONEALLY ADMINISTERED TRANS-CINNAMALDEHYDE AND TRANS-2-METHOXYCINNAMALDEHYDE

John Harrelson, Aiden-Hung Nguyen, Uyen-Vy Navarro, and Jonathon Taylor
Pacific University Oregon, United States

Hypothesis: Administration of trans-cinnamaldehyde (TCA) and trans-2-methoxycinnamaldehyde (MCA) will decrease nicotine metabolism in mice. Background: Variation in human CYP2A6-mediated metabolism modulates the pharmacological effects of nicotine and smoking behavior. TCA and MCA are two natural products present in cinnamon. Previous *in vitro* studies showed TCA and MCA are time-dependent inhibitors of human CYP2A6, and a substantial interaction with nicotine was predicted (> 4-fold AUC changes). However, *in vivo* studies of a potential interaction between nicotine and these natural compounds have not been reported. Thus, the goal was to evaluate the *in vivo* effect on nicotine metabolism by TCA and MCA using a mouse model, which has been shown to be a useful translational model to evaluate modulators of CYP2A-mediated nicotine metabolism. Methods: Two different modes of administration were selected. Injection was selected for the purpose of comparison with previous literature. Oral administration, via drinking water, was chosen to more closely resemble dietary routes of human exposure to TCA and MCA from cinnamon-containing foods and drinks. Adult male C57BL/6J mice were used throughout and were housed in groups of five. The study was approved by the IACUC of Pacific University. Mice were injected with vehicle, methoxypsoralen (15 mg/kg; positive control), TCA (114 and 57 mg/kg) or MCA (114 and 57 mg/kg). Nicotine (1 mg/kg) was administered fifteen minutes after inhibitor injection. To measure nicotine concentrations blood samples were drawn by face bleed at 5, 10, 30, 45, and 60 minutes following nicotine administration. Five to ten mice were used for each time point. For the oral administration experiment, TCA and MCA were dissolved in the drinking water at a concentration of 0.13 mg/mL, to which the mice had *ad lib.* access for three days prior to injection with nicotine. D3-labeled cotinine (internal standard) was added to blood samples, which were processed and analyzed by a Sciex 3500 LC-MS/MS to quantify nicotine and cotinine using standard curves generated in mouse plasma. *In vitro* time-dependent inhibition parameters were estimated by incubating TCA or MCA (0 – 200 micromolar) with mouse liver microsomes (5 mg/mL) for 0 to 60 minutes. At specific time points aliquots were transferred to a secondary incubation consisting of 50 μ M nicotine, 1 mM NADPH, and 1 mg/mL mouse cytosol. Each secondary incubation was quenched with ice-cold acetonitrile after incubating for 15 minutes at 37 °C, and cotinine was quantified by LC-MS/MS. Results: MCA (kinact = 0.047 per min) and TCA (kinact = 0.028 per min) were time-dependent inhibitor of nicotine metabolism in mice liver microsomes. Injection of TCA, MCA, and methoxypsoralen resulted in delayed nicotine clearance corresponding to 1.7-, 2.6-, and 2.9-fold changes in nicotine AUC (0-60 minutes). The inhibitory effect was greater with oral administration of TCA and MCA in drinking water with AUC changes of 2.2- and 9.1-fold, respectively. Conclusions: MCA is a more potent inhibitor than TCA *in vitro* and *in vivo*, which is consistent with previous studies in human liver microsomes. The evidence supports using the mouse model for future study of cinnamaldehyde-based CYP2A inhibitors.

P53 - INFLUENCE OF FOOD, SEX, AND BCRP INHIBITION ON FUROSEMIDE ORAL PHARMACOKINETICS IN RATS

Vijaya Saradhi Mettu, Sheena Sharma, and Bhagwat Prasad
Washington State University, United States

Background: Furosemide is a widely used fast-onset loop diuretic and the first-line treatment option in congestive heart failure patients, prescribed to both adult and pediatric populations. Although limited bioavailability is a concern with furosemide, a bigger problem is its inconsistent bioavailability ranging from 10-100%.¹ To explain the variable pharmacokinetics (PK), we characterized the effect of food, sex, and breast cancer resistance protein (Bcrp) inhibition on furosemide oral PK in the rat model.

Methods: A randomized crossover furosemide (5 mg/kg, oral) PK study was performed in Sprague Dawley rats (n= 6; 3 males and 3 females). The following four conditions were tested: i) fed state without BCRP inhibition, ii) fasting state without BCRP inhibition, iii) fed state with novobiocin (Bcrp inhibitor; 20 mg/kg, oral), and iv) fasting state with novobiocin. Blood and urine samples were collected and furosemide, furosemide-glucuronide, and novobiocin were quantified using a validated LC-MS/MS method. The PK data were analyzed using a non-compartmental (NCA) model utilizing MATLAB (Natick, MA) software.

Results and Conclusions: Co-administration of novobiocin increased furosemide bioavailability by >2-fold (p<0.05) in both fed and fasting states. Contrary to the negative food effect in human,² we found comparable PK of furosemide in fed and fasting states in rat model. However, we observed a predominant sex effect when furosemide was administered with novobiocin with 2-3 fold higher AUC and C_{max} in females compared to male rats. Interestingly, the sex effect on furosemide PK diminished when furosemide was co-administered with novobiocin, likely because of the inhibition of renal Bcrp that is shown to have higher expression in males compared to female rats.³ Blood concentration of furosemide-glucuronide was unaltered in fed and fasting conditions, but its renal clearance was 3-fold higher in males vs. female rats. No effect of Bcrp inhibition was observed on the PK of furosemide-glucuronide.

This study is the first to characterize the effect of Bcrp inhibition on furosemide PK in fed and fasting states. A potential

sex-dependent variability in Bcrp expression could be one of the potential mechanisms of variable furosemide PK. As furosemide has been proposed as a probe substrate of renal organic anion transporters (Oat1/3) for assessing clinical drug interactions during drug development, it is important to account for the confounding effect of Bcrp transporter and sex.

References:

1. Eillison et al., Clin J Am Soc Nephrol (2019).
2. Mccrindle et al., Br J Clin Pharmacol (1996).
3. Tanaka et al., Biochem Biophys Res Commun (2005).

P54 - USE OF *IN VITRO* DATA TOWARDS CLINICAL PREDICTION OF DRUG-DRUG INTERACTION RISK DUE TO TIME-DEPENDENT INHIBITION OF CYTOCHROME P450 1A2, 2C8, 2C9, 2C19, AND 2D6

Elaine Tseng, Jian Lin, Ethan DaSilva, Timothy Strelevitz, Theunis Goosen, and R. Scott Obach
Pfizer Inc, United States

The development of methods for prediction of CYP drug-drug interactions (DDI) from *in vitro* data for time-dependent inhibitors (TDI) continues to be of focus. Through our own recent efforts, the use of *in vitro* TDI data for the projection of DDIs for CYP3A TDIs was reported (1). This evaluation showed that both a static mathematical model utilizing estimated average unbound organ exit concentrations of TDIs and dynamic PBPK modeling (using Simcyp®) successfully project clinical DDI. In the present research, these approaches were extended to TDIs of other CYP enzymes besides CYP3A. *In vitro* TDI kinetic parameters, KI, kinact, and unbound fractions for 21 diverse compounds with clinical DDI studies were generated in human liver microsomes (HLM). All data were incorporated into the projection of the magnitude of DDIs using mechanistic static models and Simcyp®. Like CYP3A, the analysis suggests that for the mechanistic static model, use of estimated average unbound exit concentration of the inhibitor from the liver resulted in a successful prediction of observed magnitude of clinical DDIs and was similar to Simcyp®. Overall, predictions of DDI magnitude (i.e. fold increase in AUC of a CYP-specific marker substrate) were within 2-fold of actual values. Geometric mean-fold errors were 1.7 and 1.5 for static and dynamic models, respectively. Projections of DDI from both models were also highly correlated to each other ($r^2 = 0.92$). This exercise demonstrates that DDI can be reliably predicted from *in vitro* TDI data generated in HLM for all CYP enzymes. Simple mechanistic static model equations as well as more complex dynamic PBPK models can be employed in this process.

Reference:

1. Tseng E, Eng H, Lin J, Cerny MA, Tess DA, Goosen TC, Obach RS. (2021) Static and Dynamic Projections of Drug-Drug Interactions Caused by Cytochrome P450 3A Time-Dependent Inhibitors Measured in Human Liver Microsomes and Hepatocytes. Drug Metab Dispos. Oct;49(10):947-960.

P55 - PHYSIOLOGICALLY BASED PHARMACOKINETIC (PBPK) MODELING OF PYROTINIB TO UNDERSTAND THE IMPACT OF INTERPLAY BETWEEN CYP3A4 AND P-GP ON ITS DDIs WITH CYP3A4 INHIBITORS/INDUCERS

Tarang Vora¹, Grace Fraczkiwicz¹, Kaijing Zhao², Shaorong Li², Kai Shen², Miao Liu³, Shuyu Sun³, and Mingyan Zhou³
¹Simulations Plus, Inc., United States, ²Jiangsu Hengrui Medicine Co. Ltd, China, and ³Luzsana Biotechnology, Inc., United States

Objectives: Pyrotinib is a novel and irreversible dual pan-ErbB receptor tyrosine kinase inhibitor developed for treating HER2-positive advanced solid tumors. Pyrotinib, a BCS Class III compound, is primarily metabolized by CYP3A4, and *in vitro* assay suggested a potential substrate for P-gp efflux transporter. The objective was to use the PBPK model of pyrotinib to understand how the interplay of CYP3A4 and P-gp can affect the drug-drug interactions (DDI) for pyrotinib when co-administered with CYP3A4 inhibitors/inducers.

Methods: The full PBPK model for pyrotinib was developed utilizing GastroPlus®v.9.8.2. The volume of distribution was calculated using Lukacova w/lysosomal binding method. Tissue: plasma partition coefficients for all tissues were calculated based on *in vitro* / *in silico* (ADMET® Predictor v10.0.0.0) physicochemical properties of pyrotinib. The matching human PBPK physiologies were generated by the PBPKPlus™ module based on the gender, average body weight, age, and height for each dosing group. The Advanced Compartmental Absorption and Transit (ACAT™) model was used to describe the intestinal dissolution and absorption of pyrotinib. The *in vitro* passive permeability (Caco-2 cell line) was converted to human jejunal permeability using built-in GastroPlus correlation between Caco-2 permeability and *in vivo* jejunal permeability. Two different models were developed to account for pyrotinib metabolism by CYP3A4 and CYP2C8 with and without P-gp efflux transporter in the gut. The kinetic parameters Vmax and Km were optimized against

the observed plasma profiles. Both models' performance was evaluated by the ratio of predicted/observed for C_{max} and AUC at five different dose levels. Simulations for pyrotinib were performed to reproduce the observed DDI effects.

1. 80 mg of pyrotinib with co-administration of CYP3A4 inhibitors itraconazole (200 mg once daily for 14 days) and fluconazole (400 mg on day 1 and 200 mg once daily from day 2 to day 13)
2. 400 mg of pyrotinib with co-administration of CYP3A4 inducer rifampicin (600 mg once daily for 14 days) and efavirenz (600 mg once daily for 16 days)

The previously built PBPK models for perpetrator compounds that are part of GastroPlus DDI standards database were used.

Results: The developed model with and without P-gp reproduced the observed pyrotinib plasma concentration profiles for all the doses within 0.8 - 1.3 prediction fold error. The model without P-gp efflux transporter could not reproduce the observed DDI with itraconazole (C_{max} - 3.79-fold and AUC - 11.79-fold). The predicted DDI effect with itraconazole was over-predicted by 2.68-fold for C_{max}, but AUC was reasonably matched (0.97-fold). In case of the model with P-gp efflux, DDI prediction with itraconazole was 4.92 and 9.22-fold for C_{max} and AUC, respectively. The DDI predictions with fluconazole, rifampicin, and efavirenz were within a 2-fold error and Guest limits for the model with P-gp (Table-1).

Conclusion: The PBPK model for pyrotinib accounting for P-gp efflux and CYP3A4 metabolism in the gut successfully explains the interplay between P-gp and CYP3A4. A P-gp efflux becomes more effective in the event of CYP3A4 inhibition in the gut and that was responsible for a lower DDI effect for C_{max} than AUC.

Table – 1: DDI predictions summary

Victim	Perpetrator	Ratio (DDI / Baseline)				Guest limits			
		Obs	Pred	Obs	Pred	Up Lim	Low Lim	Up Lim	Low Lim
		C _{max}		AUC _t		C _{max}		AUC _t	
Pyrotinib 80 mg*	ITC 200 mg	3.79	10.17	11.79	9.22	6.83	2.10	22.83	6.09
Pyrotinib 80 mg†	ITC 200 mg	3.79	4.92	11.79	9.22	6.83	2.10	22.83	6.09
Pyrotinib 400 mg†	RIF 600 mg	0.11	0.06	0.04	0.03	0.21	0.06	0.08	0.02
Pyrotinib 80 mg†	Fluco 400/200 mg	2.40	2.25	3.57	2.94	4.05	1.42	6.39	1.99
Pyrotinib 400 mg†	Efavi 600 mg	0.33	0.29	0.20	0.25	0.58	0.19	0.37	0.11

* Model without P-gp transporter; † Model with P-gp transporter

ITC: Itraconazole; RIF: Rifampicin; Fluco: Fluconazole; Efavi: Efavirenz

P56 - ENZYME- AND TRANSPORTER-MEDIATED CLINICAL DRUG INTERACTIONS WITH DRUGS APPROVED BY THE U.S. FOOD AND DRUG ADMINISTRATION IN 2021: WHAT CAN BE LEARNED FROM NEW DRUG APPLICATION REVIEWS?

Jingjing Yu, Isabelle Ragueneau-Majlessi, and Yan Wang
UW Drug Interaction Solutions, United States

The mechanistic evaluation of enzyme- and transporter-based drug-drug interactions (DDIs) during drug development is critical to support management strategies in the clinic. In the present work, DDI data for small molecular drugs approved by the U.S. Food and Drug Administration in 2021 (N = 36) were analyzed using the University of Washington Drug Interaction Database. The mechanism(s) and clinical magnitude of these interactions were characterized based on information available in the new drug application reviews. DDI data from dedicated clinical trials, pharmacogenetics studies, physiologically-based pharmacokinetics (PBPK) modeling and simulations, and population PK analyses were examined. Positive study results (~140 studies), defined as mean area under the curve ratios (AUCRs) ≥ 1.25 for inhibition DDIs or pharmacogenetics studies and ≤ 0.8 for induction DDIs, were then fully analyzed. When new drugs were evaluated as victims of enzyme-based DDIs, a total of 18 drugs (50%) had positive results with inhibition and induction of CYP3A explaining most of the observed interactions (~85%). Six drugs, namely atogepant, finerenone, ibrexafungerp, infigratinib, mobocertinib, and voclosporin, were found to be sensitive substrates of CYP3A, with AUCRs of 5.45-18.55 when co-administered with the strong marker inhibitors itraconazole or ketoconazole. Of note, all of them were also substrates of P-gp *in vitro*, confirming the strong association between CYP3A and P-gp. Avacopan and belzutifan were found to be moderate sensitive substrates (AUCRs 2-5) of CYP3A and UGT2B17, respectively. Regarding transporters, only two drugs, atogepant (P-gp and OATP1B1/1B3) and odevixibat (P-gp), were clinical substrates of transporters, with a maximum AUCR of 2.85 for atogepant following single dose rifampin administration due to inhibition of OATP1B1/1B3. As perpetrators, only one drug, viloxazine, was considered a strong inhibitor of CYP1A2 (caffeine AUCR 5.83). No drug exhibited strong inhibition of transporters. The following drugs were found to be moderate inhibitors: asciminib (CYP2C9), belumosudil (CYP3A), fexinidazole (CYP1A2 and CYP2C19), and ibrexafungerp (OATP1B3). No strong inducer of

enzymes or transporters was identified. Four drugs showed induction, with sotorasib showing the maximum induction and considered a moderate inducer of CYP3A (midazolam AUCR 0.47). As expected, all DDIs with AUCRs ≥ 5 or ≤ 0.2 (≥ 5 -fold change) and almost all those with AUCRs of 2-5 and 0.2-0.5 (2- to 5-fold change) triggered dosing recommendations in the product labels. PBPK modeling and simulations continued to be increasingly used as alternatives to dedicated DDI clinical trials, with 10 drugs evaluated as victims and 5 drugs as inhibitors using *in silico* evaluations. Similar to drugs approved in recent years, oncology was the most represented therapeutic area, including 31% of 2021 approvals. However, drugs found to be either sensitive substrates or strong inhibitors of enzymes included treatments for a variety of diseases, e.g., antifungals, cancer treatments, central nervous system agents, depression treatments, and immune system agents. Understanding the mechanisms and clinical extent of DDIs with these newly approved drugs will certainly help guide DDI management strategies in patient populations who often receive polypharmacy.

P57 - IN VITRO EVALUATION OF PROTAC® DEGRADER ARV-110 (BAVDEGALUTAMIDE) FOR CYTOCHROME P450- AND TRANSPORTER-MEDIATED DRUG-DRUG INTERACTION

George Zhang

Arvinas Inc., United States

ARV-110, also known as bavdegalutamide, is an orally bioavailable PROTAC® degrader of androgen receptor (AR) and currently is being developed for the treatment of prostate cancer in a phase 2 clinical trial. *In vitro* studies were conducted to assess the potential of ARV-110 as a perpetrator to cause cytochrome P450 (CYP) and transporter-mediated drug-drug interactions (DDI). The induction potential of ARV-110 on CYP enzymes was assessed in cryopreserved human hepatocytes from three donors. Following treatment for 48 h, mRNA levels for CYP1A2, 2B6, 2C8, 2C9, 2C19, and 3A4 were determined by semiquantitative real-time PCR. The potential of ARV-110 to cause direct and time-dependent inhibition of the activities of CYP1A2, 2B6, 2C8, 2C9, 2C19, 2D6, and 3A4 was evaluated in pooled human liver microsomes (HLM). In addition, the inhibition potential against efflux transporters (Pgp, BCRP, and BSEP) and uptake transporters (NTCP, MATE1, MATE2-K, OATP1B1, OATP1B3, OAT1, OAT3, and OCT2) was assessed using single transporter over-expressed cell monolayers (MDCK II or HEK293) or inside-out vesicles. The results showed that ARV-110 at concentrations ranging from 0.01 to 3 μM did not induce mRNA of CYP1A2, 2B6, 2C8, 2C9, and 2C19 for all three lots. A slight induction of CYP3A4 mRNA was observed with a maximal 2.8-3.3-fold (1-2% of positive control response) at 0.1 μM and 0.03 μM across hepatocyte lots. No direct or time-dependent inhibition was observed for any of the CYP isoforms after incubating HLM with ARV-110 at concentrations of 0.013-15 μM except for a >2.5-fold shift after a 30 min-preincubation with an IC₅₀ value of 6.0 μM for CYP2C8, but this time-dependent inhibition was reversible. ARV-110 did not inhibit any of the uptake transporters up to 15 μM tested. ARV-110 exhibited low permeability in MDCK II cell monolayers and did not inhibit BCRP and Pgp in the MDCKII bidirectional assays up to 3 μM . In contrast, ARV-110 inhibited BCRP and Pgp in the vesicle assays in a concentration-dependent fashion, with IC₅₀ values of 0.12 μM and 0.19 μM , respectively. ARV-110 also inhibited BSEP in the vesicle assays with IC₅₀ of 0.10 μM . These data demonstrate that ARV-110 has a low potential to cause significant DDI via modulation of CYP enzymes or inhibition of uptake transporters. Clinical DDI studies with Pgp and BCRP substrates are under investigation.

P58 - ALTERNATIVE CYP3A4 INDUCERS FOR RIFAMPIN

Kuan-Fu Chen and Hannah Jones

Simcyp Limited (Division of Certara), United States

Rifampin is the most frequently used inducer in drug-drug interaction (DDI) studies to evaluate the impact of CYP3A4 induction on the PK of investigational drugs. However, recently MNP (1-methyl-4-nitrosopiperazine), a nitrosamine compound classified as a human carcinogen, has been found above the acceptable limit (0.16 ppm) in rifampin products. There is a need to find an alternative CYP3A4 inducer due to the impurity issue. In this work, phenytoin, phenobarbital, efavirenz, and carbamazepine were investigated to be used as an alternative CYP3A4 inducer. Physiologically-based pharmacokinetic (PBPK) simulation was performed in Simcyp (version 20) to compare induction potentials between rifampin (600 mg QD) and the proposed inducers, including phenytoin (300 mg QD), phenobarbital (100 mg QD), efavirenz (600 mg QD), and carbamazepine (100 mg BID on Day 1-2, 200 mg BID on Day 3-4, 300 mg BID on Day 5-14). The library compounds were used as default with no modification. For each inducer, simulation of 10 trials of 10 healthy males aged 20-50 years was carried out. An inducer was dosed for 2 weeks (Day 1 – 14), followed by co-administration of the inducer and midazolam on Day 15. Midazolam AUC_{0-24h} and C_{max} were simulated in the presence and absence of inducers. Based on the simulated midazolam DDI-to-control AUC_{0-24h} and C_{max} ratios, carbamazepine was determined to be the strongest CYP3A4 inducer second to rifampin (AUCR = 0.208 vs. 0.0709; C_{max}R = 0.259 vs. 0.107), which is followed by phenytoin, phenobarbital, and efavirenz. Subsequently, carbamazepine induction was further explored in different dosing scenarios to achieve higher induction potentials. At the highest dose level simulated (i.e., 600 mg BID on Day 11 – 14), the induction effects were close to those following rifampin (AUCR = 0.119 vs. 0.0709; C_{max}R = 0.157 vs. 0.107). We concluded that carbamazepine is the primary CYP3A4 inducer alternative for rifampin.

P59 - CHARACTERIZATION OF JNJ-2482272 [4-(4-METHYL-2-(4-(TRIFLUOROMETHYL)PHENYL)THIAZOLE-5-YL)PYRIMIDINE-2-AMINE] AS A STRONG AHR ACTIVATOR IN RAT AND HUMAN

Kevin Coe¹, James William Higgins², Perry Leung¹, Brian Scott¹, Judith Skaptason³, Yuen Tam¹, Laurie Volak¹, Jennifer Kinong⁴, Heather Mcallister¹, Nathan Lim¹, Michael Hack¹, and Tatiana Koudriakova¹

¹Janssen Research & Development, United States, ²Trestle Biotherapeutics, United States, ³Neurocrine Biosciences, Inc, United States, ⁴Pfizer, United States

JNJ-2482272, under investigation as an anti-inflammatory agent, was orally administered to rats q.d. at 60 mg/kg for six consecutive days. Despite high plasma exposure after single administration, JNJ-2482272 had plasma concentrations beneath the lower limit of quantification after multiple day administration. To determine if the loss of drug exposure was due to autoinduction, plated rat hepatocytes were treated with JNJ-2482272 for two days. Compared to the vehicle treated cells, a concentration-dependent increase was observed in the formation of hydroxylation and glucuronidation metabolites, which coincided with greater expression of P450s and UGTs in rat hepatocytes. CYP1A1, CYP1A2, CYP1B1, and UGT1A6 transcripts were predominantly induced, suggesting that JNJ-2482272 is an activator of the aryl hydrocarbon receptor (AhR). In a human AhR reporter assay, JNJ-2482272 demonstrated potent AhR activation with an EC₅₀ value of 0.768 nM, a potency more comparable to the strong AhR activator and toxin 2,3,7,8-tetrachlorodibenzodioxin (TCDD) than to weaker AhR activators 3-methylcholanthrene (3-MC), β -naphthoflavone (β NF), and omeprazole (OME). In plated human hepatocytes, JNJ-2482272 induced CYP1A1 gene expression with an EC₅₀ of 20.4 nM and increased CYP1A activity > 50-fold from basal levels. In human recombinant P450s (rCYPs), JNJ-2482272 was exclusively metabolized by the CYP1 family of enzymes and most rapidly by CYP1A1. The summation of these *in vitro* findings bridges the *in vivo* conclusion that JNJ-2482272 is a strong autoinducer in rats and potentially in humans through potent AhR activation. In addition, the low nanomolar AhR potency of JNJ-2482272 is remarkable for a molecule intended as a medicinal agent and illustrates the possibility for a 'non-classical' AhR ligand to bear 'classical' AhR ligand potencies.

P60 - FIVE DONORS, THREE ENDPOINTS, ONE WELL; EVALUATION OF A STREAMLINED POPULATION APPROACH TO DETERMINE INDUCTION POTENTIAL OF NEW CHEMICAL ENTITIES.

Cody Fullenwider¹, Matthew Albertolle¹, and Diane Ramsden²

¹Takeda Pharmaceuticals, United States and ²AstraZeneca, United States

The modulation of drug metabolizing enzymes and transporters (DME&T) can lead to important clinical drug-drug interactions. As such, the potential for a new chemical entity (NCE) to activate nuclear receptor pathways involved in regulation of DME&T is routinely assessed within the research stage of the drug discovery process and regulatory agencies have issued guidance on how to generate and interpret the data. Currently the gold standard is to conduct *in vitro* induction studies in hepatocytes from three separate donors and monitor for changes in CYP1A2, CYP2B6 and CYP3A4 mRNA levels as sensitive markers of activation of aryl hydrocarbon receptor (AhR), constitutive androstane receptor (CAR) and pregnane X receptor (PXR), respectively. While mRNA has demonstrated useful, as an endpoint to measure induction in isolation of competing DDI mechanisms, there is still a tendency for overprediction of induction based DDI risk and significant variability in induction response across donors. Recently coupling induction parameters generated from protein levels with PBPK modeling has successfully recovered clinical changes for a handful of inducers. The goal of this work was to expand the understanding of translation of data generated with mRNA, protein levels and enzyme activity by a. developing a robust method to determine the enzyme activity, mRNA expression and CYP protein expression from a single 96 well incubation and b. to evaluate the CYP induction potential of multiple known clinical CYP inducers in five human hepatocyte donors plated individually or as a pool. These studies enabled comparison of the three induction endpoints (enzyme activity, mRNA and protein) from five unique human donors and established the validity of a multi-donor pool as a streamlined approach to conduct induction risk assessment.

P61 - EXPRESSION DYNAMICS OF GENES INVOLVED IN XENOBIOTICS METABOLISM AFTER EXPOSURE TO NUCLEAR RECEPTOR LIGANDS OF NR1I SUBFAMILY IN 3D PRIMARY HUMAN HEPATOCYTE SPHEROIDS

Petr Pavek

Charles University, Faculty of Pharmacy in Hradec Kralove, Czech Republic

The pregnane X receptor (PXR) and the constitutive androstane receptor (CAR) are ligand-activated nuclear receptors controlling hepatocyte expression of numerous genes. Although expression changes in xenobiotic-metabolizing, lipogenic, gluconeogenic, and bile acid synthetic genes have been described after the xenosensor activation, the temporal dynamics of their target expression are largely unknown. 3D spheroids of primary human hepatocytes (PHHs) are the most phenotypically relevant hepatocyte model. We used 3D PHHs to assess time-dependent expression profiles of prototypic PXR/CAR-controlled genes involved in xenobiotic, lipid, and glucose metabolism in the time course of 168 h. We observed a similar bell-shaped time-induction pattern for xenobiotic-handling genes CYP3A4, CYP2C9, CYP2B6, and MDR1 mRNA after PXR and CAR. CYP3A4 mRNA has similar induction profiles after activating PXR, CAR and vitamin D (VDR) receptors. However, we also observed either biphasic profiles or oscillation for genes involved in endogenous

metabolism such as FASN, GLUT2, G6PC, PCK1, and CYP7A1. Moreover, we calculated half-lives of CYP3A4 and CYP2C9 mRNA under induced or basal conditions. The study shows the importance of long-term time-expression profiling of xenosensor target genes after inducers exposure in phenotypically stable 3D PHHs.

The project is funded by InoMed project (CZ.02.1.01/0.0/0.0/18_069/0010046).

P62 - DEVELOPMENT OF A STRATEGY TO IDENTIFY AND EVALUATE LIGAND AND INDIRECT ACTIVATORS OF RAT CAR

Takumi Sato, Ryota Shizu, Yoshie Miura, Takuomi Hosaka, Takamitsu Sasaki, Yuichiro Kanno, and Kouichi Yoshinari
University of Shizuoka, Japan

Constitutive androstane receptor (CAR) is a nuclear receptor that plays a key role in drug metabolism and disposition. Additionally, some CAR activators induce non-genotoxic liver cancer in rodents, and thus the information on whether a chemical compound activates CAR or not is useful for predicting its carcinogenicity and elucidating the mechanism. CAR is activated by not only ligands but also indirect activators, which induce the nuclear accumulation of CAR for target gene expression without binding to the receptor. In immortalized cells, transiently expressed CAR is spontaneously translocated to the nucleus and promotes the expression of its target genes, even in the absence of activators. For these reasons, conventional reporter assay using immortalized cell lines with CAR expression plasmid is inappropriate for evaluating the chemical activation of CAR. In this study, we aimed to establish a strategy to evaluate rat CAR (rCAR) activation.

Based on previous reports, we investigated the influences of mutations around the rCAR AF2 domain, which interacts with coactivators, and found that the mutant rCAR-3A-G354Q, containing the G354Q substitution and the insertion of three Ala residues between helices 11 and 12, showed lower constitutive activity and higher ligand responsiveness than wild-type rCAR. We then screened >300 compounds to identify rCAR activators. At first, rat primary hepatocytes were treated with each test compound and determined mRNA levels of Cyp2b1, a representative rCAR target gene. Then, the compounds that significantly increased the mRNA levels were subjected to a reporter assay with rCAR-3A-G354Q. Among them, six compounds induced reporter gene expression more than 2-fold against vehicle-treated groups and were implicated as stronger rCAR ligands than known ligands clotrimazole and artemisinin. Among them, five compounds were intraperitoneally administered to male SD rats to investigate whether these compounds activate rCAR *in vivo*, and three compounds were found to increase hepatic Cyp2b1 mRNA levels, suggesting that these compounds are rCAR ligands that work *in vivo*. In the meantime, the results obtained with rat primary hepatocytes and reporter assay indicated that several compounds were indirect rCAR activators because they induced Cyp2b1 mRNA levels in rat hepatocytes but did not activate rCAR-3A-G354Q. Since indirect CAR activators are known to display negligible species differences, we treated human hepatocyte-like HepaRG cells with these compounds and determined CYP2B6 mRNA levels. The results showed that six out of eight compounds tested increased CYP2B6 mRNA levels, suggesting that these compounds are indirect rCAR activators.

Taken together, the present results suggest that the combined measurement of Cyp2b1 mRNA levels in rat primary hepatocytes and rCAR-3A-G354Q activation in reporter assay is useful to evaluate the potency of chemical compounds for rCAR activation and to distinguish between direct and indirect rCAR activators.

P63 - REVISITING THE IMPACT OF ST. JOHN'S WORT ON CYP3A METABOLISM IN RATS – A COMPARATIVE STUDY

Anima Schäfer, Marta Rysz, Julia Schädeli, Michelle Fehr, Michelle Hübscher, Isabell Seibert, and Henriette Meyer zu Schwabedissen
University of Basel, Switzerland

Nuclear receptors (NR) play a pivotal role in maintaining homeostasis in living beings by transcriptional regulation of their target genes upon ligand binding. One well-known NR is the pregnane X receptor (PXR) which accepts a variety of xenobiotics as activating ligands. Importantly, for PXR species specific ligands have been reported with rifampicin and pregnenolon-16 α -carbonitrile as two well-known examples that solely activate the human or the rodent PXR, respectively. Another compound which is famous for its binding to the human PXR is the St. John's wort (SJW) constituent hyperforin. For this molecule selectivity for human PXR has also been shown in *in vitro* experiments [1]. However, there are *in vivo* studies in rats reporting decreased plasma concentrations of Cyp3a substrates after pretreatment with SJW while enzyme activity and/ or expression was shown to be increased [2, 3]. It is aim of this study to further investigate the impact of hyperforin on rat Cyp3a metabolism comparing two SJW formulations. One formulation was Hyperiplant® which contains a high amount of hyperforin (3-6 mg/ 100 mg extract) and the other was Rebalance® containing very low amounts of hyperforin (<0.2 mg/ 100 mg extract).

Cell based reporter gene assays using the synthetic reporter construct CYP3A4-XREM-Luciferase were performed. In presence of rat PXR, both formulations showed transactivation of the reporter gene. Furthermore, both formulations increased Cyp3a1 mRNA expression in rat hepatoma cells as quantified by real-time PCR. However, in both experiments hyperforin did not exert a transcriptional effect. Importantly, in human liver cells or using human PXR, induction or

transactivation was limited to Hyperiplant® and hyperforin. Subsequently, we conducted an *in vivo* rat study. In rats, expression of hepatic Cyp3a1 mRNA was significantly induced by a 10-day treatment with Hyperiplant® (400mg/ kg). No such effect was observed for Rebalance® (400mg/ kg). Hepatic abundance of Cyp3a1 protein was significantly increased upon both treatments with a higher effect for Hyperiplant®. However, Hyperiplant®, but not Rebalance® increased hepatic Cyp3a-activity as assessed by the formation of 6-β-OH-testosterone in liver microsomes isolated after *in vivo* treatment.

In conclusion, treatment of rats with the SJW extracts mimics the hPXR-mediated changes in drug metabolism *in vivo*. However, our *in vitro* data suggest that the impact on rat Cyp3a1 is independent of the hyperforin content and may involve another so far unknown mechanism.

References:

1. Tirona, R.G., et al., Identification of amino acids in rat pregnane X receptor that determine species-specific activation. *Mol Pharmacol*, 2004. 65(1): p. 36-44.
2. Ho, Y.F., et al., Effects of St. John's wort extract on indinavir pharmacokinetics in rats: differentiation of intestinal and hepatic impacts. *Life Sci*, 2009. 85(7-8): p. 296-302.
3. Qi, J.W., et al., Time-dependent induction of midazolam-1-hydroxylation enzymes in rats treated with St. John's wort. *Biol Pharm Bull*, 2005. 28(8): p. 1467-71.

P64 - STRUCTURAL CHARACTERIZATION OF CONSTITUTIVE TRANSCRIPTIONAL ACTIVITY OF THE NUCLEAR RECEPTOR PXR AND THE GENERATION OF LIGAND-SENSITIVE PXR MUTANTS.

Ryota Shizu, Hikaru Nishiguchi, Sarii Tashiro, Takumi Sato, Ayaka Sugawara, Takuomi Hosaka, Yuichiro Kanno, Takamitsu Sasaki, and Kouichi Yoshinari
University of Shizuoka, Japan

Pregnane X receptor (PXR) is a nuclear receptor that is highly expressed in the liver and activated by numerous xenobiotics. Ligand binding to PXR activates it to induce the transcription of target genes, such as those encoding drug-metabolizing enzymes and drug transporters. Since PXR induces xenobiotic metabolism and disposition and may cause drug–drug interactions, PXR activation by xenobiotics has been extensively studied for drug development and food and chemical safety. Although PXR is a ligand-activated nuclear receptor, it is reported that PXR has constitutive transcriptional activity regardless of ligand binding, which sometimes hampers the investigation of PXR activation by compounds of interest. In this study, we demonstrate the mechanism causing the constitutive transcriptional activity of PXR and report the construction of PXR mutants that drastically suppress basal transcriptional activity while maintaining high ligand sensitivity.

In the reported crystal structures of unliganded PXR, the C-terminal coactivator binding motif in helix 12 (H12) was found to be stabilized, while it was destabilized in other unliganded nuclear receptors. Since Phe420, located in the loop between H11 and H12, is thought to interact with Leu411, Ile414, and Q415 in H11 and Met425 in H12 to stabilize these C-terminal helices in human PXR, we substituted Phe420 to Ala (PXR-F420A) and separately inserted three alanine residues directly after Phe420 (PXR-3A). The mutation of L411A, I414A, or Q415A was also introduced in human PXR. The transcriptional activity of wild-type and mutant PXRs were determined by reporter assay in COS-1 cells. The interaction between PXR mutants and coregulators were assessed by mammalian two-hybrid assays.

The PXR-F420A or PXR-3A mutants showed drastically reduced basal activity and enhanced responses to various ligands, which was further augmented by co-expression of the coactivator PGC1α. Mutations at L411A, I414A, or Q415A also decreased the basal activity and the mutants were activated in a ligand-dependent manner. In mammalian two-hybrid assays, wild-type PXR bound to coactivators in the unliganded state, whereas the PXR mutants bound to corepressors in the absence of ligand and ligand binding induced the replacement of corepressors with coactivators. We conclude that the intramolecular interactions of Phe420 with several amino acid residues in H11 and H12 stabilize H12 to recruit coactivators even in the absence of ligands and this stabilization contributes to the basal transcriptional activity of PXR.

P65 - 1-AMINOBENZOTRIAZOLE (ABT) IS NOT AN IDEAL PAN-CYP INHIBITOR FOR REACTION PHENOTYPING OF LOW CLEARANCE COMPOUNDS IN LONG-TERM CELL CULTURE MODELS

Krishna Aluri, Marina Slavsky, Cameron Parsons, Nireesh Hariparsad, and Diane Ramsden
AstraZeneca, United States

1-aminobenzotriazole (ABT) is commonly used as a non-selective inhibitor of cytochrome P450 (CYP) enzymes to delineate their role in the metabolism of xenobiotics. Reaction phenotyping of low clearance compounds has been attempted using long-term hepatocyte models such as HepatoPac® and Hurel® with ABT (1 mM) as a pan-inhibitor of CYPs. By inhibiting all CYPs the fraction metabolized by other pathways including UDP-glucuronosyltransferases (UGTs), sulfotransferases (SULTs) and aldehyde oxidases (AOs) can be determined. While it has been reported that ABT can

inhibit and induce activity of non-CYP enzymes this hasn't been comprehensively investigated¹. The goal of this work was to investigate the inhibition and induction potential of ABT. This was accomplished using plated hepatocytes, Hurel® and recombinant enzymes. As a first step the stability of ABT was investigated using the Hurel® co-cultured hepatocyte model. This data confirmed that ABT concentrations did not significantly decrease over the length of the metabolic stability assay (72 h). Multiple concentrations of ABT were then incubated along with a range of CYP and UGT substrates to determine Fm CYP. These data demonstrated that ABT treatment significantly inhibited the clearance of a non-selective UGT substrate 4-methyl umbelliferone. The ability of ABT to inhibit selective UGTs was then characterized for nine hepatic UGTs using recombinant enzymes. In addition, the potential for ABT to induce nuclear receptors involved in the regulation of drug metabolizing enzymes was explored. ABT has previously been reported to induce enzymes regulated through PXR/CAR1. The potential for ABT to mediate induction of enzymes regulated through AhR, CAR and PXR was determined using a RIS calibrated hepatocyte donor and in the Hurel® model. Dose-dependent increases in mRNA levels were observed for CYP1A2, CYP2B6, CYP3A4, and UGT1A1. This work demonstrates that ABT is not an ideal pan-CYP inhibitor for reaction phenotyping of low clearance compounds and highlights that further work is needed to identify appropriate inhibitors in these models.

References:

1. Yang, K., Hye Koh, K., & Jeong, H. (2010). Induction of CYP2B6 and CYP3A4 expression by 1-aminobenzotriazole (ABT) in human hepatocytes. *Drug metabolism letters*, 4(3), 129-133.
2. Yang, K., Hye Koh, K., & Jeong, H. (2010). Induction of CYP2B6 and CYP3A4 expression by 1-aminobenzotriazole (ABT) in human hepatocytes. *Drug metabolism letters*, 4(3), 129-133.

P66 - FOUR STEPS TO ACCURATELY SELECT ENZYME INHIBITION MODELS AND DETERMINE INHIBITION CONSTANT (KI) VALUES FOR CYP INHIBITION BY MRTX COMPOUND A, A PROTOTYPICAL SOS1 INHIBITOR

Natalie T. Nguyen

Mirati Therapeutics, Inc., United States

The inhibition constant, K_i , is the FDA recommended parameter to use for calculating an investigational drug product's potential for clinical CYP-related drug-drug interactions (DDIs). However, measuring K_i is an extensive process and compounds are typically assumed competitive inhibitors with K_i estimated as $IC_{50}/2$. As an example, MRTX Compound A was estimated to pose DDI risks for CYP1A2, CYP2C9, CYP2C19, CYP2D6, and CYP3A4/5 based on R1 value calculations when using $K_i = IC_{50}/2$ ($R1 \geq 1.02$, the basic model of reversible inhibition)¹ and clinical studies using sensitive index substrates therefore recommended by the FDA¹. As a follow up, K_i measurements were done using a semi-automated assay in 384-format and data were processed using four steps: 1) use a Michaelis-Menten substrate-velocity plot to determine V_{max} and K_m for each inhibitor concentration, 2) determine the type of inhibition based on the increasing/decreasing trend for V_{max} and K_m 3) create reciprocal plot (Lineweaver-Burk) and confirm the type of inhibition, and 4) select the correct equation in Prism (GraphPad by Dotmatics) software based on inhibition type and calculate K_i . Based on this four-step process compound A was determined to exhibit competitive inhibition of CYP2C19 and CYP3A4/5, non-competitive inhibition of CYP1A2, and mixed inhibition of CYP2C9 and CYP2D6. Calculation of more appropriate R1 values based on measured K_i values resulted in removal of the potential for CYP1A2 and 2C19 clinical DDI by Compound A.

P67 - LOCALIZATION OF ADDUCTS FORMED BY REACTIVE METABOLITES IN CYP2C9 IMPACTS PRESENCE OF TIME DEPENDENT INHIBITION

Ellen Riddle, Alex Zelter, and Nina Isoherranen

University of Washington, United States

A major concern for drug-drug interactions (DDI) includes the irreversible inhibition of cytochrome P450 enzymes (CYPs). Time dependent inhibition (TDI) may occur via adduction of CYP enzymes by reactive drug metabolites. Traditional methods to detect and identify reactive metabolites during drug development include glutathione trapping, radiolabeled compounds, or metabolite identification. We hypothesize that the consequences of protein adduction via reactive metabolites (such as toxicity or enzyme inactivation) are the result of which proteins are adducted and the precise locations of those adducts. Traditional methods of adduct identification do not yield information regarding the precise proteins and amino acids that are adducted and thus cannot be used to study the impact of adduct location on TDI or toxicity. The goal of this project is to establish a relationship between protein inactivation and the specific amino acid residues that are adducted. The above hypothesis was tested using a combination of both *in vitro* and proteomic methods with CYP2C9 as a model enzyme, and raloxifene and tienilic acid as the inhibitors. *In vitro* IC_{50} shift experiments used CYP2C9 supersomes with a 30 minute pre-incubation in the presence or absence of the respective inhibitor, and the substrate at the experimentally determined K_m to establish time-dependent inhibition. Adduct formation with CYP2C9 was

assessed using novel proteomic tools and LC-MS/MS to identify and localize CYP2C9 adducts formed by reactive metabolites. Both raloxifene and tienilic acid are known substrates of CYP2C9 that form reactive metabolites from this enzymatic step. When tested with a standard IC50 experiment, raloxifene and tienilic acid inhibited CYP2C9 mediated metabolism (IC50 of 0.8-1.1 and 4.18 μ M, respectively). Using an IC50 shift experiment as described above, tienilic acid was found to be a TDI of CYP2C9 (14-fold shift in the IC50), whereas raloxifene did not cause an IC50 shift with CYP2C9. Surprisingly, incubation of raloxifene with CYP2C9 supersomes resulted in formation of raloxifene-protein adducts on multiple residues in CYP2C9. These adducts were then visualized using Limelight and quantified using DIA analysis. Raloxifene was found to form multiple unique adducts on CYP2C9 - despite the lack of TDI. These findings suggest that although adducts of the inhibitors are present with CYP2C9, inactivation is dependent on the localization and abundance of adducts present. Additionally, this implies that some adducts do not have any consequences for the enzymatic function of the CYP and that the reactive metabolite can leave the active site and still go on to adduct the enzyme, but not impact metabolite formation kinetics. Overall, a definitive characterization of the specific adducts formed is necessary to understand the functional consequences of protein adduction.

P68 - ENTERIC VERSUS HEPATIC URIDINE 5'-DIPHOSPHO (UDP)-GLUCURONOSYLTRANSFERASE (UGT) ACTIVITY: A COMPARISON OF CRYOPRESERVED HUMAN INTESTINAL MUCOSA (CHIM) AND CRYOPRESERVED HUMAN HEPATOCYTES (CHH) IN THE ENZYME KINETICS OF β -ESTRADIOL, CHENODEOXYCHOLIC ACID,

Albert Li¹ and Ming-Chih Ho²

¹Discovery Life Sciences, United States and ²Discovery Life Sciences In Vitro ADMET Laboratories

An orally-administered drug is firstly metabolized enterically, either by the intestinal flora or by the enterocytes during the absorption process. Upon entering the portal circulation, the absorbed drug and the enteric metabolites are subjected to hepatic metabolism, followed by the distribution of the unmetabolized parent drug and the hepatic metabolites into the systemic circulation. An accurate assessment of the potential *in vivo* drug metabolic fates of orally administered drugs therefore would require a thorough understanding of both enteric and hepatic drug metabolism enzymes. We report here a comparison of human enteric and hepatic UDP-glucuronosyltransferase (UGT) activities using pooled donor cryopreserved human hepatocytes (PHH) and pooled donor cryopreserved human intestinal mucosa (PCHIM). The metabolic pathways quantified and the respective predominant UGT isoforms were β -estradiol 3-glucuronidation (UGT1A1), chenodeoxycholic acid (CDCA) glucuronidation (UGT1A3), propofol O-glucuronidation (UGT1A9), zidovudine (AZT) glucuronidation (UGT2B7), trifluoperazine N-glucuronidation (UGT1A4), serotonin glucuronidation (UGT1A6), and raloxifene 6-glucuronidation (hepatic UGT1A1, 1A9, and extrahepatic UGT1A8). The apparent Km (μ M) and Vmax (pmol/min/mg protein) values are: b-estradiol (Km: 55.9 (PCHIM), 92.5 (PHH); Vmax: 28.7 (PCHIM), 33.6 (PHH); CDCA (Km: 8.8 (PCHIM), 20.1 (PHH); Vmax: 457.4 (PCHIM), 351.4 (PHH); trifluoperazine (Km: 29.0 (PCHIM), 82.6 (PHH); Vmax: 3.48 (PCHIM), 286.3 (PHH); propofol (Km: 187.0 (PCHIM), 285.2 (PHH); Vmax: 17.0 (PCHIM), 173.1 (PHH); AZT (Km: 787 (PCHIM), 279 (PHH); Vmax: 7.43 (PCHIM), 135.6 (PHH); raloxifene (Km: 0.47 (PCHIM), 34.5 (PHH); Vmax: 46.6 (PCHIM), 171.4 (PHH). Apparent intrinsic clearance calculated as Vmax/Km, show that enteric and hepatic clearance are similar for b-estradiol, and CDCA; hepatic clearance significantly higher than enteric clearance for trifluoperazine, propofol, and AZT; and enteric clearance significantly higher than hepatic clearance for raloxifene. Our results suggest that CHIM and PHH represent *in vitro* experimental systems for the relative roles of enteric and hepatic metabolism on the metabolic fates of orally administered drugs. We believe that findings from the two intact cell systems with intact plasma membranes, uninterrupted enzymes and cofactors at physiological concentrations may provide information supplementary to that from cell free systems such as human liver and intestinal microsomes.

P69 - CONVERSION OF DRUG METABOLITES BACK TO PARENT DRUGS BY HUMAN GUT MICROBIOTA IN AN EX VIVO FERMENTATION SCREENING PLATFORM

Evita van de Steeg¹, Frank Schuren¹, R.Scott Obach², Birol Usta¹, Margreet Heerikhuisen¹, Hakim Rahaoui¹, Steven Erpelinck¹, Irene Nooijen¹, and Wouter Vaes¹

¹TNO, Netherlands and ²Pfizer, United States

Introduction: Oral administration of drugs is an attractive, non-invasive mode of delivery of pharmaceuticals to patients. When arriving in the colon, they encounter thousands of microbial species that reside in the large intestine, including bacteria, viruses, and fungi. Here complex drug-microbial interactions may occur. Although the liver is regarded as major organ for drug metabolism, current insights into the role of our gut microbiome in drug metabolism may shine new light on this. One of the aspects is the role of gut microbiota in enterohepatic circulation. Intestinal bacteria secrete enzymes such as β -glucuronidase, sulfatase and β -glucosidase which can deconjugate the drug metabolites excreted in the bile and release the parent compound for absorption into the systemic circulation.

Methods: To investigate human colon microbiota-mediated deconjugation of drug metabolites, an ex vivo fermentation screening platform was used in which human colonic microbiota conditions are simulated. A set of 8 drug metabolites (acetaminophen sulphate, mycophenolic acid glucuronide, sertraline-N-CO-glucuronide, benzydamine N-oxide,

imipramine N-oxide, SN38 glucuronide (SN38G), raloxifene 4'-glucuronide and raloxifene 6'-glucuronide) was incubated for 6 and 24 hours with human healthy adult colon microbiota under strictly anaerobic conditions. In order to determine the kinetics of the metabolic conversion, SN38G was applied as a model drug. Linearity of the metabolic conversion was studied over 6h, and kinetics of the metabolic conversion was studied at multiple concentrations of SN38G (5, 25, 50 and 100 μM). All samples were analyzed using high-performance liquid chromatograph–UV–high-resolution mass spectrometry analysis.

Results: All drug metabolites showed microbiota-based conversion to parent drug within 6h, demonstrating different reaction types including phenol sulfate hydrolysis, phenol glucuronide hydrolysis, acyl glucuronide hydrolysis, carbamoyl glucuronide hydrolysis, and N-oxide reduction. Deconjugation of SN38G into SN38 was linear up to 4h of incubation, with an average V_{max} of 333 $\mu\text{mol}/\mu\text{g}$ bacterial DNA/h (95% confidence interval (CI): 285-403) and average K_m of 28 μM (95% CI: 17-45).

Conclusion: We present a new research tool to investigate human colon microbiota-based drug metabolism, including conversion of drug metabolites back to parent in a qualitative and quantitative manner. Combined with intestinal absorption, hepatic uptake and metabolism and renal clearance data, these microbiome conversion data will be used in physiologically-based pharmacokinetic (PBPK) model to predict enterohepatic circulation and plasma kinetics in humans. Research directed at personalized variation in drug metabolism is considered as a next step.

P70 - UPDATED STATUS ON THE COLOR DEVELOPERS CURRENTLY USED IN THERMAL PAPERS ON THE FRENCH MARKET, RELATED HAZARDS AND HUMAN EXPOSURE RISKS

Daniel Zalko, Anne Hillenweck, Marine Valleix, Elodie Person, Sandrine Bruel, Sylvie Chevolleau-Mege, Olha Tsykhotska, Florence Blas-Y-Estrada, and Laurent Debrauwer
INRAE, France

Introduction: Thermal printing solutions are increasingly used, with a worldwide market of thermal papers (TP) estimated over 4 billion US\$ in 2021 and expected to exceed 6 billion US\$ by 2028. This includes POS (point-of sale) solutions, but also self-adhesive labels and many other types of tickets. TP technology is based on the presence of a colorless dye and of a color developer (CD) within the blank ticket. Their reaction under heat (printers heads) produces the coloration, following proton exchange between the CD (a proton donor) and the dye. Since the 1970's, bisphenol A (BPA) has been the main CD used in TP. Following drastic restrictions in several countries, including the EU, BPA is being gradually replaced by alternative CD, including other bisphenols such as bisphenol S (BPS) and analogues, but also non-bisphenol substances such as Pergafast-201 (PF-201). Unlike their other uses for the manufacture of plastics and epoxy resins as polymers, in TP, bisphenols are present as monomers, e.g. as free and potentially active endocrine disrupting substances (EDC). Materials and Methods: >200 TP collected in France between July 2021 and May 2022, including POS but also adhesives used for parcel shipping and foods labeling were extracted and screened by HPLC/UV-DAD for the presence of CD. Their structures were confirmed by high resolution mass spectrometry (UHPLC-ESI/HRMS). Results: the current French market study demonstrates that following the ban of BPA in the EU, which entered into force in January 2020, BPS, and to a lesser extent PF-201, are the main CD present in TP used or available in France. Other CD, including D-8 (isopropyl-BPS), TGSH (4,4'-Sulfonylbis [2-(2-propenyl)phenol]) and BPS-MAE were also occasionally detected. Of note, BPA can still be found in a number of TP, and some specific solutions (like hard paper tickets) appear to be more often than others based on D-8. Conclusions: BPS, despite its EDC properties, is the major replacement CD in TP available on the French market, similar to the situation that prevails in regions and countries in which BPA is not yet regulated for its use in TP. Human exposure to this EDC and to BPS and analogues, but also to PF201, can be expected from skin contact, both as regards professionals and consumers. Additional studies are being carried out *in vitro/ex-vivo* to reach a better assessment of the fate and transdermal exposure route to these substances, in particular as regards the latter molecule, for which very little toxicological data is currently available.

P71 - TRANSPORTER KINETICS AND MODULATION OF THE ORGANIC CATION TRANSPORTER OCT1 (SLC22A1) IN 3D CULTURED PRIMARY HUMAN HEPATOCYTES

Alina Meyer, Niklas Handin, Malin Stüwe, Jens Eriksson, Mikael E. Sellin, and Per Artursson
Uppsala University, Sweden

Both two-dimensional and newly emerging three-dimensional cell models of primary human hepatocytes (PHH) are commonly used tools to study liver disease and function *in vitro*[1]. 3D PHH spheroids maintain a differentiated phenotype with preserved metabolic function for weeks in culture[2]–[5]. However, transporter function has not yet been investigated in PHH spheroids. Here, we investigate transporter kinetics of the organic cation transporter 1 (OCT1, encoded by SLC22A1) in PHH spheroids cultivated in 384-well format, using the fluorescent model substrate ASP+ (4-(4-(Dimethylamino)styryl)-N-methylpyridinium Iodide). First, the expression of all ASP+ transporters was quantified by global proteomics. Next, time- and concentration-dependent studies of the uptake of ASP+ were performed and validated by live cell imaging. Short-term (10 min) studies were performed with direct inhibitors of OCT1. Finally, the long-term (7 - 14 days) effects of potential OCT1 modulators on transport activity were investigated. For a subset of these modulators, no

previous assays with prolonged exposure in hepatic models have been reported. The selected compounds affected or induced nuclear receptors, DILI, steatosis, cholestasis and inflammation. The results indicate that PHH spheroids express the OCT1 protein at high levels and that OCT1 is the major or only transporter for ASP+ in these PHH spheroids. The affinity (Km) of ASP+ to OCT1 was comparable to previously published data in different 2D cultures. The direct OCT1 inhibitors reduced the uptake of ASP+ in the spheroids. In contrast to previous reports of up-[6] or downregulated[7]–[9] OCT1 mRNA expression, transporter function was stable in all tested long-term conditions, suggesting that OCT1 function remains stable during perturbation of the cellular homeostasis. Our results show that PHH spheroids express fully active OCT1 and that transporter kinetics can be studied in individual spheroids using fluorescent probes. Since the spheroids remain fully functional for up to several weeks in culture, they can be used to investigate perturbation to cellular functions over longer periods (days).

References:

1. R. J. Weaver *et al.*, "Managing the challenge of drug-induced liver injury: a roadmap for the development and deployment of preclinical predictive models," *Nat Rev Drug Discov.* vol. 19, no. 2, pp. 131-148, Feb. 2020, doi: 10.1038/s41573-019-0048-x.
2. C. C. Bell *et al.*, "Comparison of Hepatic 2D Sandwich Cultures and 3D Spheroids for Long-term Toxicity Applications: A Multicenter Study," *Toxicological Sciences*, vol. 162, no. 2, pp. 655-666, Apr. 2018, doi: 10.1093/toxsci/kfx289.
3. N. Handin, *Proteomics informed investigation of human hepatocytes and liver tissue*, vol. 298. Uppsala: Acta Universitatis Upsaliensis, 2021. doi: 10.33063/diva-446954.
4. S. U. Vorrink, Y. Zhou, M. Ingelman-Sundberg, and V. M. Lauschke, "Prediction of Drug Induced Hepatotoxicity Using Long-Term Stable Primary Hepatic 3D Spheroid Cultures in Chemically Defined Conditions," *Toxicol Sci*, vol. 163, no. 2, pp. 655-665, Jun. 2018, doi: 10.1093/toxsci/kfy058.
5. K. P. Kanebratt *et al.*, "Primary Human Hepatocyte Spheroid Model as a 3D In Vitro Platform for Metabolism Studies," *Journal of Pharmaceutical Sciences*, vol. 110, no. 1, pp. 422-431, Jan. 2021, doi: 10.1016/j.xphs.2020.10.043.
6. A. Rulcova *et al.*, "Glucocorticoid receptor regulates organic cation transporter 1 (OCT1, SLC22A1) expression via HNF4a upregulation in primary human hepatocytes," *Pharmacol Rep*, vol. 65, no. 5, pp. 1322-1335, 2013, doi: 10.1016/s1734 1140(13)71491-9.
7. L. Hyrsova *et al.*, "The pregnane X receptor down-regulates organic cation transporter 1 (SLC22A1) in human hepatocytes by competing for ('squelching') SRC-1 coactivator," *Br J Pharmacol*, vol. 173, no. 10, pp. 1703-1715, May 2016, doi: 10.1111/bph.13472.
8. M. Saborowski, G. A. Kullak-Ublick, and J. J. Eloranta. "The Human Organic Cation Transporter-1 Gene Is Transactivated by Hepatocyte Nuclear Factor-4a," *J Pharmacol Exp Ther.* vol. 317, no. 2, pp. 778-785, May 2006.
9. M. Vee, V. Lecreur, B. Stieger, and O. Fardel, "Regulation of Drug Transporter Expression in Human Hepatocytes Exposed to the Proinflammatory Cytokines Tumor Necrosis Factor- or Interleukin-6," *Drug metabolism and disposition: the biological fate of chemicals*, vol. 37, pp. 685-93, Mar. 2009, doi: 10.1124/dmd.108.023630.

P72 - PROTEOME DECONVOLUTION OF LIVER BIOPSIES REVEALS HEPATIC CELL COMPOSITION AS AN IMPORTANT MARKER OF CELL SPECIFIC RESPONSES

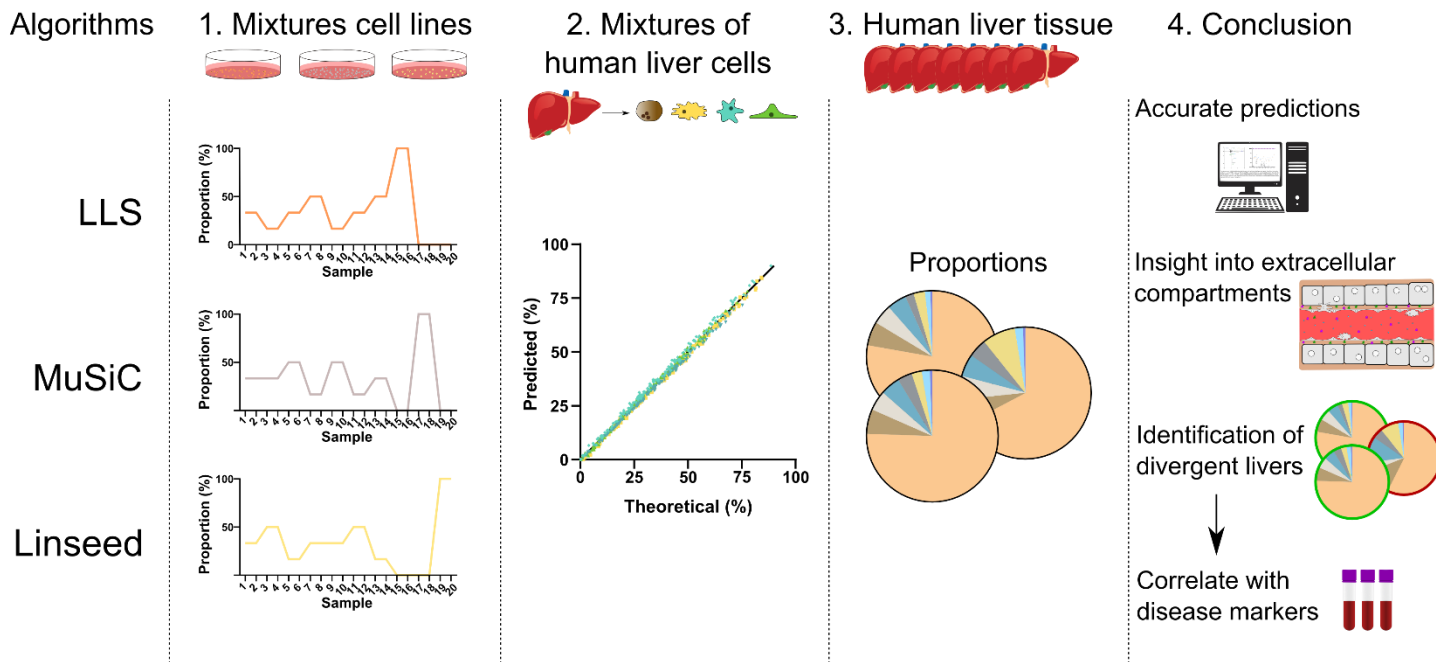
Per Artursson¹, Niklas Handin¹, Di Yuan¹, Magnus Ölander¹, Christine Wegler¹, Cecilia Karlsson^{2,3}, Rasmus Jansson-Jansson-Löfmark², Jøran Hjelmæsæth^{4,5}, Anders Åsberg⁵, Volker Lauschke⁶, and **Rebekkah Hammar**¹

¹Uppsala University, Sweden, ²AstraZeneca, Sweden ³Sahlgrenska Academy, Sweden, ⁴Vestfold Hospital Trust, Norway, ⁵University of Oslo, Norway, and ⁶Karolinska Institutet, Sweden

Human liver tissue is composed of heterogeneous mixtures of different cell types and analysis of their cellular composition can provide information on hepatic physiology, effects of drug treatment and disease progression. Deconvolution algorithms for the identification of cell types and their proportions have recently been developed for transcriptomic data. However, no method for the deconvolution of bulk proteomics data has been presented to date. Here, we investigate whether proteomes, which usually contain less data than transcriptomes, can provide useful information after deconvolution using different algorithms. We demonstrate that proteomes from mixtures of cell lines, isolated primary liver cells, and human liver tissue can be deconvoluted with high accuracy and, in contrast to transcriptome-based deconvolution, liver tissue proteomes also provided information about extracellular compartments. Importantly, we show using proteomics data from liver biopsies of 56 patient biopsies undergoing Roux-en-Y gastric bypass surgery that proportions of immune and stellate cells correlate with inflammatory markers and altered composition of extracellular matrix proteins characteristic of early-stage fibrosis. In summary, our results demonstrate that proteome deconvolution

can be used as a molecular microscope to investigate the cellular and extracellular composition of tissue samples, thereby providing an important toolset for the identification of cell-type specific events in biopsy samples after drug exposure and disease-specific large-scale proteome collections.

Proteomics informed deconvolution



P73 - AN *IN VITRO* INVESTIGATION OF CANNABIDIOL METABOLISM AND HEPATOTOXICITY USING THREE-DIMENSIONAL HUMAN HEPATOCYTE SPHEROIDS

Jessica Beers, Shalon Harvey, and Klarissa Jackson
 University of North Carolina at Chapel Hill, United States

Cannabidiol (CBD) is a pharmacologically active component of cannabis that has gained widespread popularity as a natural product and dietary supplement. In 2018, CBD was approved by the FDA for treating seizures due to Lennox-Gastaut and Dravet syndrome, two rare and severe forms of epilepsy in children(1). During clinical trials, CBD was found to cause a severe and dose-limiting hepatotoxicity in 13% of treated patients(1). The risk for this adverse effect was greatly increased for patients concomitantly taking valproate, another hepatotoxic antiepileptic drug. CBD-induced hepatotoxicity can exhibit a delayed onset, with initial signs of toxicity appearing up to 18 months after starting treatment, particularly if it is taken with valproate(1). CBD is extensively metabolized in the liver and is associated with multiple metabolism-mediated drug interactions(2,3); however, the mechanism(s) of CBD-mediated hepatotoxicity in combination with valproate are not well understood. The purpose of this study is to determine the mechanism(s) of CBD-related toxicity and interactions with valproate using three-dimensional (3D) human hepatocyte spheroids. 3D spheroids are a novel *in vitro* hepatocyte model that offers numerous advantages over traditional culture methods, including higher throughput, improved sensitivity to hepatotoxic drugs, and increased viability over extended culture periods, thus allowing detection of delayed onset toxicity(4). Spheroid-qualified human hepatocytes from four individual donors were used to evaluate the dose- and time-dependent cytotoxic effects of CBD and valproate. Following spheroid formation over 6 days, spheroids were treated with increasing doses of CBD and valproate, and spheroid morphology, viability (ATP release), and urea production were measured on days 7, 14, and 21 after initial seeding. While no toxicity was observed following 24 hours of drug exposure, a delayed onset dose-dependent toxicity was observed on days 14 and 21. This study is the first to examine the toxic relationship between CBD and valproate using this comprehensive *in vitro* approach. Future studies will examine drug metabolite formation, cell stress, and antioxidant response pathways following CBD and valproate treatment.

References:

1. Greenwich Biosciences Inc. Epidiolex (Cannabidiol) [Prescribing Information]. 2020.
2. Jiang, R.; Yamaori, S.; Takeda, S.; Yamamoto, I.; Watanabe, K. Identification of Cytochrome P450 Enzymes Responsible for Metabolism of Cannabidiol by Human Liver Microsomes. *Life Sci.* 2011, 89, 165–170.
3. Bansal, S.; Maharao, N.; Paine, M. F.; Unadkat, J. D. Predicting the Potential for Cannabinoids to Precipitate Pharmacokinetic Drug Interactions via Reversible Inhibition or Inactivation of Major Cytochromes P450. *Drug Metab. Dispos.* 2020, 48, 1008–1017.
4. Bell, C. C.; Hendriks, D. F. G.; Moro, S. M. L.; Ellis, E.; Walsh, J.; Renblom, A.; Fredriksson Puigvert, L.; Dankers, A. C. A.; Jacobs, F.; Snoeys, J.; Sison-Young, R. L.; Jenkins, R. E.; Nordling, Å.; Mkrtchian, S.; Park, B. K.; Kitteringham, N. R.; Goldring, C. E. P.; Lauschke, V. M.; Ingelman-Sundberg, M. Characterization of Primary Human Hepatocyte Spheroids as a Model System for Drug-Induced Liver Injury, Liver Function and Disease. *Sci. Rep.* 2016, 6, 25187.

P74 - OPTIMIZATION OF HEPATOCYTE BINDING ASSAY CONDITIONS TO ADDRESS LOW COMPOUND RECOVERY ISSUES IN EARLY DRUG DISCOVERY

Megha Chandrashekar and Guo Zhong
Amgen, United States

Hepatocyte binding assays are routinely performed in early drug discovery to determine fraction unbound ($f_{u,hep}$), which is an important parameter used for *in vitro-in vivo* correlations. A widely accepted industry standard of three freeze-thaw (3 F/T) cycles is typically used to significantly reduce enzyme activity and prepare “inactive” hepatocytes for the binding assay. The percentage of compound recovery is routinely monitored. Recently, we discovered that one set of Amgen compounds with a similar core chemical structure showed low compound recovery (<50%) when performing the hepatocyte binding assay in mouse hepatocytes, even though these compounds are chemically stable in buffer. Our preliminary data indicated that the depletion of these compounds still occurred in “inactive” mouse hepatocytes and a time-dependent formation of metabolites derived from hydrolysis was observed in parallel. All the data suggested that the activity of some metabolic enzymes remained in hepatocytes after 3 F/T cycles causing the depletion of these compounds. In order to address the low compound recovery issue and obtain reliable $f_{u,hep}$ values for this set of Amgen compounds, the assay conditions for the hepatocyte binding assay were optimized in the current study. “Inactive” mouse and human hepatocyte were prepared under five different conditions, including 1) 3 F/T, 2) 6 F/T, 3) 3 F/T + 1 hour incubation at 65°C, 4) 3 F/T + 24 hours at room temperature (RT), and 5) 3 F/T + 24 hours at RT + 1 hour incubation at 65°C. The compound depletion rate in “inactive” hepatocytes prepared from different conditions were measured either at 37°C or 4°C. Tested compounds included two representative Amgen compounds (K1 and K2) and several probe substrates for various hepatic metabolic enzymes. Buffer control and viable hepatocytes control groups were also included in the current study. Our data showed that significant depletion of K1 and K2 still occurred at 37°C in “inactive” mouse and human hepatocytes prepared from condition 1-3 and after 45-min incubation about 30-50% of compounds were depleted, while in hepatocytes prepared from condition 4 and 5 the depletion rate at 37°C was close to zero. With GDC-0834 and irinotecan as substrates, in comparison to the depletion rate in viable mouse hepatocytes the compound depletion rate in “inactive” hepatocytes at 37°C was reduced about 80% under condition 1-2 and >90% under condition 3-5. For other substrate compounds, including midazolam, umbelliferone and benzydamine, the compound depletion rate at 37°C was reduced >90% in hepatocytes prepared from all five conditions when compared to that measured in viable hepatocytes. In addition, when the compound depletion was performed under 4°C, little or no compound depletion was observed for all the tested compounds in “inactive” hepatocytes prepared from 3 F/T. To summarize, in order to address the low compound recovery issue in the hepatocyte binding assay, hepatocytes can be left at RT for 24 hours after 3 F/T cycles to further reduce enzyme activity, or the hepatocyte binding assay can be performed under 4°C if the impact of low temperature on $f_{u,hep}$ is minimal for the target compounds.

P75 - ROLE OF OXIDATIVE STRESS IN HEPEXTEND SUPPLEMENT MEDIATED IMPROVEMENT IN METABOLIC AND TRANSPORTER FUNCTION OF PRIMARY HUMAN HEPATOCYTES

Rohit Jindal, Julia Tritapoe, Chris Dulany, and David Kuninger
Thermo Fisher Scientific, United States

Primary human hepatocyte (PHH) cultures play important role in drug discovery and development. The ability to maintain various Cytochrome P450 (CYP450) enzymatic function and transporter activity in hepatocytes is critical for assessing drug disposition and toxicity profile. Sandwich culture of hepatocytes promote attainment of proper polarity in cultures whereby basolateral and biliary transporters are expressed on basal and apical surface, respectively. However, as the cells are plated and maintained in culture the reduction in metabolic and transporter activity occurs as the cells adapt to the culture condition. In this work, we investigated the effect of adding HepExtend supplement to media utilized during maintenance of sandwich culture of PHH and assessed its effect on 5- day cultures derived from cryopreserved cells. The

supplement improve morphology, viability (ATP levels), metabolic (CYP1A2, CYP2B6, CYP3A4) and transporter activity (uptake of taurocholate and rosuvastatin) of hepatocytes. For transporter function, both basolateral uptake and biliary efflux are enhanced upon HepExtend supplementation. In addition to the plated cells, metabolic and transporter activity was also assessed at suspension stage immediately after thawing cryopreserved cells. It was observed that metabolic function (CYP1A2 and CYP2B6) and transporter activity (uptake of taurocholate and rosuvastatin) was higher at suspension stage while CYP3A4 function was similar to the plated cultures exposed to HepExtend supplement. However, the difference in metabolic (CYP1A2 and CYP2B6) and transporter activity between suspension and 5-day plated sandwich cultures is greatly reduced by HepExtend supplementation, which is a significant improvement for sandwich cultures of PHH. To investigate the mechanism(s) responsible for improvement in metabolic and transporter activity, oxidative stress was assessed in hepatocytes exposed to maintenance media with and without HepExtend supplement. Depending on the donor, it was observed that HepExtend supplementation reduces oxidative stress in hepatocytes. Furthermore, modulation of oxidative stress in hepatocytes by supplementing the maintenance media with antioxidant improved both metabolic and transporter function. However, the levels did not reach those observed in HepExtend supplement highlighting the involvement of other mechanism(s) through which HepExtend improves metabolic and transporter function that is the subject of our current investigation. Finally, although the level of metabolic and transporter activity improvement varies from donor to donor, incorporation of HepExtend supplement can potentially expand the donor pool available for 5-day plateable studies and holds potential for improving the IVIVC (*in vitro- in vivo* correlation) of low clearance drugs.

P76 - DEVELOPMENT OF AN INTEGRATED ASSESSMENT TOOL TO CATEGORISE DILI RISK IN DISCOVERY

Barry Jones¹ and Jennifer Vance²

¹Pharmaron, United Kingdom and ²Pharmaron, United States

Idiosyncratic drug hepatotoxicity continues to be a major problem in drug development, causing over 10% of cases of acute liver failure, and leading to post marketing warnings and withdrawal of drugs.¹ Despite rigorous toxicological testing, animal studies can fail to predict the hepatotoxic responses seen in a small population of those exposed to the drug. A number of *in vitro* assays have been developed over the past years, in an aim to reduce idiosyncratic responses, focusing on exploring mechanisms which could cause hepatotoxicity, such as metabolic activation and trapping, mitochondrial toxicity and bile salt export pump (BSEP) inhibitors.² Combining these assays with physicochemical characteristics, systemic exposure and assessment of overall body burden have led to predictive models that correlate with FDA categorisation of drug induced liver injury (DILI) risk for marketed drugs.³ To aid prioritisation of clinical candidate molecules in the discovery phase we have developed a streamlined tool appropriate for use in drug discovery. The model was developed through assessment of a panel of molecules with equal distribution of clinical DILI outcome, as categorised by the FDA system.⁴ Compounds were assessed in assays for formation of glutathione adducts, multi-parametric cell health, mitochondrial toxicity and BSEP inhibition. In agreement with current thinking in the literature, the ability to form glutathione adducts did not correlate with DILI categorisation, and so this was omitted from the model. Scoring the outcomes of the remaining assays along with physicochemical descriptors and clinical dose parameters resulted in the development of a model with binary output correlating with DILI categorisation. The scoring paradigm used in the model correctly predicts 73% of the FDA categorised compounds tested with a DILI concern (29/40 compounds) and 77% without (10/13 compounds) a DILI concern. This model allows the prioritisation of candidate molecules, aiming to minimise the number of compounds entering development which may cause drug induced hepatotoxicity.

P77 - 3D SPHEROIDS USING PRIMARY HUMAN HEPATOCYTES TO PREDICT DRUG INDUCED LIVER INJURY

Barry Jones¹ and Jennifer Vance²

¹Pharmaron, United Kingdom and ²Pharmaron, United States

Primary human hepatocytes (PHHs) are considered the “gold standard” cellular model for liver functions. Although hepatocytes are often the *in vivo* targets of drug induced liver injury (DILI) PHHs are not suitable for hepatotoxicity tests under conventional 2D monolayer culture conditions, due to the rapid loss of their hepatic phenotypes, functions, and cell viability. Recent advances have shown that 3D culture of PHHs as spheroids can significantly prolong the cell viability and extend hepatic function *in vitro*.

In the present study, we validated and characterized a PHH 3D spheroid system for markers of DILI including cell viability, DNA damage, mitochondrial function, ROS reaction as well as GSH content. This involved a four-week hepatotoxicity assay with eight repeated doses of 42 test compounds. Among these 42 compounds, 7 compounds are classified as no DILI concern compounds based on clinical severity category, while the other 35 compounds are all DILI positive compounds. In addition, a cholestatic model was also established by repeatedly co-exposing with non-toxic concentrated bile acid mixture.

The activity of CYP enzymes was maintained for 4-weeks of culture and the urea production, albumin secretion and LDH release maintained stable over the 4 weeks long-term. 42 compounds were tested in the chronic hepatotoxicity assay and the cell viability IC50 value of 7 compounds classified as no DILI concern were all greater than 200 μ M. 13 of 18

compounds which are classified as low DILI concern showed a IC50 value of more than 200uM, while IC50 values for the remaining 5 compounds ranged from 10.5 uM to 361.5 uM. 18 compounds were classified as high to severe DILI concern. 2 compounds classified as severe DILI concern had no IC50 value, which were false negatives in the test. For the other severe DILI concern compounds, all had IC50 values which varied between 2uM to 180uM.

Testing 42 clinical drugs, we demonstrated that using 3D spheroids enabled chronic exposure studies which was then able to discriminate between those compounds that cause DILI and others which do not. Furthermore, co-exposing with non-toxic concentrated bile acid mixture, 3D culture can be used to detect compounds with cholestatic liability.

P78 - OPTIMIZING A MICROCAVITY PLATE-BASED HUMAN HEPATOCYTE SPHEROID MODEL FOR *IN VITRO* CLEARANCE STUDIES

David Kukla, Mei Feng, Lance Heinle, Yueting Wang, and David Stresser
AbbVie, United States

Background: Incubation of drug candidates with hepatocyte suspensions to determine intrinsic clearance is common in drug discovery. However, metabolically stable compounds (e.g., < 15% loss over four-hour hepatocyte viability window, 1E6 cells/mL) necessitate alternative approaches to generate reliable clearance estimates. Self-assembled aggregates of hepatocytes (spheroids) have been shown to support morphology, viability, functions, and drug metabolizing enzymes for weeks *in vitro*. Extended incubation times in this model could permit sufficient metabolic loss to obtain reliable measurements within typical LC/MS/MS analytical precision limits. Recently, the utility of spheroids within 96-well ultra-low attachment (ULA) plates for predicting clearance has been demonstrated. To overcome the limited number of cells (~1.5-2k/well) and lower turnover in single spheroid applications, multiple spheroids in a single well would be desirable. Recently, this limitation has been addressed with Elplasia® microcavity plates from Corning that enable ~80 spheroids to be cultured in a single well on a 96-well plate. Objective: In the Elplasia system, we undertook a systematic evaluation of assay conditions, including the evaluation of seeding strategies, spheroidal size, and culturing techniques in the effort of enhancing primary hepatocyte functions and longitudinal stability of drug metabolizing enzymes, while demonstrating their utility for clearance prediction and metabolite identification. Additionally, co-cultures with nonparenchymal cells were fabricated to further support hepatocyte functions. The vastly higher cell number per incubation would be expected to result in sufficiently rapid metabolic loss for reliable quantitation. Methods: Spheroids of varying size were fabricated by altering the initial seeding density of hepatocytes (~16-160k) per well within 96-well Elplasia plates. As comparisons, single spheroids were fabricated by seeding 1.5k hepatocytes/well in 96-well ULA plates and monolayers were formed by seeding 50k hepatocytes/well in collagen coated 96-well plates. Albumin/urea production and cytochrome P450/FMO activities were assessed regularly with probe substrates. Multiple test compounds of varying metabolic stability were evaluated, with some results supplemented with metabolite formation data. Results: Robust spheroids were formed within ~3-5 days. Generally, decreasing the number of hepatocytes per spheroid, promoted albumin/urea production and improved P450 activities on a per cell basis. Unlike monolayers that exhibited a decline in viability and hepatic functions within days; both conventional and Elplasia spheroids displayed prolonged viability for at least 13 and 21 days, respectively. However, Elplasia spheroids functionally outperformed single spheroids with ~2-fold higher albumin production, 1.3-1.6-fold higher urea production, and elevated cytochrome 450 (i.e., ~3-4-fold higher 3A4 activity) on a per cell basis after 1-2 weeks. We speculate that the higher performance in Elplasia spheroids is due to the smaller spheroid diameter compared to conventional spheroids, which may improve nutrient exchange and reduce the likelihood of necrotic core formation. As anticipated, elevating the spheroid density per well in the Elplasia model resulted in higher parent loss for low turnover compounds, often enabling the measurement of intrinsic clearance whereas the single spheroid per well model failed to yield quantifiable clearance values. This optimized model is expected to be suitable not only for intrinsic clearance measurements but also applications requiring long term incubations (toxicity, metabolite ID, induction, etc).

P79 - HUMAN HEPATOCYTE SPHEROIDS - EVALUATION OF DRUG METABOLIZING ENZYME ACTIVITY AND CLINT

Ting Wang and Klairynne Raymond
Boehringer Ingelheim, United States

Spheroids consisting of primary human hepatocytes (PHH) are emerging as a more physiologically relevant 3D cell culture system, with distinct advantages over conventional hepatocyte 2D culture. We evaluated the utility of PHH spheroids in *in vitro* drug metabolism studies, i.e. to profile drug metabolizing enzyme (DME) activity and test compound clearance. The enzyme activities of major Phase I (CYPs 1A2, 2B6, 2C8, 2C9, 2C19, 2D6, and 3A4) and Phase II (UGTs 1A1, 1A4, 1A9, and 2B7; SULTs 1A2 and 2A1) DMEs expressed in spheroids were measured and compared to hepatocyte suspension cultures using PHHs from the same donor. Overall, in comparison to enzyme activities in suspension hepatocytes using two donors, UGT activities were approximately the same, SULT activities increased, and CYP activities decreased in PHH spheroids. The extent of CYP activity loss appeared to be related to the donor hepatocytes used. To investigate the impact of spheroid formation on DME activity, the activity levels of CYPs 3A4, 2C9, and 2D6; UGT1A1; and SULT1A1 were assessed at various stages of the spheroid formation. UGT activity levels were

unchanged during the spheroid formation process. However, SULT 1A1 activity increased and stabilized within 24 h after cell seeding and CYP activity levels started decreasing within 24 h after cell seeding. To assess the potential application of PHH spheroids in compound clearance (CL) studies, especially for compounds exhibiting low metabolic turnover, 9 intermediate to high CL compounds and 18 low CL compounds were evaluated. Compound depletion was observed for all tested compounds, except for theophylline. Finally, the ability of 7-day incubation of PHH spheroids without media change was demonstrated with respect to retention of cell viability and enzyme activity. Overall, PHH spheroids demonstrate good retention of Phase II DME activity levels, but rapidly lose CYP450 activity. Longer incubation times (7 days) enables measurement of depletion of low turnover compounds.

P80 - ABSTRACT WITHDRAWN

P81 - THE ROLE OF MYELOPEROXIDASE IN CLOZAPINE-INDUCED INFLAMMATION: LINKING REACTIVE METABOLITE FORMATION AND IDIOSYNCRATIC DRUG-INDUCED AGRANULOCYTOSIS

Samantha Sernoskie, Alison Jee, and Jack Uetrecht

University of Toronto, Canada

Background: Although clozapine has unmatched efficacy in schizophrenia treatment, it is rarely prescribed due to the serious risk of idiosyncratic drug-induced agranulocytosis (IDIAG). Progression to IDIAG, a reaction believed to be mediated by the adaptive immune system, is rare and, consequentially, the mechanism of onset remains poorly defined.[1] However, most patients experience an early inflammatory response during clozapine treatment, which we believe is a necessary but, alone, insufficient step in the mechanism of IDIAG. Using preclinical models that recapitulate this innate response, we have established that clozapine activates inflammasomes.[2] We have also demonstrated that myeloperoxidase, an enzyme in neutrophils, generates a reactive clozapine nitrenium ion that irreversibly modifies proteins,[3] but how clozapine bioactivation triggers immune activation remains undetermined. Thus, the aim of this work was to link these early mechanistic events, concentrating on the involvement of myeloperoxidase and subsequent release of inflammatory mediators, including damage-associated molecular patterns (DAMPs).

Methods and Results: *In vitro*, PMA-differentiated THP-1 macrophages were incubated with clozapine (1-10 µg/mL) for up to 24 hours. The irreversible inhibitor PF-1355 (0.1-15 µg/mL) was employed to block myeloperoxidase activation, and decreased myeloperoxidase activity was confirmed using chlorination and peroxidation enzymatic assays. Using western blotting with an anti-clozapine antibody developed in-house, a decrease in clozapine covalent binding was observed with myeloperoxidase inhibition. Clozapine-induced secretion of inflammatory mediators (e.g., cytokine/DAMP IL-1β, chemokine CXCL1) was also attenuated. *In vivo*, female Sprague Dawley rats were administered clozapine (30 mg/kg, IP) ± PF-1355 (100 mg/kg, PO) and immune changes were evaluated over 24 hours. Immune phenotyping was conducted using differential blood counts and confirmed via flow cytometry. Myeloperoxidase activity and clozapine covalent binding in neutrophils was decreased by myeloperoxidase inhibition. Furthermore, clozapine-induced increases in neutrophils and inflammatory mediators (e.g., CXCL1, glucocorticoid corticosterone, acute phase reactant α-1-acidglycoprotein, DAMP calprotectin) in the blood, liver, spleen, and bone marrow were also attenuated by myeloperoxidase inhibition.

Conclusions: These data support the working hypothesis that a myeloperoxidase-generated reactive metabolite triggers the release of DAMPs, which in turn, induces the inflammatory response to clozapine. Ultimately, a better mechanistic understanding of the early events involved in the immune response to clozapine may elucidate ways to prevent IDIAG, enabling safer, more frequent therapeutic use of this highly efficacious drug. Moreover, the inflammatory mediators elucidated here may represent biomarkers that are conserved across multiple drugs associated with the risk of various idiosyncratic drug reactions, which may facilitate development of specific screening tools for novel drug candidates. This research was supported by CIHR, NSERC, Mitacs, OGS, and UofT.

References:

1. Sernoskie SC, Jee A, Uetrecht JP. The emerging role of the innate immune response in idiosyncratic drug reactions. *Pharmacol. Rev.* 2021;73(3):861–896.
2. Sernoskie SC, Lobach AR, Kato R, et al. Clozapine Induces an Acute Proinflammatory Response That Is Attenuated by Inhibition of Inflammasome Signaling: Implications for Idiosyncratic Drug-Induced Agranulocytosis. *Toxicol. Sci.* 2022;186(1):70–82.
3. Liu ZC, Uetrecht JP. Clozapine is oxidized by activated human neutrophils to a reactive nitrenium ion that irreversibly binds to the cells. *J. Pharmacol. Exp. Ther.* 1995;275(3):1476–1483.

P82 - APPLICATIONS OF PHYSIOLOGICALLY-BASED PHARMACOKINETIC MODELS TO INVESTIGATE FOOD EFFECTS ON ORAL ABSORPTION OF IBUPROFEN SODIUMLisa Cheng¹, Po-Chang Chiang², and Harvey Wong¹¹The University of British Columbia, Canada and ²Genentech Inc., United States

Physiologically-based pharmacokinetic (PBPK) models representing drug transit through the gastrointestinal tract have been applied to predict food effects on the rate and extent of oral absorption. The traditional advanced compartmental and transit (ACAT) model [1], featuring a one compartment stomach, seven compartment small intestine, and one compartment colon, is extensively used, and when investigating food effects, the stomach compartment is associated with pH 5. However, clinical studies have indicated that gastric pH following food consumption is dynamic wherein after meal intake, gastric acidity initially decreases to the pH 4.5 to pH 5.0 range and re-acidification is observed over several hours [2,3]. Previous literature suggests that the gastric pH describing the fed state is not well captured in pharmacokinetic models [4], which results in a less than desirable degree of confidence in food effect predictions of ionizable compounds. We hypothesize that the integration of a more physiologically representative fed gastric pH profile will improve the predictive power of PBPK models. To explore this hypothesis, the ACAT model was modified to incorporate a four-compartment stomach corresponding to pHs of 5, 3.5, 2, and 1.5. The oral pharmacokinetics of ibuprofen sodium (a representative weak acid) was simulated to investigate whether a four-compartment stomach model could capture the changes in ibuprofen sodium oral pharmacokinetics associated with food consumption. A comparable area under the curve (AUC_{0-inf}), a decrease in maximum plasma concentration (C_{max}), and a delay in the time to reach C_{max} (t_{max}) were previously reported when ibuprofen sodium administered with food [5]. The modified ACAT model simulated fed plasma concentration–time profile for ibuprofen sodium which showed similar trends to observations in clinical trials [5]. The fed state resulted in a similar predicted AUC_{0-inf} when compared to the fasted state, an approximate 49% reduction in C_{max} (38% observed), and a ~5-fold increase in t_{max} (3-fold observed). These preliminary findings demonstrate a proof-of-concept and suggest that a more physiologically representative gastrointestinal pH profile integrated into mechanistic models may better capture the food effect trends for ibuprofen sodium.

References:

1. Yu, L.X.; Amidon, G.L. A Compartmental Absorption and Transit Model for Estimating Oral Drug Absorption. *Int. J. Pharm.* 1999, 186, 119–125, doi:10.1016/S0378-5173(99)00147-7.
2. Dressman, J.B.; Berardi, R.R.; Dermentzoglou, L.C.; Russell, T.L.; Schmaltz, S.P.; Barnett, J.L.; Jarvenpaa, K.M. Upper Gastrointestinal (GI) PH in Young, Healthy Men and Women. *Pharm. Res.* 1990, 07, 756–761, doi:10.1023/A:1015827908309.
3. Koziolok, M.; Schneider, F.; Grimm, M.; Modeß, C.; Seekamp, A.; Roustom, T.; Siegmund, W.; Weitschies, W. Intra-gastric PH and Pressure Profiles After Intake of the High-Caloric, High-Fat Meal as Used for Food Effect Studies. *JCR* 2015, 220, 71–78, doi:10.1016/j.jconrel.2015.10.022.
4. Chiang, P.C.; Nagapudi, K.; Dolton, M.J.; Liu, J. Exploring Multicompartment Plug Flow–Based Model Approach in Biopharmaceutics: Impact of Stomach Setting and the Estimation of the Fraction Absorbed of Orally Administered Basic Drugs. *J. Pharm. Sci.* 2020, 109, 1261–1269, doi:10.1016/j.xphs.2019.11.021.
5. Legg, T.J.; Laurent, A.L.; Leyva, R.; Kellstein, D. Ibuprofen Sodium Is Absorbed Faster than Standard Ibuprofen Tablets: Results of Two Open-Label, Randomized, Crossover Pharmacokinetic Studies. *Drugs R. D.* 2014, 14, 283–290, doi:10.1007/s40268-014-0070-8.

P83 - VITAMIN K1 METABOLISM - THE ROAD LESS TRAVELED: UTILITY OF NON-LINEAR MIXED EFFECT MODELS IN THE EVALUATION OF COMPLEX GENOMIC TRAITS

Nathan Alade, Allan Rettie, and Kenneth E. Thummel

University of Washington, United States

In pharmacogenomic studies, the use of human liver microsomes as a model system to evaluate the impact of complex genomic traits (i.e., linkage-disequilibrium patterns, coding and non-coding variation, etc.) on drug metabolism remains challenging. An example of this is the CYP4F2*3 coding variant, which has been shown to decrease vitamin K (VK) metabolic clearance *in vitro* and is associated with altered pharmacodynamic effects *in vivo*. On average, CYP4F2*3 carriers receiving coumarin-based anticoagulation therapy (i.e., warfarin) require higher doses to achieve a therapeutic INR. It has been proposed that an increase in hepatic VK levels caused by reduced metabolic clearance antagonizes the effect of warfarin, which could help explain in part the wide range in warfarin dose requirements across the population. However, metabolic contributions from CYP4F11 and complex linkage disequilibrium (LD) patterns across the CYP4F gene loci make it incredibly difficult to quantify the true effect size of causal variants. To accurately predict the true effect size of such traits requires large richly sampled datasets representative of the study population; however, the accumulation of this data can be labor intensive and time-consuming if the study design and bioanalytical methods are not high throughput. To overcome these challenges, we propose the use of non-linear mixed effect models (NLME) as an

unconventional approach to evaluate the impact of complex genomic traits on the metabolism of xenobiotics *in vitro*. We hypothesize that the inclusion of diplotype data capturing genetic variability across CYP4F2 and CYP4F11 can improve the genotype-phenotype association relative to the CYP4F2*3 V433M amino acid substitution alone, in relation to vitamin K metabolism. In this study, we evaluated the impact of CYP4F2/CYP4F11 diplotype on vitamin K metabolic activity using a non-linear mixed-effect Michaelis-Menten model (NLME-MM) developed in the software program R. Preliminary data demonstrates an NLME-MM model can predict Michaelis-Menten parameters at an individual, subgroup, and population level using a sparse dataset consisting of strategically sampled concentration-response points from a large pool of donors. We envision the utility of this approach extending beyond pharmacogenomic applications and potentially providing population-level confidence intervals or covariate adjustments for kinetic parameters obtained *in vitro* for use in auxiliary bottom-up IVIVE approaches (i.e., PBPK modeling).

This work was supported in part by funding from the National Institutes of Health, P01 GM116691.

P84 - PROTEIN ABUNDANCE OF RAT P-GP AND BCRP EFFLUX TRANSPORTERS IN TRANSFECTED MDCK, MDCKII, LLC-PK1 CELL MONOLAYERS AND RAT BRAIN MICROVESSELS

Zubida Al-majdoub¹, Janita Hogan², Jingjing Guo², Jonathan Cheong³, Kunihiro Mizuno⁴, Tom De Bruyn³, Raymond Evers⁵, Anne Kanta⁴, Michael Zientek⁴, Aleksandra Galetin¹, Amin Rostami-Hodjegan¹, and Kayode Ogungbenro¹
¹The University of Manchester, United Kingdom, ²Merck, United States, ³Genentech, United States, ⁴Takeda, United States, and ⁵Johnson & Johnson, United States

Transporters expressed in the Blood-Brain Barrier (BBB) modulate the translocation of endogenous and exogenous substances between systemic blood and brain tissue and can affect drug efficacy/toxicity that are linked to the central nervous system (CNS).

In vitro-in vivo extrapolation (IVIVE) of transporter clearances requires scaling factors that would account for the differences in the abundance of transporters between cellular systems and brain tissue.

The aim of this work was to estimate the magnitude of *in vivo* efflux transport of drugs via P-glycoprotein (P-gp) and BCRP by linking the drug affinity to the transporters and the abundance of proteins in various *in vitro* model systems and in the Sprague Dawley rat brain. The abundances of P-gp and BCRP were measured in MDCK, MDCKII and LLC-PK1 cell lines transfected with either rat or human transporter cDNAs and in rat brain microvessels.

A targeted quantitative QconCAT-based proteomics protocol was used for all the samples. P-gp and BCRP scaling factors were generated according to relative expression of transporters in cell lines and brain microvessels. Human and rat P-gp and BCRP were detected in the relevant transfected cell lines. In addition, abundance of endogenous P-gp and Bcrp transporters was monitored in all cell lines used. As these endogenous transporters may contribute to observed transport, necessary corrections should be made to account for their role. P-gp transporter in rat brain microvessels was found to be 4- to 5- fold higher compared to rat P-gp in MDCK cells. The reverse trend was apparent for Bcrp transporter, as its expression in rat brain microvessels was found to be 20- fold lower compared to rat Bcrp in MDCK cells. The current work supports proteomics-informed translation of *in vitro* P-gp-related kinetics of drugs within a physiologically based pharmacokinetic (PBPK) modelling framework.

P85 - ISOLATED PRIMARY ENTEROCYTES AND 3D ENTEROIDS AS INTESTINAL *IN VITRO* ADME MODELS REFLECTIVE OF NATIVE EPITHELIUM

Merve Ceylan, **Rebekkah Hammar**, Maria Letizia Di Martino, Jens Eriksson, Ana Lopes, Elina Jonasson, Magnus Sundbom, Martin Skogar, Patrik Lundquist, Mikael Sellin, and Per Artursson
Uppsala Universitet, Sweden

In vitro assessment of human intestinal drug ADME is desirable in a drug development setting. Short lifespans and poor culturability have historically been addressed by using tumor-derived lines such as Caco-2 cells. Major drawbacks are, however, poor reflection of ADME protein levels and the different cell types found in the native epithelium(1). Fresh or cryopreserved primary cell isolates and stem-cell derived organoids capture the different intestinal cell types, but ADME characterization in these models has thus far been limited. Enzymatically isolated primary intestinal cells have been reported as an *in vitro* system for assessing native intestinal metabolic activity.(2,3) Extending these short-term models to other ADME processes would be beneficial, yet enzymatic isolation harbors the risk of damaging membrane proteins such as transporters. We therefore first devised a gentle, non-enzymatic shaking approach(4) to generate a native enterocyte model for use as an *in vitro* ADME reference. Having this benchmark of native ADME in place, we desired to create a more sustainable and long-term alternative. We therefore hypothesized that stem-cell derived enteroids could be driven towards native ADME protein expression levels by adjusting apicobasal polarity. Healthy, normal jejunal tissues were obtained from the surgery waste of donors. Primary enterocytes were isolated as a single-cell suspension via a gentle, non-enzymatic shaking approach. Viability and apoptosis were assessed using image cytometry. 3D enteroids were established from crypts as basal-out cultures in Matrigel before being transferred to suspension culture. Enteroid apicobasal polarity and differentiation were tuned by adjusting culturing conditions.(5) Suspended enteroids were then

imaged via live-cell confocal microscopy. ADME protein profiling of native tissue, primary cell isolates, and enteroids was performed using label-free quantitative mass spectrometry-based global proteomics. Drug ADME was assessed in primary cell isolates and enteroids using model substrates followed by LC-MS analysis. After optimization, jejunal primary enterocytes were isolated at viabilities of >90% and exhibiting <20% apoptosis. Live-cell microscopy confirmed enteroid barrier function and apicobasal polarity. Proteomic analysis indicated that non-enzymatically isolated primary enterocytes and apical-out, differentiated enteroids exhibit ADME protein profiles better comparable to native tissue than the current golden standard, Caco-2 cells. Protein profiles correlated with detected drug and metabolite levels in both models. Preliminary results indicate that both novel *in vitro* models will provide a more *in vivo*-like alternative for establishing in-vitro-in-vivo correlations. Non-enzymatically isolated primary enterocytes constitute a novel short-term *in vitro* gold reference standard for assessing native intestinal ADME proteins. Enteroids, which are suitable for long-term cultivation, are a reasonable alternative to this reference when differentiated in apical-out polarity.

References:

- Olander, M., Wiśniewski, J. R., Matsson, P., Lundquist, P. & Artursson, P. The Proteome of Filter-Grown Caco-2 Cells With a Focus on Proteins Involved in Drug Disposition. *Journal of Pharmaceutical Sciences* **105**, 817–827 (2016).
- Ho, M.-C. D., Ring, N., Amaral, K., Doshi, U. & Li, A. P. Human Enterocytes as an In Vitro Model for the Evaluation of Intestinal Drug Metabolism: Characterization of Drug-Metabolizing Enzyme Activities of Cryopreserved Human Enterocytes from Twenty-Four Donors. *Drug Metab Dispos* **45**, 686–691 (2017).
- Li, A. P. *et al.* Cryopreserved Human Intestinal Mucosal Epithelium: A Novel In Vitro Experimental System for the Evaluation of Enteric Drug Metabolism, Cytochrome P450 Induction, and Enterotoxicity. *Drug Metab Dispos* **46**, 1562–1571 (2018).
- van der Post, S. & Hansson, G. C. Membrane Protein Profiling of Human Colon Reveals Distinct Regional Differences. *Molecular & Cellular Proteomics* **13**, 2277–2287 (2014).
- Co, J. Y. *et al.* Controlling Epithelial Polarity: A Human Enteroid Model for Host-Pathogen Interactions. *Cell Rep* **26**, 2509–2520.e4 (2019).

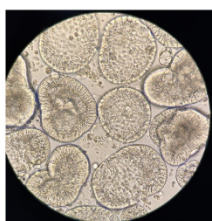


Figure 1. Differentiated human apical out organoids. (Light microscope, magnification 40x, numerical aperture 0.5)

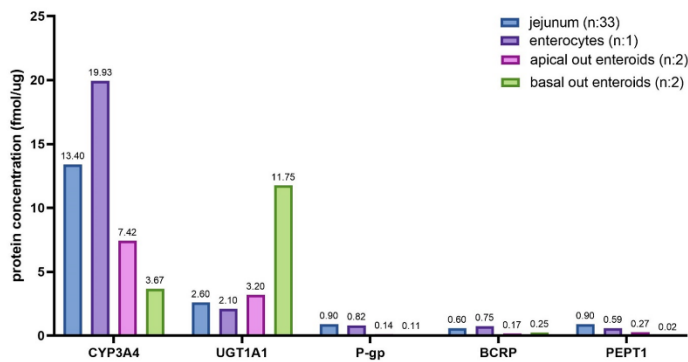


Figure 2. Clinically important ADME protein expression in human jejunum, enterocytes, and organoids.

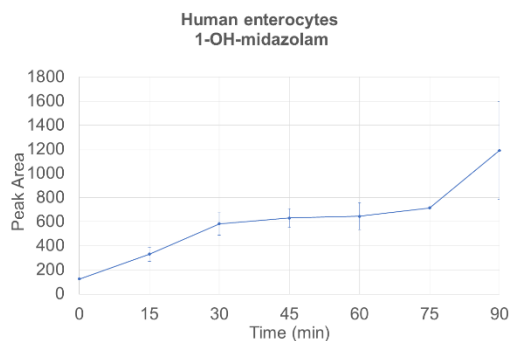


Figure 3. 1-OH-midazolam formation in human enterocytes. [Substrate 1 μ M midazolam, Hu21je] (Cell amount: 1E6/well)].

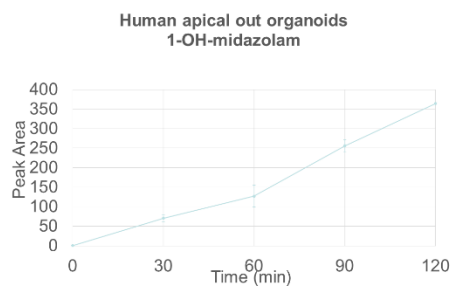


Figure 4. Metabolite formation in human apical out organoids. [Organoid amount per well: 100 organoids].

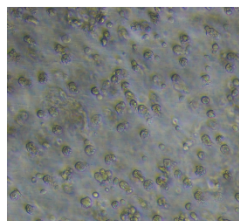


Figure 5. Micrographs of enterocytes immediately after isolation from jejunal tissue (Magnification 40x).

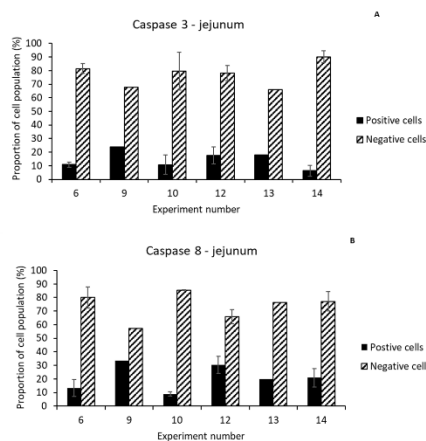


Figure 6. Visual representation of jejunal apoptosis data (by experiment number). The proportion of cells with and without active caspase was measured in the Caspase 3 (A) and Caspase 8 (B) assays

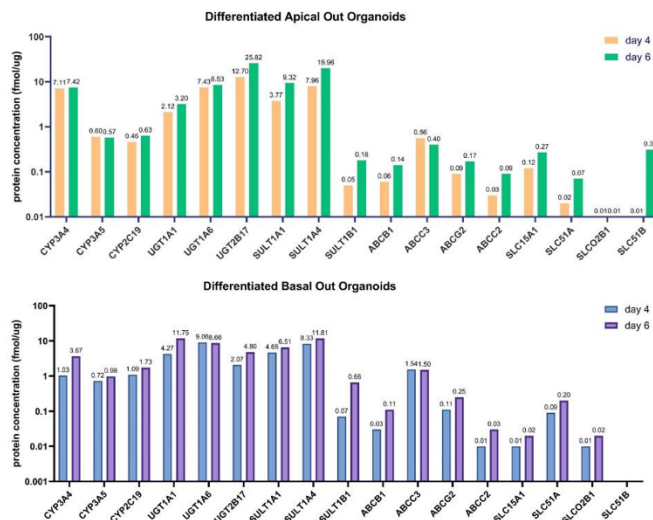


Figure 7. Protein concentrations of main ADME proteins in differentiated organoids, apical out (top) and basal out (bottom).

P86 - ISOLATED PRIMARY COLONOCYTES AND 3D COLONOIDS AS INTESTINAL *IN VITRO* ADME MODELS REFLECTIVE OF NATIVE EPITHELIUM

Rebekkah Hammar, Maria Letizia Di Martino, Ana Lopes, Jens Eriksson, Wilhelm Graf, Patrik Lundquist, Mikael Sellin, and Per Artursson
Uppsala Universitet, Sweden

With colonic inflammatory disorders on the rise globally, the need for *in vitro* assessment of human colonic drug ADME is growing. Historically, high turnover and difficulties in culturing have been addressed by using immortalized intestinal cell lines. Notable shortcomings are, however, inadequate reflection of ADME protein levels and the spectrum of cell types found in the native epithelium(1). Though fresh or cryopreserved primary cell isolates and stem-cell derived organoids reflect the spectrum of intestinal cell types, ADME characterization in these models is incomplete. Native intestinal metabolic activity has been assessed *in vitro* using enzymatically isolated primary intestinal cells(2,3). As enzymatic isolation introduces a risk of damaging membrane proteins such as transporters, these short-term models are not suitable for assessing other ADME processes. Therefore, we first generated a native colonocyte model for use as an *in vitro* ADME reference via a gentle, non-enzymatic shaking approach(4). With this native ADME standard in place, our next step was to create a more sustainable and long-term alternative. We therefore hypothesized that stem-cell derived colonoids could be driven towards native ADME protein expression levels by maintaining them in suspension culture. From the surgery waste of donors, healthy, normal colon tissues were obtained. Our gentle, non-enzymatic shaking approach yielded isolated primary colonocytes as a single-cell suspension. Image cytometry was used to assess viability and apoptosis. 3D colonoids were established from crypts as basal-out cultures in Matrigel before being transferred to suspension culture. By adjusting culturing conditions, colonoid apicobasal polarity and differentiation were tuned(5). Live-cell confocal microscopy was used to image suspended colonoids. Label-free quantitative mass spectrometry-based global proteomics was used for ADME protein profiling of paired native tissue, primary cell isolates, and colonoids. After optimization, primary colonocytes were isolated at viabilities of >95% and exhibiting <10% late apoptosis. Colonoid barrier function and apicobasal polarity were confirmed via microscopy. Proteomic analysis indicated that non-enzymatically isolated primary colonocytes and suspension-grown colonoids are closer to native protein profiles than immortalized intestinal cell lines are. Our preliminary results point towards both novel *in vitro* models providing a more *in vivo*-like alternative for establishing in-vitro-in-vivo correlations. For assessing native colonic ADME proteins, non-enzymatically isolated primary colonocytes constitute a novel short-term *in vitro* gold reference standard. Colonoids, suitable for long-term cultivation, appear to be a reasonable alternative to this reference when grown in suspension.

References:

- Olander, M., Wiśniewski, J. R., Matsson, P., Lundquist, P. & Artursson, P. The Proteome of Filter-Grown Caco-2 Cells With a Focus on Proteins Involved in Drug Disposition. *Journal of Pharmaceutical Sciences* **105**, 817–827 (2016).
- Ho, M.-C. D., Ring, N., Amaral, K., Doshi, U. & Li, A. P. Human Enterocytes as an In Vitro Model for the Evaluation of Intestinal Drug Metabolism: Characterization of Drug-Metabolizing Enzyme Activities of Cryopreserved Human Enterocytes from Twenty-Four Donors. *Drug Metab Dispos* **45**, 686–691 (2017).
- Li, A. P. *et al.* Cryopreserved Human Intestinal Mucosal Epithelium: A Novel In Vitro Experimental System for the Evaluation of Enteric Drug Metabolism, Cytochrome P450 Induction, and Enterotoxicity. *Drug Metab Dispos* **46**, 1562–1571 (2018).
- van der Post, S. & Hansson, G. C. Membrane Protein Profiling of Human Colon Reveals Distinct Regional Differences. *Molecular & Cellular Proteomics* **13**, 2277–2287 (2014).
- Co, J. Y. *et al.* Controlling Epithelial Polarity: A Human Enteroid Model for Host-Pathogen Interactions. *Cell Rep* **26**, 2509–2520.e4 (2019).

Preliminary figures:

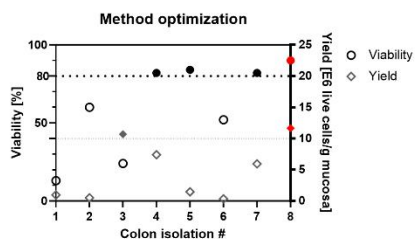


Figure 1. Non-enzymatic colonocyte isolations in chronological order. Filled icons are above thresholds of 80% viability and 10 E6 cells/g mucosa, respectively. Red icons indicate most recent isolation (June 2022).

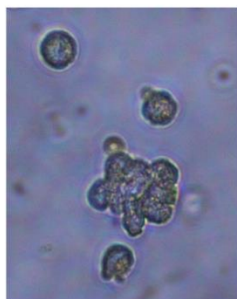


Figure 2. Micrograph (40x) of non-enzymatically isolated colonocytes directly post-isolation.

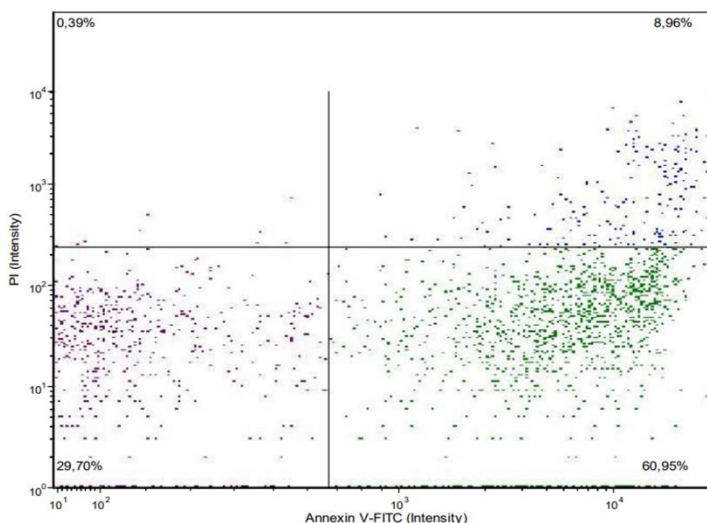


Figure 3. Image cytometry apoptosis data from non-enzymatically isolated colonocytes directly post-isolation, as measured by Annexin-V-FITC fluorescence.

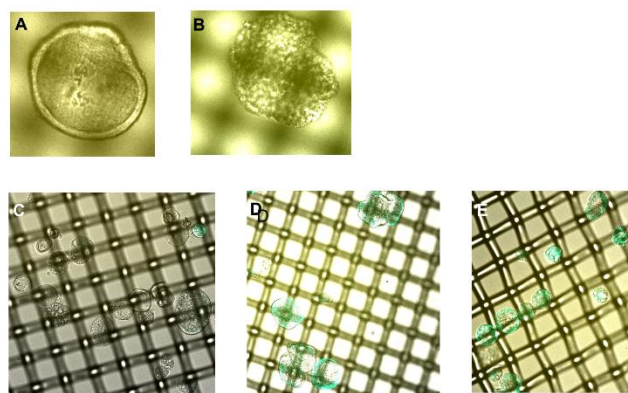


Figure 4. Still shots from live microscopy assay for barrier integrity and apicobasal polarity of suspension-grown colonoids (magnification 10x). Yellow background from lucifer yellow. Green fluorescence due to uptake of BODIPY-C12 (fluorescently labeled fatty acid analog) according to differentiation stage and polarity. A: Basal-out colonoid maintained in growth medium. B: The colonoid shown in panel A after barrier disruption with EGTA. C: Basal-out colonoids maintained in differentiation medium. D: Apical-out colonoids maintained in growth medium. E: Apical-out colonoids maintained in differentiation medium.

Gene names	Colon	Colonocytes	4-G	6-G	4-D	6-D
CYP3A4	0.00	0.02	0.00	0.00	0.18	0.21
CYP3A5	0.02	0.08	0.00	0.00	0.02	0.00
SULT1A1	1.52	2.18	0.00	0.62	4.83	3.25
SULT1A4;SULT1A3	6.10	3.90	1.45	1.86	15.85	11.33
DPP3	1.53	0.57	1.68	2.02	2.34	3.58
DPP4	0.33	0.00	0.09	0.10	0.61	0.00
MUC13	0.65	0.85	0.21	0.10	11.66	5.16
MUC5AC	0.03	0.09	0.10	0.07	5.85	1.18
FABP1	986.74	896.71	317.50	226.97	1091.70	631.00
ABCB1	0.18	0.39	0.01	0.00	2.48	1.50
ABCG2	0.00	0.00	0.00	0.00	0.19	0.00

Figure 5. Preliminary ADME proteomics data (protein concentrations in fmol/μg total protein) of paired colon tissue, non-enzymatically isolated colonocytes, and colonoids grown for 4 or 6 days in growth (G) or differentiation (D) medium.

P87 - AN ENCOUNTER WITH A NEXT GENERATION BLOOD-BRAIN BARRIER PBPK MODEL WITH ENHANCED PROTEOMIC-INFORMED TRANSPORTER IVIVE CAPABILITIES

Janita Hogan¹, Zubida Al-majdoub², Jingjing Guo¹, Jonathan Cheong³, Kunihiro Mizuno⁴, Tom De Bruyn³, Raymond Evers⁵, Anne Kanta⁴, Michael Zientek⁴, Aleksandra Galetin², Amin Rostami-Hodjegan², and Kayode Ogungbenro²

¹Merck, United States, ²The University of Manchester, United Kingdom, ³Genentech, United States, ⁴Takeda, United States, and ⁵Johnson & Johnson, United States

Efflux transporters expressed on the blood-brain barrier can limit the penetration of central nervous system (CNS) acting small molecules in the brain. Although transporter liability can be assessed qualitatively via efflux ratios, quantitative translation of *in vitro* transporter activity to *in vivo* for accurate prediction of CNS pharmacokinetics has not been well established. Proteomics-informed *in vitro in vivo* extrapolation (IVIVE) is proposed here to translate *in vitro* P-gp transporter kinetics within a physiologically based pharmacokinetic (PBPK) paradigm and to assist with the local drug exposure predictions in the brain. *In vitro* transporter kinetics assays were performed in MDCK, MDCKII, and LLC-PK1 cell monolayer transfected with rat P-gp for a set of six commercially available compounds with varying affinities for the transporter (donepezil, loperamide, phenytoin, quinidine, risperidone, and verapamil). Modeling of *in vitro* data was performed using a three-compartment mechanistic model to estimate the active transport clearance via P-gp and passive diffusion clearance across the epithelial cell membrane. The inclusion of nonspecific binding, accounting for the loss of compound during the experiment, improved the fitting to observed data. There was up to 3-fold difference in estimated P-gp-mediated clearance across cell lines, due to the differences in corresponding transporter abundances. The *in vitro* P-gp mediated clearance was then translated to *in vivo* using a scaling factor accounting for the differences in P-gp abundance between the cell lines and rat brain tissue (data for both obtained by the same LC-MS/MS-based quantitative QconCAT targeted proteomics method). Scaled P-gp-mediated clearance was implemented in a six-compartment brain PBPK model, which included the blood-brain barrier as a separate compartment. Other drug-specific and system (physiological) model parameters were derived from literature and *in silico* predictions. The PBPK model simulations were in agreement with *in vivo* concentration-time profiles in blood, neural intracellular fluid, and cranial cerebrospinal fluid, obtained from terminal rat studies. The inclusion of the proteomics-informed scaling factor led to more accurate brain K_p predictions. The current work provides a mechanistic framework for the analysis of efflux transporter kinetic data and translation to *in vivo* brain exposure.

P88 - A COMPARISON OF THE *IN VITRO IN VIVO* CORRELATION OF SMALL MOLECULE METABOLISM IN THREE LONG-TERM PRIMARY HUMAN HEPATOCYTE CULTURE MODELS

Hlaing Maw, Ting Wang, Klairynne Raymond, Alexander Byer-Alcorace, Stephanie Piekos, Tom Chan, and Mitchell Taub
Boehringer Ingelheim Pharmaceuticals, Inc., United States

Metabolite identification studies using plasma from clinical trials generate pivotal data, where human metabolites are identified to address requirements of FDA MIST and EMA ICH M3 guidelines^{1,2}. The majority of marketed small molecule drugs are metabolized in the liver where high levels of the major drug metabolizing enzymes are expressed in the parenchymal hepatocytes. Isolated human hepatocytes in a suspension format (SHH) are routinely used as an *in vitro* tool to investigate hepatic metabolism. However, the usage of SHH is limited by a relatively short incubation time (≤ 6 h), which can be inadequate to form metabolites for slowly metabolized compounds. New long-term primary human hepatocyte culture models such as spheroids, HepatoPac, and most recently the Tri-Culture system (TCS), have been developed to address this challenge. The objective of this study is to evaluate these three models as *in vitro* tools to generate Phase I and II metabolites and compare the ability of these systems to generate metabolites observed *in vivo*. Two slowly metabolized compounds, BI-A and BI-B were incubated with suspended hepatocytes for 6 h and with spheroids, TCS, or HepatoPac for 168 h. The metabolism of BI-A and BI-B in SHH was low, as parent represented $> 99\%$ of total drug related material (TDRM). Two oxidative metabolites, and 6 oxidative or glucuronidated metabolites were identified in SHH incubations with BI-A and BI-B, respectively. When BI-A was incubated with HepatoPac, spheroids, or TCS, between 5 and 9 metabolites were identified and parent represented 35-55% of TDRM. One unique *in vivo* pathway was amide hydrolysis of the mono-oxidative and dehydrogenated metabolite of BI-A, M526. Both M232 and M312 metabolites from hydrolysis of the amide bond in M526 were detected at trace levels (0.4-0.9% TDRM) in spheroids and TCS, but not in SHH or HepatoPac. All other *in vivo* Phase I and/or II metabolites were identified in all three systems evaluated. When BI-B was incubated with spheroids or TCS, 5 oxidative, 3 glucuronidated and 1 oxidative-glucuronidated metabolites were identified, with parent representing 94% of TDRM. In human plasma, 2 oxidative metabolites (each $< 1\%$ TDRM) and one oxidative-glucuronide metabolite (4% TDRM) were identified. Overall, the three long-term culture models investigated can generate clinically relevant metabolites. All three systems are capable of generating metabolites more extensively than SHH, which is relevant for slowly metabolized compounds, and as such are suitable tools to predict *in vivo* metabolism and metabolite formation.

References:

1. U.S. Food and Drug Administration (2020) Safety Testing of Drug Metabolites: Guidance for Industry. Center for Drug Evaluation and Research, US Food and Drug Administration, US Department of Health and Human Services, Rockville, MD.
2. European Medicines Agency (2009) ICH topic M3 (R2) non-clinical safety studies for the conduct of human clinical trials and marketing authorization for pharmaceuticals. European Medicines Agency, London, UK.

P89 - ESTABLISHMENT OF *IN VITRO* ASSAYS TO PREDICT THE *IN VIVO* CLEARANCE OF PEPTIDES IN RAT

Anna Vildhede, Annika Janefeldt, Ann-Sofie Sandinge, Maria Englund, Marie Persson, Constanze Hilgendorf, and Ulrik Jurva
AstraZeneca, Sweden

Predicting *in vivo* pharmacokinetic parameters, such as metabolic clearance, from *in vitro* data is a crucial part of the drug discovery process in order to rank compounds for progression and to guide optimization of compound metabolic stability. For peptide drugs, there is no well-proven strategy in place for the *in vitro-in vivo* extrapolation (IVIVE) of metabolic clearance. As a result, optimization of the metabolic clearance of peptide drugs is mostly driven by preclinical *in vivo* studies, rendering the drug development process slow, expensive, and ethically challenging. To enhance the *in vitro* ADME tool box available for peptide drug development, the aim of our study was to establish *in vitro* assays that are predictive of the metabolism observed *in vivo* for bicyclic peptides in rat. For a set of 15 bicyclic peptides, the *in vitro* metabolic stability in rat blood and plasma did not correlate with the *in vivo* clearance. To rule out any potential impact of the choice of anticoagulant on measured plasma clearance, the metabolic stability in EDTA plasma was compared with that in citrate and heparin plasma, resulting in generally very similar half-lives and no improvement of the *in vitro-in vivo* correlation. Since the liver and kidneys are suggested to be two of the main sites for peptide degradation, the *in vitro* metabolic stability of 44 different peptides (mainly bicyclic) was subsequently studied in suspended hepatocytes and kidney homogenate/S9 fraction. The kidney-derived *in vitro* systems were used interchangeably in this study since they produced comparable clearance values. Although the scaled hepatocyte clearance predicted the *in vivo* clearance within 2-fold for half of the peptides (55%), a fourth of the peptides were underpredicted by more than 3-fold. IVIVE based on kidney homogenate/S9 clearance was associated with a larger underprediction of the *in vivo* clearance and only a handful of peptides (22%) were predicted within 2-fold. Clearly, neither of these *in vitro* systems performed sufficiently well on their own; however, when adding together the scaled liver and kidney clearances, an improved IVIVE was obtained with 64% of predictions falling within 2-fold and 82% within 3-fold of observed values. In summary, we have identified kidney homogenate/S9 fraction as a complement to hepatocytes for the prediction of *in vivo* metabolic CL of peptides. These *in vitro* assays have the potential to replace animal studies during the drug discovery phase, making the drug development process faster, cheaper and more sustainable from an ethical perspective.

P90 - STRATEGIES TO IMPROVE BEYOND RULE OF 5 COMPOUND RECOVERIES WITHIN INVITRO ASSAYS: EFFECT OF VARIOUS EXCIPIENTS

Julius O. Enoru, Anand Joshi, Yongjin Yao, Purvi Jejurkar, and David Stresser
AbbVie, United States

Drugs require a certain degree of lipophilicity in order to achieve sufficient oral absorption and tissue penetration. However, high lipophilicity is often associated with poor aqueous solubility and high non-specific binding, particularly to plastic-based apparatus routinely used in *in vitro*-ADME assays. The high propensity to exhibit non-specific binding and low solubility yields low recovery values and inaccurate ADME parameters that are critical for human dosing and pharmacokinetic projections. Recently, Solutol® (also known as Kolliphor HS15) has been shown to improve recovery of lipophilic molecules in a protein binding equilibrium dialysis assay¹. We aimed to investigate the potential role of Solutol and other excipients to improve the recovery of lipophilic compounds and thus enhance the robustness of *in vitro* assays performed with these “problematic” compounds. Initial investigations were conducted with venetoclax, a compound known to exhibit high non-specific binding to incubation apparatus. In this study, we evaluated the effect of Solutol, poloxamer 407, kollidon 90, sodium dodecyl sulfate (SDS), D-α-tocopheryl polyethylene glycol succinate (TPGS1000) and TWEEN 20 on the recovery of venetoclax in potassium phosphate buffer pH 7.4 in 96-well polypropylene deep well plates. The venetoclax recovery in blank buffer was very low, <5%. In the presence of Solutol and TPGS1000, the recovery improved to >60% at final excipient concentration of 0.004% (w/v) and 0.002% (w/v), respectively. TWEEN 20 improved venetoclax recovery to 52% at a concentration of 0.004% (v/v). Poloxamer 407 (0.0035% (w/v)), kollidon 90 (5% (w/v)), SDS (0.0115% (w/v)) had lower improvements (<34%) in the recovery of venetoclax. Further, as HBSS is the buffer of choice for permeability studies, Solutol, TWEEN 20, SDS, TPGS200, 1000, 4000 and 6000 were evaluated in this matrix with venetoclax. Solutol was able to achieve recoveries of >65% at 0.004% w/v, TPGS1000 at 0.001%w/v, TPGS 4000 at 0.002%w/v and TPGS 6000 at 0.004% w/v compared to blank (38-48.7%). While these excipients displayed promise in mitigating non-specific binding, it will be critical that they display minimal impact on biological activity for their potential

utility as excipients in various *in vitro* ADME assays. For example, Solutol and TPGS appear to display strong inhibition of P-gp at "optimal" recovery-enhancing concentrations of 0.004% w/v and 0.001% w/v, respectively. These results offer promise towards improving the reliability of testing Bro5 compounds in *in vitro* ADME assays.

References:

1. Abhishek Srivastava, Andy Pike, Beth Williamson, Katherine Fenner: A Novel Method for Preventing Non-specific Binding in Equilibrium Dialysis Assays Using Solutol® as an Additive. *Journal of Pharmaceutical Sciences* 110 (2021) 1412-1417.

P91 - A VALIDATED SOLUTION FOR SHIPPING PRIMARY HUMAN PROXIMAL TUBULE CELL MONOLAYERS BETWEEN LABORATORIES

Lucy Gentles, Claire Devlin, Cindy Carr, and Colin Brown
Newcells Biotech, United Kingdom

aProximate™ is a highly sophisticated, near-physiological proximal tubule cell (PTC) model that is a proven market-leader in the study of transporters and drug-drug interactions. One issue with primary cell cultures is the short time window they remain differentiated and functional, which has hindered the sharing of this model between laboratories. To overcome this and ship cells globally in an assay-ready format, a safe and reliable short-term preservation method was developed and internally validated, pausing cells at hypothermic temperatures for up to 5 days. Human PTCs were isolated from the cortex tissue of 17 nephrectomies and grown on Transwell® filter supports to functional maturity. Membrane barrier integrity was quantified by transepithelial electrical resistance (TEER), with values of more than 60 Ω.cm² used as quality control (QC) to indicate a fully established, polarized monolayer. Cells were placed into metabolic stasis, using a formulated biogel and maintained at 4°C for 3 or 5 days to simulate shipping conditions. Subsequently, cells were revived to 37°C and left to recover until the minimum TEER QC value was reached. TEER recovery was cold-time dependent, with plates shipped for 3 and 5 days taking 24hr and up to 72hr respectively. Following 5 days of hypothermic preservation and a 48-72hr recovery phase, monolayers remained differentiated and exhibited a single-layer cobblestoned epithelium, morphologically akin to pre-shipment control. Monolayers were viable and metabolically active, indicated by way of ATP assay (>100 % of control, n = 9 kidneys). Extensive positive immunofluorescent staining of the tight junction protein, ZO1, was demonstrative of an uncompromised cell membrane barrier. At the mRNA level, relative expression of the key drug transporters OCT2, MDR1 and MATE1 were stable relative to control (85.2%, 103.3% and 106.2% respectively, n=4). Functionally, monolayers conserved the mechanics to facilitate the OCT2-mediated basolateral uptake and MATE-mediated efflux of 14C creatinine. The efflux ratio for creatinine in shipped cells was 1.8 ± 0.16 fold and was not significantly different from time-matched control monolayers (n = 10 kidneys, paired t test, P > 0.01). Likewise, the basolateral : apical creatinine uptake ratio was 3.5 ± 0.43 and was not significant from time-matched control monolayers (n = 17 kidneys, paired t test, P > 0.05). Taken together, these data suggest that coating PTCs at hypothermic temperatures offers the possibility of shipping a viable and functional model across the world with improved confidence, overcoming a major limitation in the widespread use of primary cell models.

P92 - EFFECT OF DRUGS THAT CAUSE CHOLESTATIC DRUG-INDUCED LIVER INJURY ON BILE ACID TRANSPORT AND METABOLISM

Thomas Kralj¹, Chitra Saran², Kenneth Brouwer¹, Kim Brouwer², and Darren Creek³

¹BioIVT, United States; ²University of North Carolina at Chapel Hill, United States and ³Monash University, Australia

Background: Drug-induced liver injury (DILI) is the leading cause of acute liver failure and a major reason for liver transplantation. Cholestatic DILI can occur as the sole DILI phenotype or as a comorbidity with other DILI phenotypes. Cholestasis is characterized by impaired hepatic bile flow and may be induced by several different mechanisms. In order to reduce the occurrence of cholestatic DILI and other forms of adverse drug reactions (ADR), it is vital to develop the tools and knowledge to comprehensively screen drugs for toxicologic safety. C-DILI™ and B-CLEAR® assays can be used to screen drugs for cholestatic hepatotoxic potential and the capacity to impair biliary transport, respectively. Methods: Transporter Certified™ primary human hepatocytes (PHH) were cultured in a sandwich configuration, and HuH-7 cells were cultured for 4 weeks with 1 μM dexamethasone and overlaid to facilitate canalicular formation and biliary excretion of bile acids [1]. PHH and HuH-7 cells were treated with fialuridine, pioglitazone, ritonavir, and troglitazone, which have been associated with severe ADR. Results: Based on the C-DILI™ assay using PHH (n=3), ritonavir (125 μM) and troglitazone (50 μM) demonstrated a significant potential for cholestatic hepatotoxicity after a 24-h exposure. Additionally, pioglitazone (100 μM), ritonavir (25 μM) and troglitazone (75 μM) impaired biliary transport of taurocholate based on the B-CLEAR® assay in HuH-7 cells (n=3) after a 24-h exposure. The biliary excretion index (BEI) of taurocholate decreased for pioglitazone, ritonavir, and troglitazone exposures from control values of 43-50% to 6%, 10%, and 24%, respectively. Fialuridine, a drug associated with ADR mortalities, did not demonstrate any potential for

cholestatic hepatotoxicity or a reduction in BEI. Ultra-high-resolution mass spectrometry metabolomics was used to identify changes in the abundance of bile acid-associated metabolites in PHH (n=4) caused by these four drugs after a 24-h exposure. Ritonavir, pioglitazone, and troglitazone reduced the cellular abundance (expressed as % of control) of taurocholate (4.8-46%), glycocholate (1.3-31%), taurochenodeoxycholate (3.5-9.8%), and glycochenodeoxycholate (4.5-5.3%); the cellular abundance of chenodeoxycholate, taurine and glycine were unaffected. However, treatment with fialuridine increased the cellular abundance (expressed as % of control) of taurocholate (161%), taurochenodeoxycholate (209%) and chenodeoxycholate (288%) with no effect on any other bile acid or associated metabolites. Proteomic analysis of PHH whole cell lysates (n=4) following a 24-h exposure to pioglitazone, ritonavir, and troglitazone revealed an increase in metabolic enzymes, including cytochrome P450 (CYP) 3A4, CYP3A5 and CYP reductase. Conclusions: Drugs such as pioglitazone, ritonavir, and troglitazone may initially impair bile acid transport, which can then induce an adaptive response including increased phase I metabolism and decreased cellular abundance of bile acids. The net effect of a compound on these multiple pathways may determine the compound's potential to cause cholestatic liver injury.

Supported by PharmAlliance; NHMRC #APP1148700; NIH R35 GM122576

Reference:

1. Kang HE, Malinen MM, Saran C, Honkakoski P, Brouwer KLR. Optimization of Canalicular ABC Transporter Function in HuH-7 Cells by Modification of Culture Conditions. *Drug Metab. Dispos.* 2019;47(10):1222-30.

P93 - CHARACTERIZATION OF XENOBIOTIC DISPOSITION POTENTIAL OF PLACENTAL CELL LINES (JEG-3, JAR, BEWO, AND HTR-8/SVNEO) AND PLACENTAL TISSUE THROUGH QUANTITATIVE GLOBAL PROTEOMICS

Laken Kruger¹, Samantha Lapehn², Guihua Yue², Daniel A. Enquobahrie³, Qi Zhao⁴, Khyobeni Mozhui⁴, Theo K. Bammler³, James MacDonald³, Alison Paquette², Sheela Sathyanarayana^{2,3}, and Bhagwat Prasad¹

¹Washington State University, United States ²Seattle Children's Research Institute, United States, ³University of Washington, United States, and ⁴University of Tennessee Health Science Center, United States

The placenta is a heterogenous fetal organ that is composed of multiple cell types maintaining various critical functions throughout pregnancy. *In vitro* models of the placenta are important for studying toxicity and related pathophysiological mechanisms of xenobiotic exposure on specific pathways in a high-throughput manner. Selecting the correct cell line for specific research questions is vital for translating *in vitro* data to humans. In this study, we compared the global proteomic profiles of four placental cell lines (JEG-3, JAR, BeWo, and HTR-8/SVneo) to placental villous tissue collected at the end of gestation to determine how these cell lines relate to placental biology, specifically their xenobiotic disposition potential. The cell lines were cultured and harvested inhouse and the tissues (n=99) were obtained from the Conditions Affecting Neurocognitive Development and Learning in Early Childhood (CANDLE) study(1). The membrane and non-membrane (soluble) protein fractions were isolated from cell lines and tissues, the tissue fractions from all 99 donors were pooled, and digested (in triplicate) using trypsin before nanoLC-MS analysis. Global proteomics analysis of the cells and tissue pool detected between 1,866-2,716 proteins in the membrane fraction and 1,676-2,506 proteins in the soluble fraction. Out of these, 1,239 membrane and 1,010 soluble proteins were ubiquitously detected in all groups. The cell lines that were the most concordant with the placenta tissue were BeWo and JEG-3, whereas JAR and HTR-8/SVneo showed less overlap. Out of 5 syncytiotrophoblast markers (CYP19A1, ABCG2, CSH2, PSG5, and PSG9), BeWo and JEG-3 cells expressed CYP19A1, ABCG2, and CSH2; JAR cells only expressed CYP19A1; and as expected the extravillous trophoblast cell line (HTR-8/SVneo) did not express any of these markers. With respect to xenobiotic disposition proteins, 15 proteins were expressed in the pooled placental sample. Out of these 15 proteins, BeWo, JEG-3, JAR, and HTR-8/SVneo cells expressed 10, 9, 8, and 7 proteins, respectively. Quantitatively, BeWo cells had similar levels of CYB5A to the pooled placenta tissue (p>0.05), while JEG-3, JAR, and HTR-8/SVneo cells showed 1.6, 2.5, and 15-fold higher levels, respectively. CYP19A1 was significantly lower (p<0.05) in BeWo, JAR, and JEG-3 cells by 27.2, 197.5, and 7.1-fold, respectively. Taken together, cell line selection must be carefully considered when studying xenobiotic transformation to ensure that the appropriate metabolic genes are expressed for the precursor drug of interest. Our results clearly suggest that BeWo and JEG-3 cells are more similar to the pooled placental tissue in relation to the relative quantity and composition of xenobiotic disposition proteins.

Reference:

1. Sontag-Padilla, L. M. et al. The Urban Child Institute CANDLE Study: Methodological Overview and Baseline Sample Description. (2015).

P94 - DEVELOPMENT OF A HIGH-THROUGHPUT TIME DEPENDENT INHIBITION OF CYP450 ASSAY IN CRYOPRESERVED HUMAN HEPATOCYTES

Yau Yi Lau, Eunice Choi, Megan Metallides, Jennifer Pham, Teresa Sierra, Bharat Misra, and **Sravani Adusumalli**
Cyprotex, United States

Purpose: Time-dependent inhibition (TDI) of human cytochrome P450s is a major cause of clinical drug-drug interactions. Under and over prediction of *in vivo* DDIs have been observed when inhibition assays were performed in human liver microsomes. Human hepatocytes provide the closest *in vitro* model to intact liver with both phase I and II enzymes and transporters that may modulate the effects of TDI on clinical DDIs. This poster presents a high-throughput TDI assay for 7 major CYP450s (CYP1A2, CYP2B6, CYP2D6, CYP2C8, CYP2C9, CYP2C19, and CYP3A4) using cryopreserved human hepatocytes in 384-well plate.

Methods: Time and cell density linearity

Optimum cell density and incubation time for each isoform were determined using a range of cell concentrations (0.1, 0.25 and 0.5 million cells/mL) across several incubation times. Briefly, each substrate was pre-incubated with media for 10 minutes and cryopreserved human hepatocytes were added to initiate the reaction. An aliquot was taken from the reaction mixture at 0, 5, 10, 15, 30, and 60 minutes and terminated.

Determination of Km and Vmax

Using the cell density and incubation time determined in the previous section, the metabolite formation of the substrate was measured with several concentrations of probe substrate covering the expected range of Km values were incubated with cryopreserved human hepatocytes.

CYP450 hepatocyte inhibition assay

The hepatocyte inhibition assay is performed in a high-throughput 384-well format. Test compounds are serially diluted to 7 different concentrations in DMSO and further diluted into William's E media containing L-glutamine and HEPES (final DMSO concentration = 0.25%). Cryopreserved human hepatocytes with and without inhibitor at 7 concentrations are pre-incubated for 30 minutes. Probe substrate for each isoform at a concentration close to the Km values are then added and incubated for an appropriate time period determined from previous section. All incubations are done at 37°C in a CO₂ incubator.

All reactions are terminated by adding acetonitrile containing internal standard. Samples are centrifuged and the resulting supernatant is transferred for analysis using LC-MS/MS methods.

Results: The time linearity results showed that 30 min preincubation with inhibitor and 10 min incubation after addition of substrates were enough for the determination of IC₅₀ shift. Time-dependent inhibition in human hepatocytes was observed for all isoforms using the control inhibitors for each isoform. In general, the observed fold shifts were higher in hepatocytes than in microsomes indicating that human hepatocyte system is more sensitive than microsomal system. The data obtained using 384-well format was comparable with 96-well format.

Conclusion: A robust, high-throughput TDI assay using cryopreserved human hepatocytes was developed using 384-well plates which significantly lowers labor and cost in comparison. Hepatocyte system is a more complete representative of the *in vivo* liver system which contains both phase I & II enzymes and transporters. This assay can be of great importance to better predict the possible DDIs in the *in vivo* situation. This high-throughput assay is especially useful for screening compounds that show phase II metabolism and enzyme-transporter interplay.

P95 - CYTOTOXIC REACTIVE METABOLITE ASSAY WITH PERMEABILIZED CRYOPRESERVED HUMAN HEPATOCYTES FOR THE IDENTIFICATION OF DRUG CANDIDATES WITH POTENTIAL TO CAUSE IDIOSYNCRATIC DRUG-INDUCED LIVER INJURIES

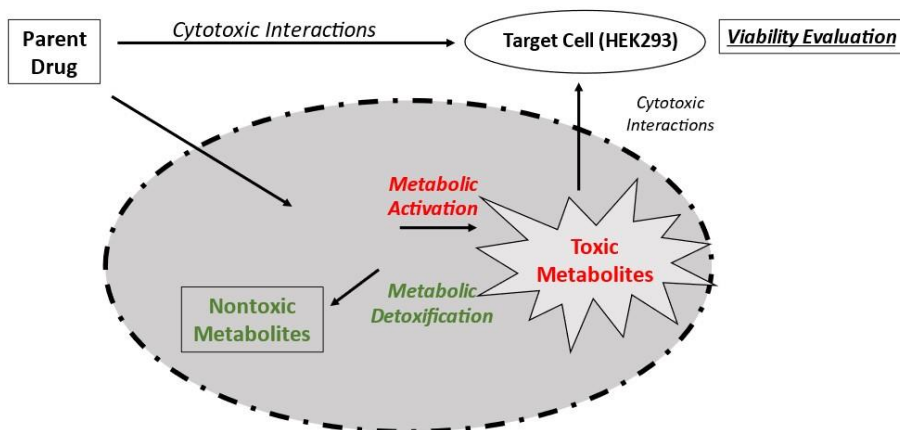
Albert Li

Discovery Life Sciences, United States

We report here a novel *in vitro* experimental system, the metabolism-dependent cytotoxicity assay (MDCA), for the definition of the roles of hepatic drug metabolism in toxicity, especially in the identification of chemical structures with idiosyncratic drug induced liver injuries (iDILI) potential. MDCA employs permeabilized cofactor-supplemented cryopreserved human hepatocytes (MetMax™ human hepatocytes, MMHH), as an exogenous metabolic activating system, and HEK-293 cells, a cell line devoid of drug metabolizing enzyme activity, as target cells for the quantification of drug toxicity. MMHH was supplemented with specific cofactors to identify key metabolic activation and detoxification pathways. We propose here that Metabolism-Dependent Cytotoxicity Index (MDCI), calculated as a ratio of the IC₅₀ values for drug cytotoxicity in the absence to that in the presence of each of the cofactors in MDCA, may provide a quantitative measure of the effects of drug metabolism on toxicity. MDCI values less than 1 indicates metabolic detoxification (higher IC₅₀ values in the presence of the cofactor), and that higher than 1 representing metabolic activation (lower IC₅₀ values in the presence of the cofactor). Six drugs with clinically significant hepatotoxicity, resulting in liver failure or a need for liver transplantation: acetaminophen, amiodarone, cyclophosphamide, ketoconazole, nefazodone and troglitazone were evaluated. All six drugs exhibited cytotoxicity enhancement by NADPH, suggesting metabolic activation via phase 1 oxidation. Attenuation of cytotoxicity by UDPGA was observed for acetaminophen and

troglitazone, by PAPS for acetaminophen and troglitazone, and by GSH for all six drugs. Our results suggest that drugs with iDILI potential may be identified via two key properties: 1. Metabolic activation by oxidative metabolism indicated by NADPH enhancement of cytotoxicity. 2. Attenuation of NADPH-dependent cytotoxicity by GSH as an indication of cytotoxic reactive metabolite formation. MDCA can be applied towards the elucidation of metabolic activation and detoxification pathways, especially in the identification of cytotoxic reactive metabolite formation. The MDCA is intended to supplement current analytical approaches for the evaluation of reactive metabolite formation to guide structure optimization to minimize hepatotoxic liability via the provision of toxicological significance of the reactive metabolites observed. Elucidation of key drug metabolism pathways for drug toxicity with MDCA may allow the assessment of metabolism-based risk factors for drug toxicity for identification of human populations susceptible to iDILI.

Metabolism Dependent Cytotoxicity Assay (MDCA)



P96 - ABSTRACT WITHDRAWN

P97 - METHODS FOR SEMI-AUTOMATING THE CYTOCHROME P450 INHIBITION CONSTANT (KI) ASSAY IN 384-FORMAT

Cody Parker

Mirati Therapeutics, United States

Determination of cytochrome P450 (CYP) inhibition constant (Ki) values are highly involved, time-consuming experiments that generates thousands of samples per CYP examined, which typically translates to multiple days of liquid chromatography-mass spectroscopy/mass spectroscopy (LC-MS/MS) data acquisition. The various inhibitor-substrate concentration combinations needed to determine the Ki values makes it challenging to generate incubation plates by hand. Our objective was to develop a more efficient method to determine CYP Ki values for drug development candidates and in this poster we present a semi-automated, more reliable Ki assay by utilizing acoustic liquid handling (Echo 650 Series, Beckman Coulter) and a 384-well plate format. Automated dispensing reduce sample preparation time significantly and the 384-well plate format enables inclusion of 8 inhibitor and 6 substrate concentrations for both control and test compound (n=4 each) in a single experiment for each CYP. Timepoints are collected for every 2 minutes up to 10 min (20 min for CYP2C19) to ensure the linear range is captured correctly for each CYP enzyme. In addition, LC-MS/MS acquisition time is reduced by pooling samples from different probe substrates so data for multiple CYPs can be collected in one injection. These optimized processes used in conjunction dramatically increase the overall efficiency of the CYP Ki assay while improving the quality of the data generated. The assay was validated and the control inhibitor values generated for multiple CYPs (CYP1A2 0.0071 μM , CYP2C8 0.0189 μM , CYP2C9 0.373 μM , CYP2C19 0.116 μM , CYP2D6 0.0281 μM , CYP3A4/5 0.016 μM) correlated well with literature values. The experimental procedure and a comparison of resulting control inhibitor Ki values with literature data will be presented.

P98 - ABSTRACT WITHDRAWN

P99 - CHARACTERIZATION OF CLEARANCE MECHANISMS IN AN ALL-HUMAN CELL BASED TRI-CULTURE SYSTEMStephanie Piekos¹, **Mitchell Taub**¹, Edward LeCluyse²¹Boehringer Ingelheim Pharmaceuticals, United States and ²LifeNet Health LifeSciences, United States

Routine use of primary human hepatocytes (PHHs) for clearance estimations of low-turnover compounds has been restricted in part by the lack of a suitable technology that is convenient, supports a multitude of donor lots, and maintains the metabolic pathways of PHHs over prolonged culture periods. To address these limitations, an all-human tri-culture system has been developed comprised of cryopreserved PHHs and primary feeder cells (FCs) consisting of stromal and endothelial cells at a 1:1 ratio. Frozen FCs were thawed and seeded onto 24-well collagen coated plates and allowed to attach. Cryopreserved adult PHHs were then thawed and plated onto the FCs, creating a Tri-Culture System (TCS). Basic morphology and functionality, including formation of functional bile canaliculi, albumin (Alb) synthesis and urea production, were evaluated over a 4-week culture period. Cytochrome P450 (CYP), UDP-glucuronosyltransferase (UGT) and aldehyde oxidase (AO) activities also were determined over a 2-4week period. The ability of the TCS to predict *in vivo* non-renal clearance of two slowly cleared compounds was also evaluated. PHHs from multiple adult donor lots in the TCS exhibited a healthy and stable morphology, including multicellular cluster formation, for up to 30 days in the 24-well format. Extensive anastomosing networks of bile canaliculi were identified with CDFDA staining after day 5 of culture with well-formed tight and gap junctions that remained stable throughout the remainder of the culture period. Albumin and urea production levels were maintained in the TCS for an 4-week period. CYP1A2, CYP2C9, CYP2D6, and CYP3A4 specific activities were maintained at stable levels over the culture period. E2-3G production (UGT1A1) was stable between day 5 and 28 of culture, while AZT-G (UGT2B7) was well-maintained but exhibited greater variability over the 4-week culture period. AO specific activity was greater than in suspended hepatocytes and stable over at least a 14-day period. The TCS was also able to predict the hepatic clearance of alprazolam and tolbutamide within 2-fold of reported *in vivo* values. Overall, these results show that the triculture model represents a convenient, stable all-human hepatic culture system that maintains both hepatocellular morphology and metabolic function for up to 1 month.

P100 - BULK AND SINGLE CELL PROTEOMICS REVEAL CONVERGENT RESPONSES TO HEPATOTOXIC DRUGS EFAVIRENZ, NEVIRAPINE, AND ACETAMINOPHEN IN HUMAN HEPATOCYTES**Yuting Yuan**, Benjamin Orsburn, and Namandjé Bumpus

Johns Hopkins University, United States

Drug-induced hepatotoxicity remains a leading cause of the withdrawal of drugs from the global market¹. We aimed to employ bulk and single cell mass spectrometry (MS)-based proteomics to investigate the impact of a subset of known hepatotoxic drugs, namely, efavirenz (EFV)², nevirapine (NVP)³, and acetaminophen (APAP)⁴ on the human hepatocyte proteome *in vitro*⁵. Our hypothesis is that the concurrent application of bulk and single cell proteomics in these studies will identify shared mechanisms and/or protein signatures that can be leveraged to understand and predict hepatotoxicity in response to a range of drugs.

Cultured cryoplateable hepatocytes were incubated for 24 hours with EFV, NVP and APAP individually at their IC₅₀ or IC₉₀ concentrations to induce hepatotoxicity (EFV IC₅₀ 10 μ M and IC₉₀ 90 μ M; NVP IC₅₀ 90 μ M and IC₉₀ 200 μ M; APAP IC₅₀ 1.5 μ M and IC₉₀ 800 μ M). Traditional bulk proteomics was performed using the combined lysates of thousands of drug- or DMSO-treated cells. To better understand potential cell-to-cell variability in the proteomic response, single cell proteomics was performed on a second set of identically treated cells⁶.

Using bulk proteomics, more than 3,000 proteins were identified. Statistical analysis of the biological and technical replicates of each dosage condition revealed proteins that were differentially abundant when compared to DMSO-treated cells. We observed 19 proteins with significantly different relative abundance following exposure of cultured hepatocytes to the IC₅₀ and IC₉₀ concentrations of EFV, NVP and APAP (p-value < 0.05, Log₂ fold change < -1)⁷. For instance, a decrease in the levels of ataxin-2, which is involved in regulating mRNA translation through interactions with the poly(A)-binding protein⁸, and the cytokine-like proteins serum amyloid family proteins 1, 2 and 4 (SAAs) that have become recognized for their role in cell-cell communication as well as feedback in inflammatory and protective pathways⁹, was observed. To test a role for cytochrome P450-dependent metabolism of EFV, NVP and APAP in the proteomic changes observed, hepatocytes were preincubated with the P450 inhibitor 1-aminobenzotriazole (ABT) before treatment with EFV, NVP and APAP¹⁰. In the presence of ABT, the EFV-, NVP-, and APAP-mediated decreases in the abundance of ataxin-2 and SAAs were not significantly different from DMSO-treated controls with the cutoff of p-value < 0.05, Log₂ fold change < -1, indicating a role for P450-dependent metabolism. Using single cell proteomics, we determined that the decrease in the levels of ataxin-2 and SAAs was detectable and heterogeneous at the level of individual hepatocytes following treatment with EFV, NVP and APAP at their respective IC₉₀ concentrations. Of note, principal component analysis revealed that the proteomic profiles of hepatotoxic drug-treated cells and DMSO control-treated cells could largely be separated into two discrete clusters. Taken together, these data suggest that ataxin-2 and SAA proteins in hepatocytes are modulated in response to hepatotoxic drugs and single cell proteomics can provide insight into the magnitude and heterogeneity of this response within individual cells.

P101 - SYNERGISTIC EFFECTS OF OCHRATOXIN A AND HEAT STRESS IN A KIDNEY MICROPHYSIOLOGICAL SYSTEM**Jade Yang**¹, Wei Yang Chen¹, Tomoki Imaoka², Catherine Yeung¹, and Edward Kelly¹¹University of Washington, United States and ²Daiichi Sankyo, Japan

Mirroring the rise in chronic kidney disease (CKD), the number of reported cases of chronic kidney disease of unknown etiology (CKDu) have increased in rural populations in countries like Nicaragua, El Salvador, Sri Lanka, and India. CKDu is predominantly seen in young and middle-aged adults that are nondiabetic and have normal blood pressure, pointing to risk factors outside of traditional causes of CKD. Postulated risk factors vary greatly by region, but some proposed risk factors include Ochratoxin A (OTA) and heat stress. OTA is a foodborne mycotoxin from the *Penicillium* and *Aspergillus* fungal species that has been found to be nephrotoxic, hepatotoxic, and carcinogenic in animal studies. We hypothesized that there is a synergistic effect between exposure to OTA and transient heat stress. To assess this relationship, primary human proximal tubule epithelial cells (PTECs) were cultured with OTA (0, 1, and 10 μ M) for 48 hours in the presence or absence of transient heat stress (24 hours at 39 °C, followed by 24 hours of recovery at 37 °C) in both 2D well plates and 3D culturing devices or microphysiological systems (MPS). Viability assays showed little change in OTA induced cytotoxicity with the addition of heat stress, however, transcriptomic data sheds light on the potential synergistic effect of OTA and heat. Amongst the thousands of genes that were differentially expressed with OTA treatment, CDKN1A (p21) and CDKN2A (p16) were of particular interest due to their role in causing cell cycle arrest at G1/S, and G2/M checkpoints in the case of CDKN1A. Both genes showed increased expression with 1 μ M OTA treatment, and interestingly, larger positive log fold change in the presence of heat. Previous work from our group displayed that bioactivation and subsequent elimination increased or decreased, respectively, OTA toxicity by inhibiting phase I and phase II metabolizing enzymes. As a result, we were interested in investigating how liver metabolism of OTA would alter its effect on the kidney proximal tubule. Using a novel flow-directed liver and kidney MPS, we can probe the direct effects of OTA on primary human hepatocytes, as well as OTA's metabolites on PTECs. Thus far, we found that 10 μ M OTA treatment caused a 4-fold decrease in human serum albumin production after 48 hours and data that suggests OTA metabolism in the liver may lessen OTA nephrotoxicity.

P102 - ABSTRACT WITHDRAWN**P103 - ABSTRACT WITHDRAWN****P104 - "MIST" STUDIES: A COMPARISON OF METHODOLOGIES FOR EARLY DETECTION OF DISPROPORTIONATE HUMAN METABOLITES****Eleanor Barton**, and Ray Cooke*Pharmaron UK Ltd., United Kingdom*

The regulatory guidance (Metabolites in Safety Testing (MIST) and Considerations for Human Radiolabelled Mass Balance Studies) recommend early assessment for the presence of unique or disproportionate human metabolites, by comparison to the non-clinical (toxicology) species. The definitive approach is to perform a radiolabelled human mass balance study; however, it is not always feasible to perform such a study very early in the clinical development of a drug. Several methods for early detection of disproportionate metabolites have been published. In the last 2 years Pharmaron have performed more than 10 "MIST" studies using high resolution, liquid chromatography-mass spectrometry (LC-MS); this poster presents a comparison of the advantages and disadvantages of each approach, along with a novel hybrid approach we have developed. Where a radiolabelled drug has been synthesised, dosed to animals and plasma samples from this study are available a semi-quantitative approach can be taken (CP Yu et al[1]), whereby the ratio between the radioactive peak and the LC-MS peak in the animal sample provides a "factor" used to estimate the absolute concentration of each metabolite in the (matrix matched) non-radiolabelled human plasma samples. An alternative approach is to calculate the exposure multiples of metabolites between species (Shuguang Ma et al[2]). By matrix matching, plus addition of an internal standard, the peak area ratio of each metabolite to the internal standard can be compared between the human and animal samples to indicate whether the metabolite in question is present at higher levels in the human sample than in the animal samples. The benefit of the radiolabelled approach is that semi-quantitative, absolute concentrations can be determined. However, the limitations are that only metabolites observed in the animal samples can be semi-quantified, all such metabolites need to be well chromatographically resolved, and of course the radiolabelled samples are needed. With the exposure multiple method, no absolute concentration value can be calculated, however it is possible to calculate the exposure multiple for any metabolite, either previously observed or just theoretically predicted, thus increasing the chances of detecting a unique or highly disproportionate metabolite. Furthermore, chromatographic resolution is less important, as specificity is achieved from the accurate mass, mass spectrometry. At Pharmaron a hybrid approach has also been developed whereby the samples are matrix matched and internal standard added, including the radiolabelled samples where available. The absolute concentration of metabolites

observed in the radiolabelled animal samples can therefore be semi-quantified in the human samples, however the exposure multiples can also be calculated for metabolites not seen in the radiolabelled animal samples.

References:

1. Yu CP, Chen CL, Gorycki FL, Neiss TG (2006): A rapid method for quantitatively estimating metabolites in human plasma in the absence of synthetic standards using a combination of liquid chromatography/mass spectrometry and radiometric detection. *Rapid Commun. Mass Spectrom.* 21, 497-502.
2. Shuguang Ma, Zhiling Li, Keun-Jong Lee, and Swapan K. Chowdhury (2010): Determination of Exposure Multiples of Human Metabolites for MIST Assessment in Preclinical Safety Species without Using Reference Standards of Radiolabelled Compound. *Chem. Res. Toxicol.* 2010, 23, 1871-1873

P105 - EXAMINING THE NEPHROTOXICITY INDUCED BY BENZALKONIUM CHLORIDES IN 2D AND 3D-CULTURED HUMAN PROXIMAL TUBULE EPITHELIAL CELLS

Marie Brzoska, Ryan Seguin, Jade Yang, Edward Kelly, and Libin Xu
University of Washington, United States

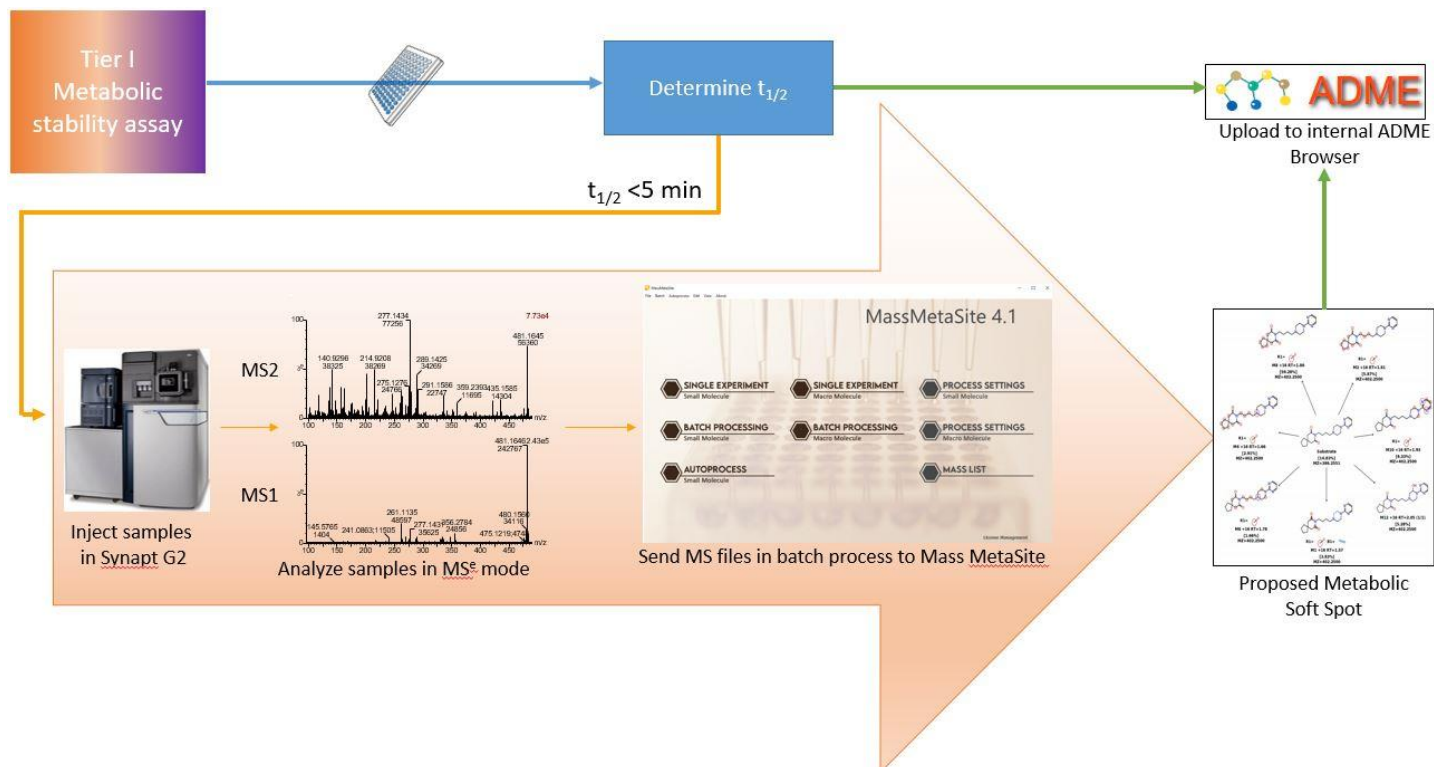
Benzalkonium chlorides (BACs) are widely used antimicrobials in a variety of consumer products and settings, including disinfectants, medical products, and food-processing industry. Though initially recognized as safe, the FDA has called for additional safety data on BAC use in consumer products. Their toxicity becomes especially important during the COVID-19 pandemic due to increased use of BAC-containing disinfectant products. BAC exposure in rats led to their accumulation primarily in the kidney (42-fold higher than blood); In contrast, accumulation did not occur in the liver, likely due to efficient metabolism of BACs by hepatic cytochromes P450 (CYPs), mainly CYP4F isoforms and CYP2D6. Thus, we hypothesized that BAC-metabolizing capacity determines the extent of buildup of BACs in the kidney and subsequent kidney injury. Human kidney and liver microsomes were incubated with 1 μM C12-BAC over 8 time points between 0 and 64 minutes, and LC-MS analysis showed C12-BAC was consumed much slower in the kidney microsomes than the liver microsomes, with the half-lives being 50 and 2.5 min, respectively. We then used cell viability assays to investigate the nephrotoxicity of C10-, C12-, C14- and C16-BAC and their ω -OH metabolites ranging from 0 – 40 μM over 48 hours in 2D-cultured human proximal tubule epithelial cells (PTECs). In general, the parent compounds displayed much larger cytotoxicity (6-24-fold) than their ω -OH metabolites, suggesting BAC metabolism by CYPs detoxifies BACs. EC50 for C12-BAC is approximately 4 μM while the EC50 for the C14- and C16-BACs is around 1 μM . The EC50 value for C10-BAC was not captured in the concentration range examined. BAC-metabolizing CYP4F11 and CYP4F12 are expressed in the kidney, but administration of a CYP4F inhibitor, HET0016, to inhibit the metabolism of BACs did not significantly increase the cytotoxicity of parent BACs, suggesting that BAC metabolism by the kidney is not sufficient to detoxify them. We then examined the nephrotoxicity of BACs using a kidney-on-a-chip microphysiological system (MPS), in which the microenvironment of the chip mimics the functional characteristics of human proximal tubules. We found that 1 μM of BACs exert potent toxicity to human PTECs in the kidney MPS system, comparable to the toxicity exerted by a known nephrotoxin, Polymyxin B, at a higher concentration (50 μM). To summarize, our data suggests that the kidney has smaller BAC-metabolizing capacities than the liver and that BACs can potentially cause nephrotoxicity in humans.

P106 - METABOLITE ELUCIDATION USING TIER ONE DATA (MET-OD)

Elias Carvalho Padilha, Pranav Shah, Jordan Williams, and Xin Xu
National Center for Advancing Translational Sciences (NCATS), United States

Hepatic metabolic stability is an important parameter in drug discovery because it can prevent a drug from attaining sufficient *in vivo* exposure, producing short half-lives, poor oral bioavailability and low plasma and tissue concentrations. At NCATS, we determine metabolic stability with a high-throughput, substrate-depletion method or the *in vitro* half-life ($t_{1/2}$) approach (a Tier I ADME assay) with rat liver microsomes (RLM). In case a compound is found to be unstable, chemists will modify the structure to achieve more stable molecules. This iterative process continues until an optimal lead compound is selected. However, without knowing the metabolic soft spots (sites of metabolism), chemists have to rely on their intrinsic chemistry knowledge to presume or speculate the metabolic soft spots. This could make the structure optimization process cumbersome, laborious, and time/resource intensive. In this study, we aimed to develop and validate a rapid metabolite identification process based on Tier I metabolic stability data or so called "Metabolite Elucidation using Tier One Data (MET-OD)" approach. In this framework, we automatically run fragmentation analysis on mass spectrum of low stable ($t_{1/2} < 5$ min) compounds and obtain information on the metabolic soft spots along with stability data. Experimentally, the same sample that is used to determine metabolic stability can be used for fragmentation analysis to identify metabolic soft spots with the software Mass MetaSite/WebMetabase (Figure 1). In this way, chemists will gain additional information on how to modify unstable compounds to achieve more stable compounds in fewer iterations. Thus, it will save time, cost and valuable resources. To validate whether this procedure will capture the metabolites properly, we

ran the MET-OD pipeline using 48 known compounds with $t_{1/2} < 5$ min. These compounds were submitted to our Tier I RLM stability assay, where compounds ($1 \mu\text{M}$) were incubated with RLM (0.5 mg/mL) in 100 mM phosphate buffer ($\text{pH } 7.4$) along with NADPH regenerating system for 15 minutes at 37°C . Results obtained from the rapid metabolite identification (MET-OD) were compared to that from the conventional metabolite identification (MetID) assay, which was performed at a higher compound concentration ($10 \mu\text{M}$) and higher microsomal protein concentration (1 mg/mL). Additionally, the chromatographic system was coupled with a PDA detector to observe if the major metabolites observed using mass spectrometry was the same as in UV detection. Preliminary results indicate $\sim 75\%$ correlation between MetID and MET-OD for the detection of the highest metabolites. This level of detailed information early in the drug discovery process will reduce the number of iterations in developing stable lead candidates and accelerate translational research.



P107 - METABOLIC PATHWAYS OF ICLEPERTIN: CLINICAL INSIGHT FROM PRECLINICAL DATA

Tom Chan¹, Aaron Teitelbaum², Pingrong Liu¹, Klairynne Raymond¹, Holly Maw¹, Young-Sun Scaringella¹, Alexander Byer-Alcorace¹, Andrea Whitcher-Johnstone¹, Ting Wang¹, Bachir Latli¹, and Mitchell Taub¹

¹Boehringer Ingelheim Pharmaceuticals Inc., United States and ²Boehringer Ingelheim Pharma GmbH & Co. KG, Germany

Iclepertin (BI 425809) is a glycine transporter 1 (GlyT1) inhibitor being developed for the treatment of Cognitive Impairment Associated with Schizophrenia (CIAS). In this work, the metabolic profile of BI 425809 in plasma, urine and feces was characterized in samples collected from healthy male volunteers administered a single oral dose of ^{14}C -labeled BI 425809 in a human absorption, distribution, metabolism, and excretion (hADME) trial. Twenty metabolites were identified in human plasma and excreta including the major plasma metabolites BI 758790 (M530) and BI 761036 (M232). Neither of these major metabolites was found to be pharmacologically active against a panel of 100 off targets as well as against GlyT1 and GlyT2. While the pharmacokinetic (PK) profile of M530 closely followed that of BI 425809, the PK profile of M232 was characterized by a much longer t_{max} (192 h) and terminal $t_{1/2}$ (243 h) than BI 425809 ($t_{\text{max}} = 1.5 \text{ h}$ and $t_{1/2} = 51 \text{ h}$). Follow-up *in vitro* studies were conducted to probe the metabolic pathways involved in the metabolism of BI 425809 to M530 and M232 using hepatic subcellular fractions, recombinant enzymes, and human plasma. The data indicate that BI 425809 is readily oxidized by CYP3A4 to form a putative carbinolamine that can undergo further metabolism via two main pathways. In the first pathway, the carbinolamine spontaneously undergoes ring opening to form an aldehyde, M528. M528 is further reduced by cytosolic carbonyl reductase 1 (CBR1) to form M530. In the second pathway, the carbinolamine is further oxidized to form an n-acetyl acetamide metabolite, BI 764352 (M526). M526 is subsequently hydrolyzed in the plasma by albumin to form M232. Enzyme kinetic studies using recombinant CYP3A4

revealed that the Clint of BI 425809 via the pathway which forms M528 is >1200-fold higher than the pathway which forms M526, explaining the long t_{max} value of M232. Although the formation of M526 is very slow, the long elimination t_{1/2} of M232 drives its high exposure and C_{max} after multiple dosing. These data highlight the key role of CYP3A4 in forming both major metabolites and helps to explain the unique plasma profile of the major BI 425809 metabolite, M232.

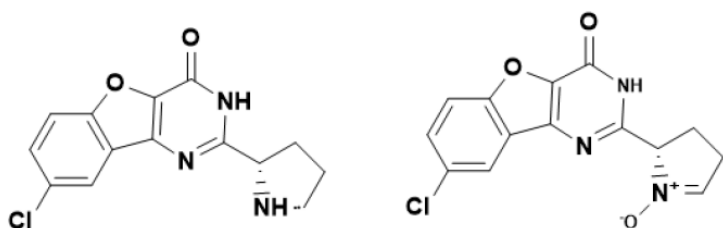
P108 - IDENTIFICATION, SEMIQUANTITATION, STRUCTURE ELUCIDATION, AND REACTION PHENOTYPING OF A MAJOR CIRCULATING METABOLITE IN HUMANS ADMINISTERED WITH BMS-863233

Weiqi Chen, Sarah Traeger, Wenying Li, and Ramaswamy Iyer

BMS, United States

An unusual P+14 metabolite (BMS-959208) was identified in human plasma following multiple oral dosing of BMS-863233, a potent ATP-competitive, reversible, and selective CDC7 inhibitor. Based on levels of BMS-959208 that were obtained by LC-MS/MS-based semi-quantitation without a reference standard, BMS-959208 was a likely major circulating metabolite in humans. Biosynthesis of BMS-959208 with S9 fractions from Arocolor-1524 induced rats followed by semi-preparative HPLC purification yielded enough BMS-959208 for structure elucidation via NMR analysis. Subsequently, cytochrome P450 (CYP) reaction phenotyping was carried out to identify the enzymes involved in the formation of BMS-959208. Incubations of BMS-863233 at concentrations of 5 and 50 μM were conducted with cDNA-expressed human CYPs and FMOs, and the rate of formation of BMS-959208 was measured by LC/MS/MS analysis. The results indicated that CYP1A2 was the major enzyme responsible for the formation of BMS-959208. Other enzymes, CYP 1A1, CYP2C19 and FMO3, may have also contributed to the formation of BMS-959208. To confirm the involvement of CYP1A2 and other enzymes, 50 μM of BMS-863233 was incubated with a panel of human liver microsomes (HLM) from individual donors that had wide ranges of variation in activities of CYP1A2 and CYP2C19. Furthermore, BMS-863233 was incubated with human liver microsomes in the presence of chemical inhibitors for CYP1A2 and CYP2C19. BMS-863233 was also incubated with HLM heated at 45 °C for 5 minute to deactivate FMOs. Results from these studies confirmed that CYP1A2 is the major enzyme involved in the formation of BMS-959208.

Figure 1. Molecular structures of BMS-863233 and BMS-959208



P109 - HEPATIC GLUCURONIDATION AND BIOACTIVATION RESISTANCE OF THE NATURAL PRODUCT QUEBECOL IN HUMAN AND RAT LIVER MICROSOMES

Gabriel Dalio Bernardes da Silva, and Ed Krol

University of Saskatchewan, Canada

Quebecol (2,3,3-tri-(3-methoxy-4-hydroxyphenyl)-1-propanol) is a polyphenolic compound, which is formed during maple syrup production from *Acer saccharum* spp. The name of quebecol was assigned because of the world's premier producer of maple syrup, the Canadian province of Quebec. A number of structural analogues of quebecol have been synthesized and their pharmacological properties investigated however, there are no reports on the hepatic metabolism of quebecol. This interest in therapeutic properties spurred us to investigate the *in vitro* Phase I and II metabolism of quebecol. We anticipated phase II metabolism would predominate, and we observed extensive metabolism resulting in the formation of three glucuronide metabolites in both rat liver microsomes (RLM) and human liver microsomes (HLM). To further understand the hepatic contribution to first-pass glucuronidation we have validated an HPLC method following FDA and EMA guidelines (selectivity, linearity, accuracy, precision, and auto-sampler stability) to quantify quebecol in microsomes. *In vitro* enzyme kinetics were performed for quebecol glucuronidation by HLM including 8 concentrations from 5-30 μM. We determined a Michaelis-Menten constant (K_M) of 5.1 μM, intrinsic clearance (Cl_{int}) of 0.04 mL/min/mg, and maximum velocity (V_{max}) of 0.22 μmol/min/mg. In contrast, we were unable to detect any P450 metabolites for quebecol in either HLM or RLM. In spite of the presence of three phenols that could form para-quinone methides, we found no evidence of reactive intermediate formation by performing glutathione (GSH) trapping experiments. To confirm this, we prepared quinone standards of quebecol using manganese dioxide, and the quinones were trapped as GSH

adducts. Rather than observe the expected para-quinone methides, we instead observed ortho-quinone formation resulting from manganese dioxide-mediated dealkylation, suggesting that quebecol is resistant to reactive intermediate formation.

P110 - SALMON GILL EPITHELIAL CELL MODEL FOR XENOBIOTIC METABOLISM

Lada Ivanova, **Christiane Fæste**, and Anita Solhaug

Norwegian Veterinary Institute, Norway

Fish are exposed to xenobiotics in the water. Gills are complex organs, functioning as exchange point with and barrier against the environment at the same time. Here, we have characterized the metabolic capacity of the ASG-10 gill epithelial cell line from Atlantic salmon (1). CYP1A expression was confirmed by using the EROD assay and immunoblot with specific antibodies. Performing *in vitro* metabolism experiments with typical substrates in the ASG-10 cells, followed by liquid chromatography mass spectrometry (LC-MSMS), we were able to establish the presence of several other CYP and UGT enzymes. In addition, enzymatic activities associated with esterases and acetyl transferases were evaluated by studying the biotransformation of benzocaine (BZ) (ethyl 4-aminobenzoate). This local anesthetic is frequently used in experiments with fish by bath exposure, either at concentrations in the range 1 to 5 mL/L, allowing recovery, or up to 25 mL/L, leading to death. Pharmacokinetics in different fish species are temperature-dependent, with a fast uptake, relatively high volume of distribution and at least two-compartment plasma elimination, exhibiting an initial half-life of about 1 h and a slow terminal phase (2). We were able to determine the three main BZ metabolites that have been described after *in vivo* exposure in fish: N-acetylbenzocaine (acetylBZ), p-aminobenzoic acid (PABA) and p-N-acetyl-aminobenzoic acid (acetylPABA). They are products of acetylation and hydrolysis reactions and primarily excreted through the gills. The ASG-10 cells further produced hydroxy-benzocaine (BZOH), a metabolite known to induce methemoglobinemia in mammals, and benzocaine-glucuronide (BZ-GlcA) (3). The findings were compared to metabolite profiles obtained from incubations with salmon liver S9 and microsomes, and from the plasma of salmon euthanized with BZ. Both, BZOH and BZ-GlcA were identified in fish for the first time, giving further insight into BZ toxicity and kinetics in fish, and demonstrating the applicability of the ASG-10 cell line for biotransformation studies.

References:

1. Gjessing MC, Aamelfot M, Batts WN, Benestad SL., Dale OB., Thoen E, Weli S, Winton JR (2018). Development and characterization of two cell lines from gills of Atlantic salmon. *Plos one*, 13: e0191792.
2. Meinertz, J. R., Stehly, G. R., & Gingerich, W. H. (1999). Metabolism, elimination, and pharmacokinetics of the fish anesthetic benzocaine. In *Xenobiotics in Fish* (pp. 189-200). Springer, Boston, MA.
3. Hartman N, Zhou H, Mao J, Mans D, Boyne M, Patel V, Colatsky T (2017). Characterization of the methemoglobin forming metabolites of benzocaine and lidocaine. *Xenobiotica*, 47:431-438.

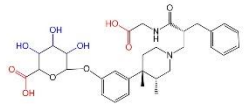
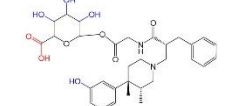
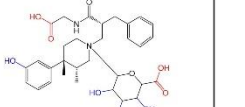
P111 - DETERMINATION OF ACYL-, O-, AND N-GLUCURONIDE USING CHEMICAL DERIVATIZATION COUPLED WITH LIQUID CHROMATOGRAPHY – HIGH RESOLUTION MASS SPECTROMETRY

Abhi Shah, **Yukuang Guo**, and SeanZhu

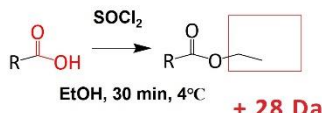
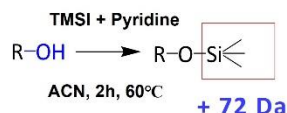
Takeda, United States

Glucuronidation is the most common phase II metabolic pathway to eliminate small molecule drugs from the body. However, determination of glucuronide structure is quite challenging by mass spectrometry due to its inability to generate structure informative fragments about the site of glucuronidation. Herein we described a simple method to differentiate acyl-, O-, and N-glucuronides using chemical derivatization. The idea is that derivatization of acyl-, O- or N-glucuronide of a molecule results in predictable and different numbers of derivatized functional groups, which can be determined by the mass shift using mass spectrometry. The following two reactions were applied to specifically derivatize carboxyl and hydroxyl groups that are present on the aglycone and its glucuronide metabolite. Carboxyl groups were activated by thionyl chloride followed by esterification with ethanol. Hydroxyl groups were derivatized via silylation by 1-(trimethylsilyl)imidazole. The mass shift per derivatized carboxyl and hydroxyl group was +28.031 Da and +72.040 Da, respectively. This approach was successfully validated using commercial glucuronide standards including benazepril acyl-glucuronide, raloxifene O-glucuronides, and silodosin O-glucuronide. In addition, this approach was applied to determine the type of glucuronide metabolites that were isolated from liver microsomal incubation, where alvimopan and diclofenac acyl-glucuronides, darunavir, haloperidol, and propranolol O-glucuronides, and darunavir N-glucuronide were identified. Lastly, this approach was successfully utilized to elucidate the definitive structure of a clinically observed metabolite, soticlestat O-glucuronide. In conclusion, a novel efficient and cost-effective approach was developed to determine acyl-, O-, and N-glucuronide using chemical derivatization coupled with liquid chromatography-high resolution mass spectrometry.

Chemical derivatization approach to differentiate acyl-, O-, and N-glucuronides

Glucuronide	O-gluc	Acyl-gluc	N-gluc
Structure			
Number of -OH	3	4	4
Number of -COOH	2	1	2

Reactions



Samples analysis



4 LC-HRMS with Thermo Orbitrap Elite

P112 - DAPL1 AFFECTS PERINATAL MOUSE SENSITIVITY TO MATERNAL TCDD EXPOSURE: COMPARATIVE STUDY USING HOMOZYGOUS FETUSES FROM DAPL1 HETEROZYGOUS DAM

Hong-bin Chen¹, Jorge Carlos Pineda Garcia¹, Yukiko Hattori¹, Tomoki Takeda^{1,2}, Ren-shi Li¹, Yoshitaka Tanaka, and **Yuji Ishii**¹

¹Graduate School of Pharmaceutical Sciences, Kyushu University, Japan and ²Japan Bioassay Research Center, Japan

Death-associated protein-like 1 (DAPL1) is widely expressed in cells above the proliferative compartment in various epithelia. DAPL1 may be involved in the early stages of epithelial cell differentiation [1]. Maternal exposure to dioxin reduces the number of growth hormone (GH)-positive cells in the pituitary gland of fetal rats. DAPL1 knockdown in primary cultured fetal pituitary cells also reduces GH expression levels [2]. Compared with rats, maternal exposure to 2,3,7,8-tetrachlorodibenzo-p-dioxin (TCDD) at a low dose (1 µg/kg) is insufficient to effectively reduce the GH expression in mice fetuses [3]. We used our recently established Dapl1-knockout (KO) mice [4] to examine whether the deletion of Dapl1 could potentiate or not the effect of low-dose TCDD. The heterozygous offspring of the Dapl1-KO mouse was used to mate. The resulting pregnant mice were given oral TCDD (1 µg/kg) at gestational day (GD) 12; The fetuses were dissected at GD18 to collect the pituitary gland and related tissues and organs for genotyping. The expression of GH and other pituitary hormones in both Dapl1-KO and wild-type mice were compared to explore the associated factors of Dapl1 and TCDD. We observed that in the absence of Dapl1, a low dose of TCDD (1 µg/kg) effectively reduced GH mRNA expression in the fetal pituitary gland. This phenomenon was restricted to males. In female Dapl1-KO mice, TCDD reduced thyrotropin mRNA expression levels in the fetal pituitary. Therefore, Dapl1 alters the sensitivity of perinatal mice to TCDD at variable degrees with significant differences between genders.

This research was supported in part by the JSPS KAKENHI [Scientific Research (A) JP17H00788 and JP21H04928] and the Ministry of Health, Labor and Welfare, Japan [Research on Food Safety (H30-Designated Research-005 and R3-Designated Research JP21KA2003)].

References:

1. Sun, L., Ryan, D. G., Zhou, M., Sun, T. T. & Lavker, R. M. EEDA: a protein associated with an early stage of stratified epithelial differentiation. *J Cell Physiol* 206, 103-111 (2006).
2. Hattori, Y., Takeda, T., Fujii, M., Taura, J., Yamada, H. and Ishii, Y. Attenuation of growth hormone production at the fetal stage is critical for dioxin-induced developmental disorder in rat offspring. *Biochem Pharmacol* 186, 114495 (2021).
3. Takeda, T., Taura, J., Hattori, Y., Ishii, Y. and Yamada, H. Dioxin-induced retardation of development through a reduction in the expression of pituitary hormones and possible involvement of an aryl hydrocarbon receptor in this

defect: a comparative study using two strains of mice with different sensitivities to dioxin. *Toxicol Appl Pharmacol* 278, 220-229 (2014).

4. Chen, H. B., Pineda Garcia, J. C., Arizono, S., Takeda, T., Li, R. S., Hattori, Y., Sano, H., Miyauchi, Y., Hirota, Y., Tanaka, Y., Ishii Y. DAPL1 is a novel regulator of testosterone production in Leydig cells of mouse testis. *Sci Rep.* 11, 18532 (2021).

P113 - ASSESSING THE IMPACT OF BENZALKONIUM CHLORIDES ON GUT MICROBIOME AND LIVER METABOLISM

Vanessa Lopez¹, Joe L. Lim², Ryan P. Seguin¹, Joseph L. Dempsey², Julia Y. Cui², Libin Xu^{1,2}

¹Department of Medicinal Chemistry and ²Department of Environmental and Occupational Health Sciences, University of Washington, United States

Benzalkonium chlorides (BACs) are widely used disinfectants in a variety of consumer and food-processing settings, and the ongoing COVID-19 pandemic has led to greatly increased use of BACs. The prevalence of BACs in our daily environment raises the concern that whether regularly recurring BAC exposure could disrupt the gastrointestinal microbiota and their beneficial functions to host health. We recently reported that BACs are metabolized by cytochromes P450 (CYPs) 4Fs and 2D6 in the liver. Our preliminary data supports that biliary excretion from the liver to the intestine is the major route of elimination for BACs and their metabolites. Thus, we hypothesize that exposure to BACs alters the gut microbiome diversity and composition, which will lead to alterations in bile acid homeostasis, sterol biosynthesis, and xenobiotic metabolism in the liver. In this study, we exposed male and female mice to C12- and C16-BACs at 120 μ g/g/day for one week via oral dosing. Intestinal content from cecum was collected, and 16S rRNA sequencing was carried out on the isolated bacterial DNA. We found that exposure to either C12- or C16-BACs led to decreased alpha diversity and significantly altered composition of gut bacteria, such as the complete elimination of the actinobacteria phylum. Additionally, through a targeted bile acid quantitation analysis, we found decreases in secondary bile acids in BAC-treated mice. This finding is supported by decreases in bacteria known to metabolize primary bile acids into secondary bile acids, such as the families of Ruminococcaceae and Lachnospiraceae. Furthermore, targeted sterolomic analysis of liver extracts revealed that BACs caused overall decreased sterol abundance, including decreased cholesterol and lanosterol. Additionally, RNA sequencing revealed that C16-BAC exposure in the female cohort up-regulated of *Hmgcr*, a gene that encodes the rate-limiting enzyme for cholesterol synthesis, which is consistent with the inhibition of cholesterol biosynthesis by BACs. C16-BAC exposure in the male cohort up-regulated of *Cyp4a10*, *Cyp4f13*, *Cyp2j6* and *Cyp2c38* genes, all involved in hepatic lipid and xenobiotic metabolism. Lastly, UPLC-MS/MS analysis of intestinal sections and livers of BAC treated mice demonstrated the absorption and metabolism of BACs. Both parent compounds were detected in the liver along with their major Phase-I metabolites: the ω -OH, (ω -1)-OH, (ω -1)-ketone, and ω -COOH metabolites. Together, these data signify the potential impact BAC exposure on human health through disturbance of the gut microbiome and liver metabolism.

P114 - MECHANISTIC ANALYSIS OF OCHRATOXIN-A NEPHROTOXICITY

Anish Mahadeo¹, Edward Kelly¹, Catherine Yeung¹, Tomoki Imaoka², and Theresa Aliwarga¹

University of Washington, United States and ²Daiichi Sankyo, Japan

Chronic kidney disease (CKD) affects 20 million people in the United States alone, with over 600,000 patients receiving dialysis[1]. While diabetes, hypertension, and obesity are known risk factors for CKD, over the last 50 years, endemic hotspots of chronic kidney disease have emerged around the world, disproportionately affecting younger men who do not have these conditions, and live in tropical, agricultural communities in regions like South Asia and Central America. Since the cause(s) of these endemic nephropathies remain unclear, the condition has been termed chronic kidney disease of unknown etiology (CKDu). A recent report suggests that in the state of Tamil Nadu in India, 52% of CKD cases are of unknown origin[2]. Several environmental agents have been proposed to contribute to CKDu, including the mycotoxin ochratoxin-A (OTA), one of the most common contaminants in a wide variety of food including wheat, maize, rice, and coffee. OTA causes not only nephrotoxicity but also hepatotoxicity, genotoxicity, and carcinogenesis, however its mechanism of toxicity is poorly understood. Exposure to OTA is unavoidable, and thus chronic exposure is a concern. Based on previous work[3], it is hypothesized that OTA may hinder the nuclear translocation of antioxidant-regulator NRF2 from its cytosolic binder KEAP1, thus downregulating numerous oxidative-stress responses transcribed by NRF2. To investigate this mechanism, primary human proximal tubule epithelial cells (hPTECs) were cultured with NRF2 activators sulforaphane (SFN) or tert-butylhydroquinone (tBHQ) to induce antioxidant response genes before being challenged with OTA. Total mRNA sequencing and immunocytochemistry staining for downstream NRF2 targets were utilized for assessment.

RNA-seq analysis revealed numerous differentially expressed genes between cells treated OTA, OTA + NRF2 activators, and control media. Several NRF2 targets such as GSR and GSTP1 were found to be downregulated due to OTA, even in the presence of NRF2 activators. Interestingly, several genes involved in the hypoxic response such as HIF1 α were upregulated. Immunocytochemistry analysis of cells cultured under hypoxic conditions with OTA and NRF2 activators

revealed significant HIF1 α nuclear localization and cell death compared controls. This suggests a synergistic effect between OTA, the NRF2 pathway, and the hypoxic response pathway may be involved in OTA nephrotoxicity. Future experiments will investigate these processes in 3-D proximal tubule microphysiological systems, which have been demonstrated to replicate *in vivo* processes and microenvironment not seen in traditional cell culture. Furthermore, the role of OTA, hypoxic and oxidative stress on mitochondria will be assessed by live confocal imaging of hPTECs. To investigate the role of OTA in CKDu, plasma and urine samples from CKDu patients in Sri Lanka will be analyzed by LC-MS/MS for the presence of OTA.

References:

1. Wang, V., et al., The Economic Burden of Chronic Kidney Disease and End-Stage Renal Disease. *Semin Nephrol*, 2016. 36(4): p. 319-30.
2. Parameswaran, S., et al., A Newly Recognized Endemic Region of CKD of Undetermined Etiology (CKDu) in South India-"Tondaimandalam Nephropathy". *Kidney Int Rep*, 2020. 5(11): p. 2066-2073.
3. Imaoka, T., et al., Microphysiological system modeling of ochratoxin A-associated nephrotoxicity. *Toxicology*, 2020. 444: p. 152582.

P115 - PREDICTING REACTIVITY TO DRUG METABOLISM: BEYOND CYPs

Mario Öeren, Peter Hunt, and Matthew Segall
Optibrium Ltd., United Kingdom

Understanding the metabolism of novel compounds at the molecular level is of critical importance for successful drug discovery projects. The use of *in silico* methods allows chemists to optimise the metabolic properties of new chemical entities both quickly and cost-effectively (or identify situations, when an acceptable balance of said properties is not possible). Furthermore, potential toxic metabolites can be identified early in a drug discovery project.

Historically, predictive models have targeted prediction of metabolism by human isoforms of the Cytochrome P450 (CYP) family of enzymes due to their importance in the metabolism of drug-like compounds, in particular the modification phase. However, studies on how to predict metabolism for other enzymes in the modification phase, such as Aldehyde Oxidases (AOX) and Flavin-containing Monooxygenases (FMO), and conjugation phase enzymes, such as Uridine 5'-diphosphoglucuronosyl-transferases (UGT), are increasing in prevalence.

The study presents methods for predicting isoform-specific metabolism by human AOXs, FMOs and UGTs. The models use semi-empirical quantum mechanical simulations, validated using experimentally obtained data and density functional theory calculations, to estimate the reactivity of each potential site of metabolism in the context of the whole molecule. Ligand-based models, trained and tested using high-quality regioselectivity data, combine the reactivity of the potential site of metabolism with the orientation and steric effects of the binding pockets of the different enzyme isoforms. The resulting binary classification models, which predict if a site is metabolised by a specific isoform of these enzyme families, achieve Cohen kappa coefficients from 0.62 to 0.94.

P116 - ADAGRASIB METABOLISM AFTER SINGLE AND MULTIPLE ORAL DOSING IN HUMANS

Lisa Rahbaek, Chris Wegerski, Natalie T. Nguyen, Cornelius Cilliers, Lauren Hargis, Matthew A. Marx, James G. Christensen, and Jonathan Q. Tran
Mirati Therapeutics, United States

Adagrasib (MRTX849) is a covalent KRASG12C inhibitor in development for treatment of patients with KRASG12C-mutated non-small cell lung cancer. Adagrasib metabolism was investigated after a single oral dose of 600 mg adagrasib containing 1 μ Ci of [¹⁴C]-MRTX849 in five healthy subjects. [¹⁴C]-MRTX849-derived metabolites were quantified by liquid chromatography-accelerator mass spectroscopy. Additionally, adagrasib metabolism was evaluated after multiple dosing of the proposed therapeutic dose 600 mg twice daily for eight days in four patients. MRTX849-derived metabolites were semi-quantified by liquid chromatography-ultraviolet-high resolution mass spectroscopy/mass spectroscopy. Following a single oral dose, adagrasib underwent extensive metabolism with three abundant (>10% of AUC for the drug-related materials) circulating plasma metabolites (M68, M55a and M11). However, M55a was not detected in human plasma at steady state after multiple dosing at 600 mg twice daily. Both M68 and M11 are not human specific metabolites and do not contribute significantly to the pharmacological activity of adagrasib. Based on *in vitro* human recombinant cytochrome P450 (rCYP) mapping data M68 is not formed by a single rCYP whereas M11 is formed by rCYP2C8. In conclusion, adagrasib metabolism was adequately characterized following a single and multiple dosing in humans.

P117 - OXIDIZED METABOLITES AND UNUSUAL CONJUGATES OF AZD9496 BY MICROBIAL BIOTRANSFORMATION

Julia Shanu-Wilson¹, Ravi Manohar¹, Richard Phipps¹, Jonathan Steele¹, Stephen Wrigley¹, Liam Evans¹, Tashinga

Bapiro², and Andrew Sykes²¹Hypha Discovery, United Kingdom and ²AstraZeneca, United Kingdom

AZD9496 is an orally active selective estrogen receptor degrader (SERD) whose clinical development was discontinued by AstraZeneca for treatment of estrogen receptor-positive breast cancer in favor of AZD9833, which is currently in clinical trials.

CYP2C8 is largely responsible for biotransformation of AZD9496 to two hydroxylated metabolites observed in human liver microsomes and plasma; M3 (major) and M5 (minor). The two metabolites are diastereoisomers but whose configuration is unknown [1].

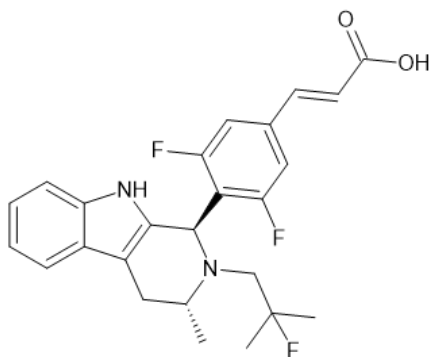
Screening of AZD9496 using microbial biotransformation and PolyCYPs enzyme incubations resulted in the formation of multiple derivatives. A total of 15 derivatives were isolated. Of the oxidized derivatives produced, 2 active metabolites were confirmed as the human metabolites M3 and M5.

Analysis of the microbial biotransformation reactions also revealed the formation of a number of conjugates with unusual mass additions, as well as a glucuronide. Three microbial strains were scaled up to generate sufficient material of the unknown conjugates for purification and structure elucidation by NMR.

All three strains produced conjugates subsequently identified as amino acid adducts, including glycine, alanine, serine and glutamine conjugates. One of these strains also produced a conjugate with an N-acetylcysteine addition to the indole aromatic ring with further oxidation in the same molecule, most likely to an N-oxide.

The formation of amino acid conjugates of drugs containing carboxyl groups is a known but uncommon biotransformation observed during microbial biotransformation of drug compounds. The generation of the amino acid conjugates involves the consecutive action of acyl CoA synthetase and amino acid N-acyltransferases, via an acyl-CoA intermediate. It is not known if any of the conjugates produced through microbial biotransformation of AZD9496 are formed in human or other mammalian systems.

Biotransformation by microbes and PolyCYPs enzymes are established techniques for generating late-stage oxidized derivatives as a lead optimization strategy. Here we show an example of the use of microbial biotransformation to create unusual conjugates.



Reference:

1. Complete Substrate Inhibition of CYP2C8 by AZD9496. Tashinga E. Bapiro, Andy Sykes, Scott Martin, Michael Davies, James W. T. Yates, Matthias Hoch, Helen E. Rollison and Barry Jones. *Drug Metabolism and Disposition*, 2018, 46 (9) 1268-1276; DOI: <https://doi.org/10.1124/dmd.118.081539>

P118 - ACYL MIGRATION AND STABILITY OF THC-COOH-GLUCURONIDE IN BIOLOGICAL MATRICES

Nina Isoherranen and Keiann Simon

University of Washington, United States

11-Nor- Δ^9 -Tetrahydrocannabinol-9-carboxylic acid glucuronide (THC-COOH-Glucuronide), a major circulating metabolite of Δ^9 -Tetrahydrocannabinol (THC), is a 1- β -O-acyl glucuronide. This metabolite is analogous to a similar glucuronide metabolite of Cannabidiol (CBD). Acyl glucuronides undergo acyl migration forming β -glucuronidase-resistant isomeric 2-, 3-, and 4-O-acyl glucuronides. THC-COOH-Glucuronide also may be degraded to its aglycon 11-nor- Δ^9 -Tetrahydrocannabinol-9-carboxylic acid (THC-COOH). THC-COOH-Glucuronide is hydrolyzed by β -glucuronidases and non-specific esterases, and it is degraded at alkaline pH and higher temperature conditions. We hypothesized that acyl migration and instability of the THC-COOH-Glucuronide, occurring in biological matrices, potentially impacts sample stability and pharmacokinetic analyses. The aim of this study was to determine the acyl glucuronide migration rates in different biological matrices and to establish the stability of THC-COOH-glucuronide in biological samples. THC-COOH-Glucuronide was incubated in phosphate buffer (pH 7.4), in plasma, in urine, and in phosphate buffer with albumin (pH

7.4), all at 37 °C for 0-48 hours. The incubated samples were analyzed using liquid chromatography tandem mass spectrometry (LC-MS/MS) and LC-UV, monitoring THC-COOH-Glucuronide, its acyl migration products and THC-COOH. Acyl migration was observed in all matrices with THC-COOH-Glucuronide and the time courses of degradation were generated. The formation of THC-COOH was observed in all samples. However, the additional formation of an unknown THC-COOH isomer from THC-COOH-glucuronide was observed in plasma and in buffer containing 2 mg/mL albumin. In light of this investigation, instability of THC-COOH-Glucuronide in biological matrices becomes important in quantitative pharmacological and biomarker analysis, and in cannabinoid incubations that require biological temperature conditions (37 °C) and the addition of albumin. Further studies to determine the impact of sample handling and sample storage on quantitation of THC-COOH-glucuronide and THC-COOH are needed. The significance of potential acyl migration products *in vivo* requires further investigation.

P119 - LC-MS METHOD FOR DETECTION OF 1ST, 2ND AND 3RD GENERATION OLIGONUCLEOTIDE THERAPEUTICS IN LIVER AND KIDNEY HOMOGENATE SAMPLES FOR METABOLISM STUDIES

Irina Slobodchikova, Wei Lu, and Greg Kilby
Alliance Pharma, United States

Oligonucleotide-based therapeutics is an emerging and fast growing area. Oligonucleotide-based drugs show a potential in the treatment of a wide variety of genetic disorders and infections and as use for vaccines. Understanding the metabolism of oligonucleotides and evaluation of safety of potential drug candidates with the use *in vitro* models including liver and kidney tissue homogenates is important for successful drug development process. However, this process is complex from sample preparation and chromatography prospective compared to small molecule analysis. The goal of the project is to optimize sample preparation and LC-MS methodology for 1st, 2nd and 3rd generation oligonucleotides including phosphorothioate, 2'-O-methyl and locked oligonucleotides, and phosphoramidate morpholino oligonucleotides. Protein Metrics software will be used for high- throughput oligonucleotide data analysis.

For an initial proof of concept study, we optimized liquid-liquid extraction with phenol/chloroform/isoamyl alcohol mixture (25:24:1 v/v) to reach high analyte recovery, good selectivity and minimal matrix effects. During LC-MS method development, different columns, mobile phase modifiers, and gradients were evaluated for suitable separation and intensity of parent oligonucleotides. Preliminary results show effective separation and sufficient intensity of phosphorothioate, 2'-O-methyl and locked oligonucleotides using an Agilent Poroshell 120 EC-C18 column and the mobile phase A containing 25 mM 1,1,1,3,3,3-hexafluoro-2-propanol/ 8mM trimethylamine in water and mobile phase B containing methanol in negative electrospray ionization mode, while phosphoramidate morpholino oligonucleotide requires additional optimization to obtain high signal intensity.

The study will examine optimal conditions for biotransformation studies of a wide variety of modified oligonucleotide therapeutics.

P120 - ROLE OF MIR-7-5P IN MITOCHONDRIAL METABOLISM

Gavin Traber, Mei-Juan Tu, Neelu Batra, Colleen Yi, and Ai-Ming Yu
University of California, Davis - School of Medicine, United States

RNA interference (RNAi) provides researchers with a versatile means to modulate target gene expression and develop new therapies [1,2,3]. MicroRNAs (miRNAs) compose one major form of genome-derived RNAi molecules converge into RNA-induced silencing complexes to achieve post-transcriptional gene regulation [1,2]. Recently, several miRNAs have shown clinical relevance as putative xenobiotics to manipulate and rebalance miRNA profiles to combat disease [3,4,5,6]. Of these miRNAs, miR-7-5p (miR-7) is known to downregulate genes important in metabolism and mitochondrial function including EGFR [7,8,13] and VDAC1 [9,10,11], and proposed to downregulate mitochondrial genes AGK [12,13], PPIF [12,14,15], and DTYMK [11,12,13]. However, most available miRNA reagents on the market today are miRNA mimics that are chemically synthesized *in vitro* and artificially modified [16,17]. By contrast, our laboratory has developed a novel technology to bioengineer RNAi agents (BioRNA) *in vivo*, including miR-7, by utilizing specific tRNA/pre-miRNA carriers [18]. Using this technology, we aim to develop a novel BioRNA/miR-7 as an anticancer xenobiotic agent through endogenous RNAi mechanisms to regulate mitochondrial metabolism. Thus far, we have successfully cloned and overexpressed BioRNA/miR-7 in *Escherichia coli* as verified by Sanger sequencing and RNA gel electrophoresis, respectively. Additionally, we have isolated BioRNA/miR-7 from total bacterial RNA by anion exchange Fast Protein Liquid Chromatography to attain a purity of 98.7% as determined by reverse phase High Performance Liquid Chromatography, and an endotoxin level of 0.68 (EU/μg RNA) as determined with an endotoxin assay kit. Moreover, we have validated the processing of BioRNA/miR-7 to target miR-7-5p in human non-small cell lung cancer (NSCLC) cells by stem-loop reverse transcription real-time qPCR assay and assessed the functional capability of BioRNA/miR-7 to regulate known miR-7 target gene expression in comparison to a commercial miR-7 mimic by Western blot analysis. Furthermore, we have established the effects of BioRNA/miR-7 on mitochondrial function with a Seahorse Analyzer and compared treatment-induced changes in mitochondrial morphology by confocal microscopy. The success of the BioRNA technology together

with previous and preliminary data on miR-7 suggests that miR-7 plays an important role in mitochondrial metabolism, and BioRNA/miR-7 may be developed as a new therapeutic RNA for the treatment of NSCLC.

Acknowledgements: This study is supported by the National Institute of General Medical Sciences [R35GM140835] and National Cancer Institute [R01CA225958 and R01CA253230], National Institutes of Health. Gavin M. Traber is supported by a National Institutes of General Medical Sciences-funded Pharmacology Training Program Grant [T32GM099608].

References:

1. Fire A, Xu S, Montgomery MK, Kostas SA, Driver SE and Mello CC (1998) Potent and specific genetic interference by double-stranded RNA in *Caenorhabditis elegans*. *Nature* **391**:806-811.
2. Sen GL and Blau HM (2006) A brief history of RNAi: the silence of the genes. *FASEB J* **20**:1293-1299.
3. Setten RL, Rossi JJ and Han SP (2019) The current state and future directions of RNAi-based therapeutics. *Nat Rev Drug Discov* **18**:421-446
4. Yu AM, Choi YH, and Tu MJ (2020) RNA Drugs and RNA Targets for Small Molecules: Principles, Progress, and Challenges. *Pharmacol Rev.* **72**(4):862-898.
5. Yu AM and Tu MJ (2022) Deliver the promise: RNAs as a new class of molecular entities for therapy and vaccination. *Pharmacol Ther.* **230**:107967.
6. Traber GM and Yu AM (2022) RNAi Based Therapeutics and Novel RNA Bioengineering Technologies. *Journal of Pharmacology and Experimental Therapeutics*. (In press).
7. Webster RJ, Giles KM, Price KJ, Zhang PM, Mattick JS, and Leedman PJ (2009) Regulation of epidermal growth factor receptor signaling in human cancer cells by microRNA-7. *J Biol Chem.* **284**(9):5731-41.
8. Che TF, Lin CW, Wu YY, Chen YJ, Han CL, Chang YL, Wu CT, Hsiao TH, Hong TM, and Yang PC (2015) Mitochondrial translocation of EGFR regulates mitochondria dynamics and promotes metastasis in NSCLC. *Oncotarget.* **6**(35):37349-66.
9. Wang F, Qiang Y, Zhu L, Jiang Y, Wang Y, Shao X, Yin L, Chen J, and Chen Z (2016) MicroRNA-7 downregulates the oncogene VDAC1 to influence hepatocellular carcinoma proliferation and metastasis. *Tumour Biol.* **37**(8):10235-46.
10. Camara AKS, Zhou Y, Wen PC, Tajkhorshid E, and Kwok WM (2017) Mitochondrial VDAC1: A Key Gatekeeper as Potential Therapeutic Target. *Front Physiol.* **8**:460.
11. Chaudhuri AD, Choi DC, Kabaria S, Tran A, and Junn E (2016) MicroRNA-7 Regulates the Function of Mitochondrial Permeability Transition Pore by Targeting VDAC1 Expression. *J Biol Chem.* **291**(12):6483-93.
12. Agarwal V, Bell GW, Nam JW, and Bartel DP (2015) Predicting effective microRNA target sites in mammalian mRNAs. *Elife.* **4**:e05005.
13. Chou YT, Lin HH, Lien YC, Wang YH, Hong CF, Kao YR, Lin SC, Chang YC, Lin SY, Chen SJ, Chen HC, Yeh SD, and Wu CW (2010) EGFR promotes lung tumorigenesis by activating miR-7 through a Ras/ERK/Myc pathway that targets the Ets2 transcriptional repressor ERF. *Cancer Res.* **70**(21):8822-31.
14. Coleman O, Suda S, Meiller J, Henry M, Riedl M, Barron N, Clynes M, and Meleady P (2019) Increased growth rate and productivity following stable depletion of miR-7 in a mAb producing CHO cell line causes an increase in proteins associated with the Akt pathway and ribosome biogenesis. *J Proteomics.* **195**:23-32.
15. Gupta MK, Sahu A, Sun Y, Mohan ML, Kumar A, Zalavadia A, Wang X, Martelli EE, Stenson K, Witherow CP, Drazba J, Dasarathy S, and Naga Prasad SV (2021) Cardiac expression of microRNA-7 is associated with adverse cardiac remodeling. *Sci Rep.* **11**(1):22018.
16. Morena F, Argentati C, Bazzucchi M, Emiliani C, and Martino S (2018) Above the Epitranscriptome: RNA Modifications and Stem Cell Identity. *Genes (Basel).* **9**(7):329.
17. Yu AM, Jian C, Yu AH, and Tu MJ (2019). RNA therapy: Are we using the right molecules? *Pharmacol Ther.* **196**:91-104.
18. Li PC, Tu MJ, Ho PY, Batra N, Tran MML, Qiu JX, Wun T, Lara PN, Hu X, Yu AX, and Yu AM (2021) *In vivo* fermentation production of humanized noncoding RNAs carrying payload miRNAs for targeted anticancer therapy. *Theranostics.* **11**(10):4858-4871.

P121 - NOVEL BIOENGINEERED MIR-1291 MODULATES XENOBIOTIC NUTRIENT TRANSPORTERS AND METABOLIC ENZYMES TO CONTROL CELL METABOLISM

Mei-Juan Tu, Yi-Mei Wang, and Ai-Ming Yu

University of California, Davis - School of Medicine, United States

Vitamin B6 (VB6) belongs to a class of water-soluble essential nutrients consisting of six compounds that could be interconverted by specific enzymes in a biosystem. The bioactive form of vitamin B6, pyridoxal-5'-phosphate (PLP), functions as a coenzyme in more than 100 metabolic reactions including amino acid biotransformation, one-carbon metabolism, and carbohydrate metabolism. Thus, it is not surprising that dysregulation of cellular VB6 metabolism is

associated with the progression and diagnosis of multiple kinds of diseases. In addition, VB6 (Pyridoxine, Nestrex, or Neuro-K) has been approved by the US FDA for the treatment of drug-induced vitamin deficiency and hereditary disorders, and it is also commonly used as a dietary supplement. Our previous studies have demonstrated that microRNA-1291-5p (miR-1291-5p or miR-1291) acts as a tumor suppressor, whereas it is downregulated in pancreatic cancer (PC) patient tissues and cell lines. This study is to investigate the role of miR-1291 in the control of nutrient metabolism and develop miR-1291-based therapy. We first employed our newly-invented RNA bioengineering technology to achieve high-level and large-scale, *in vivo* fermentation production of a fully-humanized biologic miR-1291 agent (BioRNA/miR-1291) at a high-degree of homogeneity (> 4 mg BioRNA per liter of culture and > 97% purity). RNA sequencing studies revealed that BioRNA/miR-1291 was selectively processed to target miR-1291-5p to modulate the transcriptome in PC cells. Proteomics study showed that a number of proteins were reduced remarkably in AsPC-1 cells by BioRNA/miR-1291, among which the pyridoxine 5'-phosphate oxidase (PNPO), a rate-limiting enzyme of PLP synthesis, was revealed as a direct target of miR-1291-5p. Besides PNPO and the previously-reported glucose transporter SLC2A1/GLUT1, amino acid transporter SLC7A5/LAT1 was verified as a direct target for miR-1291-5p. Downregulation of PNPO, LAT1, and GLUT1 protein expression by biological miR-1291 led to sharp alteration of homeostasis of glucose, amino acids, and VB6 in human PC cells, and subsequent suppression of glycolysis capacity and mitochondrial function as well as the increase of oxidative stress. Combination treatment with bioengineered miR-1291 and 5-FU exerted strong synergism in the inhibition of PC cell and organoid proliferation *in vitro*. In addition, miR-1291 mono- and combination therapy were effective to control tumor growth in pancreatic cancer patient-derived xenograft (PDX) mouse models. These results demonstrate a critical role for miR-1291 in the regulation of xenobiotic/nutrient metabolism which provide insight in developing new therapeutic strategies via targeting tumor metabolism.

P122 - METABOLITE IDENTIFICATION BY INTEGRATION OF DATA ACQUISITION, DIFFERENTIAL MASS SPECTROMETRY, AND DATA PROCESSING TECHNIQUES: APPLICATION TO GLUCAGON-LIKE PEPTIDE-1 (GLP-1) METABOLITE DETECTION AND IDENTIFICATION

Pengcheng Wang¹, Amanda Cirello¹, Mithat Gunduz¹, John Davis¹, and Markus Walles²

¹Novartis Institutes for Biomedical Research, Inc, United States and: ²Novartis Institutes for Biomedical Research, Switzerland

Therapeutic peptides are composed of a series of alpha amino acids usually with molecular weights of 500-5000 Da. An increasing number of therapeutic peptides and peptide conjugates have been entering clinical trials and have been successfully approved for human use. Understanding the metabolic fate is critical for discovery and preclinical and clinical development of therapeutic peptides. Despite the increase of application of various software and data processing techniques, metabolite detection and identification of complex therapeutic peptides remains challenging. We aim to evaluate and develop an integrated strategy to identify metabolites of therapeutic peptides from complex biologic matrices. We used glucagon-like peptide-1 (7-37, GLP-1) as a case example. The metabolic fate of GLP-1 was investigated in rat and human liver lysosomes, as well as in rat, monkey and human liver S9 fractions. High-performance liquid chromatography-high resolution mass spectrometry (HPLC-HRMS) was used for metabolite analysis. For data acquisition, we evaluated the AcquireX™ intelligent data acquisition workflow to enhance real-time, selective data-independent LC-MSn data acquisition. For metabolite detection, we evaluated and demonstrated that differential mass spectrometry (computational method for detecting differences of MS features) was able to distinguish and detect metabolites. For metabolite structural elucidation, we evaluated different data processing platforms (MassMetaSite, Biopharma Finder, ProMass) to unambiguously characterize metabolite structures. This work highlighted that integration of data acquisition, differential mass mass spectrometry, and data processing techniques provided an applicable strategy for metabolite identification of therapeutic peptides from complex biological matrices.

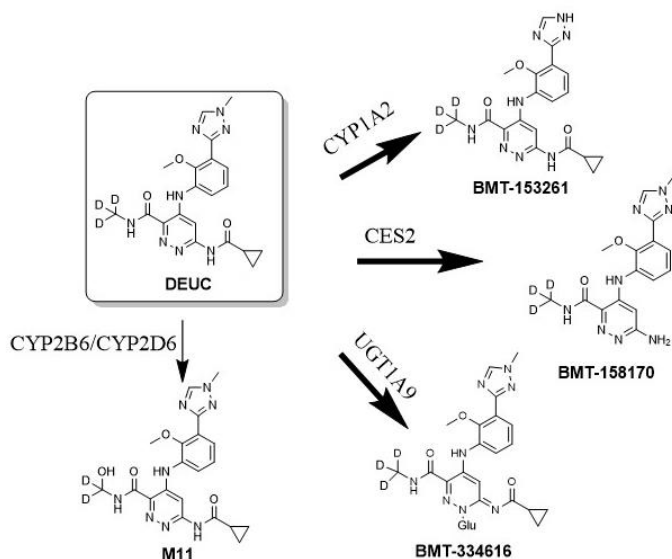
P123 - CHARACTERIZATION OF THE METABOLIC PATHWAYS OF DEUCRAVACITINIB (BMS-986165)

Ming Yao, Xiaomei Gu, Anjaneya Chimalakonda, Ramaswamy Iyer, and Wenying Li

Bristol-Myers Squibb Co, United States

Deucravacitinib (DEUC, BMS-986165), a highly selective and potent small molecule inhibitor of the cytokine signaling kinase, tyrosine kinase 2 (TYK2), is currently under development as an oral treatment for autoimmune disorders associated with TYK2-dependent pathways. Results from *in vitro* metabolism studies indicated that DEUC was metabolized via four primary biotransformation pathways, namely N-demethylation at the triazole moiety to form BMT 153261, cyclopropyl carboxamide hydrolysis to form BMT-158170, N-glucuronidation to form BMT-334616, and monooxidation at the deuterated methyl group to form M11. Enzymes involved in these biotransformation pathways were investigated using recombinant enzymes and HLM with selective inhibitors, and the results showed 1) the formation of BMT 153261 was mainly mediated by CYP1A2, with minor contribution from CYP2B6 and CYP3A4/5; 2) the formation of BMT-158170 was catalyzed by CES2; 3) the formation of BMT-334616 was mediated by UGT1A9; and 4) CYP2B6 and CYP2D6 were the enzymes responsible for formation of M11. *In vivo* ADME studies indicated that all 4 biotransformation pathways were present in every species (humans, mice, rats, and monkeys). In humans, each of the 3 major metabolic

pathways (formation of BMT-153261, BMT-158170, and BMT-334616) was responsible for < 25% of the DEUC elimination, while contribution of the minor pathway (formation of M11) to the elimination was < 6%. Thus, coadministration of agents that modify activities of CYP1A2, UGT1A9, CES2, CYP2B6, or CYP2D6 was not expected to produce clinically relevant changes in DEUC exposures in humans. Consistently, no clinically meaningful effect on DEUC exposure was identified when DEUC was co-administered with fluvoxamine (strong CYP1A2 inhibitor), ritonavir (CYP1A2 inducer), and diflunisal (UGT1A9 inhibitor).



In vitro and in vivo primary biotransformation pathways of DEUC

P124 - METABOLITE IDENTIFICATION, CATABOLISM AND COMPOUND DEGRADATION STUDIES FOR ANY MOLECULE SIZE AND HRMS DATA SOURCE

Ismael Zamora¹, Luca Moretoni², Fabien Fontaine¹, Tatiana Radchenko¹, Albert Garriga¹, Xavier Pascual¹, Nadia Zara³, and Pol Gimenez¹

¹Lead Molecular Design, S.L., Spaine, ²Molecular Discovery /Molecular Horizon, Italy, and ³Molecular Discovery, Italy

Introduction: The study of compound degradation in the context of Drug metabolism or/and Chemical degradation studies have an important role in drug discovery with an impact in the development of a new chemical entities. These studies have 2 components one related to the quantification and the calculation of compound clearance or degradation constants and another one related to the elucidation of the products (degradants or metabolites) formed during the experiment. We are presenting in here a solution developed over the last 15 years that consider both aspects for molecules of any size and for almost any instrument vendor and acquisition mode data source.

A collection of algorithms were developed to perform the two major tasks that are needed in theses studies: peak detection and structure assignment. The peak detection algorithms consider the specific needs for each compound class, i.e. it can use the Monoisotopic mass for molecules smaller than 4000 amu, the most abundant isotope for molecules until 20.000 amu or the average mass for bigger ones. The structure assignment algorithm has been developed to be able to work with a set of atoms and bonds like the ones described in small molecule or monomers like in oligonucleotides, peptides or proteins or a combination of both molecule representation.

Using the developed approaches, we analyzed a collection of experimental data for a set of small molecules, protacs peptides, oligonucleotides or proteins where the data was collected on a Waters Synapt/ Xevo/Vion/ Bioaccord, Thermo Q-Exactive, Agilent QToF, Sciex TripleToF/Zeno, Bruker TimmToF instrument. The degradation studies presented where done on in-vitro metabolite systems like human liver microsome, human hepatocyte, protease incubation or forced degradation analysis.

Results will be presented for each of the compound classes: a) small molecular metabolism in Human liver microsomal for nefazodone measured in 4 different instrument/acquisition modes (Waters Synapt MSe, Sciex Tripe ToF SWATH, Bruker QToF and Aglient All Ions); b) force degradation studies for lanzoprazol measures in Agilent QToF and Thermo Q-Exactive; c) Protac Hepatocyte degradation study on a Thermo DDS d) Somatostatine metabolism study using a Waters acquisition, e) Semiclutide degradation from a Waters Vion; f) Oligonucleotide (sense and antisense chain analysis) from a Thermo DDS analysis

In all cases the computation of the clearance and/or degradation contact will be presented together with a collection of

the metabolites found. The analysis of the fragmentation data will be shown for one case of the Nefazone and the oligonucleotide studies.

P125 - AUTOMATIC QUANTIFICATION WORKFLOW USING HIGH RESOLUTION MASS SPECTROMETRY

Ismael Zamora¹, Fabien Fontaine¹, Pol Giménez¹, Christopher Kochansky², and Kevin Bateman²

¹Lead Molecular Design, S.L., Spain and ²Merck, United States

Calibration lines in drug quantification workflows are traditionally determined using QQQ instruments that have high sensitivity and where the ion selectivity is gained by using multiple reaction monitoring. This workflow needs a previously identified transition to be monitored to obtain the needed selectivity for the compound of interest. In this work we demonstrate an automated methodology to perform quantification studies based on high-resolution mass spectra data. We obtain selectivity based on the high resolution, low ppm difference between the observed and the theoretical m/z computed from the compound formula. We gain the needed sensitivity by automatically considering multiple m/z ions, including adducts and fragments, in the computation of the peak areas.

The methodology has been developed using MSe data acquired on a Waters Xevo G2XS Qtof mass spectrometer. A peak analysis is done in the high and low collision energy traces. The m/z of each of the identified peaks in both MS functions are then compared to the m/z obtained for the parent molecular formula, the multiple charges, the adducts and/or the theoretically generated fragments. The list of experimental peaks that matches any of the computed m/z is then submitted to the quality peak analysis (criteria: number of points per peak, ppm, signal/noise ratio, etc.). The area for each of the m/z is computed (isolated or in combination) using an auto-adjusting extraction window and later used in a regression analysis that has multiple acceptance criteria.

The data for the working example is obtained for a compound at 10 different concentration levels: 1, 2, 5, 10, 20, 50, 100, 200, 500, 1000, 2000, 5000, 10000 ng/mL measured in triplicate. The peak quality criteria were based on a minimum of eight scan points per peak, a difference in Retention Time between samples lower than 0.05 min, the ions with a difference between the observed and the computed m/z lower than 15 ppm. The extraction window was auto-adjustable, the noise evaluation time range (peak units) was set to 6, and the Minimum signal/noise ratio to 3. The maximum variation of nominal concentration of each sample and the average, as well as the maximum CV was set to 25% for a point to be accepted for regression. For a line to be accepted a minimum number of concentration levels was set to 6 with a minimum replication of 2 and a maximum fold change between consecutive points was 10. Three lines can be derived to cover the wider dynamic range, the LLoQ and the ULOQ using different weighting factors. In the example that will be shown the best fragments for quantification are obtained even in the absence of the M+H ion due to in-source fragmentation. The regression line obtained covered the dynamic range from 2 to 10000 with all the quality controls fulfilled with a combination of two m/z. It is also observed that due to the different ion intensity and noise evaluation for each ion it was necessary to perform an automatic optimization of parameters for the best peak quality.

P126 - COMPARISON OF CID AND EAD FRAGMENTATION WITH AUTOMATED ASSIGNMENT FOR SMALL MOLECULE STRUCTURE ELUCIDATION

Ismael Zamora¹, Fabien Fontaine¹, Christopher Kochansky², Kevin Bateman², Jason Causon³, and Jose Castro-Perez³

¹Lead Molecular Design, S.L., Spain, ²Merck, United States, and ³Sciex, United States

Collisional-induced dissociation (CID) has been the main workhorse for small molecule structure elucidation in drug metabolite identification studies. Software tools, such as MassMetasite, have been developed to assist in the automatic interpretation of CID MS/MS spectra. The challenge with CID is that for many drug metabolites, non-informative fragmentation occurs, resulting in a lack of useful structural assignments for these metabolites. Commercialization of electron activated dissociation (EAD) on a quadrupole time of flight mass spectrometer provides a potentially powerful new tool for small molecule structure elucidation in drug discovery. Automated interpretation of EAD MS/MS spectra using existing algorithms needs to be tested, modified, and implemented. A comparison of CID and EAD fragmentation using automated interpretation will be presented in this work.

Small molecule drugs were incubated in rat hepatocytes at 1 μ M. Time points: 0, 30 and 120 min were pulled from the incubation and quenched with 1 volume of CH₃CN. Samples were vortexed, centrifuged, and the supernatant transferred to an HPLC vial for analysis.

LC separation was performed on a Phenomenex Luna Omega Polar C18, 150 mm column using 0.5 μ L or 5 μ L injection volumes. Gradient separation 0.1% formic acid in water and acetonitrile was performed over 4.75 minutes from 5%B to 95%B with a total of 6.5 minutes.

The samples were analysed using ZenoTOF 7600 CID-IDA(DDA) and EIEIO IDA(DDA). TOFMS was scanned between m/z 100-1000, CID/EAD MS/MS from 60-1000. Data was processed in MassMetaSite with CID and EAD fragmentation. EAD is a free electron fragmentation mode recently introduced to accurate mass LC-MS/MS. It utilizes high energy electrons which allows for the dissociation of singly charged precursors, in this work an electron kinetic energy of 10 eV was utilized. The MS/MS spectra show significant increases in the number of fragment ions observed when going from Zeno CID to Zeno EAD spectra. The larger number of fragment ions makes it even more important for automated

assignment using software tools such as MassMetasite. Many of the new fragments are the result of radical bond cleavage driven by electron-impact excitation of ions from organics (EIEIO) mechanism. Typical software algorithms for MS/MS focus on even electron species, typical of CID fragmentation. With EAD and the production of odd electron fragments, modification of the algorithm is required. The results to date show much richer fragmentation spectra using EAD versus CID and that the modified algorithm can assign the new odd electron fragments.

Following analysis of metabolic studies with 5 compounds - diclofenac (shown here), verapamil, nefazodone, buspirone and a Merck compound (shown here):

EAD fragmentation is complementary to CID fragmentation

For metabolism studies EAD can enable a much more informative spectra which can help in structure elucidation

EAD offers unique fragmentation for molecules in which CID does not offer key diagnostic fragments

P127 - *IN VITRO* METABOLITE PROFILING COMPARISON OF RADIOACTIVE 14C-LABELED MYCLOBUTANIL, TRICYCLAZOLE, OXYFLUORFEN, PRONAMIDE, BIPHENYL, AND BUTOXYETHYLBENZOATE IN RAT LIVER MICROSOMES AND RAT LIVER METMAXTM HEPATOCYTES

Fagen Zhang, Lynn McClymont, Debbie McNett, Matthew LeBaron, and Sue Marty

The Dow Chemical Company, United States

Evaluation of *in vitro* metabolism is a quick and efficient way to examine the generation of metabolites that may be formed *in vivo*. Currently, the most common *in vitro* systems are liver microsomes and liver hepatocytes. Among these two major systems, liver hepatocytes are more advantageous than liver microsomes as hepatocytes more closely resemble the *in vivo* system vs. liver microsomes. Traditionally, cryopreserved hepatocytes required laborious handling procedures, which increased study costs significantly. Recently, a novel hepatocyte system (MetMaxTM) was developed that allows simplified, microsome-like handling and experimental protocols, and has been used for *in vitro* metabolite determination for many pharmaceuticals. In the current study, metabolism of radioactive 14C-labeled non-pharmaceutical chemicals (myclobutanil, tricyclazole, oxyfluorfen, pronamide, biphenyl, and butoxyethylbenzoate) was evaluated in both a rat liver microsomal system and a rat liver hepatocyte MetMaxTM system. The resulting metabolite HPLC/RAM profiles were similar between the two test systems for myclobutanil, tricyclazole, oxyfluorfen, and pronamide. In contrast, these two metabolic systems resulted in substantially different metabolite profiles for biphenyl and butoxyethylbenzoate where more *in vivo*-relevant metabolite profiling were formed with the MetMaxTM system. The current study results showed that metabolite profiling generated by MetMaxTM depended on the chemical structure(s) of the parent compounds, but for some chemicals, MetMaxTM may provide a more similar to *in vivo* metabolism system compared to hepatic microsomes.

P128 - COMBINING PRODUCT ION FILTERING, 2-PYRIDINE CARBOXALDEHYDE-TAGGING, AND BACKGROUND SUBTRACTION FOR STUDYING MACROCYCLIC PEPTIDE METABOLISM AND SOFTSPOTS

Haiying Zhang, Zhigang Lyu, Silvi Chacko, Kathy Mosure, Matt Soars, Michael Poss, and Joe Cannon

Bristol-Myers Squibb, United States

Macrocylic peptides are emerging as a new class of therapeutically promising compounds that can modulate protein functions. However, metabolic characterization of macrocylic peptides has been challenging because of the structural similarity of the metabolites to endogenous components and the complexity of the cyclic nature of the peptides. 2-pyridine carboxaldehyde (2-PCA) is a selective reagent for derivatization at the alpha amine of peptides [1], and we have demonstrated that for macrocylic peptides this derivatization offers a unique mass tag diagnostic to highlight the first amino acid of newly linearized peptide metabolites [2]. Here we present methodology for metabolite profiling of macrocylic peptides in complex biological matrices leveraging the 2-PCA derivatization and a combination of two data-processing techniques: background subtraction and product ion filtering. After 2-PCA derivatization of metabolite samples, high resolution LC/MS data was obtained for each sample with both molecular ion scans and all-ion fragmentation (AIF) scans. After applying a background subtraction technique [3] to remove irrelevant sample matrix ions including those from 2-PCA derivatized sample matrices, extracted ion chromatograms were generated on the background-subtracted AIF dataset, based on a unique tag mass of the 2-PCA moiety which was a universal fragment ion in AIF data for all newly linearized metabolites of macrocylic peptides (a.k.a., the product ion filtering.) The end result of these processes was that the metabolite peaks in the samples were revealed with high selectivity, along with the molecular ion and fragmentation information of each metabolite peak that was obtained in the same round of LC/MS analysis, allowing for facile identification of the metabolite peaks in the samples and the determination of the relevant metabolic soft spots of the macrocylic peptides. This method was demonstrated in the profiling of the metabolism of two commercially available cyclic peptides, JB1 and Somatostatin, in rat small intestine luminal contents. The method was also successfully applied for the first time for rapid and unambiguous detection of circulating metabolites of macrocylic peptides *in vivo*, providing helpful information in guiding chemistry optimization efforts and generating crucial *in vitro-in vivo* correlations for commonly used preclinical species.

References:

1. J.I. MacDonald, H.F. Munch, T. Moore, M.B. Francis. One-step site-specific modification of native proteins with 2-pyridinecarboxyaldehydes. *Nat. Chem. Biol.* 2015, 11, 326.
2. H. Zhang, S. Chacko, J. R. Cannon. 2-Pyridine Carboxaldehyde for Semi-Automated Soft Spot Identification in Cyclic Peptides. *Int. J. Mol. Sci.* 2022, 23, 4269.
3. H. Zhang, M. Grubb, W. Wu, J. Josephs, W.G. Humphreys. Algorithm for Thorough Background Subtraction of High-Resolution LC/MS Data: Application to Obtain Clean Product Ion Spectra from Nonselective Collision-Induced Dissociation Experiments. *Anal. Chem.* 2009, 81, 2695.

P129 - NOVEL N+-METHYLATION OF TASELISIB (GDC-0032): STRUCTURAL CHARACTERIZATION AND REACTION PHENOTYPING

Weiping Zhao, Cyrus Khojasteh¹, Laurent Salphati¹, Sungjoon Cho¹, Zhang², Shuguang Ma¹, and Bin Wang³

¹Genentech, United States, ²Global Blood Therapeutics, United States, and ³The Coca-Cola Company, United States

Taselisib (also known as GDC-0032) is a potent and isoform-selective PI3K Inhibitor that “Spares” PI3K α . During the drug development of taselisib, the mass balance studies were conducted following single oral doses of ¹⁴C-taselisib in rats, dogs and humans. While oxidation and amide hydrolysis were major metabolism pathways in three species, methylation was also the major metabolism pathway in dogs. To determine the structure of methylation metabolite (M17) in dogs, the deuterium label exchange experiment and M17 was isolated from dog bile and feces followed by NMR analysis had been conducted. The structure of M17 had been identified to be N-methylation on triazole moiety.

In vitro experiment showed that only dog hepatocytes generated M17 while human, mouse, rat and monkey hepatocytes didn't. Both dog liver cytosol and microsomes could mediate M17 generation from taselisib suggesting that multiple methyltransferases (MT) were involved in that reaction. In order to determine which MT were involved in the formation of M17, several methyltransferase inhibitors were tested with dog hepatocytes incubated with taselisib. 2,3 dichloro-methyl benzylamine (DCMB) significantly inhibited methylation of taselisib (98%). DCMB is a thiol methyltransferase (TMT) inhibitor. Therefore, TMT might play a role in the methylation of taselisib in dogs. Since DCMB may not inhibit only TMT, this study cannot rule out that other methyltransferases might also be involved in the methylation of taselisib. The role of another N-methyltransferase, NNMT, on the N-methylation of taselisib was investigated using the recombinant dog NNMT enzyme. The data suggested that dog NNMT played a minor role, which was consistent with the minimal effect of the NNMT inhibitor 1-methyl nicotinamide, on taselisib methylation.

In summary, the structure of dog-specific methylation metabolite (M17) and enzymes potentially mediating methylation were characterized.

P130 - ABSTRACT WITHDRAWN**P131 - BLOCKING ALDEHYDE OXIDASE METABOLISM TO MITIGATE TOX FINDINGS**

Justin Ly¹, Satoko Kiyota², Hank La¹, Liling Liu¹, Jack Terret³, and Steve Magnusen³

¹Drug Metabolism and Pharmacokinetics, Genentech, Inc., United States, ²Safety Assessment, Genentech, Inc., United States ³Discovery Chemistry, Genentech, Inc., United States

Purpose: Aldehyde oxidase (AO) is a metabolizing enzyme, located in the cytosolic compartment of tissues in many organisms, and it plays an important role in the metabolism of many drugs and xenobiotics. It catalyzes oxidations of azaheterocycles, oxidations of aldehyde, hydrolysis of amides, and various reductions, effecting mainly nitro, N-oxide, and isoxazole moieties. AO-mediated metabolism presents a unique challenge to drug discovery due to (1) limited understanding of AO enzyme compared to other drug metabolizing enzymes, such as CYPs and UDP-glucuronosyltransferases (UGTs), and (2) the widespread use of structural motifs that are AO substrates. Due to insufficient understanding of AO expression and its activity in various tissues, it is a challenge to accurately predict human pharmacokinetics of drug candidates that are mainly metabolized by AO enzyme. In addition, oxidative metabolites generated from AO metabolism might pose a risk of safety related issues. The purpose of this work was to identify, assess, and modify compound X to mitigate its tox liabilities.

Methods/Results: Compound X, which contained a hypoxanthine substructure, was considered structural alert for being substrate of AO. Thus following incubation in hepatocytes of various species, compound X's main route of elimination was determined to be mediated by AO in rodent, cyno, and human hepatocytes by generating M7 and M8 as major metabolites; but not in dog hepatocytes, as dogs do not express AO enzyme. Furthermore, incubation of compound X in S9 along with and without AO inhibitor, Hydralazine, resulted in a reduction of 96% and 97% of M7 formation in cyno and human S9, respectively; and a reduction of 97%, 95%, and 100% of M8 formation in rat, cyno, and human S9, respectively. Following multiple doses of Compounds X in rat and cyno toxicology studies, oxidative metabolites (M7 and M8) were detected in abundance in circulation and these metabolites were found to effect the coagulation parameters by

prolonging the prothrombin time (PT) and activated partial thromboplastin time (aPTT). Blocking the site of metabolism of compound X with a methyl group resulted in Compound Y that generated less M7 and M8 which caused less effect on PT and aPTT in rats and cynos. *In vitro* incubation of Compound Y in rat, cyno, an human S9 also resulted in low levels of M7 and M8.

Conclusion: These data suggested that M7 and M8 were the metabolites generated mainly through AO enzyme, and reducing their formations mitigated tox findings. Until a better understanding of AO biology (expression and activity) in various tissues of humans and preclinical species, it is a common practice in drug discovery to identify, assess, and modify structural features of drug candidate that have AO-mediated metabolism, so that elimination pathways can be diversified to include other drug metabolizing enzymes.

P132 - IN VITRO-IN VIVO METABOLITE PROFILING AND IDENTIFICATION OF OLIGONUCLEOTIDE

Gengyao Qin, Qiandan Miao, Liqi Shi, Weiqun Cao, Yi Tao, and Liang Shen
WuXi AppTec Co. Ltd., China

Oligonucleotides are synthetic single or double strands of modified RNA (ribonucleic acid) or DNA (deoxyribonucleic acid), less than 100 nt (nucleotides), which can be used to modulate gene expression by binding to RNA or DNA through Watson–Crick base pairing. They can, in theory, target any gene of interest since only the right nucleotide sequence along the targeted DNA or RNA needs to be selected, so, oligonucleotides should be much more specific than small molecule drugs.[1]

“Appropriate bioanalytical methods should be used to characterize the parent oligonucleotide and any relevant metabolites, including chain-shortened metabolites.” had been listed in the considerations in FDA guidance (June 2022). As for all marketed oligonucleotide drugs, the materials for *in vitro* and *in vivo* metabolic studies were submitted for IND filings to clarify the metabolic behaviors and clearance pathways.

Based on the HRMS technology and related software, a strategy has been set up for oligonucleotides in *in vitro* (plasma, liver microsomes, liver S9 fractions and liver homogenate) and *in vivo* (plasma, urine, feces and tissues) metabolism studies to characterize the relevant metabolites and indicate the *in vitro-in vivo* metabolic correlation. The metabolism of Oligo A was evaluated *in vitro* in mouse, rat, dog, monkey and human liver S9 fractions, and *in vivo* in monkey liver samples. Metabolic profiling in human liver S9 fractions did not identify any metabolites unique to human *in vitro*. The major metabolites 3' n-1 of AS, 3GalNAc loss of SS and 3GalNAc_linker loss of SS in monkey liver were also identified in *in vitro* monkey and human liver S9 fractions.

The strategy presented here can be used for the metabolism of oligonucleotides for IND filing. Additionally, metabolic profiling in *in vitro* and *in vivo* models can help to develop the analytical methods for clinical trial, and to monitor the major components of parent related oligonucleotides in human.

Reference:

1. Lara Moumné, et al. Oligonucleotide therapeutics: from discovery and development to patentability. *Pharmaceutics*, 2022, 14, 260.

P133 - ABSTRACT WITHDRAWN

P134 - FREQUENCY OF THE I/D VARIANT IN THE ACE1 GENE AMONG THE CIRCASSIAN SUBPOPULATION IN JORDAN

Laith AL-Eitan¹, Nama'a Abu-Seini¹, Saif Alahmad, **Nancy Hakooz**², and Rana Dajani³

¹Jordan University of Science and Technology, Jordan, ²School of Pharmacy-University of Jordan, Jordan, and ³The Hashemite University, Jordan

Angiotensin-Converting Enzyme, ACE, plays an important role in pathways that contribute to the regulation of blood pressure and fluid homeostasis. It is the target of a major class of antihypertensive drugs, ACE inhibitors; such as captopril and enalapril. The allele and genotype frequencies of an insertion/deletion (I/D) (rs4646994) polymorphism have been implicated in many conditions such as coronary heart diseases (Vladeanu et al., 2020), COVID-19 mortality and morbidity rates (Mir et al., 2021) and with the increased risk of multiple myeloma (Zmorzynski et al., 2019). The allele and genotype frequencies of an insertion/deletion (I/D) (rs4646994) polymorphism found in ACE widely differ among populations.

The present study aims to determine allele and genotype frequencies of the ACE I/D polymorphism among the Circassian subpopulation in Jordan. The difference in the genotype frequency between the Circassians and a number of populations in the world was investigated. Moreover, we have examined if there is any difference in the allele and genotype frequencies of the ACE I/D polymorphism based on sex. A total of 123 unrelated healthy Circassian individuals' blood samples were collected. DNA was extracted and genotyped. We found that the D allele frequency (66%) is double the I

allele frequency (34%) in Circassians. We also found that the genotype frequency of the ACE I/D polymorphism is significantly different in comparison to most populations. Furthermore, no significant differences were reported in the allele and genotype frequencies between Circassians males and females. In conclusion, we have demonstrated that the Circassian subpopulation might be at risk for acute coronary disease, infection and death from COVID-19 and higher risk of multiple myeloma because they carry the D allele.

References:

1. Mir, M. M. et al. (2021) 'Strong association of angiotensin converting enzyme-2 gene insertion/deletion polymorphism with susceptibility to sars-cov-2, hypertension, coronary artery disease and covid-19 disease mortality', *Journal of Personalized Medicine*. doi: 10.3390/jpm11111098.
2. Vladeanu, M.-C. et al. (2020) 'Angiotensin-converting enzyme gene D-allele and the severity of coronary artery disease', *Experimental and Therapeutic Medicine*. doi: 10.3892/etm.2020.8978.
3. Zmorzynski, S. et al. (2019) 'ACEinsertion/deletion polymorphism (rs4646994) is associated with the increased risk of multiple myeloma', *Frontiers in Oncology*. doi: 10.3389/fonc.2019.00044.

P135 - METABOLIC EFFECTS OF PERFLUOROOCCTANE SULFATE IN MULTIPLE ORGANS OF RATS USING NUCLEAR MAGNETIC RESONANCE-BASED METABOLOMICS

Ching-yu Lin

National Taiwan University, Taiwan

Perfluoroalkyl substances are a group of chemicals widely used in industry and commercial products, such as stain resistant cookware and breathable waterproof textiles. The chemicals are commonly detected in human biofluids. Among those perfluoroalkyl substances, perfluorooctane sulfate (PFOS) is the most frequently detected one. However, the potential adverse effects and possible mechanisms of PFOS are still unclear. We hypothesize that PFOS cause molecular perturbations and disrupt intracellular homeostasis, which may lead to adverse effects. Those molecular changes are organ-specific. Metabolomics is a high throughput and sensitive approach to investigate changes of small molecules in a biological system, which can be correlated with environmental stress such as toxicant exposure. In this study, we intend to understand the potential toxic effects of PFOS and suggest possible toxic mechanisms through metabolomics approach. In order to understand the organ-specific biochemical responses caused by PFOS, an animal experiment was conducted followed by nuclear magnetic resonance (NMR)-based metabolomic analysis. After male Sprague-Dawley rats were treated with a series dose of PFOS by oral for 21 days, their organs, including liver, lungs, heart, kidneys, pancreas, and testis, were collected. Metabolites from tissues were extracted and analyzed by high-resolution NMR. Then, the spectra were processed and analyzed by multivariate analysis, specifically, partial least squares discriminant analysis (PLS-DA). Metabolic changes were identified in each organ. The PLS-DA score plots revealed that the metabolite perturbations in the lungs, liver, heart, kidneys, and testes were notably correlated with PFOS exposure. Numerous metabolites from those organs were significant changed after Kruskal-Wallis tests. The changes of those metabolites are related with alteration of glycogen synthesis, glycogenolysis, and ketogenesis in the liver. Moreover, disturbances in amino acid metabolism were discovered in the kidneys, lungs, liver, and testes. We conclude that metabolomics is a feasible tool to identify target organs and suggest potential health effects of PFOS.

P136 - CYP4F2*3 (V433M) POLYMORPHISM IMPACTS BENZALKONIUM CHLORIDE METABOLISM IN AN ALKYL CHAIN LENGTH-DEPENDENT MANNER

Linxi Zhu

University of Washington, United States

Benzalkonium chlorides (BACs) are a class of quaternary ammonium compounds. They are among the most common active ingredients in disinfectants used in domestic cleaning, industrial processing, and clinical settings. BACs are primarily metabolized by cytochrome P450 (CYP) enzymes through ω -hydroxylation by CYPs 4F2 and 4F11 and (ω -1)-hydroxylation (or further internal oxidation) by CYPs 2D6 and 4F12. These primary metabolites are further metabolized to ω -carboxylic acid and (ω -1)-ketone products. We hypothesize that CYP polymorphism is a major determinant of inter-individual variability in BAC persistence in humans. CYP4F2 was previously found to be an ω -hydroxylase of C16 BAC, but not of C12 BAC. In this work, we investigated the impact of CYP4F2 polymorphism (*1/*1, *3/*3, and *1/*3) on C12 and C16 BAC metabolism in 4F2-genotyped and pooled (from 10 individuals for each genotype) human liver microsomes (HLM). Wild-type (WT) (4F2*1/*1) HLM exhibited a 2.08-fold higher metabolic rate for C16 BAC than 4F2*3/*3; However, for C12 BAC, this ratio was only 1.09. The heterozygote (4F2*1/*3) HLM metabolic rates of both C12 and C16 BACs were close to WT, being 80% and 88% of the WT metabolic rates, respectively. The fraction metabolized (fm) of carboxylic acid for C16 BAC are 0.72 (*1/*1), 0.54 (*1/*3) and 0.22 (*3/*3), whereas for C12 BAC, this fm in all three variants are less than 0.05, suggesting CYP4F2 is a major contributor to the formation of ω -carboxylic acid from C16-BAC, but not C12-BAC.

The use of the specific CYP2D6 inhibitor quinidine in all three groups of 4F2-genotyped HLM confirmed the significant contribution of CYP2D6 to (ω -1)-hydroxylation of both C16- and C12-BACs. Inhibition of CYP2D6 had a greater effect on C12 BAC metabolism than C16 BAC, reducing their (ω -1)-hydroxy metabolites by 67% and 55%, respectively, in WT HLM. In conclusion, the impact of 4F2*3 polymorphism on BAC metabolism in HLM was far greater for C16 BAC than for C12 BAC. Inhibition of 2D6 by quinidine was not necessary to observe this effect, indicating that the 4F2*3 polymorphism alone can substantially reduce C16 BAC metabolism in HLM. This study suggests that individuals with the CYP4F2 poor metabolizer genotype could be more susceptible to BAC exposure.

P137 - A NOVEL THREE-DIMENSIONAL IMAGING AND ASSESSMENT OF THE NEW ZEALAND WHITE RABBIT EYE

Lydia Andrews-Jones¹, **Gianna Ferron**², Ronnie Nie¹, John Masterson¹, Jie Shen¹, Joshua Rowe¹, Stefan Linehan², and Tim Ragan²

¹AbbVie, Inc., United States and ²TissueVision Inc., United States

When attempting to evaluate and understand ocular pathologic processes, histologic methods allow the most detailed morphologic evaluation of ocular changes but are limited to two-dimensional (2D) imaging. These can be compared back to in-life morphologic evaluations from modalities such as OCT and funduscopy but special stains and detail is lacking. There is great benefit to be able to evaluate the full, intact structure of the eye with three-dimensional (3D) modeling. Histologic preparation of the eye requires technical expertise to maintain the structures, especially the retina, in anatomically correct alignments for pathology evaluation. Rabbits are one of the most commonly used species in ocular studies, yet rabbit eyes are notoriously one of the most technically difficult eyes to work with and achieve sufficient histologic preparations for. Here we report a novel 3D assessment of the New Zealand White rabbit eye using the TissueVision, Inc. (TVI) TissueCyte Serial Two-Photon Plus (STP2) imaging platform. Fixed rabbit eye samples were embedded in an agarose block and polymerized in an embedding matrix to provide stability for 100 micron-thick sectioning. Samples were imaged using two-photon excitation and targeted regions of interest were assessed. Gross tissue anatomy was visualized via autofluorescence, and collagen signatures of the cornea and sclera were visualized via second harmonic generation (SHG) imaging. High-resolution fully aligned datasets were produced for each eye. Targeted regions of muscle, retina, iris, ciliary body, and lens were visualized via autofluorescence. An assessment of collagen in the cornea and sclera revealed distinctive collagen fibril bundle organization. The ability to process intact New Zealand White rabbit eyes using the STP2 imaging platform demonstrates a novel method to produce a 3D model of total gross morphology and collagen signatures of the cornea and sclera. This finding elucidates great potential for the future evaluation of disorders of the eye. This proof-of-concept study used 100 micron-thick sections. Future studies will look at thinner sections, and collection of slices of interest for further histologic processing using traditional methods for detailed morphologic evaluation in targeted areas of the 3D structure. The combination of these methods will allow both the traditional evaluation of lesions in the eye and a 3D reconstruction of the eye as a whole with relative positioning, with future application in evaluating pharmacodynamics and pharmacokinetics of drug treatment.

P138 - NOVEL WHOLE-BRAIN SERIAL TWO-PHOTON PLUS AND MALDI-IHC IMAGING OF AMYLOID-BETA PLAQUE DYNAMICS IN PRE-CLINICAL ALZHEIMER'S DISEASE ANIMAL MODELS

Gianna Ferron¹, Stefan Linehan¹, Tim Ragan¹, Michael Sasner², Kevin Elk², and Dylan Garceau²

¹TissueVision Inc., United States and ²The Jackson Laboratory, United States

Alzheimer's Disease (AD) has a strong spatial-temporal component to its progression, where different brain regions are affected by amyloid-beta ($A\beta$) plaque deposition at varying time points. Standard imaging and analysis platforms can neglect these details, as they lack the ability to pair high-yield whole-brain imaging with region-specific quantitation. Furthermore, many $A\beta$ analyses require homogenization of tissue, prohibiting secondary analysis. To address this gap, we have developed a novel high-throughput whole-brain imaging pipeline for pre-clinical AD models to quantitatively track plaque progression as a function of brain region across time while producing indexed tissue sections for MALDI-IHC staining and imaging mass spectrometry (IMS) analysis. $A\beta$ plaques in the well characterized 5XFAD mouse model of AD were labeled with Methoxy-X04, an $A\beta$ plaque-specific compound, prior to trans-cardial perfusion and whole-brain excision. The brains were processed on the TissueCyte Serial Two-Photon Plus (STP2) imaging platform to produce fully aligned multi-channel volumetric datasets, yielding high resolution 3D models of each brain. Registration to the Allen Mouse Brain Common Coordinate Framework (CCFv3) and region-specific plaque analysis were conducted to determine plaque size, density, and total number per animal brain. Resulting sections were evaluated with MALDI-IHC for $A\beta$ 42, pTau, MAP2, GAD67, GLUT1, NeuN, synapsin, myelin and neurogranin tags. The analysis of whole-brain plaque distribution in the 5XFAD mouse model revealed distinct spatial-temporal changes across the brains. STP2 imaging, combined with CCFv3 mapping and MALDI-IHC analysis allowed for targeted evaluation of $A\beta$ plaques. Our novel technology has great promise for quantifying the spatial-temporal $A\beta$ plaque efficacy of AD animal models, and the production of translatable pre-clinical AD drug discovery data. The high sensitivity and precision of the STP2 platform

combined with the high multiplexity of MALDI-IHC and IMS imaging can benefit region-specific disease progression compared to standard laboratory approaches.

P139 - ANTIBACTERIAL EFFICACY OF THE MACROCYCLIC DEPSIPEPTIDE TEIXOBACTIN IN THE NEUTROPENIC MOUSE PK-PD MODEL OF THIGH INFECTION

Peng Hsiao¹, Zammany Kline¹, Daniel Carney¹, Jeremiah Joseph¹, Sara Kalina¹, Ying Zhang¹, Livia Ferrari², Paola Savoia², Antonio Felici², and Antoine Henninot¹

¹Ferring Research Institute Inc., United States and ²Aptuit (Verona) S.r.l., Italy

Teixobactin, a macrocyclic depsipeptide discovered in Gram-negative *Eleftheria terrae* represents a novel class of peptidoglycan synthesis inhibitors that is highly potent, with no observable resistance against a broad range of Gram-positive microbes including methicillin-sensitive *Staphylococcus aureus* (MSSA) and vancomycin-resistant *Enterococci* (VRE). Minimum inhibitory concentrations (MIC) of teixobactin against MSSA and VRE were determined to be 0.138 and 0.453 µg/mL, respectively. The pharmacodynamics (PD) of Teixobactin against MSSA and VRE were investigated using the neutropenic mouse thigh infection model. Mice with ca. 1.2E+06 CFU/thigh at the initiation of therapy were administered with 1, 5, or 20 mg/kg Teixobactin bolus intravenously. Teixobactin was effective at inhibiting both MSSA and VRE in a dose dependent manner. The maximal bacterial reduction counts in thigh tissues at 24 hr for MSSA and VRE were – 4.0 and – 2.8 log₁₀ CFU/thigh, respectively. Further refined fractionized dose study against MSSA was conducted at dose range from 1 to 30 mg/kg (in 1, 2 or 4 equally fractionated doses) over 24 hr. Of all the PK parameters evaluated (C_{max}/MIC, AUC/MIC, and fT > MIC), the percentage of a 24 hr dosing interval at which the free Teixobactin plasma concentration exceeded 4X the MIC was the best linked with efficacy (fT > 4XMIC; R₂ = 0.92).

P140 - EFFECT OF FOOD ON PHARMACOKINETICS AND PHARMACODYNAMICS OF HIP1601, A DUAL DELAYED-RELEASE FORMULATION OF ESOMEPRAZOLE, IN HEALTHY SUBJECTS

Sejung Hwang¹, Joo Young Na¹, Jae-Yong Chung², In-Jin Jang¹, and SeungHwan Lee¹

¹Seoul National University College of Medicine, South Korea and ²Seoul National University Bundang Hospital, South Korea

A novel dual delayed-release formulation of esomeprazole (HIP1601) was developed to prolong the effect of esomeprazole inhibiting gastric acid secretion. This study investigated the food effect on the pharmacokinetics (PK) and pharmacodynamics (PD) of HIP1601. A randomized, open-label, single-dose, 2-period, 2-sequence crossover study was conducted in healthy Korean subjects. Subjects were orally administered a single dose of HIP1601 40 mg with fasted and fed state respectively in each period. PK characteristics and PD characteristics evaluated through continuous 24-hour intragastric pH monitoring in fasted and fed state were compared between two conditions. A total of 23 subjects completed the study and included in PK analysis. PD analysis was conducted in 21 subjects except 2 subjects because of the inappropriate pH profiles. The systemic exposure of esomeprazole after a single dose of HIP1601 in the fed state decreased compared to that in the fasted state. However, the percent decrease from baseline in integrated gastric acidity and the percent of time pH over 4 were not significantly different between the two conditions. In conclusion, although the systemic exposure of esomeprazole decreased when HIP1601, a dual delayed-release esomeprazole, was administered in the fed state compared to that in the fasted state, the degree of gastric acid secretion inhibition was not clinically different regardless of food intake.

P141 - TOXICOKINETICS OF ORALLY MICRO-DOSED [14C]-BENZO[A]PYRENE FOLLOWING DIETARY INTERVENTION WITH BRUSSELS SPROUTS AND 3,3'-DIINDOLYLMETHANE (DIM) SUPPLEMENTS USING UPLC-ACCELERATOR MASS SPECTROMETRY (UPLC-AMS)

Monica Maier

Oregon State University, United States

Benzo[a]pyrene (BaP) is formed by incomplete combustion of organic materials (petroleum, coal, tobacco, etc.) and is ubiquitous in the environment. It is designated by the International Agency for Research on Cancer as a group 1 known human carcinogen; a classification supported by numerous studies in preclinical models and epidemiology studies of exposed populations. 3,3'-diindolylmethane (DIM), a naturally-occurring compound found in cruciferous vegetables like Brussels sprouts (BS), a popular dietary supplement, and is an effective dietary chemopreventive agent. Following dietary intervention with BS or DIM supplements this study follows uptake, metabolism, and elimination of [14C]-BaP at environmentally relevant concentrations in human plasma over a 48-h period using UPLC-accelerator mass spectrometry (UPLC-AMS). Volunteers were micro-dosed with 50 ng (5.4 nCi) [14C]-BaP following seven days on a cruciferous vegetable restricted diet, or the same diet supplemented daily with 50 g/day of BS or 300 mg (two 150 mg daily doses) of BioResponse-DIM®. Both BS and DIM reduced total [14C]-BaP and metabolites recovered from plasma by 56-67% relative to non-intervention. Supplementation markedly reduced T_{max} and C_{max} for [14C]-BaP, but not AUC_{0→∞},

indicative of slower but not reduced overall absorption. The earliest eluting [¹⁴C] peak, likely BaP conjugates, exhibited significantly reduced C_{max} and AUC_{0→∞}. BaP-9,10-dihydrodiol, also had a supplement-dependent reduction in C_{max}. Toxicokinetic constants for other metabolites followed the same pattern as BaP while metabolite profiles remained consistent with non-intervention. Non-compartmental analysis did not indicate alterations in clearance suggesting neither DIM nor BS supplements acted through induction or inhibition of BaP metabolism, mechanisms thought to be important in preclinical models. Although the number of subjects and large interindividual variation seen are limitations of this study, it represents the first human trial showing dietary intervention altering toxicokinetics of a defined dose of a known human carcinogen.

P142 - PROTEOMIC QUANTIFICATION OF RECEPTOR TYROSINE KINASES INVOLVED IN CANCER DEVELOPMENT AND PROGRESSION IN PATIENTS WITH COLORECTAL CANCER LIVER METASTASIS

Areti-Maria Vasilogianni¹, Zubida M. Al-Majdoub¹, Brahim Achour¹, Sheila Annie Peters², Amin Rostami-Hodjegan¹, and Jill Barber¹

¹The University of Manchester, United Kingdom and ²Merck KGaA, Germany

Colorectal cancer is a leading cause of death, with half of the patients having liver metastasis. Receptor tyrosine kinases (RTKs) are important regulators of various cellular processes and pathways and changes in their expression can have a negative impact on cancer progression and response to therapeutic intervention. Many anti-cancer drugs act as receptor tyrosine kinase inhibitors (RTKIs) for the treatment of colorectal cancer liver metastasis (CRLM). Despite the high incidence of CRLM, quantitative data in liver tissue from CRLM patients are scarce. This study aimed to investigate, for first time, the protein expression of 21 RTKs in CRLM. LC-MS/MS targeted proteomics was used to quantify the target proteins in human liver microsomes from 15 human healthy livers from healthy donors and 18 cancerous (2 primary and 16 metastatic) liver samples matched with 18 normal liver tissues from cancer donors. The findings demonstrated, for the first time, lower expression of EGFR, INSR, VGFR2 and AXL, and higher expression of IGF1R, in tumours relative to normal livers. EPHA2 was upregulated in tumours compared with histologically normal livers and PGFRB increased in tumours relative to normal and healthy tissues. Expression of VGFR1/2, PGFRA, KIT, CSF1R, FLT3, FGFR1/3, ERBB2, NTRK2, TIE2, RET, and MET was comparable among healthy, normal and tumour samples. Significant, moderate correlations were observed ($R_s > 0.50$, $p < 0.05$) for EGFR with INSR and KIT, while FGFR2 correlated with PGFRA and VGFR1 with NTRK2 in healthy livers. In histologically normal tissue, there were correlations between TIE2 and FGFR1, EPHA2 and VGFR3, FGFR3 and PGFRA ($p < 0.05$). EGFR correlated with INSR, ERBB2, KIT and EGFR, and KIT with AXL and FGFR2. In tumours, CSF1R correlated with AXL, EPHA2 with PGFRA, and NTRK2 with PGFRB and AXL. Sex, liver lobe and body mass index of donors did not correlate with the abundance of RTKs, whereas their age correlated. RTKs relative abundance distribution was also assessed. RET was the most abundant in normal and healthy livers (~35%), while PDGFB was highest in tumours (~47%). 22 drug-metabolizing enzymes (DMEs) and 25 transporters were previously measured in the same sets of samples with LC-MS/MS targeted proteomics. Among those proteins, cytochrome P450 (CYP) enzymes, uridine 5'-diphospho-glucuronosyltransferases (UGTs), ATP-binding cassette (ABC) and solute carrier (SLC) transporters were quantified. These are important for the metabolism and disposition of RTKIs. The current study revealed several correlations between the abundance of RTKs (pharmacodynamic markers) and proteins relevant to drug pharmacokinetics (enzymes and transporters). The implementation of these correlations should allow more realistic virtual populations to be generated, allowing better prediction of exposure and response to drugs. Overall, this study demonstrated perturbed expression of several RTKs in cancer and these patterns are of high value as biomarkers for liver cancer metastases.

P143 - DEVELOPMENT OF AN *IN VIVO* MODEL TO STUDY ACQUISITION OF ANTIBIOTIC RESISTANCE USING A CLINICALLY RELEVANT DOSING STRATEGY AND "HUMANIZED" ANTIMICROBIAL EXPOSURES

Noelle Williams, Xiaoyu Wang, Erika Serrano Diaz, Laura Coughlin, Marguerite Monogue, Andrew Koh, and Erdal Toprak

UT Southwestern Medical Center, United States

Antibiotic misuse has led to the development of bacterial resistance, causing nearly 35,000 deaths annually in the United States. Sub-inhibitory antibacterial concentrations may cause selective pressure for resistance development. While antimicrobial plasma exposures in humans have been well defined, there are limited data describing these concentrations throughout the gastrointestinal tract, a potential breeding ground for antimicrobial resistance due to its innate microbiota and potential genetic exchange. To understand the mechanisms driving the development of resistance, we developed an *in vivo* murine model that allows for the complex interplay of host and bacteria in a setting where antibiotic exposures mimic those in humans. Clearance of most antibiotics are quite rapid in mice and in order to simulate human exposures, previous studies have utilized uranyl nitrate to impair renal clearance coupled with dosing every few hours. We utilized a refillable and programmable iPRECIO® pump to deliver the antibiotic cefepime at a concentration equivalent to human trough levels coupled with a subcutaneous dose to better mimic human pharmacokinetics. Compound levels in both plasma and the GI system were evaluated by LC-MS/MS in order to understand the concentrations bacteria will

encounter. Mice implanted with subcutaneous iPRECIO® pumps containing 20 mg/ml cefepime, which released drug at a rate of 4 µL/hr, showed steady state plasma concentrations of cefepime of 3.4 µg/mL similar to trough concentrations achieved in patients receiving 2 g of cefepime every 8 hours (1). A bolus subcutaneous injection of 50 mg/kg in the mouse resulted in a peak plasma concentration of 55 µg/ml and an AUC of 42 hr*µg/mL. Peak plasma concentrations in humans receiving a single 2 g dose as a 30 min infusion are 126 µg/mL with an AUC of 245 hr*µg/mL. The combination of a 100 mg/kg subcutaneous dose with continuous exposure from the iPRECIO® pumps would, therefore, be expected to match the human C_{max} and trough. As %time>MIC for the infecting organism determines cefepime efficacy, this dosing approach should allow one to modulate exposures and evaluate development of bacterial resistance when concentrations are above and below this threshold. Surprisingly, cefepime concentrations in colon fecal material were much higher than those observed in the plasma after the subcutaneous dose. To our knowledge, there is no information on the concentration of cefepime in human feces, but it may be lower since cefepime shows renal clearance. To properly model exposures of the microbiome to antibiotics like cefepime, then, it may be necessary to also measure human fecal concentrations and adjust dosing in the mouse model. Our data demonstrate that programmable, re-fillable pumps can simulate human antibiotic plasma trough concentrations in mice but gut concentrations may determine effects on the microbiome.

Reference:

1. Barbhuiya, RH, ST Fogue, CR Gleason, CA Knupp, KA Pittman, DJ Weidler, H Movahhed, J Tenney, RR Martin (1992). Pharmacokinetics of cefepime after single and multiple intravenous administrations in healthy subjects. *Antimicrobial Agents and Chemotherapy* 36:552-557.

P144 - DETERMINING EFFECT OF ISOTRETINOIN ON CYP2D6 AND CYP3A4 ACTIVITY IN PATIENTS WITH SEVERE ACNE

Yugian Zhao, Jay C. Vary Jr., Aprajita S. Yadav, Lindsay C. Czuba, Sara Shum, Jeffrey LaFrance, Nina Isoherranen, and Mary F. Hebert

University of Washington, United States

All-trans-retinoic acid (atRA), the active metabolite of retinol (vitamin A), and its isomer 13cisRA increase the expression of small heterodimer partner (SHP), which leads to increased binding of SHP to hepatocyte nuclear factor 4α (HNF4α) blocking the CYP2D6 gene promoter leading to decreased CYP2D6 expression in human hepatocytes (reference 2) and in CYP2D6 transgenic mice (reference 1). In addition, retinoids have been shown to induce CYP3A4 and activate Pregnane X Receptor (PXR) *in vitro* (reference 2). Based on *in vitro* to *in vivo* predictions, we hypothesized that administration of isotretinoin (13cisRA) would decrease the activity of CYP2D6 and increase CYP3A4 activity. The aim of this study was to test this hypothesis and determine whether isotretinoin administration decreases CYP2D6 activity and increases CYP3A4 activity in patients with severe acne treated with isotretinoin. A total of 33 patients (22 females and 11 males) with severe acne who were anticipated to receive isotretinoin for therapeutic reasons, but overall in good health were recruited. The mean age of the participants was 23.2±5.7 years. All participants were genotyped for CYP2D6 and their CYP2D6 activity scores (AS) were: 0 (n=2), 0.5 (n=1), 1 (n=5), 1.5 (n=5), 2 (n=17), 2-2.5 (n=1), and 3 (n=2). All participants took dextromethorphan (DM) 30 mg orally on study day 1 (pre-isotretinoin) and study day 2 (concomitant isotretinoin 0.5-1 mg/kg/day orally for > 1 week) as a safe, dual-probe substrate for CYP2D6 and CYP3A4. Plasma concentrations of atRA, 13cisRA, and 4oxo13cisRA were measured on both study days. Plasma (2 hrs after dosing) and 0-4 hour urine collection concentrations of DM and its metabolites were measured using validated LC-MS/MS methods. The retinoid concentrations in plasma increased 100-1000-fold with isotretinoin administration compared to endogenous concentrations. The CYP2D6 activity marker, urine dextromethorphan (DX)/DM metabolic ratio (MR), trended towards being lower with isotretinoin (17.1±11.7) compared to pre-treatment control (31.9±50.1, p=0.08) for CYP2D6 extensive metabolizers (AS: 1, 1.5, and 2 (n=27)) using paired Wilcoxon signed-rank test. When all participants were combined, no significant differences in the CYP3A4 marker 3-methoxymorphinan (3MM)/DM MRs in plasma (0.09±0.06 vs 0.08±0.04) or urine (0.14±0.15 vs 0.10±0.07) were observed between isotretinoin treatment and control study days, respectively. Large inter-individual variabilities in plasma and urine DX/DM MRs were observed among participants with the same and differing activity scores. A positive correlation was observed between plasma and urine DX/DM MRs.

References:

1. Koh KH, Pan X, Shen HW, Arnold SL, Yu AM, Gonzalez FJ, Isoherranen N, Jeong H. Altered expression of small heterodimer partner governs cytochrome P450 (CYP) 2D6 induction during pregnancy in CYP2D6-humanized mice. *J Biol Chem*. 2014 Feb 7;289(6):3105-13. doi: 10.1074/jbc.M113.526798. Epub 2013 Dec 6. PMID: 24318876; PMCID: PMC3916516.

2. Stevison F, Kosaka M, Kenny JR, Wong S, Hogarth C, Amory JK, and Isoherranen N (2019) Does In Vitro Cytochrome P450 Downregulation Translate to In Vivo Drug-Drug Interactions? Preclinical and Clinical Studies With 13-cis-Retinoic Acid. *Clinical and Translational Science* 12:350–360.

P145 - PARENT-METABOLITE PHARMACOKINETIC MODELING, TISSUE DISTRIBUTION, AND BIOTRANSFORMATION STUDIES OF NOVEL EDARAVONE ORAL PRODRUG

Dong Wook Kang¹, Ju Hee Kim¹, **Seok-jin Cho**¹, Young Bean Hong¹, Yong-Bok Lee², and Hea-Young Cho¹
¹CHA University, South Korea and ² Chonnam National University, South Korea

Edaravone is a neuroprotective agent for the treatment of amyotrophic lateral sclerosis and is thought to delay the decline in muscle strength and the progress of muscular atrophy. Not only is edaravone administered via IV infusion, but also it should be administered in 14-day cycle with a 14-day drug-free period. To ease the burden on patients and caregivers, a novel edaravone oral prodrug TEJ-1704 was developed. The current study aimed to evaluate the nonclinical properties of TEJ-1704 and edaravone. 30 mg/kg of edaravone and 99 mg/kg of TEJ-1704 (30 mg/kg as edaravone) were orally administered to rats, respectively, for evaluating pharmacokinetics (PKs), tissue distribution, and metabolite conversion ratio (biotransformation of TEJ-1704 to edaravone). The concentrations of edaravone and TEJ-1704 in the plasma and six different tissues were quantified using the validated UPLC-ESI-MS/MS method. The PK parameters (t_{1/2}, T_{max}, C_{max}, and AUC_{inf}) of edaravone were estimated, and the metabolite conversion ratio of TEJ-1704 was calculated based on the AUC of both parent drug and metabolite. The parent-metabolite pharmacokinetic modeling was carried out and internally validated using diagnostic plots, bootstrapping, and visual predictive checks. The T_{max}, C_{max}, AUC_{inf}, and t_{1/2} of edaravone were estimated to be 0.4 hr, 35420.4 ng/mL, 47059.7 ng·hr/mL, and 1.7 hr in the reference group (edaravone-administered group), and 0.7 hr, 3285.6 ng/mL, 40361.9 ng·hr/mL, and 12.9 hr in the test group (TEJ-1704-administered group), respectively. The T_{max}, C_{max}, AUC_{inf}, and t_{1/2} of TEJ-1704 were estimated to be 0.7 hr, 3680.0 ng/mL, 50370.8 ng·hr/mL, and 13.2 hr in the test group. In the test group, TEJ-1704 lasted for more than 10 hours and was continuously metabolized to edaravone until all TEJ-1704 is depleted. Thus, t_{1/2} of edaravone in the test group was about 7.6 times longer (1.7→12.9 hr) than that of the reference group. The C_{max} of edaravone in the test group was about 0.09-fold lower (35420.4→3285.6 ng/mL) than in the reference group. The T_{max} and AUC_{inf} of edaravone were not significantly different between the test and the reference groups. The metabolic conversion ratio (metabolite-to-parent drug AUC ratio) was 0.80. After the administration of TEJ-1704, the tissue distribution of edaravone was ranked as follows: Gastrointestinal tract > Kidney > Liver > Heart > Lung > Brain. The parent-metabolite PK model with first-order absorption and elimination was developed and well described the observed data of edaravone and TEJ-1704. The results of model validation did not show any visible trend or model misspecification implying the model was robust and reliable. In conclusion, the increased t_{1/2} and decreased C_{max} of edaravone (even if the similar systemic exposure) in the test group suggest the possibility of TEJ-1704 as the prodrug of edaravone.

P146 - NONLINEAR MIXED-EFFECTS MODELLING TO REVISIT ETHANOL PHARMACOKINETICS

Sören Büsker¹, Alan Wayne Jones², Robert G. Hahn³, Max Taubert¹, Ulrich Klotz⁴, Matthias Schwab⁵, and **Uwe Fuhr**¹
¹University of Cologne, Faculty of Medicine and University Hospital Cologne, Germany, ²Linköping University, Sweden, ³Research Unit, Södertälje Hospital and Karolinska Institutet at Danderyds Hospital (KIDS), Sweden, ⁴Dr. Margarete Fischer-Bosch-Institute of Clinical Pharmacology and University of Tübingen, Germany, and ⁵Dr. Margarete Fischer-Bosch-Institute of Clinical Pharmacology; University of Tübingen, and Departments of Clinical Pharmacology, Pharmacy and Biochemistry, University Hospital Tübingen, Germany

Ethanol (“alcohol”) is among the most important recreational drugs in most countries. Excessive drinking and drunkenness have a major impact on public health and many other societal aspects. Understanding the pharmacokinetics (PK) of ethanol is important because of potential drug-alcohol interactions, in forensic science when investigating alcohol-related crimes, and even for the consumer to adjust her or his activities according to the expected blood alcohol concentrations (BAC). While ethanol PK has been extensively studied since the 1930s, some issues are unresolved, including the role of first-pass metabolism in conjunction with the various effects of food. Many respective conclusions were derived from comparisons of the AUC (area under the BAC vs. time curve) which is inappropriate in the presence zero order elimination processes. We re-evaluated blood alcohol concentration (BAC) profiles from three published clinical studies reporting on oral (1,2), intraduodenal (2), and intravenous (2,3) administration of ethanol with and without food using the nonlinear mixed-effects modelling software NONMEM version 7.5.0 (ICON Development Solutions, Ellicott City, Maryland, USA). Available data included 1,510 BACs obtained in 72 healthy subjects (60 male, 12 female, age range 20-60 years). After establishing individual models for each study, a common model for all data was generated. In all cases, two-compartment models with first-order absorption and Michaelis-Menten elimination kinetics provided the best description of the BAC profiles. In the common analysis, bootstrap median values and 95% CIs for ethanol bioavailability was estimated to be 94.4% [91.8-97.2 %] and 98.2% [95.1-100 %] after oral and intraduodenal administration, respectively. The absorption rate constant (K_a) depended on the site of intestinal administration and was higher in the fasted state: K_{a,duodenal,fed} 11.4 1/h [6.9-21.0 1/h]; K_{a,oral,fed} 1.44 1/h [1.20-1.77 1/h]; K_{a,oral,fasted} 3.67 1/h [2.95-4.68 1/h]. Model

fitting improved much when an independent food effect (as a factor) on maximum elimination rate (V_{max}) was included. Estimates of V_{max} (fasted) and food effect were 6.31 g/h [95% CI: 6.04-6.59 g/h] and 1.39-fold [95% CI: 1.33-1.46-fold], respectively. Simulations based on the common model confirmed that AUC decreases when reducing the oral or intravenous input rate of ethanol, irrespective of any first pass metabolism. Simulated AUC_{0-10h} for a 75 kg subject was 2.34 g/L*h in the fed state and 3.83 g/L*h in the fasted state after an oral dose of 45 g ethanol. This difference was mainly attributable to the food effect on elimination and less to that on absorption rate. Our results help to understand human PK of ethanol and the interpretation of BAC results in clinical and forensic medicine. (1) Jones AW. Interindividual variations in the disposition and metabolism of ethanol in healthy men. *Alcohol* 1984;1:385-91. (2) Ammon E, Schäfer C, Hofmann U, Klotz U. Disposition and first-pass metabolism of ethanol in humans: Is it gastric or hepatic and does it depend on gender? *Clin Pharmacol Ther* 1996;59:503-13. (3) Hahn R, Norberg A, Gabrielsson J, Danielsson A, Jones AW. Eating a meal increases the clearance of ethanol given by intravenous infusion. *Alcohol* 1994;29:673-7.

P147 - CHARACTERIZATION OF TRANSPORTER-MEDIATED DISPOSITION OF HEPATOBILIARY IMAGING AGENTS IN ISOLATED PERFUSED RAT LIVERS USING A MULTI-COMPARTMENT PHARMACOKINETIC MODEL

Angela Jeong¹, Catherine Pastor, and ¹Kim Brouwer

¹University of North Carolina, Chapel Hill, United States and ²University Hospital of Geneva, Switzerland

[Introduction] Hepatobiliary magnetic resonance imaging (MRI) and single-photon emission computed tomography (SPECT) are used for quantification of liver function. Metabolically stable hepatobiliary imaging agents [e.g., gadobenate dimeglumine ([¹⁵³Gd]BOPTA), mebrofenin ([^{99m}Tc]MEB)] are transported into hepatocytes by organic anion-transporting polypeptides (Oatps) and excreted into the extracellular space via basolateral multidrug resistance-associated protein 3 (Mrp3) or into bile via canalicular Mrp2. In this study, we developed a multi-compartment pharmacokinetic model to quantify transporter-mediated distribution of [^{99m}Tc]MEB and [¹⁵³Gd]BOPTA between hepatic compartments using previously obtained ex vivo data [1]. [Methods] Sprague-Dawley rat livers (n=6/agent) were perfused in a single-pass manner with 64μM [^{99m}Tc]MEB or 200μM [¹⁵³Gd]BOPTA for 30min followed by a 30-min washout phase. A gamma counter was placed over livers and concentration-time profiles were estimated in the extracellular space, hepatocytes, and bile canaliculi after adjustment for intrahepatic volume ratios, as detailed previously [1]. Hepatic disposition profiles of [¹⁵³Gd]BOPTA in a rat model of sinusoidal obstruction syndrome induced by monocrotaline (MCT) gavage (n=4), characterized by impaired biliary excretion [2], also were used for model analysis. A multi-compartment model was constructed in Phoenix WinNonlin v8.3. Volumes of extracellular space (2.46ml) and bile canaliculi (0.047ml) were fixed to literature values. Other parameters were obtained by simultaneously fitting the 5-compartment model (extracellular space, hepatocyte, bile canaliculi, and perfusate outflow) to the concentration-time profiles, where perfusate outflow was separated into two compartments (substrate effluxed from hepatocytes and substrate that did not enter hepatocytes) to improve the precision of estimates for Mrp3-mediated efflux rate constants. [Results] The 5-compartment model adequately described [^{99m}Tc]MEB and [¹⁵³Gd]BOPTA concentration-time data based on the goodness-of-fit and CV%<10% for all estimated parameters (Table1). The model estimated Oatp-mediated hepatocyte uptake rate constant was much higher for [^{99m}Tc]MEB than [¹⁵³Gd]BOPTA (22.5min⁻¹ vs 6.77min⁻¹), whereas the Mrp3-mediated efflux rate constant of [^{99m}Tc]MEB was lower than [¹⁵³Gd]BOPTA (0.00014min⁻¹ vs 0.022min⁻¹). The estimated hepatocyte distribution volume of [¹⁵³Gd]BOPTA was much larger than [^{99m}Tc]MEB suggesting that the two substrates have different distribution within hepatocytes (20.8ml vs 7.77ml). The rate constant for Mrp2-mediated biliary excretion of [¹⁵³Gd]BOPTA was greatly reduced in MCT-treated rats (8.11E-05min⁻¹ vs 0.054min⁻¹), while the Mrp3-mediated efflux rate constant was increased (0.07min⁻¹ vs 0.022min⁻¹). [Conclusion] The 5-compartment model developed herein adequately characterized the transporter-mediated uptake and excretion of the two hepatobiliary imaging substrates. This model also demonstrated how increased Mrp3-mediated efflux compensated for decreased MRP2-mediated biliary excretion in livers from MCT-treated rats.

Table 1. Model parameter estimates

Parameter	[^{99m} Tc]MEB-Control		[¹⁵³ Gd]BOPTA-Control		[¹⁵³ Gd]BOPTA-MCT	
	Estimate	CV%	Estimate	CV%	Estimate	CV%
K_{uptake} (min ⁻¹)	22.5	2.29	6.77	6.43	4.51	8.54
K_{outflow} (min ⁻¹)	1.60	5.08	34.2	3.87	30.5	4.61
K_{efflux} (min ⁻¹)	0.00014	6.95	0.022	6.30	0.07	5.56
$K_{\text{BileCanaliculi}}$ (min ⁻¹)	0.079	3.39	0.054	3.95	8.11E-05	20.14
$K_{\text{BileOutflow}}$ (min ⁻¹)	3.67	2.06	166.0	7.01	0.35	21.31
$V_{\text{hepatocyte}}$ (ml)	7.77	3.55	20.8	5.41	20.8	Fixed

References:

1. Pastor and Brouwer. New pharmacokinetic parameters of imaging substrates quantified from rat liver compartments. *Drug Metab. Dispos.* 50(1):58-64,2022.
2. Schiffer et al. Hepatic regeneration is decreased in a rat model of sinusoidal obstruction syndrome. *J. Surg. Oncol.* 99(7):439-46,2009.

P148 - POPULATION PHARMACOKINETICS OF CEFEPIME IN CRITICALLY ILL ADULT PATIENTS WITH HOSPITAL-ACQUIRED OR VENTILATOR-ASSOCIATED PNEUMONIA**Dong-Hwan Lee***Hallym University Sacred Heart Hospital, South Korea*

This study aimed to investigate the population pharmacokinetic (PK) profile and determine the optimal dosage regimen of cefepime in critically ill adult patients with hospital-acquired pneumonia (HAP) or ventilator-associated pneumonia (VAP). Population-PK models for cefepime were developed using a nonlinear mixed-effect modeling approach. The percentage of time within 24 h in which the free concentration exceeded the minimum inhibitory concentration (MIC) at a steady state (50% $fT > MIC$, 100% $fT > MIC$, and 100% $fT > 4 \times MIC$) for various combinations of dosage regimens and renal function was explored using Monte Carlo simulation. Twenty-one patients were prospectively enrolled in this study. Cefepime PK was best described using a two-compartment model in which creatinine clearance (CLCR) through Cockcroft-Gault (CG) was a significant covariate for the total clearance of cefepime. The simulation results to determine the optimal cefepime dosing regimen for 50% $fT > MIC$ as treatment target with $C_{min} < 20$ mg/L as safety target showed that a dosage regimen of 2 g through intravenous (IV) infusion every 12 h administered over 4 h was optimal at an MIC of 4 mg/L, rather than the currently recommended dosage regimen of 2 g administered through IV infusion every 8 h, in patients with normal renal function (CLCR = 90–130 mL/min). For a treatment target of 100% $fT > MIC$ with $C_{min} < 35$ mg/L as a safety target, a dosage regimen of 0.75 g administered through continuous infusion over 24 h would be sufficient at an MIC equal to or less than 8 mg/L in patients with renal dysfunction (CLCR = 10–30 mL/min). Our results suggest that clinicians should consider renal function and potential neurotoxicity when deciding the dosing regimen of cefepime in critically ill patients with HAP or VAP. Therapeutic drug monitoring (TDM) to adjust cefepime trough levels may be useful to improve clinical outcomes and reduce cefepime neurotoxicity.

P149 - THE STRATEGY FOR EFFICACY EVALUATION OF THE MESENCHYMAL STEM CELL THERAPEUTICS: PHARMACOKINETIC STUDY OF ADJUVANT CHEMOTHERAPY IN RECURRENT GLIOBLASTOMA PATIENTS**Young Bean Hong**, Dong Wook Kang, Seok-Jin Cho, Ju Hee Kim, and Hea-Young Cho*College of Pharmacy, CHA University, South Korea*

Glioblastoma is an aggressive type of cancer in the brain with a high propensity for recurrence. However, conventional adjuvant chemotherapy is limited due to blood-brain barrier (BBB) related impediments to the delivery. MSC11FCD is anti-cancer cellular therapeutics based on mesenchymal stem cell (MSC) that contains the cytosine deaminase gene. It functions by converting 5-fluorocytosine (5-FC) to 5-fluorouracil (5-FU) in the injection site. The MSC is expected that it can track remaining glioblastoma cells and induce cell death after resection surgery. Although 5-FU should be investigated for its pharmacokinetics (PKs) to evaluate MSC11FCD efficacy in brain tissue, direct quantification of 5-FU is virtually impossible due to the inability to collect brain samples from patients. This study aimed to indirectly evaluate the efficacy of MSC11FCD in a clinical trial for recurrent glioblastoma patients by investigating the PKs of 5-FC as a prodrug of 5-FU. During resection surgery of glioblastoma, the patients (n=10) were injected MSC11FCD and administered 5-FC (150 mg/kg, QID for 7 days) after the surgery. Plasma samples were collected up to 3, 51, 99, and 147 h after the first administration of 5-FC and analyzed by the simultaneous bio-analysis method using the HPLC-UV system. The PK model of 5-FC was developed and validated for PK evaluation reliant on the existence of MSC. The PK parameters and the results of simulations were estimated using WinNonlin software and were contrasted through the existence of MSC. The PK model, which assumed the patients have no MSC, was the 1-compartment model without lag-time and applied to fit the observed plasma concentration of 5-FC in patients. All the results of diagnostic plots and the model validation indicated that the developed PK model of 5-FC well described the observation values of PK data. According to the existence of MSC, the elimination rate constant (K_e) was calculated differently. K_e increased 0.09 ± 0.01 (1/h) to 0.30 ± 0.02 (1/h) through injection of MSC. The results of simulations show that the predicted plasma concentrations at steady-state (C_{ss}) of 5-FC in patients who have the MSC was about $49.48 \pm 1.00\%$ of the C_{ss} of 5-FC assuming the absence of MSC. It suggested that the additional elimination pathway of 5-FC exists in patients with MSC11FCD. These results could be used as scientific evidence of the efficacy of MSC11FCD for recurrent glioblastoma.

P150 - PBPK SIMULATION-BASED EVALUATION OF ISONIAZID DISPOSITION IN PREGNANCY FOR NAT-2 FAST AND SLOW ACETYLATORS

Ogochukwu Amaeze, and Nina Isoherranen
University of Washington, United States

Isoniazid (INH) is a first-line anti-tubercular drug for treating latent tuberculosis infection (LTBI) and tuberculosis (TB) disease. INH is primarily metabolized by N-acetyltransferase 2 (NAT-2), which has a highly polymorphic gene, segregating the human populations into fast, intermediate, and slow metabolizer phenotypes. This genetic polymorphism accounts for the majority of pharmacokinetic (PK) variability observed for INH and impacts INH exposure resulting in hepatotoxicity, treatment failure, or drug resistance. TB during pregnancy poses a substantial risk of morbidity and mortality to the pregnant woman and the fetus if left untreated. Current WHO TB treatment guidelines recommend using the same regimens and dosages for non-pregnant and pregnant populations. INH is the preferred agent for TB prevention and treatment of LTBI in pregnancy; it is also a core component of the standard TB treatment regimen for active TB disease. Reported plasma INH exposure during pregnancy varies widely between studies and is poorly understood. Pregnancy may influence NAT-2 activity and hence, INH disposition during pregnancy, leading to altered efficacy or toxicity of INH compared to non-pregnant women or men. We hypothesized that PBPK modeling could be used to predict INH disposition across the gestational timeline in different populations. Our study aimed to develop and verify a pregnancy INH PBPK model for NAT-2 fast and slow acetylators (FA and SA) and apply it to predict INH disposition throughout the pregnancy timeline and establish NAT-2 changes during pregnancy. Integrating prior *in vitro* data, clinical PK data, and relative abundance of NAT-2 in FA and SA, a PBPK model for INH in FA and SA was developed and verified using the Simcyp simulator V21. First, a model of intravenous INH was developed and verified for the non-pregnant population. Second, the model was expanded to incorporate oral absorption parameters. Model performance was evaluated by comparing the predicted PK parameters (AUC and C_{max}) to clinical studies data and employing a goodness-of-fit test. Third, the model was extended to the pregnant population by incorporating pregnancy-induced physiological changes in the Simcyp simulator pregnancy population. The model was then applied to predict INH disposition in the different pregnancy stages. This work demonstrates a promising approach for predicting INH exposure and disposition for different NAT-2 acetylator phenotypes and model-informed dosing in pregnancy. The next step will be to incorporate INH metabolites into the model to evaluate the effect of pregnancy on NAT-2 activity in different acetylator phenotypes.

Funding: Bill and Melinda Gates Foundation (INV 029091).

P151 - APPLICATION OF PBPK MODELING TO ASSESS PUR1900, AN INHALED FORMULATION OF ITRACONAZOLE, AS AN INHIBITOR OF CYP3A4 METABOLISM

Mackenzie Bergagnini-Kolev
Certara, United States

PUR1900, a dry powder formulation of itraconazole being developed for oral inhalation for the treatment of allergic bronchopulmonary aspergillosis in patients with asthma. Itraconazole and its primary metabolite, hydroxy-itraconazole (OH-itraconazole), are both potent inhibitors of CYP3A4 in the gut and liver. Through inhalation of PUR1900, high concentrations of itraconazole may be delivered to the lungs while limiting systemic exposure. Lower systemic exposure of itraconazole and OH-itraconazole may reduce the DDI liability of PUR1900 as a CYP3A4 perpetrator. An itraconazole PBPK model was previously developed to simulate the concentration-time profiles of itraconazole and OH-itraconazole after administration of itraconazole as an oral solution. This PBPK model (Simcyp Simulator, V19) was modified to simulate administration by oral inhalation. The PBPK model parameters describing the fraction absorbed and rate of absorption from the lung, as well as the fraction of inhaled dose swallowed, were optimized by fitting these parameters to the observed plasma concentration data collected in a clinical study in which 35 mg of PUR1900 was administered once a day (QD) for 14 days (1). Simulated population geometric mean itraconazole and OH-itraconazole area under the curve (AUC)_{0-24h} values at steady state (by Day 14) were within 0.96-fold and 1.68-fold respectively of observed data from a Phase 1 clinical trial. The PUR1900 PBPK model was then applied to predict the DDI liability of PUR1900 inhibition of CYP3A4, using the sensitive substrate midazolam as the victim drug. Multiple-dose PUR1900 was simulated at 35 mg (QD) for 14 days to reach steady-state. A single dose of midazolam (5 mg orally) was simulated in the presence or absence of steady-state PUR1900. Under these conditions, the population simulated geometric mean ratios (GMR) of midazolam AUC_{0-inf} and maximum drug concentration (C_{max}) were 1.22 and 1.12, respectively. This minimal change in midazolam exposure in the presence of PUR1900 (35 mg QD) is less than 1.25-fold and considered no interaction. In conclusion, PBPK modelling of PUR1900 after the administration of multiple inhaled doses predicts that effects of PUR1900 on CYP3A4 substrates are minimal. Based on the criteria of the FDA DDI guidance, no clinically significant CYP3A4 DDI was predicted after the administration of 35 mg of PUR1900 QD for 14 days (2).

References:

1. Hava DL, Tan L, Johnson P, Curran AK, Perry J, Kramer S, Kane K, Bedwell P, Layton G, Swann C, Henderson D, Khan N, Connor L, McKenzie L, Singh D, Roach J. A phase 1/1b study of PUR1900, an inhaled formulation of itraconazole, in healthy volunteers and asthmatics to study safety, tolerability and pharmacokinetics. *Br J Clin Pharmacol*. 2020 Apr;86(4):723-733. doi: 10.1111/bcp.14166. Epub 2020 Jan 16. PMID: 31696544; PMCID: PMC7098863.
2. FDA DDI Guidance (2020). Clinical Drug Interaction Studies — Cytochrome P450 Enzyme- and Transporter-Mediated Drug Interactions, Guidance for Industry. U.S. Department of Health and Human Services, Food and Drug Administration, Center for Drug Evaluation and Research (CDER).

PF152 - COMPARATIVE ANALYSIS OF SHORT-CHAIN AND LONG-CHAIN PER- AND POLYFLUOROALKYL SUBSTANCES USING PHYSIOLOGICALLY-BASED TOXICOKINETIC MODELLING

James Chun Yip Chan¹, Sheng Yuan Chin¹, Jieying Lin¹, and Shawn Pei Feng Tan²

¹Agency for Science, Technology and Research, Singapore and ²University of Manchester, United Kingdom

Humans are exposed to environmental contaminants such as per- and polyfluoroalkyl substances (PFAS) through consumer products, contaminated food and water sources. Highly persistent in the environment and humans with unusually long half-lives, the bioaccumulation of PFAS in humans is associated with adverse health effects including cancer, thyroid hormone disruption, reduced kidney function. Long-chain PFAS such as perfluorohexanesulfonic acid (PFHxS, 6 carbons), perfluorooctanesulfonic acid (PFOS, 8 carbons) and perfluorooctanoic acid (PFOA, 8 carbons) have half-life estimates of 7, 3.3-5.4 and 1.3-3.9 years respectively, while short-chain PFAS such as perfluorobutanoic acid (PFBA, 4 carbons) and perfluorobutanesulfonic acid (PFBS, 4 carbons) have estimated half-lives of 3 and 28 days respectively. In general, their half-lives in humans are partially correlated with chain length. Although extensive biomonitoring studies have been conducted to estimate PFAS half-lives using human blood and urine samples, these estimates lack confirmation in human toxicokinetic studies, while animal half-life estimates exhibit major discrepancies and are generally unreliable for extrapolation. The limited understanding of PFAS toxicokinetics and the underlying mechanisms controlling their half-lives hinders their safety assessment. Here, we performed a comparative analysis of the 5 aforementioned PFAS using bottom-up, physiologically-based toxicokinetic (PBTk) models constructed in the Simcyp Simulator®. As these PFAS are metabolically inert and strong acids with limited passive permeability, their excretion will depend on transporters in the liver and kidney. We generated an extensive panel of *in vitro* transporter kinetic data for hepatic transporters OATP1B1, OATP1B3, OATP2B1 and NTCP; and renal transporters OAT1, OAT3, OAT4 and URAT1. The kinetic data were scaled to *in vivo* clearances using quantitative proteomics-based *in vitro*-to-*in vivo* extrapolation (IVIVE), and then used to parameterize our *in silico* models without relying on empirical fitting to clinical data or extrapolations from animal data. Our simulations successfully recapitulated the trend of half-lives for PFAS where PFBA < PFBS < PFOA < PFOS < PFHxS, as similarly observed in biomonitoring studies. Kinetic analyses showed that short-chain PFAS were substrates of fewer transporters than long-chain PFAS, and exhibit lower intrinsic clearances for these transporters. Sensitivity analyses indicated renal (and not biliary) clearance as the major elimination pathway of PFAS. For long-chain PFAS, their *in vivo* persistence is largely driven by extensive renal reabsorption, which was less prominent for short-chain PFAS. In addition, short-chain PFAS exhibit a higher unbound fraction in plasma, resulting in a greater contribution of renal filtration to their elimination. Collectively, these lead to shorter half-lives for the short-chain PFAS. Our models present a mechanistic explanation of the key processes controlling PFAS half-lives. We recommend that the design of next-generation PFAS should focus on reducing plasma protein binding and renal reuptake transporter affinities to limit their systemic retention and biological half-lives.

PF153 - DELINEATING THE COMPLEX INTERPLAY OF ENZYMES AND TRANSPORTERS IN GOVERNING THE ABSORPTION AND DISPOSITION OF ATORVASTATIN AND THE METABOLITES USING PHYSIOLOGICALLY BASED PHARMACOKINETIC (PBPK) MODELING

Revathi Chapa, and Grazyna Fraczekiewicz

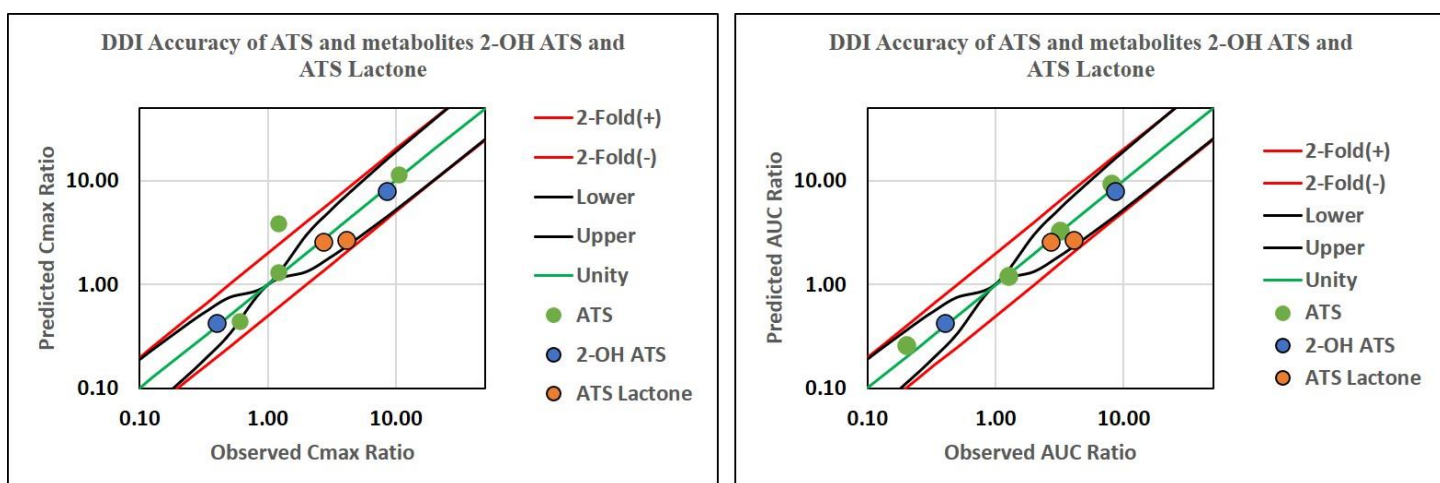
Simulations Plus, United States

Statement of Hypothesis: Atorvastatin (ATS) is widely used to treat high cholesterol and potentially lower the risk of cardiac complications. Absorption and disposition of atorvastatin and the metabolites 2-hydroxy atorvastatin (2-OH ATS), 4-OH atorvastatin (4-OH ATS) and atorvastatin lactone (AL) is governed by complex interplay of enzymes and transporters. To delineate the role of their individual contributions, we developed a mechanistic physiologically based pharmacokinetic (PBPK) model using a middle-out approach which incorporates the *in vitro* and *in vivo* information that represents all the key mechanisms that reproduced the observed clinical data of atorvastatin and its metabolites 2-OH ATS, 4-OH ATS and AL, where the individual role of enzymes and transporters involved was simultaneously verified using drug-drug interaction (DDI) studies with rifampicin, gemfibrozil and itraconazole.

Methods: The Advanced Compartmental Absorption and Transit (ACAT™)/PBPK model was developed by integrating

1) apical efflux by P-gp and BCRP in the gut 2) CYP3A4 mediated hydroxylation in gut and liver 3) UGT1A1 and UGT1A3 mediated glucuronidation in gut and liver 4) OATP1B1 and OATP1B3 mediated hepatic uptake and 5) biliary efflux mediated by P-gp. The model was implemented in GastroPlus® v.9.8.2 (Simulations Plus, USA) using *in silico*, *in vitro* and fitted parameter values. The formation of 2-OH ATS and 4-OH ATS by CYP3A4 mediated hydroxylation and AL by UGT1A1/1A3 mediated glucuronidation (glucuronide to lactone formation is assumed to be spontaneous) were also included in the model. The model was verified using clinical data of ATS and metabolites after oral ATS administration of doses 10 to 80 mg in fasted and fed state. In addition, the effect of rifampicin (pan inhibitor and inducer of enzymes and transporters), gemfibrozil (OATP inhibitor) and itraconazole (strong CYP3A4 inhibitor) on the pharmacokinetics (PK) of ATS and the metabolites were also studied.

Results and Conclusions: The developed model adequately described the PK of ATS and its metabolites 2-OH ATS, 4-OH ATS and AL for all the doses studied. The simulated plasma concentration-time profiles closely matched the observed profiles and all simulated PK parameters (C_{max} and AUC) were within 2-fold of the observed values under fasting and fed conditions. The simulated DDI ratios of C_{max} and AUCs for ATS and its metabolites with rifampicin and gemfibrozil are in reasonable agreement with the upper and lower limits of GUEST Criterion1. In the DDI study with itraconazole, while the simulated DDI ratio of AUC was well predicted, the simulated DDI ratio of C_{max} did not fall within the GUEST limits. Overall, our model accurately predicts the PK of ATS and its metabolites for the entire dose range including the DDIs.



Reference:

1. Guest, E. J., L. Aarons, J. B. Houston, A. Rostami-Hodjegan and A. Galetin (2011). "Critique of the two-fold measure of prediction success for ratios: application for the assessment of drug-drug interactions." *Drug Metab Dispos* 39(2): 170-173.

P154 - EVALUATING THE UTILITY OF TAPE STRIPPING DATA IN THE QUANTITATIVE DERIVATION OF PARTITION COEFFICIENTS CRITICAL FOR DERMAL PBPK MODEL DEVELOPMENT

Jing Yi Eleanor Cheong, Anjiah Nalaparaju, Chiang Huay Freda Lim, and Chun Yip James Chan
 Agency for Science, Technology and Research Singapore, Singapore

Diffusion and partition coefficients across the different skin layers govern the rate and extent of skin permeation. These compound-dependent parameters, coupled with formulation-specific attributes and skin physiology, form the key components of dermal physiologically-based pharmacokinetic (PBPK) models. Consequently, the predictive potential of any dermal PBPK model is contingent on the incorporation of accurate coefficients, particularly in the stratum corneum (SC), which represents the main resistance to skin penetration. Diffusion through the heterogeneous two-phase structure of the SC layer requires active partitioning between (1) SC lipids and the vehicle (K_{SClip:vehicle}), and (2) SC lipids and corneocytes. Unfortunately, quantitative structure–activity relationships (QSAR) relating experimental measurements of K_{SClip:vehicle} to physicochemical properties of the permeant lack applicability when vehicle characteristics deviate from the dataset utilized for QSAR model development. Additionally, *in vitro* permeation testing using Franz cell assays measure bulk transport through full-thickness skin and lack granular insight into SC concentrations crucial to guide determinations of corneocyte permeability. In this study, we evaluate the utility of tape stripping data to parameterize K_{SClip:vehicle} and corneocyte permeability for two diclofenac formulations: Pennsaid® (diclofenac sodium topical solution 2%) and Voltaren® (diclofenac sodium topical gel 1%).¹ All PBPK simulations were performed using the Multi-Phase Multi-Layer Mechanistic Dermal Absorption model implemented in the Simcyp® Version 21 simulator. Figure 1 outlines the strategy adopted for systematic model development. For initial simulations of diclofenac concentrations across SC

depth, physical and structural characteristics of the drug products obtained from literature were used to define the diffusion of diclofenac within the formulations (D_{vehicle}), while $K_{\text{SCLip:vehicle}}$ was derived assuming a completely aqueous formulation. Partition ($K_{\text{SCLip:water}}$) and diffusion coefficients (D_{SCLip}) within the SC were predicted with QSAR models, while corneocyte permeability was represented by the default value ($1\text{E-}5\text{ cm/h}$) within the simulator. Iterative dermal PBPK model refinement involved the incorporation of $K_{\text{SCLip:vehicle}}$ calculated using estimated diclofenac concentrations at the outer surface of the SC ($C_{\text{SC},0}$) and non-ionized concentrations of diclofenac in the vehicle available for permeation. Lastly, corneocyte permeability was optimized to fit both the SC concentration-depth profile as well as the amount of diclofenac recovered from the tape stripping studies. Preliminary simulations using optimized QSAR-predicted $K_{\text{SCLip:water}}$ and D_{SCLip} as well as empirically derived $K_{\text{SCLip:vehicle}}$ and corneocyte permeability markedly overestimated observed diclofenac concentrations across SC depth for both formulations. Introduction of the revised $K_{\text{SCLip:vehicle}}$ enabled better recapitulation of the SC concentration-depth profiles and yielded predicted diclofenac amounts in the SC that were within two fold of the observed values. Sensitivity analyses also established that a consistent corneocyte permeability value of $1\text{E-}5\text{ cm/h}$ across both formulations provided the best congruence with measured SC amounts. In summary, our research exemplified how tape stripping data could be applied to mitigate existing uncertainties surrounding the quantitative derivation of partition coefficients critical for dermal PBPK model development. To circumvent the need for *in vivo* tape stripping data for emerging, untested formulations, future work will explore the feasibility of performing such tape stripping experiments using *ex vivo* human skin.

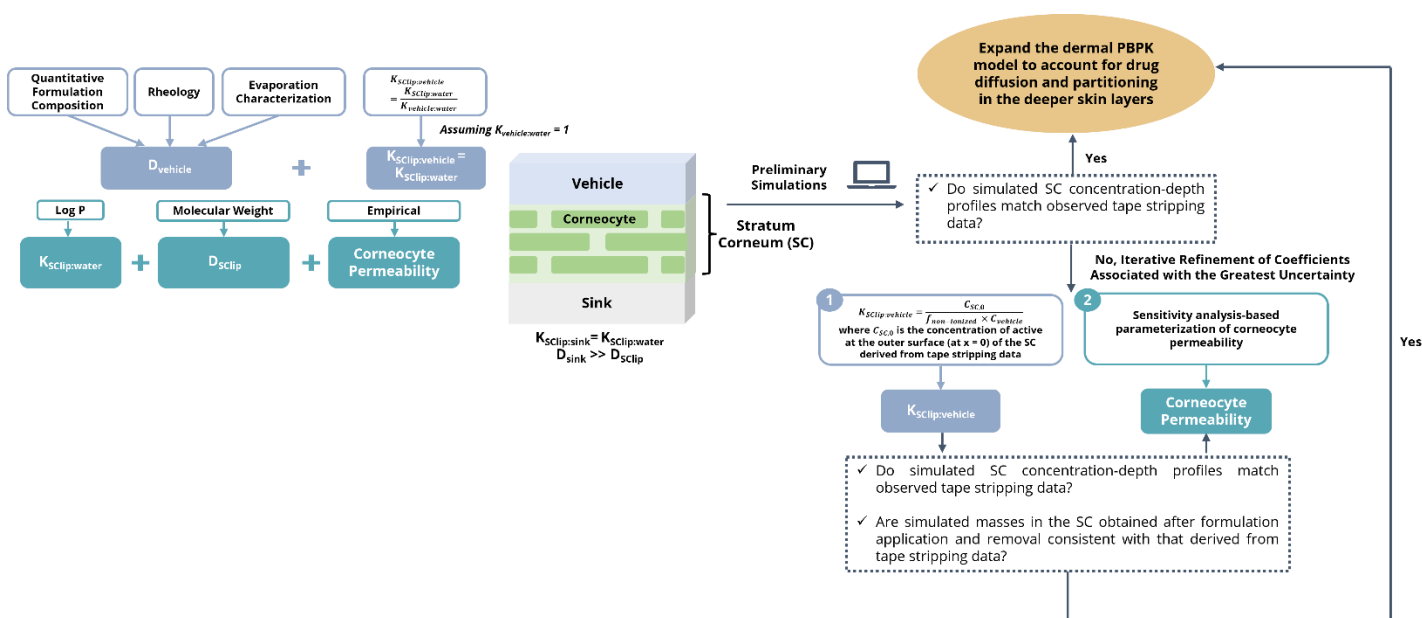


Figure 1. A systematic modelling workflow describing the use of tape stripping data in the optimization of partition and diffusion coefficients governing drug transfer from the vehicle into the stratum corneum (SC) and its subsequent disposition within the SC.

Reference:

1. Cordery, S. F. et al. *Int. J. Pharm.* 529, 55–64 (2017).

P155 - MECHANISTIC UNDERSTANDING OF TRANSPORTER-DEPENDENT DISPOSITION OF PERFLUOROCTANESULFONIC ACID USING PHYSIOLOGICALLY-BASED TOXICOKINETIC MODELLING

Sheng Yuan Chin¹, Jiaying Lin¹, Shawn Pei Feng Tan², and James Chun Yip Chan¹

¹Agency for Science, Technology and Research (A*STAR), Singapore and ²University of Manchester, United Kingdom

Perfluorooctanesulfonic acid (PFOS), an environmental toxicant, is found ubiquitously in consumer products and industrial manufacturing. PFOS is highly persistent in the environment and in humans as it is highly resistant to metabolic degradation, while long-term exposure is associated with adverse health effects such as high cholesterol, thyroid disorders, cancers and reproductive diseases. Bio-monitoring studies estimate the human half-life of PFOS at a remarkable 3-5 years. However, due to safety concerns, this has not been confirmed in prospective human toxicokinetic (TK) studies, and the mechanisms underlying its *in vivo* persistence remain unclear. To address these gaps, we constructed a bottom-up, physiologically-based toxicokinetic (PBTK) model to explore the mechanisms controlling the unusual disposition of PFOS and predict its half-life and tissue concentrations. As PFOS is metabolically inert, biliary and/or renal excretion are believed to be the main elimination routes. Given that PFOS is highly charged at physiological pH due to its estimated pKa of -1.01 and is also highly plasma protein bound (99.52%), it likely exhibits limited passive

permeability, thus its disposition is heavily dependent on xenobiotic transporters. In our study, we characterized *in vitro* PFOS kinetics for 4 hepatic (OATP1B1, 1B3, 2B1 and NTCP) and 4 renal (OAT1, 3, 4 and URAT1) uptake transporters using stably transfected cell lines. These were subsequently scaled up to *in vivo* levels using quantitative proteomics-based *in vitro*-to-*in vivo* extrapolation (IVIVE), then used to parameterize permeability limited organ models within the Simcyp Simulator®. Our predicted PFOS half-life of 4.97 years closely matches the estimates from bio-monitoring studies. Sensitivity analyses indicated renal clearance as the major elimination pathway instead of biliary excretion. Within renal clearance, there are two processes that are mainly driven by transporters, namely tubular secretion and reabsorption. We demonstrated that extensive tubular reabsorption driven by OAT4 and URAT1 is the key to the prolonged half-life of PFOS. In addition, our detection of previously unreported background transport of PFOS in the wild-type HEK293 and CHO cell lines led us to uncover a novel transporter for PFOS, which is highly likely to be the monocarboxylate transporter 1 (MCT1). The ubiquitous presence of MCT1 in human tissues may drive greater tissue penetration of PFOS and contribute to its *in vivo* persistence. Additionally, our model can predict the *in vivo* PFOS tissue concentrations, which can be correlated with tissue toxicodynamic studies, and used to determine external/internal exposure relationships. Lastly, with appropriate adjustments of physiological parameters, we envision that our model can be extrapolated to vulnerable and clinically inaccessible populations to study their TK profiles for PFOS. In short, we built the first mechanistic, bottom-up PBTK model with the extensive incorporation of transporter kinetics to explain the mechanism behind the prolonged half-life of PFOS.

P156 - PHYSIOLOGICALLY BASED PHARMACOKINETIC MODELLING APPROACHES FOR GENDER-SPECIFIC RISK ASSESSMENT OF N-NITROSODIMETHYLAMINE (NDMA)

Seok-jin Cho¹, Dong Wook Kang¹, Ju Hee Kim¹, Yong-Bok Lee², and Hea-Young Cho¹

¹CHA University, South Korea and ²Chonnam National University, South Korea

Recently, the global pharmaceutical industry was alerted by the presence of N-nitrosodimethylamine (NDMA) in several pharmaceuticals which prompted recalls. NDMA can be present in drug products due to various reasons, such as the use of contaminated solvents and catalysts during the manufacturing process and the instability of the substance itself. Regulatory agencies worldwide are making efforts to mitigate the risks from NDMA by investigating the root causes of the impurity and establishing its acceptable intake (AI) limit. This study aimed to suggest a methodology for risk assessment of NDMA through physiologically based pharmacokinetic (PBPK) models in rats and humans. For accurate human risk assessment, gender differences in pharmacokinetics and tissue distribution of NDMA were investigated in rats before the model construction. After intravenous (1 mg/kg) or oral (1, 3, and 10 mg/kg) administration of NDMA in male and female rats, the biological samples (plasma, six different tissues, urine, and feces) were collected and analyzed using UPLC-APCI-MS/MS method. As a result, only the 1 mg/kg oral dosing group showed statistically significant differences between genders in the area under the curve from time 0 to infinity, peak plasma concentration, and apparent clearance. For tissue distribution, there were no gender differences in tissue-plasma partition coefficient in all groups, and NDMA is mainly distributed in the kidney and gastrointestinal tract. Based on the *in vivo* results of NDMA, PBPK models of male and female rats were constructed, respectively. After final verification of the developed rat PBPK models through sensitivity analysis, the models were extrapolated to human PBPK models with human physiological parameters. The established models were applied to gender-specific risk assessment with the oral exposure scenario designed as the AI limit (96 ng/day) of NDMA in drug products recommended by the FDA. In this scenario, it was assumed that the daily NDMA exposures of adult men and women were 1.37 ng/kg/day and 1.66 ng/kg/day, respectively, based on the AI limit. Through the PBPK model-based reverse dosimetry approach, the reference doses (RfD) of 233.52 ng/kg/day (men) and 128 ng/kg/day (women) were estimated from no observed adverse effect level for NDMA in rats. When comparing the calculated RfD with the daily exposure according to gender, the margin of exposure was calculated as 170.45 (men) and 77.11 (women), which suggested that the AI limit of NDMA currently regulated by the FDA is sufficiently lower than the RfD. In this study, the PBPK models established a correlation between the NDMA exposure and external dose in humans. These models will provide valuable tools for risk assessment with biomonitoring data in the future.

P157 - DEVELOPMENT OF A PHYSIOLOGICALLY-BASED PHARMACOKINETIC MODEL FOR PRACINOSTAT IN GASTROPLUS

Jeff Clarine, Cody Parker, Natalie T. Nguyen, and Lisa Rahbaek

Mirati Therapeutics Inc., United States

Pracinostat is an orally available histone deacetylase inhibitor and Jayaraman¹ previously described the preclinical metabolism and disposition of pracinostat and predicted the human pharmacokinetics (PK) by allometric scaling and physiologically -based pharmacokinetic (PBPK) modeling in the Simcyp SimulatorTM (Certara). In this poster we describe the development of a pracinostat PBPK model in GastroPlus (Simulations Plus) utilizing the model building strategy presented by Miller². Pracinostat is a basic, moderately lipophilic, highly soluble compound with high permeability that undergoes first pass metabolism¹. According to the Extended Clearance Classification System (ECCS)³, it is a Class 2 compound, suggesting clearance is primarily driven by metabolism. The PBPK model described herein is built on

previously published in-vitro and in-vivo PK data^{1,4} as well as in-vitro ADME data generated at Mirati Therapeutics Inc. Models were developed in GastroPlus to simulate the plasma exposures of pracinostat after intravenous and oral administration to mice, rats, and dogs and oral administration to humans. In this poster we provide the pracinostat PK data predicted by allometric scaling and the two PBPK modelling softwares with a comparison to the observed human exposures after an oral 10 mg dose to patients.

References:

1. Jayaraman R, Pilla Reddy V, Pasha MK, Wang H, Sangthongpitag K, Yeo P, Hu CY, Wu X, Xin L, Goh E, New LS, Ethirajulu K. Preclinical metabolism and disposition of SB939 (Pracinostat), an orally active histone deacetylase inhibitor, and prediction of human pharmacokinetics. *Drug Metab Dispos.* 2011 Dec;39(12):2219-32. doi: 10.1124/dmd.111.041558. Epub 2011 Aug 26. PMID: 21873472.
2. Miller NA, Reddy MB, Heikkinen AT, Lukacova V, Parrott N. Physiologically Based Pharmacokinetic Modelling for First-In-Human Predictions: An Updated Model Building Strategy Illustrated with Challenging Industry Case Studies. *Clin Pharmacokinet.* 2019 Jun;58(6):727-746. doi: 10.1007/s40262-019-00741-9. PMID: 30729397.
3. Varma MV, Steyn SJ, Allerton C, El-Kattan AF. Predicting Clearance Mechanism in Drug Discovery: Extended Clearance Classification System (ECCS). *Pharm Res.* 2015 Dec;32(12):3785-802. doi: 10.1007/s11095-015-1749-4. Epub 2015 Jul 9. PMID: 26155985.
4. Sohlenius-Sternbeck AK, Terelius Y. Evaluation of ADMET Predictor in Early Discovery Drug Metabolism and Pharmacokinetics Project Work. *Drug Metab Dispos.* 2022 Feb;50(2):95-104. doi: 10.1124/dmd.121.000552. Epub 2021 Nov 8. PMID: 34750195.

P158 - ABSTRACT WITHDRAWN

P159 - PREDICTING DELTA-9-TETRAHYDROCANNABINOL (THC) SYSTEMIC EXPOSURE AND RESPONSE IN HUMANS FOLLOWING DIFFERENT ROUTES OF CANNABIS PRODUCTS ADMINISTRATION USING PARENT-METABOLITE PBPK/PD MODELING

Mayur K. Ladumor, and Jashvant D. Unadkat
University of Washington, United States

Background: The use of cannabis (aka marijuana) products for medicinal and non-medicinal purposes continues to increase globally. The cannabis constituent delta-9 tetrahydrocannabinol (THC) and its active metabolite, 11-hydroxy-THC (11-OH-THC), produce the intoxicating (pharmacodynamics, PD) effect of cannabis. The magnitude of the intoxicating effect and severity of adverse events associated with cannabis products varies considerably between individuals [1]. This is likely due to the large inter-individual variability in THC pharmacokinetics (PK, which drives its PD) and potential variability in the cannabinoid 1 receptor pathway. THC is primarily cleared from the body by cytochrome P450 2C9 metabolism to its intoxicating metabolite, 11-OH-THC [2]. We hypothesized that the PK-PD relationship of THC will differ between different routes of cannabis administration (oral vs. IV/inhalation), because the plasma concentration ratio of 11-OH-THC to THC will be higher after oral vs. IV/inhalation administration. To establish cannabis dose equivalence between different routes of administration, we aimed to build a parent-metabolite PBPK/PD model to quantitatively predict THC and its 11-OH-THC systemic exposure and response (on a visual analogue scale) in healthy adult experienced cannabis users after oral or IV/inhalation use of cannabis products.

Methods: THC and 11-OH-THC PBPK models were created using MATLAB (v. R2022) and its SimBiology module (Mathworks, MA). The middle-out PBPK approach was used to predict the PK of THC/11-OH-THC after IV administration using *in vitro* experimental and *in vivo* data². First-order gut absorption model was used to predict THC/11-OH-THC PK after oral THC administration. Our previously published regional respiratory tract model was used to predict THC respiratory drug deposition and absorption using particle size distribution, inhalation characteristic, dissolution, and permeability data [3]. THC/11-OH-THC drug concentrations in the peripheral vein (rather than the central vein) were sampled. Our model was considered validated if THC/11-OH-THC PK parameters (plasma AUC or C_{max}) fell within 1.25-fold of the observed values. Given that THC and 11-OH-THC interact with the same receptor and share a common mechanism of action, the competitive interaction E_{max} model was used to predict the PD response and compared with previously published observed effect over 4 hr (on 1-10 visual analogue scale) [4]. The PD parameters were estimated by collapsing the hysteresis loop using the hypothetical effect compartment approach, using the summation of the venous plasma concentration of THC and 11-OH-THC and the PD effect as input.

Results and Conclusions: Our PBPK model predicted IV, inhalation and oral plasma AUC of THC and 11-OH-THC within 1.25-fold of the observed data. Consistent with the reported data, our model predicted plasma AUC_{0-4hr} ratio of 11-OH-THC to THC was higher (~1.3) after oral administration compared with after IV or inhalation administration (~0.09) [5]. As hypothesized, the trend of predicted EC₅₀ after different routes of cannabis administration followed the order IV > oral, confirming that 11-OH-THC is an active metabolite. Our validated PBPK/PD model can help to establish the equivalence

of cannabis products and routes of administration for both healthy as well as special populations (e.g., people with hepatic impairment).

This work was supported by the NIH [P01DA032507].

References:

1. Health alert network (HAN). Increases in Availability of Cannabis Products Containing Delta 8 THC and Reported Cases of Adverse Events. <https://emergency.cdc.gov/han/2021/han00451.asp>
2. Patilea-Vrana GI, Unadkat JD. Quantifying hepatic enzyme kinetics of (-)- Δ 9 Tetrahydrocannabinol (THC) and its psychoactive metabolite, 11-OH-THC, through *in vitro* modeling. *Drug Metabolism and Disposition*. 2019 Jul 1;47(7):743-52.
3. Ladumor MK, Unadkat JD. Predicting Regional Respiratory Tissue and Systemic Concentrations of Orally Inhaled Drugs through a Novel PBPK Model. *Drug Metabolism and Disposition*. 2022;50(5):519-28.
4. Hollister LE, Gillespie HK, Ohlsson A, Lindgren JE, Wahlen A, Agurell S. Do plasma concentrations of Δ 9-tetrahydrocannabinol reflect the degree of intoxication? *The Journal of Clinical Pharmacology*. 1981;21(S1):171S-7S.
5. Lunn S, Diaz P, O'Hearn S, Cahill SP, Blake A, Narine K, Dyck JR. Human pharmacokinetic parameters of orally administered Δ 9-tetrahydrocannabinol capsules are altered by fed versus fasted conditions and sex differences. *Cannabis and cannabinoid research*. 2019;4(4):255-64.

P160 - PHYSIOLOGICALLY BASED PHARMACOKINETIC MODELING AND SIMULATION FOR FEXUPRAZAN IN HUMAN

Kyeong-Ryoon Lee

Korea Research Institute of Bioscience and Biotechnology, South Korea

Fexuprazan is a new drug in potassium-competitive acid blocker (P-CAB) family, which inhibit gastric acid secretion and can be used to treat gastric acid-related disorders such as gastroesophageal reflux disease (GERD). The aim of this study is to develop the physiologically based pharmacokinetic (PBPK) model for understanding of clinical pharmacokinetics. Various *in vitro* and *in vivo* studies were carried out and the findings were then used to establish the PBPK model. The silico data were estimated and then used as well. The tissue distribution of fexuprazan was predicted using tissue-to-plasma partition coefficient of rats, and the volume of distribution (i.e., V_{ss}) among the species was estimated by allometric relationship. The drug was eliminated primarily via the metabolism in liver, but urinary excretion was limited (i.e., less than 2.02%). Meanwhile the fraction absorbed (F_a) was estimated to be 0.761 from the PBPK model, and the value was consistent with its physicochemical properties such as solubility and permeability. Finally, the C_{max} , AUC, and time-concentration profiles in human was predicted by the PBPK model using the learning data set, and the proposed model was validated using the validation data sets in this study. In conclusion, the pharmacokinetic profiles was well predicted by using the PBPK model with the estimated model parameters, and the major pharmacokinetic parameters was well predicted.

P161 - THE USEFULNESS OF A PHYSIOLOGICALLY-BASED PHARMACOKINETICS (PBPK) MODEL DEVELOPED IN MONKEY IN THE PREDICTION OF HUMAN PHARMACOKINETICS IN LIVER IMPAIRMENT POPULATION AND DRUG-DRUG INTERACTIONS

Xiaomin Liang¹, Megan Koleske², and Yurong Lai¹

¹*Gilead Sciences, United States and* ²*University of California, San Francisco, United States*

Drug transporters in liver contribute to the hepatic uptake, biliary clearance (CL), asymmetric liver exposure, and are targets of drug-drug interactions (DDIs). In disease state, i.e. liver cirrhosis, the changes of transporter function and as well as other physiological factors can significantly affect drug pharmacokinetics (PK). However, predicting human PK for compounds undergoing transporter mediated CL from *in vitro* data remains challenging as large and compound dependent scaling factors (SF) are needed to bridge the gap between *in vitro* and *in vivo*. Recently, we showed that the SFs of the unbound intrinsic passive (CL_{int,passive,u}), active uptake (CL_{int,active,u}), biliary (CL_{int,biliary,u}), and metabolic (CL_{int,metabolic,u}) can be drawn by comparing *in vitro* data and the fitted parameters to the plasma curve in cynomolgus monkey using a physiologically-based pharmacokinetics model (PBPK). The derived SFs can be reliably used for human PK prediction. In the current study, we used pitavastatin, a probe substrate of organic anion transporting polypeptides (OATP) as a case example, to demonstrate the usefulness of this approach. The simulated human PK profile of pitavastatin using SFs derived from the monkey model was overlaid well with observed clinical PK curved dosed intravenously, and the predicted area under the curve (AUC) was about 90% of observed AUC. The human model was further refined using clinical data from OATP or breast cancer resistance protein (BCRP) transporter genetic

polymorphism and DDI studies. The refined PBPK model was used to predict the PKs in liver impairment patient population in SimCYP (Certara). As a result, the simulated pitavastatin AUC in liver impairment population was approximately 30% or less difference from the observed AUC. The simulated PK curves were further improved by incorporating the enterohepatic recirculation into the model. Our investigation demonstrated the usefulness of a PBPK model developed and validated in monkey in the prospective human PK prediction for compounds undergoing transporter-mediated clearance. The transporter genetic polymorphism and DDI data can reliably characterize the fraction (ft) of contribution from individual transporter for model refinement. The refined PBPK model can be used to predict human PK in liver impairment patient population by incorporating the transporter and physiological factors changes. In conclusion, using pitavastatin as an example, our findings provide a framework to demonstrate that SFs calibrated from monkeys is a reliable approach for the prospective human PK prediction. The human model refined by the genetic polymorphism and DDI data can adeptly predict human PKs with liver impairment patient population.

P162 - SATURABLE RENAL REABSORPTION OF PERFLUOROCTANOIC ACID PROVIDES A UNIFIED EXPLANATION FOR ITS DIVERGENT HALF-LIVES IN HIGH AND LOW EXPOSURE SETTINGS

Jieying Lin¹, Sheng Yuan Chin², Shawn Pei Feng Tan³, Hor Cheng Koh⁴, Eleanor Jing Yi Cheong², Eric Chun Yong Chan⁵, and James Chun Yip Chan²

¹A*STAR Skin Research Labs, Agency for Science Technology and Research, Singapore, ²Singapore Institute of Food and Biotechnology Innovation, Agency for Science Technology and Research, Singapore, ³Centre for Applied Pharmacokinetic Research, School of Health Sciences, University of Manchester, United Kingdom, ⁴School of Chemical and Biomedical Engineering, Nanyang Technological University, Singapore, and ⁵Department of Pharmacy, Faculty of Science, National University of Singapore, Singapore

Notoriously known as a forever chemical, perfluorooctanoic acid (PFOA) is an environmental toxicant that is pervasive in both the environment and human body, exhibiting years-long biological half-life in humans. Human exposure occurs through various sources including contaminated food and water, and industrial and consumer products; in fact, PFOA has been detected in breast milk, umbilical cord blood and 99% of blood samples. The bioaccumulation of PFOA is associated with adverse health effects such as cancer, reduced kidney function and thyroid hormone disruption. PFOA has an estimated half-life of 1.3-3.9 years from human blood and urine samples in low exposure (70 ng/day over 2 years) biomonitoring studies, whereas a high dose (50 mg) phase I dose-escalation trial estimated a vastly shorter half-life of 116 days. Due to ethical and safety concerns, prospective studies to assess the toxicokinetics of PFOA are understandably limited. Additionally, extrapolations from animal data are unreliable as the half-life of PFOA demonstrates species-specificity. Such limitations hamper its risk assessment. In this study, we constructed the first bottom-up physiologically-based toxicokinetic (PBTK) model of PFOA to mechanistically explain its persistence in humans. PFOA is metabolically inert and exhibits poor passive permeability, hence, its disposition is heavily dependent on membrane transporters in the liver and kidney, which can influence the likelihood of organ-specific toxicity. *In vitro* transporter kinetics of hepatic transporters OATP1B1, OATP1B3, OATP2B1 and renal transporters OAT1, OAT3, OAT4, URAT1 were thoroughly characterized and scaled to *in vivo* clearances using quantitative proteomics-based *in vitro*-to-*in vivo* extrapolation (IVIVE). These data and physicochemical parameters of PFOA were subsequently used to parameterize our *in silico* model without empirical scaling. Our model successfully recapitulated both high dose plasma-concentration time profiles from the phase I dose-escalation trial, and mean serum concentrations from a low exposure biomonitoring study. The simulated half-lives under high and low exposure conditions were 173 days and 1.2 years respectively, closely matching observed data. We further inferred that the inclusion of a hypothetical, saturable, renal basolateral efflux transporter in the model was necessary to permit renal reabsorption that in turn enabled recapitulation of the years-long half-life of PFOA observed at low exposures in biomonitoring studies. This same transporter would be saturated at the high exposure conditions of the clinical study, resulting in diminished reabsorption and a dramatically shorter half-life. Interestingly, our sensitivity analyses revealed that renal, but not hepatic transporters were key drivers of the reduced clearance and prolonged half-life of PFOA. We also predicted *in vivo* tissue concentrations of PFOA for correlation with tissue toxicodynamic studies to assess organ-specific toxicities. In summary, our work provides the first unified explanation to reconcile the divergent half-lives of PFOA reported in clinical versus biomonitoring studies, and identifies key determinants of its clearance and biological persistence.

P163 - A SATURABLE PLASMA PROTEIN BINDING MODEL FROM *IN VITRO* DATA CAN PREDICT NONLINEAR PHARMACOKINETICS IN A PBPK MODEL

Louis Lin¹, Matthew Wright², Cornelis Hop², and Harvey Wong¹

¹University of British Columbia, Canada and ²Genentech, United States

When plasma protein binding (PPB) is saturable, the fraction of unbound drug (fu) can change over the course of treatment, leading to nonlinear pharmacokinetics (PK). Vismodegib, a small molecule inhibitor of the hedgehog signaling pathway, is one example that was found to display saturable binding to alpha-1-acid glycoprotein (AAG), one of the main plasma proteins, in clinical trials [1]. As a result, vismodegib reaches steady-state sooner and at a lower accumulation

than expected under typical linear PK conditions [1]. The objective of this study is to test whether this could have been predicted earlier, using a modeling approach with *in vitro* PPB data. An equilibrium dialysis assay measured binding of vismodegib (at 5.0, 20, 75, and 120 μM) to AAG (at 0.5, 1.0, and 5.0 mg/mL) or human serum albumin (HSA; at 5.0, 15, and 40 mg/mL), the two major plasma proteins. We first characterized changes in f_u by using this data to build a PPB model, which was then nested into a physiologically-based pharmacokinetic (PBPK) model to examine how the dynamic binding characteristics of vismodegib influence its concentration-time profile. Binding data to HSA was fit to a single non-saturable binding site model and binding to AAG fit best to a two-site model, with one saturable ($K_{d1.AAG} = 0.061 \mu\text{M}$) and one non-saturable ($K_{d2.AAG} = 24.5 \mu\text{M}$) binding site, according to the lowest Akaike information criterion score amongst the AAG binding models tested. The overall PPB model built using these kinetic parameters shows an approximately 3-fold increase in f_u up to clinically observed unbound concentrations of 0.15 μM at steady-state. Following incorporation into a PBPK model, the simulated concentration-time profiles were consistent with the observed and simulated drug exposure (AUC and C_{max}) was within 2-fold error. Most importantly, the PPB model was necessary to describe the nonlinear PK characteristics at steady-state in the PBPK model. When the effect of saturable PPB was removed from the PBPK model, the PK profile followed linear kinetics, suggesting that saturable PPB binding contributes significantly to nonlinear PK for vismodegib. Overall, this study illustrates how detailed *in vitro* data combined with a modeling approach can provide insight into the clinical PK profile in earlier stages for compounds with saturable PPB.

Reference:

1. Graham, R.A., Lum, B.L., Cheeti, S., Jin, J.Y., Jorga, K., Von Hoff, D.D., Rudin, C.M., Reddy, J.C., Low, J.A. and LoRusso, P.M., 2011. Pharmacokinetics of Hedgehog Pathway Inhibitor Vismodegib (GDC-0449) in Patients with Locally Advanced or Metastatic Solid Tumors: the Role of Alpha-1-Acid Glycoprotein Binding GDC-0449 Pharmacokinetics and AAG. *Clinical Cancer Research*, 17(8), pp.2512-2520.

P164 - PH-DEPENDENT STABILITY OF SIMVASTATIN: PHYSIOLOGICALLY-BASED PHARMACOKINETIC MODELING OF SIMVASTATIN AND SIMVASTATIN ACID PHARMACOKINETICS, DRUG INTERACTIONS AND FOOD EFFECT

Bridget Morse, Jeffrey Alberts, Gemma Dickinson, and Stephen Hall
Eli Lilly, United States

Simvastatin is a commonly administered therapeutic agent for the treatment of hypercholesterolemia. Simvastatin is a prodrug, administered in lactone form, and converted *in vivo* to the active metabolite simvastatin acid. The effect of CYP3A inhibitors on the pharmacokinetics (PK) of simvastatin and simvastatin acid is well-characterized in the clinic and can be pronounced, particularly the effect of grapefruit juice (GFJ), which increases exposure >10-fold. Simvastatin also demonstrates a distinctive food effect, in which the plasma acid:lactone ratio is altered. We hypothesize this is due to elevated gastric pH in the fed state. Although not fully characterized for simvastatin, nonenzymatic pH-dependent conversion between the lactone and acid forms has previously been demonstrated for atorvastatin. We have previously developed a physiologically-based pharmacokinetic (PBPK) model for atorvastatin, which incorporated acid-lactone conversion and reproduced the dose-dependent PK of atorvastatin and the observed drug-drug interactions (DDIs). In this work, we sought to characterize the conversion of simvastatin lactone-acid, and assess the predictability of simvastatin PK, DDIs and food effect using PBPK modeling. *In vitro*, the equilibrium of simvastatin lactone-acid was assessed across a pH range. Conversion between the lactone and acid was almost instantaneous at pH=1, most stable at moderate pH=3-5, and completely favored formation of simvastatin acid at pH=7.4. These data were incorporated into a PBPK model, built in Simcyp v20, in which simvastatin acid formation was included at discrete rates in each of the stomach, enterocyte, and plasma. The fraction of simvastatin metabolized by CYP3A in the gut (F_g) and liver (F_m), were included as previously determined in a model of simvastatin. Formation of simvastatin acid in the enterocyte was attributed to carboxylesterase 2 (CES2). The model was able to accurately reproduce the effects of CYP3A inhibitors on PK of simvastatin and simvastatin acid. The large effect of grapefruit juice was reproduced by including inhibition of CES2 by GFJ, accurately predicting the unique change in the plasma acid:lactone ratio (decrease of ~3-fold) compared to other CYP3A inhibitors. Changing the equilibrium of simvastatin lactone-acid in the stomach according to *in vitro* pH-dependent data reproduced the distinctive change in plasma simvastatin acid:lactone observed with food (increase of ~2-fold). By incorporating pH-dependent simvastatin acid formation at different physiologic sites, this model is able to reproduce previously unexplained clinical observations, particularly the effect of grapefruit juice and food on the pharmacokinetics of active simvastatin acid.

P165 - ELUCIDATING MECHANISMS UNDERLYING A PHARMACOKINETIC NATURAL PRODUCT-DRUG INTERACTION USING A MODELING AND SIMULATION APPROACH

James T. Nguyen¹, Rakshit Tanna¹, Dan-Dan Tian², Christopher Arian³, Nadja Cech⁴, Nicholas Oberlies⁴, Allan Rettie³, Kenneth Thummel³, and Mary Paine¹

¹Washington State University, United States, ²Eli Lilly and Company, United States, ³University of Washington, United States, and ⁴University of North Carolina Greensboro, United States

Background. The commonly used herbal product goldenseal is a well-known inhibitor of cytochrome P450 (CYP) 3A activity, as evidenced by an approximately 50% increase in the area under the plasma concentration versus time curve (AUC) of the probe drug midazolam after oral administration with goldenseal.^{1,2} The collective *in vitro* and clinical pharmacokinetic studies prompted development of a physiologically based pharmacokinetic (PBPK) model to 1) predict plasma exposure to the major goldenseal alkaloids berberine and (–)-β-hydrastine, 2) distinguish the contributions of reversible and time-dependent CYP3A inhibition by each alkaloid, and 3) determine the primary anatomical site of the interaction. **Methods.** A PBPK inhibitor model was developed for each alkaloid using the Simcyp™ population-based simulator. Physicochemical properties, CYP3A inhibition kinetics, and clinical pharmacokinetic data obtained from the literature were incorporated into the models using a middle-out approach. The models were refined by adding the dissolution rate profile and apparent absorptive permeability (Papp) for berberine and (–)-β-hydrastine, which were determined using fasted state simulated intestinal fluid and Caco-2 cell monolayers, respectively. The developed inhibitor models were combined with the midazolam substrate model to simulate alkaloid exposure and predict the magnitude of the goldenseal-midazolam interaction. Simulation outcomes were verified with data from an independent clinical pharmacokinetic study. **Results.** Total berberine and (–)-β-hydrastine content dissolved by >80% within 20 minutes, indicating that dissolution was not a limiting factor to alkaloid exposure. (–)-β-hydrastine was approximately 60-fold more permeable than berberine (Papp, 9.5x10⁻⁶ versus 1.7x10⁻⁷ cm/s). Predicted plasma AUC_{0-12h} of each alkaloid was within two-fold of the observed AUC_{0-12h} (7.29 versus 7.68 nM•h for berberine and 1,640 versus 1,190 nM•h for hydrastine). The predicted midazolam AUC_{0-12h} ratio (AUC in presence to absence of goldenseal) after multiday goldenseal administration was within 10% of the observed ratio (1.48 versus 1.39). Simulations demonstrated that goldenseal maximally decreased active CYP3A enzyme in the gut and liver by ~70% and ~10%, respectively. Removing either the (–)-β-hydrastine model or time-dependent inhibition from the simulation resulted in a predicted <5% decrease in active CYP3A enzyme in the gut and liver and no change in midazolam AUC. **Conclusions.** PBPK models incorporating experimentally determined dissolution rate profiles and absorptive permeability adequately predicted goldenseal alkaloid plasma exposure. Simulations implicated (–)-β-hydrastine as the major phytoconstituent that precipitates the observed pharmacokinetic goldenseal-midazolam interaction, primarily by inhibiting gut CYP3A via time-dependent inhibition. Modeling and simulation represent a robust technique that can be used to elucidate mechanisms underlying other natural product-drug interactions.

Supported by the National Center for Complementary and Integrative Health (U54 AT008909 and F31 AT011698).

References:

1. Gurley BJ, Gardner SF, Hubbard MA, et al. In vivo effects of goldenseal, kava kava, black cohosh, and valerian on human cytochrome P450 1A2, 2D6, 2E1, and 3A4/5 phenotypes. *Clin Pharmacol Ther.* 77(5):415-426, 2005.
2. Nguyen JT, Tian DD, Tanna RS, et al. Assessing Transporter-Mediated Natural Product-Drug Interactions Via *In vitro*-In Vivo Extrapolation: Clinical Evaluation With a Probe Cocktail. *Clin Pharmacol Ther.* 109(5):1342-1352, 2021.

P166 - PROTEOMIC CHARACTERIZATION OF CLINICALLY RELEVANT DRUG-METABOLIZING ENZYMES AND TRANSPORTERS IN THE LIVER AND DIFFERENT INTESTINAL SECTIONS OF SPRAGUE DAWLEY RAT FOR APPLICATIONS IN PBPK MODELING

Sheena Sharma¹, Guihua Yue¹, Dilip K. Singh¹, Vijaya S. Mettu¹, Deepak Ahire¹, Abdul Basit¹, Scott Heyward², and Bhagwat Prasad¹

¹Washington State University, United States and ²BioIVT, United States

Background: Animal models are extensively utilized for assessing preclinical drug pharmacokinetics (PK), drug tissue distribution, drug-drug/food interaction, and drug toxicity prior to human studies. However, translating the preclinical data to human is challenging, especially when drug metabolizing enzymes and transporters (DMET) are involved in disposition. Our specific aims are to: i) quantify clinically-relevant DMET proteins in rat liver and different sections of intestine (duodenum, jejunum, ileum, and colon) by targeted and global (untargeted) proteomics and ii) populate DMET proteomics data into rat physiologically-based PK (PBPK) model for predicting the PK of a P-gp substrate, T-3256336.

Methods: Pooled homogenates of liver (n=6) and individual intestinal sections (duodenum, jejunum, ileum and colon; n=3)

of male Sprague Dawley (SD) rats were procured from BioIVT, and the total membrane and soluble proteins were extracted. The samples were digested using trypsin, and surrogate peptides were quantified for clinically-relevant DMET proteins using targeted and global (data independent acquisition) quantitative proteomics. Proteomics data analysis was performed using Skyline and MaxQuant. Absolute protein amounts were determined using surrogate peptides as calibrators (targeted)¹ or total protein approach (TPA).² Finally, the data were integrated into PK-Sim software for PBPK modeling of a test compound, T-3256336.

Results and Conclusions: The abundance of DMET proteins using targeted and global proteomics was largely comparable, especially for high abundant proteins. Additionally, the TPA approach allowed quantification of a large set of proteins along with subcellular marker proteins (e.g., Atp1a1, calnexin and calreticulin). The majority of rat Cyp (Cyp2c11 > 3a18 > 3a1, 3a2 > 1a2, 2a2, 2c13) and Ugt (Ugt2b7 > 2b1 > 1a6 > 1a1) enzymes were detected predominantly in the liver tissue in both targeted and untargeted analysis. Ugt1a1 and 1a6 were also present in rat intestine tissue with higher abundance in jejunum and ileum compared to colon tissue. Among transporters, Ntcp, Oatp1a1, and Mrp2 were detected in the liver tissue. P-gp abundance in SD rats increased in the distal intestine consistent with human and Wistar rat data.³ Majority of the proteins were ~2-fold higher in the membrane protein fraction compared to the homogenate fraction. The following additional proteins were quantified by TPA approach: Cyps (Cyp2a1, 2c12 and 2e1), Ugts (Ugt2b10, 2b15, 2b35 and 2b37), non-Cyps (Gst, Sult, Nat, Aldh, Aox, Marc, Fmo, and Ces enzymes), and transporters (Bcrp, Bsep, Mrp3, Mrp6, Oatp1a4, and Oatp2a1). Transporters such as Bcrp, Mrp6, Oatp2a1, and P-gp were predominantly detected in intestine (ileum > jejunum). The proteomics-informed PBPK model reasonably predicted (within 2-fold) the observed PK of T-3256336, when integrated with P-gp abundance.

Overall, the global proteomics-based TPA approach was successfully utilized as a tool in quantifying DMET proteins. This was shown to be a superior technique compared to targeted proteomics, because of its ability to quantify a large set of proteins without the need for peptide standards. These findings suggest that proteomics-informed PBPK models in preclinical species can allow mechanistic PK predictions in animal models including tissue concentration predictions, which can be potentially utilized to account for inter-species differences in DMET proteins during allometric scaling.

Funding: The research was supported by Department of Pharmaceutical Sciences, Washington State University, Spokane, WA, and NICHD grant (R01.HD081299).

References:

1. Xu et al., Anal Chem (2018).
2. Wiśniewski et al., J Proteome Res (2019).
3. Mai et al., Mol Pharm (2021).

P167 - A PHYSIOLOGICALLY-BASED PHARMACOKINETIC MODEL FOR HYDROXYCHLOROQUINE AND DESETHYLHYDROXYCHLOROQUINE IN HEALTHY AND COVID-19 POPULATIONS

Claire Steinbronn¹, Daryl Murry², Yashpal Chhonker², Kate Heller¹, Meighan Krows¹, Michael Paasche-Orlow³, Anna Bershteyn⁴, Helen Stankiewicz Karita¹, Vaidehi Agrawal⁵, Mark Wener¹, Christine Johnston¹, Ruanne Barnabas⁶, and Sam Arnold¹

¹University of Washington, United States, ²University of Nebraska, United States, ³Boston University, United States, ⁴New York University Grossman School of Medicine, United States, ⁵University of Maryland-Baltimore, United States, and ⁶Massachusetts General Hospital, United States

Hydroxychloroquine (HCQ) is an established therapeutic that has been FDA-approved since 1955 and used to treat malaria, systemic and chronic discoid lupus erythematosus, and rheumatoid arthritis. Due to its multiple proposed mechanisms of action and established safety profile, HCQ is often investigated for other therapeutic uses. While HCQ has characteristics that support repurposing efforts, uncertainty about absorption, distribution, metabolism, and excretion (ADME) present hurdles when selecting a dosing regimen for any new indication. HCQ has a complex pharmacokinetic (PK) profile with a large and variable volume of distribution. Approximately 30% of HCQ is eliminated through renal excretion while the remainder is metabolized by cytochrome P450 (CYP) enzymes into three circulating metabolites, including desethylhydroxychloroquine (DHCQ). Early in the COVID-19 pandemic, clinical trials investigated HCQ for post-exposure prophylaxis (ClinicalTrials.gov: NCT04328961) and early treatment for COVID-19 (ClinicalTrials.gov: NCT04354428). Data from physiologically-based pharmacokinetic (PBPK) models were simultaneously used to develop dosing recommendations based on simulated lung concentrations. However, it was not clear if COVID-19 would impact the distribution and/or elimination of HCQ. A voluntary sub-study in both trials was implemented to collect dried blood spot samples for a PK analysis of HCQ and DHCQ from SARS-CoV-2(-) (n=19) and (+) participants (n=26). It was determined that the previously published PBPK models under-estimated the variance for both HCQ and DHCQ and over-estimated the mean DHCQ exposure in the SARS-CoV-2(-) cohort. The model performance was improved by incorporating the known variability in blood to plasma partitioning (B/P) for HCQ and DHCQ. The model adequately described the HCQ and DHCQ concentration versus time data observed in both the SARS-CoV-2(-) and (+) participants suggesting HCQ

distribution and elimination were not significantly impacted by the disease. New evidence suggests that COVID-19 has an isoform-specific impact on CYP activity. Based on these data, we developed a virtual population model to simulate how changes in CYP activity during mild COVID-19 disease would influence HCQ and/or DHCQ exposure. We found that a significant difference (AUC ratio outside of 80-125% of observed healthy values) in HCQ and DHCQ exposure would only be observed between uninfected and mild COVID-19 cases if a study were to include at least 500 subjects in both the healthy and mild COVID-19 arms. In addition, the sample size required to identify a significant difference in HCQ and DHCQ exposure depended on incorporating the B/P variability. Altogether, this work demonstrates the importance of considering B/P as an important determinant of PK variability for therapeutics with extensive blood partitioning.

P168 - PREDICTING HUMAN PHARMACOKINETICS BY USING EX VIVO MODELS AND PBPK MODELING; DEMONSTRATOR STUDY USING ROSUVASTATIN AND DIGOXIN

Lianne Stevens¹, Joost Westerhout², Jeroen Dubbeld³, Catherijne Knibbe⁴, Joanne Donkers², Ian Always³, and Evita van de Steeg²

¹LUMC & TNO, Netherlands, ²TNO, Netherlands, ³Leiden University Medical Center, Netherlands, and ⁴Leiden Academic Center for Drug Research, Netherlands

Introduction: Good prediction of the absorption, distribution, metabolism and excretion (ADME) profile of drugs is of high importance in the drug development process. However, this is often hampered by the lack of translational *in vitro* and *in vivo* models. Therefore, robust translational models are needed which can help predict the intestinal absorption, hepatic clearance (metabolic and biliary) and renal clearance of compounds. Ex vivo whole organ models, are a promising tool compared to *in vitro* models, thereby paving the way to apply physiologically-based pharmacokinetic (PBPK) modeling in a more reliable and accurate way. The aim of the current study was to demonstrate this, and incorporate ADME data of 2 model drugs (rosuvastatin and digoxin) derived from intestinal segment studies and whole organ perfused liver and kidney into a generic PBPK model to predict the drug PK profile in humans.

Methods: Three ex vivo models were developed using porcine organs to study ADME processes of rosuvastatin and digoxin. 1) the inTESTine system (n=2) to study apical to basolateral intestinal transport, determining the apparent permeability (Papp) in duodenum, jejunum, ileum and colon tissue. 2) Normothermic machine perfusion of ex vivo liver (n=2) was used to determine the hepatic uptake, clearance and biliary excretion and 3) normothermic machine perfusion of ex vivo kidney (n=2) was used to determine the renal clearance and urinary excretion.

Results: Intestinal absorption of digoxin was limited (average Papp 0.57, due to Pgp affinity of digoxin), and showing higher Papp values in the distal parts of GI tract (Papp: 1.65). Similar results were found for rosuvastatin (BCRP substrate), with average Papp value of 0.21 and 0.14 for distal GI tract. Perfused porcine livers showed to rapidly clear rosuvastatin and digoxin (to a lower extent) from the perfusate with a hepatic extraction ratio of 0.82 and 0.31, respectively. Both compounds were detected in the bile after 10 min of administration, with a biliary excretion of 23% for rosuvastatin and 51% for digoxin. The perfused kidneys showed a minimal renal excretion of both compounds (<10%). These data were incorporated into a generic PBPK model and simulations resulted in relatively accurate predictions of the plasma concentration (Area Under the Curve (AUC)), plasma peak concentration (Cmax), hepatic clearance and bioavailability when compared to human clinical studies. The predicted AUC for digoxin (32.1 ng/mL*h) and rosuvastatin (255.6 ng/mL*h) based on our data from three ex vivo models was within the range of the average AUC based on multiple human clinical studies (23.9±7.8 ng/mL*h for digoxin and 123.7±57.4 ng/mL*h for rosuvastatin). Moreover, by using the ex vivo data incorporated into a PBPK model we were able to predict to what extent the drug enters the enterohepatic circulation.

Conclusion: The combination of ex vivo gut, liver and kidney models with a generic PBPK model is a unique and powerful combination to predict ADME profile of (new) drugs, including the possibility to calculate the fraction that undergoes enterohepatic circulation. Future research is aimed at studying drug-drug interactions and the effects of disease processes.

P169 - PHYSIOLOGICALLY BASED PHARMACOKINETIC MODELS FOR KRATOM, A BOTANICAL WITH OPIOID-LIKE EFFECTS, AND KRATOM-DRUG INTERACTIONS MEDIATED BY CYP3A AND CYP2D6

Rakshit Tanna¹, James T. Nguyen¹, Nadja Cech², Nicholas Oberlies², Allan Rettie³, Kenneth Thummel³, and Mary Paine¹

¹Washington State University, United States, ²University of North Carolina at Greensboro, United States, and ³University of Washington, United States

Background. Oral formulations prepared from the leaves of the kratom (*Mitragyna speciosa*) plant are increasingly used for their opioid-like effects to self-manage opioid withdrawal symptoms and pain. Calls to US poison centers involving kratom exposures increased 52-fold from 2011-2017; one-third reported use of kratom with other drugs. Many of these drugs are metabolized extensively by cytochrome P450 (CYP) enzymes, particularly CYP3A and CYP2D6, raising concern for potential adverse kratom-drug interactions. Mitragynine, typically the most abundant alkaloid in kratom leaves, is a time-dependent inhibitor of both hepatic and intestinal CYP3A activity (midazolam 1'-hydroxylation; KI ~4 μM, kinact ~0.075 min⁻¹) and a reversible inhibitor of hepatic CYP2D6 activity (dextromethorphan O-demethylation; Ki ~1 μM).¹ We subsequently showed that a single low dose (2 g) of a well-characterized kratom product administered as a tea² to 12

healthy volunteers inhibited CYP3A but not CYP2D6 activity (midazolam AUC ratio: 1.39; dextromethorphan AUC ratio: 0.99). Hypothesis and aims. Extrapolation of these *in vitro* and clinical data to real-world scenarios involving other drugs, as well as varied mitragynine content among different kratom products and kratom consumption patterns, can be accomplished through physiologically based pharmacokinetic (PBPK) modeling and simulation. Our aims were to 1) recover mechanistic *in vitro* information describing mitragynine pharmacokinetics and 2) develop and verify mitragynine and kratom-drug interaction PBPK models. Methods. Apparent absorptive permeability (Papp) of mitragynine was determined using Caco-2 cell monolayers. Enzyme kinetics (Km, Vmax) for mitragynine elimination (fm,CYP3A4, 0.67)³ with recombinant CYP3A4 were determined using a substrate depletion approach; residual intrinsic clearance (CLint) was determined using human liver microsomes and a selective CYP3A4 inhibitor (ketoconazole, 1 μM). A bottom-up PBPK model for mitragynine was developed within the Simcyp® simulator using physicochemical and *in vitro* parameters.² The verified mitragynine (inhibitor) model was linked with either the midazolam or dextromethorphan (substrate) model using the respective inhibition mechanism and kinetic parameters to simulate kratom-drug interactions. Results. The Papp for mitragynine (3.59x10⁻⁶ cm/s) was near that of the moderate permeability drug propranolol (2.93x10⁻⁶ cm/s). Mitragynine was metabolized extensively by recombinant CYP3A4 (Km, 1.4 μM; Vmax, 18.5 pmol/min/pmol CYP3A4) and other CYPs (CLint, 20.2 μL/min/mg protein). Predicted mitragynine AUC (750 nM*h) was within 35% of observed AUC (570 nM*h). Predicted AUC ratios for midazolam (1.26) and dextromethorphan (1.06) were within 10% of observed ratios. Conclusions. PBPK models adequately predicted mitragynine systemic exposure and the observed kratom-drug interactions. These verified models can be used to predict and simulate real-world scenarios. Such information will enable the safe use of this increasingly popular botanical product, thereby addressing ongoing public health concerns.

P170 - DEVELOPMENT OF REPRESENTATIVE SENSITIVE CYP2C8 SUBSTRATE AND MODERATE CYP2C8 INHIBITOR PBPK MODELS TO SUPPORT LABELING RECOMMENDATIONS FOR TUCATINIB

Ian Templeton¹, Anthony Lee², Chris Endres², Ariel Topletz-Erickson², and Hao Sun²

¹Certara UK Ltd., Simcyp Division, United States and ²Seattle Genetics, United States

PBPK models were applied to simulate the impact of moderate CYP2C8 inhibition on tucatinib PK. The default PBPK models for gemfibrozil, and its primary metabolite gemfibrozil 1-O-β glucuronide, were modified to simulate moderate CYP2C8 inhibition. To accomplish this, the model for rosiglitazone was modified to represent a sensitive substrate of CYP2C8. The modified models were applied to find the minimum and maximum limits of CYP2C8 inhibition to achieve an >2 to < 5-fold increase in AUC of a representative sensitive CYP2C8 substrate with this representative “moderate” CYP2C8 inhibitor. Rosiglitazone is primarily metabolized by CYP2C8 (~50%). Other CYP isoforms have also been shown to contribute to rosiglitazone metabolism, although the relative contributions of other isoforms have not been determined specifically. Therefore, the remaining 50% is included in the model as non-isoform specific hepatic clearance (Yeo KR et al., 2013). The maximum AUC ratio which may be predicted under complete inhibition of a substrate with fmCYP equal to 50 % is 2-fold. Therefore, the fractional hepatic intrinsic clearance of rosiglitazone by CYP2C8 was increased to 90% in the model to better represent a sensitive CYP2C8 substrate. Gemfibrozil is a competitive inhibitor of CYP2C8. The primary metabolite gemfibrozil 1-O-β glucuronide is both a competitive and mechanism-based inhibitor of CYP2C8 (Table 4-1). A DDI simulation was conducted using the modified rosiglitazone PBPK model (fmCYP2C8 90 %) and the models for gemfibrozil and gemfibrozil 1-O-β glucuronide. To focus on the CYP2C8 component, gemfibrozil competitive inhibition of CYP3A4 was deactivated. 10 virtual trials were simulated (n=10 subjects each) with 50% female subjects, age 20 – 55 years. The simulated population geometric mean AUC ratio (GMRAUC, 90% CI) for the modified rosiglitazone model was 4.84-fold (4.46, 5.25), representing moderate CYP2C8 inhibition near the maximum (5-fold) for this category. To simulate CYP2C8 inhibition near the minimum (2-fold) for this category, the default gemfibrozil and gemfibrozil 1-O-β glucuronide models were modified to reduce the inhibition potential of each inhibitor. Gemfibrozil Ki was reduced to 0.9 μM, and the MBI component of gemfibrozil 1-O-β glucuronide was deactivated. Under these conditions, the simulated population GMRAUC (90% CI) for the modified rosiglitazone model was 2.11-fold (2.00, 2.21). The modified gemfibrozil and gemfibrozil 1-O-β glucuronide models were then utilized to simulate the impact on tucatinib exposure after administration with a moderate CYP2C8 inhibitor. The simulated population GMRAUC (90% CI) of tucatinib were 3.08-fold (2.87, 3.32) under maximum moderate CYP2C8 inhibitor conditions and 1.98-fold (1.89, 2.08) under minimum moderate CYP2C8 inhibitor conditions. Based on the simulation results, no dose modifications were proposed for the tucatinib label.

P171 - SPECIES-DEPENDENT ALPHA 1-ACID GLYCOPROTEIN BINDING AND THE IMPACT ON PLASMA PROTEIN BINDING OF PF-07321332 (NIRMATRELVIR), AN ORALLY BIOAVAILABLE SARS-COV-2 3CL PROTEASE INHIBITOR

Heather Eng, Siennah Greenfield, Alyssa Dantonio, R. Scott Obach, Li Di, and Amit Kalgutkar
Pfizer, United States

The SARS-CoV-2 3C-like protease inhibitor PF-07321332 (nirmatrelvir), in combination with ritonavir (Paxlovid™), was granted emergency use authorization in December of 2021 by the U.S. Food and Drug Administration for the treatment of mild-moderate COVID-19 in adults and children [12 years of age and older weighing at least 88 pounds (40 kg)] with a positive test for the virus that causes COVID-19, and who are at high risk for progression to severe COVID-19, including hospitalization or death. Preclinical studies characterizing the disposition of nirmatrelvir to support expedited toxicological and clinical assessments revealed species differences in plasma protein binding. The unbound fraction of nirmatrelvir in plasma, albumin, and alpha 1-acid glycoprotein (the two main plasma binding proteins) from animals and human is reported herein. Nirmatrelvir demonstrated moderate, concentration-independent (0.3-10 µM) plasma protein binding in rat, monkey, and human with mean unbound fractions ranging from 0.310–0.478. In contrast, nirmatrelvir was highly bound at low substrate concentrations and moderately bound at high substrate concentrations in rabbit plasma (fraction unbound 0.0100-0.817) and dog plasma (0.0235-0.685). The species differences were predominantly driven by concentration-dependent and saturable binding to dog and rabbit alpha 1-acid glycoprotein, and to a lesser degree, dog albumin. In a dog pharmacokinetics study, a low total plasma clearance (0.475 mL/min/kg) and low steady state distribution volume (0.20 L/kg) were observed for nirmatrelvir, presumably because of high plasma protein binding, which was unlike the moderate clearance and low-moderate steady state distribution volumes in rats (27.2 ml/min/kg, 1.8 L/kg) and monkeys (17.1 ml/min/kg, 0.33 L/kg). The high dog plasma protein binding had implications in the selection of the non-rodent toxicology species, which was ultimately selected to be non-human primate, to avoid impacting the expedited timeline to deliver a first-in-class therapy during the COVID-19 pandemic.

P172 - ANALYSIS OF RETINOL BINDING PROTEIN 4 (RBP4) AND TRANSTHYRETIN (TTR) IN PLASMA BY QUANTITATIVE LC-MS/MS: INSIGHTS INTO PLASMA PROTEOMICS

Aprajita S. Yadav, Nina Isoherranen, and Alex Zelter
University of Washington, United States

Retinol binding protein 4 (RBP4) is a 21 kDa protein that forms a tetramer with transthyretin (TTR), a 55 kDa homotetrameric protein, and binds retinol in blood with high affinity. Multiple studies in humans have shown an association between increased serum levels of retinol binding protein (RBP4) and obesity, diabetes, insulin resistance, triglyceride levels, cardiovascular disease, and chronic kidney disease [1]. However, RBP4 and TTR concentrations have typically been measured by western blots, or using enzyme linked immunoassays (ELISA) kits, which have limited dynamic range, can be variable between labs or kits, and response can be altered by disease states, matrix effects or anticoagulant [2,3]. LC-MS/MS based protein quantification has been developed as an alternative strategy for ELISAs and western blotting, but plasma proteomic analysis can be confounded by the complexity of the human plasma proteome, abundance of albumin and IgG, and the presence of protease inhibitors which can affect tryptic digest. We hypothesized that LC-MS/MS quantification of RBP4 and TTR in plasma would provide an accurate, rigorous, and reproducible method to determine the absolute concentrations of RBP4 and TTR in human plasma/serum in patients with different disease states and allow quantification of RBP4-retinol and RBP4-TTR concentration ratios. A novel, quantitative mass spectrometry based analytical method was developed and validated to allow for simultaneous targeted quantification of RBP4 and TTR in human plasma. Surrogate peptides for proteomic analysis of RBP4 and TTR were selected from *in silico* analysis and monitored following tryptic digest of purified protein standards and plasma samples. To address the phenomena of digestion quality, missed cleavages, ragged ends and variable modifications present, shotgun proteomics was employed to characterize purified RBP4 standards expressed from multiple cell systems and RBP4 and TTR in human plasma. This analysis showed the presence of peptides incorporating missed cleavages in addition to the expected fully cleaved peptides. Division of signal between multiple peptide species is an important consideration when developing quantitative assays. Yeast enolase was added as a process control and the effectiveness of reducing signal variability by normalizing to this process control was assessed. Multiple internal standards, FSGTWYAMAK[13C615N2] and YWGVASF[13C915N]LQK for RBP4 and GSPAINVAVHVFR[13C615N4] for TTR, were used to determine quantitative variability across peptides from the same protein. A set of plasma samples was quantified multiple times to address technical digest variability, inter-day digest variability, freeze-thaw stability, and autosampler stability. Instrument response linearity and matrix effects for different peptides was also assessed. Instrument variability was observed to range from 5.4 - 7.3% for different enolase peptides, digestion variability added 8 – 32.5% variation which was peptide dependent. Broadly, these results highlight the benefits of robust method development to account for incomplete digestion, efficiency of digestion with a process control and selecting appropriate normalization criteria for accurate quantification. The developed assay will provide an important new tool for understanding the validity of RBP4 and TTR as disease biomarkers.

References:

1. Blaner, Pharmacology and Therapeutics (197) 153–178. 2019
2. Hoofnagle & Wener, Journal of Immunological Methods (347) 3–11. 2009
3. Graham, et al., Diabetologia (50) 814–823. 2007

P173 - RADIOLABEL IS NECESSARY TO UNCOVER NONINTUITIVE METABOLITES OF BIIB104: NOVEL RELEASE OF [14C]NITRILE FROM THIOPHENE AND SUBSEQUENT FORMATION OF [14C]THIOCYANATE

Chungang (Chuck) Gu, Jiansheng Huang, and Christopher L. Shaffer
Biogen, United States

BIIB104 [formerly known as PF-04958242; chemical name: N-((3S,4S)-4-(4-(5-cyanothiophen-2-yl)phenoxy)tetrahydrofuran-3-yl)propane-2-sulfonamide] is a potent and highly selective AMPAR potentiator that has been investigated for the treatment of cognitive impairment associated with schizophrenia. *In vitro* metabolism studies with non-radiolabeled BIIB104 in rat, dog, and human liver microsomes showed O-dealkylation in all 3 species, tetrahydrofuran hydroxylation dominating in human and dog liver microsomes, and thiophene hydroxylation more prevalent in rat liver microsomes. Rat and dog mass balance studies with [14C]BIIB104 (radiolabel at the nitrile group) showed incomplete recovery of administered radioactivity from excreta (urine and feces) over 7 days post-dose (approximately 80% in rats and approximately 60% in dogs), as well as very long radioactivity half-lives in rat and dog plasma. Radiochromatographic metabolite profiling, as well as metabolite identification including LC-MS/MS of chemical derivatization products of [14C]cyanide and [14C]thiocyanate, revealed that [14C]cyanide is a major metabolite in rat liver microsomes, but a minor and trace metabolite in dog and human liver microsomes, respectively. Accordingly, [14C]thiocyanate was a major metabolite in rat bile and urine, but only one of many metabolites in dog bile and urine. [14C]thiocyanate accounted for the long half-lives of plasma radioactivity in both rat and dog. Unlike a literature report regarding the release of [14C]nitrile from a pyridine moiety, the release of [14C]nitrile from the thiophene of BIIB104 is not via a one-step metabolic process. Rather, the metabolic release of [14C]nitrile in the present case is postulated to follow an epoxidation-initiated ring-opening of the 5-cyanothiophene moiety based on the detection of non-radiolabeled counterpart metabolites in rat liver microsomes. This case with BIIB104 is a good example supporting the idea, as recently advocated by the US FDA in a draft guidance on mass balance studies, for completing cross-species radiolabeled ADME studies before initiating large-scale clinical trials to help avoid first finding unexpected drug metabolites during late-stage clinical development.

P174 - ABSTRACT WITHDRAWN**P175 - VERIFICATION OF THE “CARBONYL STRESS” HYPOTHESIS IN A YEAST MODEL OF REACTIVE ENDOGENOUS ELECTROPHILE TOXICITY**

Philip Burcham, and Jeevaprasath Ravikumar
University of Western Australia, Australia

Proteomic investigations have shown that numerous reactive electrophiles released from oxidized lipids contribute to protein adduction during oxidative stress, yet few studies have tested the likelihood that such damage acts additively to amplify toxicity outcomes. We thus used a simple yeast model to test the effects of concurrent exposure to subtoxic concentrations of four carbonylating electrophiles – acrolein (ACR), crotonaldehyde (CRO), 2-trans-hexenal (HEX) and vinyl ketone (MVK). The primary aim was to test the hypothesis that mixtures of carbonyl compounds produce greater toxicity when tested in combination at concentrations that are sub-toxic as individual carbonyls. We first estimated threshold toxicity values from growth curves of *S cerevisiae* (ATCC 9763) grown in 1 mL volumes of YPD media on 24-well plates in the presence of 0.02 to 10 mM concentrations of carbonylating electrophiles. Wells contained 1 million cells added from log-phase overnight cultures. Plates were incubated at 30 °C in a Synergy HTX MultiMode Microplate Reader, with automatic agitation and optical density measurements collected at 30 min interval for 18 h. The concentration of each toxic carbonyl corresponding to the Lowest Adverse Effect Level (LOAEL) was established as the lowest concentration that did not significantly reduce the Area Under the Curve (AUC) of the kinetic growth curve over the 18 h duration of the experiment, while the next lowest concentration tested served as the No Adverse Effect Level (NOAEL). The NOAEL values estimated for the four carbonyls were 0.06 mM (ACR), 0.02 mM (MVK), 0.3 mM (CRO) and 0.5 mM (HEX). In the subsequent experiments, when tested alone at the NOAEL, none of the four compounds produced significant reductions in the AUC of the growth curves relative to control, but when tested in combination, the mixtures reduced the AUC by 19% ($p < 0.05$, Dunnett's). Exposing the cells to the mixture of reactive carbonyls also produced more significant reductions in the viability of the cells than when tested alone, as assessed using the MTT assay. Use of an immunochemical assay for protein carbonyl adducts, the combination of electrophiles produced greater damage to a 150 kDa target protein that was only modestly damaged in cells exposed to each carbonyl at the NOAEL alone. Taken together, these findings suggest

that due to their ability to exert "joint toxicity" due to a shared mechanism of action, reactive carbonyls might make greater than expected contributions to many diseases that involve free radical production and autocatalytic degradation of membrane lipids.

P176 - HEPATIC UPTAKE TRANSPORT MECHANISMS OF HIF PROLYL-HYDROXYLASE INHIBITORS (DUSTATS)

Yi-An Bi, Manthena Varma, Mark West, Emi Yamaguchi, and Sangwoo Ryu

Pfizer Inc, United States

Purpose: Hypoxia-inducible factor prolyl hydroxylase Inhibitors (HIF-PHIs), also referred as 'dustats', are mostly investigational drugs that act by inhibiting hypoxia-inducible factor-proline dioxygenase (HIF prolyl-hydroxylase) which is responsible to break down the HIF under conditions of normal oxygen concentrations. Dustats including daprodustat, desidustat, enarodustat, roxadustat and vadadustat are typically low molecular weight lipophilic acids, and in this study, we evaluated the role of transporter-mediated uptake mechanisms in their hepatic clearance.

Methods: Transport assays based on plated human hepatocytes (PHH), HEK293-cell lines and low-efflux MDCK cells were applied. In PHH assay, the cells were preincubated for 10 min in HBSS buffer with or without a pan-SLC inhibitor (rifampicin SV) and selective inhibitors (rifampicin, OATPs; ketoprofen, OAT2; quinidine, OCT1 and rifampicin SV, pan inhibitor) at target concentrations. The incubation conditions were optimized; uptake clearance (CL_{up}) and passive diffusion rate were determined. Samples were analyzed by LC/MS/MS.

Results: Anionic dustats including roxadustat, daprodustat, vadadustat, and enarodustat all showed OATP1B1 and 1B3-mediated transport in HEK293 cells. OATP1B-specific transport of these compounds was also inhibitable by OATP1B inhibitors. All anionic dustats showed uptake inhibition by rifampin 20 μ M in PHH with active uptake measured in the range of 25-60% *in vitro*. Molidustat, which is neutral at physiological pH (neutral compound), did not show OATP1B-specific transporter in HEK293 cell and PHH uptake assay. Passive permeability across low-efflux MDCK cells was found to be low for all compounds (<2 x10⁻⁶ cm/sec) and the molecular weight is in the range of 300-400 Da suggesting these compounds are extended clearance classification system (ECCS) class 3A compounds. OATP1B1 substrate activity is commonly seen with high molecular weight anions/zwitterions (ECCS 1b and 3B). Significance of OATP1B in the clearance daprodustat may be deduced based on >17-fold increase in its AUC following treatment with gemfibrozil, inhibitor of CYP2C8 and OATP1B1. Clinical studies may be necessary to further evaluate uptake mechanisms for other dustats.

This study shows that the hepatic uptake for majority of the novel and emerging HIF inhibitors is primarily driven by OATP1B1/1B3, and therefore, could play a significant role in their clinical pharmacokinetics. Interestingly, all the anionic dustats evaluated are low molecular weight compounds (300-400 Da) and therefore suggests occurrence of OATP1B-mediated uptake is not uncommon in the low MW acid/zwitterion space.

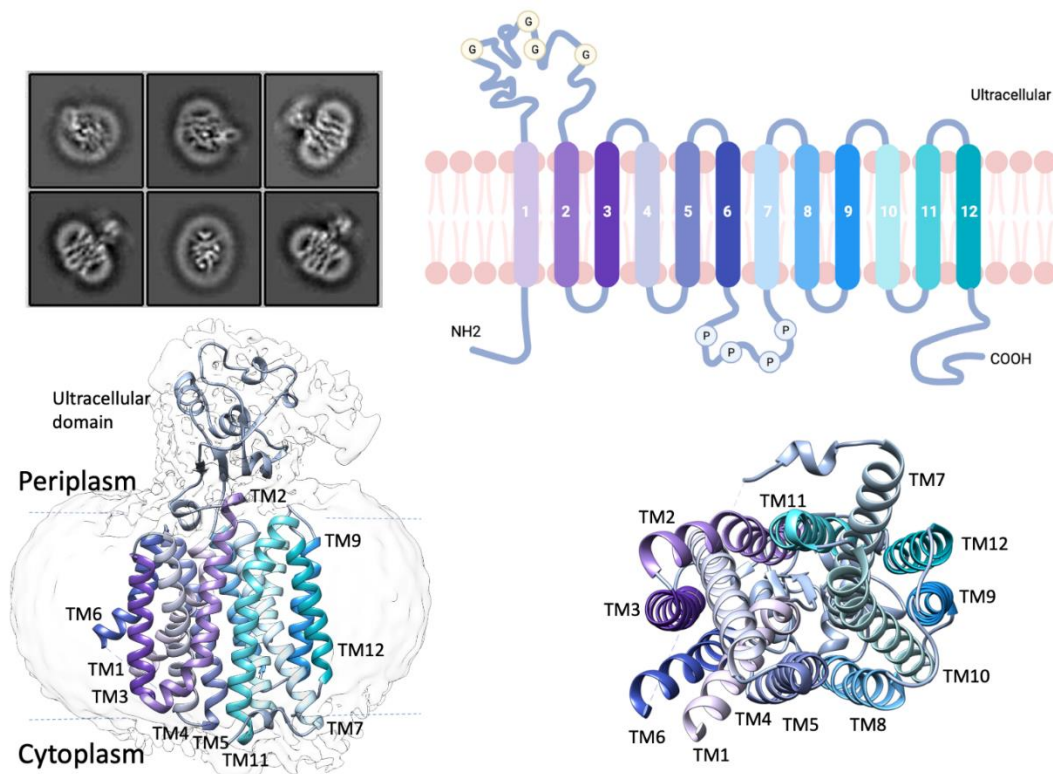
P177 - STRUCTURE, SUBSTRATE RECOGNITION AND INHIBITOR BINDING OF ORGANIC CATION TRANSPORTER 1 (SLC22A1)

Tongyi Dou, Tengfei Lian, Xiaofeng Tan, Yi He, and Jiansen Jiang

NHLBI/NIH, United States

Aim: To investigate the structure, substrate binding and inhibition mechanism of organic cation transporter 1 (SLC22A1) using Cryo-EM. **Background:** Numerous endogenous metabolites and xenobiotic drugs exist as organic ions in our body, while absorption, distribution, and excretion of these compounds are heavily dependent on various organic ion transporters. The solute carrier 22 (SLC22) family are such typical organic ion transporters comprising organic cation transporters (OCTs), organic zwitterion/cation transporters (OCTNs), and organic anion transporters (OATs), thus play a central role in the physiological homeostasis of organic ions. In addition, due to their substrate polyspecificity, SLC22s also mediate massive clinical drug-drug interactions (DDIs) that the FDA provided industrial guidelines for new chemical entities (NCEs). OCT1, highly expressed on the sinusoidal membrane of hepatocytes, is a prevalent liver drug uptake transporter that plays an important role in the distribution of the antidiabetic drug metformin and therefore affects its pharmacodynamics (PD). Combinations of nucleoside reverse-transcriptase inhibitors (NRTI) combinations are effective for long-term viral suppression, e.g., abacavir provided an effective and durable antiretroviral response that was noninferior to zidovudine, when combined with lamivudine and efavirenz. However, co-administered drugs cause drug-drug interactions and inhibit lamivudine uptake mediated by OCT1. **Results:** Here we report that by applying a stepped mask during single particle data processing, three near-atomic resolution cryo-EM structures of apo, endogenous substrate thiamine-bound, and inhibitor abacavir-bound OCT1 were solved to resolution 2.3~2.5Å. All the twelve transmembrane helices (TMs) and the periplasmic domain are clearly solved, while the cytoplasmic domain completely missing probably due to flexibility. The structure of OCT1-thiamine complex showed intracellular occluded state, with thiamine density clearly identified in the binding pocket of key residue L32, K215, W218, Q42, F245, etc. In the OCT1-abacavir structure, however, two abacavir molecule fully occupied the cavity, which is in consistent with previous literature that OCT1 show two binding sites for some inhibitors leading to picomolar strong inhibition (Minuesa G et al. Transport of lamivudine and high-affinity interaction of nucleoside reverse transcriptase inhibitors with human organic cation

transporters 1, 2, and 3. *J Pharmacol Exp Ther.* 2009 Apr;329(1):252-61). More specifically, binding of the two abacavir molecules not only occupied most residues identified in substrate-binding but also involved more residues e.g., Y36, Y222, W355, Q448, C451, D475. This in general, revealed in the first time the NRTIs' picomolar inhibition mechanism against OCT1. Conclusion: All the three OCT1 cryo-EM structures are solved without using nanobodies, with substrate-binding site clearly identified and inhibition mechanism of nucleotide reverse transcriptase inhibitor revealed. These new findings may help us better understand at the atomic level the drug transporter OCTs' mechanism of action, the clinical DDIs that OCTs mediated, therefore facilitate optimizing precision medicine and structure-based drug development.



P178 - PROTEIN ABUNDANCE OF DRUG TRANSPORTERS IN HUMAN HEPATITIS C LIVERS

Marek Drozdziak¹, Joanna Lapczuk-Romanska¹, Christoph Wenzel², Mateusz Kurzawski¹, and Stefan Oswald³

¹Pomeranian Medical University, Poland, ²University Medicine Greifswald, Germany, and ³Rostock University Medical Center, Germany

Transmembrane drug transport in hepatocytes is one of the major determinants of drug pharmacokinetics. In the study, ABC transporters (P-gp, MRP1, MRP2, MRP3, MRP4, BCRP, BSEP) and SLC transporters (MCT1, NTCP, OAT2, OATP1B1, OATP1B3, OATP2B1, OCT1, OCT3) were quantified for protein abundance (LC-MS/MS) and mRNA levels (qRT-PCR) in hepatitis virus C (HCV) infected liver samples from the Child-Pugh class A (n=30), B (n=21) and C (n=7) patients.

Protein levels of BSEP, MRP3, MCT1, OAT2, OATP1B3 and OCT3 were not significantly affected by HCV infection. P-gp, MRP1, BCRP and OATP1B3 protein abundances were upregulated, whereas these of MRP2, MRP4, NTCP, OATP2B1 and OCT1 were downregulated in all HCV samples. The observed changes started to be seen in the Child-Pugh class A livers, i.e. upregulation of P-gp, MRP1 and downregulation of MRP2, MRP4, BCRP and OATP1B3. In the case of NTCP, OATP2B1 and OCT1 decrease of the protein levels was evidenced in the class B livers. In the class C livers any other changes were noted than these in the class A and B patients. The results of the study demonstrate that drug transporter protein abundances are affected by functional state of the liver in hepatitis C patients.

The study was funded by Minister of Science and Higher Education (Regional Initiative of Excellence" in 2019-2022 project number 002/RID/2018/19 amount of financing 12,000,000 PLN).

P179 - CHARACTERIZATION OF THE TRANSPORTER-MEDIATED UPTAKE OF THE EXPERIMENTAL MALE CONTRACEPTIVE H2-GAMENDAZOLE**Raymond Hau**¹, Joseph Tash², Gunda Georg³, Stephen Wright¹, and Nathan Cherrington¹¹University of Arizona, United States, ²University of Kansas Medical Center, United States, and ³University of Minnesota, United States

The blood-testis barrier (BTB) is a selectively permeable membrane barrier formed by tight junctions between adjacent Sertoli cells (SCs) that protects developing germ cells from external pressures. Transporters expressed by SCs influence the disposition of drugs across the BTB and many drugs are incapable of accumulating in the male genital tract to pharmacologically relevant concentrations. The experimental male contraceptive, H2-gamendazole (H2-GMZ) is an anionic lonidamine analog that selectively accumulates >10-fold in the testes compared to other organs and elicits a potent anti-spermatogenic effect in rodents. However, the transporter-mediated mechanisms that permit H2-GMZ to bypass the BTB are unknown. This study was designed to characterize the human transporter-mediated processes that are involved in the uptake of H2-GMZ into human SCs. H2-GMZ uptake studies were performed in an immortalized human SC line (hT-SerC) using liquid chromatography-tandem mass spectrometry (LC-MS/MS). H2-GMZ followed Michaelis-Menten kinetics of transport into hT-SerCs, suggesting transporter-mediated entry. Additionally, H2-GMZ was co-incubated with known transporter inhibitors or competitive substrates to identify the responsible uptake transporter(s). H2-GMZ uptake was inhibited by >50% in the presence of 1 mM indomethacin, 1 mM diclofenac, 1 mM MK-571, and several related lonidamine analogs. Although other compounds caused statistically significant decreases in H2-GMZ uptake, these were minor compared to the compounds stated above. Interestingly, H2-GMZ uptake was stimulated by an acidic extracellular pH and reduced at higher pH values, which is characteristic of OATP-mediated transport. H2-GMZ uptake was also observed to be independent of extracellular Na⁺, K⁺, and Cl⁻ levels, which are also nonessential for the OATPs. Unfortunately, expression of the endogenous transporters that transport H2-GMZ into native CHO, MDCK, and HEK-293 cells facilitates even greater uptake capacity than hT-SerCs, thus limiting the viability of overexpressed transporter studies in these native cell lines. Moreover, H2-GMZ uptake was partially inhibited by 1 mM indomethacin, diclofenac, or MK-571 in each of these native cell lines. The physiological characteristics of H2-GMZ transport suggest that an OATP or OATP-like transporter may be responsible for transporting this drug into human SCs. Altogether, identification of the transporters involved in the flux of H2-GMZ may provide insight into the selectivity of drug disposition across the human BTB to understand and overcome the pharmacokinetic and pharmacodynamic difficulties presented by this barrier.

P180 - PREDICTION OF DRUG-INDUCED LIVER TOXICITY USING RATIO OF PLASMA CMAX TO IC50 FOR BSEP INHIBITION**Kan He**, Emily Qian, Qin Shi, and Lining Cai*Frontage Laboratories, Inc., United States*

Bile salt export pump (BSEP) is expressed in the basolateral membrane of hepatocyte and is responsible for transporting bile salts from hepatocytes into bile flow. BSEP is the limited step in the enterohepatic circulation of bile salts. Normally, BSEP acts like a vacuum cleaner to maintain the intracellular concentrations of bile salts at very low level. Loss-of-function mutations of BSEP cause the progressive familial intrahepatic cholestasis type 2 (PFIC2). Inhibition of BSEP by drugs is associated with drug-induced liver injury (DILI). The potentials for over 200 drugs to inhibit human BSEP activity were determined using BSEPcyte®, a hepatocyte suspension-based assay format. BSEPcyte® involves incubation of a bile salt precursor cholic acid in primary hepatocytes in suspension, and LC-MS/MS determination of the glycocholic acid and/or taurocholic acid exported into incubation medium. In general, the results demonstrated that BSEPcyte® detected more most-DILI-concern drugs than the membrane vesicle assay. This was most likely because BSEPcyte® was able to detect metabolite-mediated BSEP inhibition, and retain the uptake activity in hepatocytes for accumulation of some drugs. BSEPcyte® produced physiologically relevant IC₅₀ values, which allowed us to obtain better *in vitro* and *in vivo* correlations. BSEP inhibition was highly correlated with cholestatic and mixed liver injury. The results were further analyzed with plasma C_{max}/IC₅₀ ratios. There were 25 drugs with C_{max}/IC₅₀ ratio greater than 0.1, among them 8 drugs withdrawn from the market or discontinued from further development (troglitazone, fasiniglifam, benziodarone, benzbromarone, lumiracoxib, bromfenac, ciglitazone and fipexide), 12 drugs associated with most-DILI-concern (ritonavir, deferasirox, cyclosporine, indinavir, ketoconazole, etodolac, bosentan, leflunomide, disulfiram, diclofenac, itraconazole, ticlopidine), and 5 drugs with less-DILI-concern (saquinavir, rosiglitazone, pioglitazone, chlorpromazine). In conclusion, the results in the present study demonstrated that BSEP inhibition was highly associated with cholestatic and mixed DILI, and the C_{max}/IC₅₀ ratio > 0.1 was associated with severe DILI.

P181 - PREDICTION OF DRUG-INDUCED LIVER TOXICITY USING RATIO OF PLASMA CMAX TO MDR3 IC50**Kan He**, Emily Qian, Qin Shi, and Lining Cai*Frontage Laboratories, Inc., United States*

MDR3 is one of the few human hepatic transporters whose loss-of-function mutations cause liver failure and early death. MDR3 is responsible for transporting phosphatidylcholine (PC) from inner leaflet to outer leaflet of hepatocyte plasma membrane. The PC of the outer leaflet is extracted by bile salt micelles, which further forms the mixed micelles with cholesterol. The mixed micelles are excreted into bile flow. Inhibition of MDR3 activity by drugs is associated with drug induced liver injury (DILI). In the present study, the potentials for over 200 drugs to inhibit MDR3 activity were determined using MDR3cyte® assay format. This assay format involved incubation of d9-choline with human primary hepatocytes, activation of MDR3 with bile salt micelles and LC-MS/MS determination of d9-PC species which were transported into incubation medium. There were two major PC species transported from human hepatocytes to the extracellular medium, which was consistent with the major PC species in human bile. For all drugs causing MDR3 inhibition with IC50 < 100 µM, the plasma Cmax/IC50 ratio of the most-DILI-concern drugs were much higher than the no-DILI-concern drugs. There were 18 drugs with Cmax/IC50 ratio of 0.2, among them 9 drugs withdrawn from market (benzbromarone, benzarone, benziodarone, troglitazone, benoxaprofen, pirofen, zimeldine, ebrotidine, tasosartan), 8 drugs with boxed warning (tipranavir, pazopanib, ketoconazole, leflunomide, nefazodone, lapatinib, tolcapone and methotrexate, and 1 drug with warnings and precautions (ritonavir). In conclusion, the results from the present study demonstrated that MDR3 inhibition was highly associated with DILI, and the plasma Cmax/IC50 ratio > 0.2 was associated with severe DILI.

P182 - EVALUATION OF REMDESIVIR AS A POTENTIAL SUBSTRATE OF OATP1B1, P-GP, MRP1, AND MRP2 IN VITROM. Rasheduzzaman Jony, **Jae-Gook Shin**, Saurav Howlader, Phuoc Long Nguyen, and Yong-Soon Cho*Inje University College of Medicine, South Korea*

Remdesivir (RDV) has been demonstrated as an effective treatment for SARS-CoV-2. RDV is known to experience a significant first-pass effect [1] indicating a considerable uptake into the liver. RDV is primarily excreted through the renal route [1, 2], with tubular secretion having a considerable role. Therefore, it is crucial to investigate the role of hepatic and renal transporters in the disposition of RDV. Cellular uptake and the bidirectional assay were conducted using different cell lines stably transfected with P-glycoprotein (P-gp), breast cancer resistance protein (BCRP), multidrug resistance protein 1 and 2 (MRP1 and MRP2), bile salt export pump (BSEP), organic anion transporting polypeptide 1B1, 1B3 and 2B1 (OATP1B1, OATP1B3 and OATP2B1), organic cation transporter 1 and 2 (OCT1 and OCT2), sodium taurocholate co-transporting polypeptide (NTCP) and organic anion transporter 1 and 3 (OAT1 and OAT3). The concentration within the cell was then quantified using liquid chromatography with tandem mass spectrometry (LC-MS/MS). The amount of protein within the cells was quantified using the Bradford protein assay. The substrate kinetics parameters of RDV for transporters were estimated using the Michaelis-Menten equation with a nonlinear regression model. Uptake studies suggested that not only OATP1B1 and P-gp but also MRP1 and MRP2 accept RDV as a substrate. The transport of RDV by each transporter was markedly attenuated by the representative inhibitors, confirming the involvement of the corresponding transporters. The Km and Vmax value of RDV was estimated to be $6.21 \pm 1.9 \mu\text{M}$ and $128.3 \pm 3 \text{ pmol/min/mg protein}$ for OATP1B1, $9.89 \pm 2.47 \mu\text{M}$ and $63.70 \pm 14.69 \text{ pmol/min/mg protein}$ for P-gp, $40.56 \pm 4.72 \mu\text{M}$ and $96.78 \pm 24.18 \text{ pmol/min/mg protein}$ for MRP1, $22.91 \pm 7.78 \mu\text{M}$ and $543.73 \pm 57.61 \text{ pmol/min/mg protein}$ for MRP2, respectively. The data suggested that RDV is a potential substrate of OATP1B1, P-gp, MRP1 and MRP2 membrane transporters. These findings partially help explain the hepatic and renal disposition of RDV mechanistically.

References:

1. Yang, K., What Do We Know About Remdesivir Drug Interactions? *Clin Transl Sci*, 2020. 13(5): p. 842-844.
2. Hanafin, P.O., et al., A mechanism-based pharmacokinetic model of remdesivir leveraging interspecies scaling to simulate COVID-19 treatment in humans. *CPT Pharmacometrics Syst Pharmacol*, 2021. 10(2): p. 89-99.

P183 - INFLUENCE OF KNOCKOUT AND HUMANIZATION OF SLCO2B1 ON ATORVASTATIN DISPOSITION IN RATS**Jonny Kinzi**, Janine Hussner, Isabell Seibert, Simone Zuercher, Marta Rysz, Mirubagini Vythilingam, Oliver Schwardt, Daniel Ricklin, and Henriette Meyer zu Schwabedissen*University of Basel, Switzerland*

The organic anion transporting polypeptide (OATP) 2B1 is a transmembrane protein facilitating the disposition of molecules across cell membranes. OATP2B1 is a member of the SLCO family and is expressed throughout the human body with the highest abundance in liver [1, 2]. Previous *in vitro* data showed OATP2B1 to be involved in the transport of

various endogenous and xenobiotic molecules. However, there is still limited understanding of its *in vivo* relevance. Hereby, we report on the pharmacological phenotype of Slco2b1-knockout (Slco2b1^{-/-}) and hSLCO2B1-knockin (hSLCO2B1^{+/+}) rats assessed with the substrate atorvastatin. In detail, male rats received 2 mg/kg i.v. or 10 mg/kg p.o. of atorvastatin, respectively, and blood samples were collected over 24 hours via an implanted jugular vein catheter. Serum levels of atorvastatin were quantified using a validated LC-MS/MS method and pharmacokinetic parameters were estimated by non-compartmental analysis. Investigating the influence of OATP2B1 on systemic levels after oral administration, our findings showed a trend towards 20% higher AUC in hSLCO2B1^{+/+} compared to Slco2b1^{-/-} rats, while the apparent clearance CL/F was slightly decreased. Although it is assumed that OATP2B1 contributes to the hepatic anion elimination route, the obtained data did not support that. In a subsequent assessment of i.v. atorvastatin pharmacokinetics, humanized rats showed a 57% increase in CL in comparison to Slco2b1-knockout rats. Interestingly, we also observed a significant decrease in AUC by approximately 40% in hSLCO2B1^{+/+} compared to Slco2b1^{-/-} rats. No impact was observed comparing wildtype and Slco2b1^{-/-} animals. During the initial phase after dosing, OATP2B1 expressing animals showed lower serum levels, which led us to investigate atorvastatin tissue distribution. In hSLCO2B1^{+/+} animals, atorvastatin liver levels were significantly decreased by 41% after 1 hour of i.v. dosing, although OATP2B1 is expected to facilitate its hepatic uptake. Previously published data highlighted the pivotal role of hepatic Mdr1a/b, Bcrp and Cyp3a1/Cyp3a2 as determinants of systemic atorvastatin levels [3]. Quantification of their expression and abundance in the liver revealed a significant increase of Cyp3a1 in hSLCO2B1^{+/+} rats. This may explain the reduced amounts of atorvastatin in the liver of those animals. In conclusion, our data indicate a role of OATP2B1 in the *in vivo* handling of atorvastatin and an impact of OATP2B1 on the expression and activity of hepatic Cyp3a1 in rats. Further studies involving the novel rat models are warranted to decipher the underlying mechanism.

References:

1. Kinzi, J., M. Grube, and H. E. Meyer Zu Schwabedissen. "Oatp2b1 - the Underrated Member of the Organic Anion Transporting Polypeptide Family of Drug Transporters?". *Biochem Pharmacol* 188 (Jun 2021): 114534.
2. McFeely, S. J., L. Wu, T. K. Ritchie, and J. Unadkat. "Organic Anion Transporting Polypeptide 2b1 - More Than a Glass-Full of Drug Interactions." *Pharmacol Ther* 196 (Apr 2019): 204-15.
3. Wang, Z., H. Yang, J. Xu, K. Zhao, Y. Chen, L. Liang, P. Li, et al. "Prediction of Atorvastatin Pharmacokinetics in High-Fat Diet and Low-Dose Streptozotocin-Induced Diabetic Rats Using a Semiphysiologically Based Pharmacokinetic Model Involving Both Enzymes and Transporters." *Drug Metab Dispos* 47, no. 10 (Oct 2019): 1066-79.

P184 - CHARACTERIZATION OF NONCLINICAL DRUG METABOLISM AND PHARMACOKINETIC PROPERTIES SHOWS CONSISTENCY AMONG THREE PHOSPHORODIAMIDATE MORPHOLINO OLIGONUCLEOTIDES FDA-APPROVED FOR DUCHENNE MUSCULAR DYSTROPHY

Marie Claire Mukashyaka, Yogesh Patel, Peter Burch, Bridge Hunter, Louise R. Rodino-Klapac, and Lilly East
Sarepta Therapeutics, Inc., United States

Eteplirsen, golodirsen, and casimersen are phosphorodiamidate morpholino oligomers (PMOs) approved by the FDA for the treatment of Duchenne muscular dystrophy (DMD) in patients with mutations amenable to 51, 53, and 45 exon skipping, respectively. In general, the drug metabolism and pharmacokinetic (DMPK) properties of anti-sense oligonucleotides are not well characterized. During the development of eteplirsen, golodirsen and casimersen, DMPK properties of all three PMOs were evaluated, inclusive of plasma protein binding, metabolic stability, and interactions with cytochrome P450 (CYP) isoforms and membrane-bound drug transporters. Additionally, nonclinical distribution, metabolism, and excretion profiles of the PMOs were quantified in radiolabelled mass balance mouse studies. In mouse, rat, nonhuman primate (NHP), and human plasma the average percentage of plasma protein binding for all three PMOs was low and concentration independent rendering favorable tissue bioavailability particularly to highly perfused tissues (eteplirsen, 21.6%, 7.7%, 3.7% 13.3%; casimersen, 17%, 21.1%, 13%, 21.8%; golodirsen, 36.2%, 20.1%, 35.7%, 36.9%). None of the PMOs were found to be substrates, inhibitors, or inducers of human CYP enzymes (CYP1A2, CYP2B6, CYP2C8, CYP2C9, CYP2C19, CYP2D6, and CYP3A4/5) or of membrane drug transporters (OAT1, OAT3, OCT1, OCT2, OATP1B1, OATP1B3, MATE-1, MATE2-K, P-gp, BCRP, MRP2, or BSEP) at clinically relevant concentrations. These findings suggest minimal drug-drug interaction liability following acute and chronic PMO therapy. Following intravenous drug administration, the 3 PMOs demonstrated a dose proportional plasma PK (5 to 320 mg/kg in NHPs; 100 to 900 mg/kg in rats). The plasma concentration-time profile appeared biphasic across all PMOs with a rapid distribution phase followed by a longer terminal elimination phase. Estimated half-life for eteplirsen was 1.9–3.7 h and 1.9–4.6 h in rat and NHP, for casimersen 1–20.8 h, 8.7–12.4 h, and 1.4–6.7 h in mouse, rat and NHP, and for golodirsen 0.6–4.7 h, 2.7–11.6 h and 1.7–8.7 h in mouse, rat and NHP. The tissue biodistribution profile in mdx mice appeared similar across the three PMOs with extensive drug exposure quantified in the target muscle tissues and the highest level of drug exposure observed in the kidney. In mdx mice, renal excretion (mean recovery through 336 hours post-dose: eteplirsen, 32.3%; casimersen, 68.9%; golodirsen, 74.9%) was the primary route of elimination followed by fecal elimination (mean recovery

through 336 hours post-dose: eteplirsen, 22.1%; casimersen, 12.5 %; golodirsen, 9.6%). Consistent with the metabolic stability observed in microsomal incubations, PMOs were the only components identified in mouse plasma and urine. Collectively, the current body of work showcases the most comprehensive nonclinical PK evaluations of PMOs and highlights key DMPK features that are consistent across the PMO drug class. Importantly, these findings provide confirmatory evidence to the PMO drug class concept, which can be leveraged to accelerate and optimize future development of PMO exon skipping drug candidates.

P185 - WHY IS THE SYSTEMIC EXPOSURE OF DUAL CYP3A AND OATP SUBSTRATES GREATLY AFFECTED IN HEPATIC IMPAIRMENT? INSIGHTS FROM THE EXTENDED CLEARANCE MODEL

Flavia Storelli¹, **Mayur K. Ladumor**¹, Mayur, Xiaomin Liang², Yurong Lai², Paresh Chothe³, Osatohanmwun Enogieru⁴, Raymond Evers⁵, and Jashvant Unadkat¹

¹University of Washington, United States, ²Gilead Sciences Inc., United States, ³Takeda, United States, ⁴Amgen, United States, and ⁵Janssen Research & Development, LLC, United States

Introduction: Hepatic impairment (HI) significantly affects the systemic exposure (i.e. area-under-the-plasma concentration-time-curve, AUC) of drugs that are primarily cleared by the hepatic organic anion transporting polypeptides (OATPs) and biliary transporters (AUC increased <5-fold). However, this effect is even greater (AUC increased > 10-fold) for drugs that are dual substrates of hepatic OATPs and cytochrome P450 (CYP) 3A enzymes. Therefore, the aim of this study was to gain insight into the mechanism(s) underlying this difference using the Extended Clearance Model (ECM). **Methods:** Using the ECM and physiological changes in HI (retrieved from Simcyp version 21, Certara), we simulated the effect of HI on the AUC of IV-administered hypothetical OATP-substrates with negligible renal CL under the following two conditions: 1) when OATP-mediated uptake was the rate-determining step (RDS) in CLH of a drug (RDSCL,h = uptake), i.e. when sinusoidal efflux intrinsic clearance (CL_{int,s,ef}) is << sum of metabolic and biliary intrinsic clearances (CL_{int,met+bile}); and 2) when all the hepatobiliary clearances were the RDS (RDSCL,h=all), i.e., when CL_{int,s,ef} is >> CL_{int,met+bile}. Furthermore, to incorporate the effect of HI on gut CYP3A metabolism, we simulated the effect of HI on the AUC of orally administered atorvastatin (a dual OATP and CYP3A substrate) using previously reported hepatobiliary intrinsic clearances estimates. Then, we performed sensitivity analyses to identify potential factors contributing to the increase in atorvastatin AUC observed in HI (10-fold). **Results:** Our simulations revealed the following: first, the effect of HI on the AUC of OATP-transported drugs was larger when RDSCL,h=all vs. RDSCL,h=uptake. This is because, in HI, the decrease in hepatic CYP3A abundance is greater than that of OATP abundance. Second, when RDSCL,h=all, the magnitude of the HI effect on the AUC of drugs was sensitive to the CL_{int,s,ef}/CL_{int,met+bile} ratio; the greater the drug's CL_{int,s,ef}/CL_{int,met+bile} ratio in the absence of HI, the greater the impact of HI on AUC. Importantly, when RDSCL,h=all, the directionality (i.e., increase/decrease) of the HI effect on CL_{int,s,ef} (e.g., efflux by MRP3) significantly affected the AUC of OATP-substrate drugs. Third, the greater the contribution of metabolism vs. biliary efflux to CL_{int,met+bile}, the greater the effect of HI on the AUC of the drug. This is because, in HI, the decrease in hepatic CYP3A abundance is greater than that of biliary efflux transporters. This explains the larger HI effect on the AUC of extensively metabolized OATP substrates vs. OATP substrates mostly excreted unchanged in the bile. Fourth, the effect of HI was amplified for orally administered drugs that are extensively metabolized in the gut (i.e., low fraction escaping gut metabolism, F_g) because HI also reduces gut CYP3A abundance. **Conclusions:** The ECM can help understand the factors that drive the large changes in AUC of dual OATP and CYP3A substrates in HI. This work highlights the importance of accurately quantifying all hepatobiliary clearances, including CL_{int,s,ef}, to predict the effect of HI on the AUC of OATP substrates.

Funding: Supported by the University of Washington Research Affiliate Program on Transporters (UWRAPT) funded by Gilead Sciences, Takeda, Amgen and Janssen

P186 - ABSTRACT WITHDRAWN

P187 - QUANTITATIVE EXPRESSION OF LIPID AND NUCLEOSIDE TRANSPORTERS IN LUNG TISSUES FROM HUMAN, RAT, DOG AND CYNOMOLGUS MONKEY

Congrong Niu, Xiaodong Xie, Xiaomin Liang, and Yurong Lai
Gilead Sciences, United States

Objective: Lung transporters play critical roles in both physiological function and drug distribution. For example, the adenosine triphosphate (ATP)-binding cassette (ABC) subfamily A transporters are involved in lipid transport and play a distinct role in lipid homeostasis. The alveolar surfactant in the lung, a mixture of phospholipids, cholesterol, and hydrophobic proteins, can reduce surface tension and stabilize alveoli during respiration. Therefore, disruptions of the transporter functions can result in the surfactant dysfunction that can be implicated in the pathophysiology of several alveolar and airway diseases. On the other hand, nucleoside analog drugs that are currently used in the treatment of

cancers and viral infection are hydrophilic molecules with poor passive diffusion across cell membranes. The distribution of nucleoside analog drugs relies on solute carrier families 28 and 29 (SLC28 and SLC29) that encode concentrative and equilibrative nucleoside transporter proteins, respectively. Since animal models are routinely used to delineate the efficacy, pharmacokinetic profile and general safety, current investigation was to quantitatively determine the expressions of lipid and nucleoside transporters in the lung. The findings can be informative to interpret drug distribution and toxicity data for the translation from preclinical species to human.

Methods: The total membrane proteins were extracted from human, monkey, dog, and rat lung tissues using Native Membrane Protein Extraction Kit (Sigma-Aldrich), and subsequently treated with dithiothreitol (DTT) and iodoacetamide (IAA) followed by the digestion of trypsin. The amounts of transporter proteins were quantified using a Sciex 7500 triple-quadruple mass spectrometer coupled to a Shimadzu LC (SLC-30A) system with optimized ionization conditions. The Na⁺/K⁺ ATPase levels in the lung were measured as the membrane protein marker. Total RNA was isolated from lung tissues using a Qiagen RNeasy kit. The mRNA levels were measured by RT-qPCR. β -actin was used to normalize target gene expression.

Results and conclusion: In the current investigation, three lipid and seven nucleoside transporters were characterized. mRNA and protein levels of these transporters across species were detected by RT-qPCR and targeted quantitative proteomics methods respectively. The mRNA expression pattern agrees with the protein expression. However, no quantitative correlation can be drawn between mRNA and protein expression. The expressions of ABCA1, ABCA3 and ABCG1, the ABC transporters that are the regulators of cellular cholesterol and phospholipid homeostasis, were detected in all tested species, and found to be highest in rat. The most concentrative nucleoside transporters (CNT1/2/3) were not detectable in lung tissues except CNT1 and CNT3 were detected in rat and human respectively. Among the equilibrative nucleoside transporters (ENT1/2/3), ENT1 had highest expression across species and the expression levels in dog and rat lung tissues were much higher than those in human and monkey. Comparison of the transporter expressions across species can be useful to interpret the drug distribution of nucleoside analog drugs, and the lipid homeostasis data tested in preclinical species, and aid drug development for the treatment of pulmonary disease.

P188 - PROTEIN-MEDIATED UPTAKE EFFECT ON THREE INTESTINAL UPTAKE TRANSPORTERS SHOWS SUBSTRATE AND PH-DEPENDENT INTERACTIONS

Md Masud Parvez, Armin Sadighi, Anitha Police, and Julius O. Enoru
Abbvie Biotherapeutics, United States

Protein-mediated uptake effect (PMUE) is an emerging 'black box' in in-vitro drug-drug interaction studies and in-vitro to in-vivo extrapolations. It is known that pH can have an impact on the activity of intestinal transporters. To date, several studies have utilized plasma protein in in-vitro drug-drug interaction studies to improve the power of IVIVE. Unbound and "total IC50" concepts have also been proposed based on the concept of IC50 shift in the presence or absence of plasma protein. In this study, we investigated the effect of pH and protein on the uptake efficiency of three intestinal uptake transporters - organic anion-transporting polypeptide (OATP)-2B1, peptide transporter 1 (PEPT1), peptide transporter 2 (PEPT2) for their fluorescent and radiolabeled probe substrates. Recombinant HEK293 cells (OATP2B1, PEPT1 and PEPT2) were investigated for uptake of fluorescent (4',5'-dibromofluorescein (fDBF), fluorophore-conjugated dipeptide, β -Ala-Lys-N-7-amino-4-methylcoumarin-3-acetic acid (AMCA)), and radiolabeled ([³H]estrone 3-sulphate and [³C]glycyl-sarcosine (Gly-Sar)) substrates, under different experimental conditions – pH, presence and absence of 4% v/v human serum or 4% w/v bovine serum albumin (BSA). In addition, the inhibitory effect of erlotinib (OATP2B1) and losartan (PEPT1 and PEPT2) under these experimental conditions was investigated.

The results for fDBF uptake into HEK-OATP2B1 show 4-fold higher uptake at pH 6.5 compared to pH 7.4. In addition, at pH 6.5 the fDBF uptake was decreased to 2-fold in the presence of 4% BSA. Meanwhile no significant change in uptake was observed using 4% HSA. Moreover, erlotinib inhibited OATP2B1-mediated fDBF, increasing the IC50 by 8-fold in the presence of 4% BSA versus no BSA at pH 6.5. On the other hand, a 5-fold lower OATP2B1 mediated uptake of radiolabeled substrate [³H]ES was observed in the presence of 4% BSA vs no BSA at pH 6.5. Under these conditions, erlotinib inhibited [³H]ES uptake resulting in approximately 6-fold IC50 shift. Similarly, PEPT1 mediated fAMCA uptake was 4.3-fold higher at pH 6.5 compared to pH 7.4. Losartan, a known PEPT1 inhibitor decreased fAMCA uptake by approximately 2.8-fold in the presence of 4% BSA versus "no BSA". Consistent with PEPT1, fAMCA showed 6-fold higher uptake and 2-fold increase in losartan IC50 for PEPT2 in the presence of 4% BSA. In contrast, uptake of the radiolabeled substrate [¹⁴C]Gly-Sar did not show any significant differences in the presence or absence of 4% BSA, and neither was the inhibitory effect by losartan affected. Together, these findings suggest the importance of different experimental conditions and substrate selectivity for the intestinal uptake transporters-mediated study. This information could be very valuable in designing an *in vitro* intestinal uptake transporter DDI studies and proof valuable for performing precise *in vivo* extrapolations.

P189 - EVIDENCE OF ALBUMIN-MEDIATED UPTAKE PHENOMENON WITH RENAL ORGANIC ANION TRANSPORTER 1

Shawn Pei Feng Tan, Susan Murby, Amin Rostami-Hodjegan, Daniel Scotcher, and Aleksandra Galetin
University of Manchester, United Kingdom

The inclusion of human serum albumin (HSA) or plasma has been reported to increase the unbound intrinsic uptake clearance ($CL_{int,u}$) of highly bound substrates of hepatic transporters [1,2]. However, limited evidence is available for the relevance of albumin-mediated uptake for renal transporters. In this study, conditionally immortalised proximal tubular epithelial cells transduced with organic anion transporter 1 (OAT1) were utilised to investigate the albumin-mediated uptake effect. Two OAT1 probes were investigated, adefovir (clinical OAT1 probe, $f_u,p = 0.98$) and 4-pyridoxic acid (PDA, OAT1/3 endogenous biomarker, $f_u,p = 0.081$). Uptake of PDA was measured in the absence and presence of HSA at 0.5, 1.0, 2.0 and 4.0%, coupled with parallel measurements of fraction unbound in the incubation buffer. Two experimental designs were compared, either keeping total or unbound PDA concentration constant in the presence of 0.5 – 4.0% HSA. In both cases, the addition of HSA led to similar effects to the $CL_{int,u}$. In comparison to the control scenario (no albumin), at 1 and 4% HSA, $CL_{int,u}$ increased by 1.5 and 2.7-fold (total PDA constant) and 2.0 and 3.2-fold (unbound PDA constant) respectively. The addition of unbound 300 μ M probenecid to the 1% HSA condition led to a 7-fold decrease to the $CL_{int,u}$, confirming the presence of albumin-mediated uptake phenomenon and rules out the possibility that this was caused by non-specific binding of HSA-bound PDA. The inclusion of 1% HSA resulted in 1.6-fold increase in adefovir $CL_{int,u}$ versus the control condition, opposite to expectations of no effect for highly unbound drugs like adefovir [2]. This highlights the need for including highly unbound drugs when evaluating the albumin-mediated uptake phenomenon. In conclusion, this study has confirmed the presence of an albumin-mediated uptake effect with a highly-protein bound endogenous substrate of OAT1/3. Keeping total or unbound PDA concentration constant between the various HSA concentrations led to similar effects on the fold-change of PDA $CL_{int,u}$, but the latter benefits from better analytical sensitivity. Studies investigating the effect on a larger range of OAT1/3 substrates with various extents of protein binding are ongoing.

References:

1. Miyauchi S, Kim SJ, Lee W, et al. Consideration Of Albumin-Mediated Hepatic Uptake For Highly Protein-Bound Anionic Drugs: Bridging The Gap Of Hepatic Uptake Clearance Between In Vitro And In Vivo. *Pharmacol Ther.* 2022 Jan;229:107938.
2. Francis LJ, Houston JB, Hallifax D. Impact of Plasma Protein Binding in Drug Clearance Prediction: A Data Base Analysis of Published Studies and Implications for In Vitro-In Vivo Extrapolation. *Drug Metab Dispos.* 2021 Mar;49(3):188-201.

P190 - RAT AS A MODEL FOR PREDICTING HUMAN RENAL ORGANIC ANION TRANSPORTER-MEDIATED DRUG-DRUG INTERACTIONS

Aarzo Thakur, Vijaya Mettu, James T. Nguyen, Mary F. Paine, and Bhagwat Prasad
Washington State University, United States

The use of endogenous metabolites as transporter biomarkers to predict transporter-mediated drug-drug interactions (DDIs) is emerging, with the goal of facilitating safe and cost-effective drug development. Organic anion transporters (OAT/Oat1/3) are solute carrier transporters expressed on the basolateral membrane of kidney proximal tubule cells, facilitating the uptake of several drugs and endogenous metabolites for renal secretion. Inhibition of OAT1/3 by probenecid in human participants has been associated with elevated plasma concentrations of various endogenous metabolites, including pyridoxic acid and kynurenic acid.^{1,2} The objective of this study was to evaluate whether changes in putative Oat biomarkers in rat blood and urine due to transporter inhibition can be extrapolated to OAT activity in humans. We conducted a pharmacokinetic DDI study in rats ($n=6$) involving the OAT/Oat substrate furosemide (5 mg/kg i.v.) and inhibitor probenecid (10 mg/kg i.v.). Blood and urine were collected from 0-8 h and analyzed for furosemide, probenecid, pyridoxic acid, kynurenic acid, and creatinine by liquid-chromatography tandem mass spectrometry (LC/MS/MS). In the absence of probenecid, average (\pm S.D.) furosemide area under the blood concentration-time curve (AUC) was 40 ± 7 and 47 ± 7 μ M \cdot h in female and male rats, respectively. Whereas, furosemide AUC more than doubled in female and male rats (235 ± 94 versus 105 ± 21 μ M \cdot h) in the presence of probenecid. The higher AUC in females can be attributed to elevated probenecid blood concentrations, which was likely due to lower probenecid renal elimination, leading to the higher magnitude of interaction. In the presence of probenecid, at 1 h, furosemide blood concentration correlated with pyridoxic acid ($r^2=0.97$) and kynurenic acid ($r^2=0.78$) concentration. These observations suggest that pyridoxic acid or kynurenic acid blood concentrations may be used to predict changes in furosemide (or potentially other drug substrate) blood concentrations upon Oat inhibition. Average renal clearance (CL_{renal}) ratio, calculated as the ratio of CL_{renal} in the presence to absence of probenecid, for furosemide, pyridoxic acid, kynurenic acid, and creatinine was 0.35, 0.73, 0.77, and 0.95, respectively, consistent with the literature supporting the utility of pyridoxic acid and kynurenic

acid as biomarkers of OAT1/3.1,2 The AUC of furosemide, pyridoxic acid, kynurenic acid, and creatinine measured in two human participants from an ongoing clinical probenecid-furosemide DDI study were at least 2.2, 2.3, 1.7, and 1.2 -fold higher, respectively, in the presence of probenecid. The average CLrenal ratio for furosemide, pyridoxic acid, kynurenic acid, and creatinine in these participants was 0.41, 0.60, 0.73, and 1.00, respectively, consistent with the rat data. The similar CLrenal ratios between rats and humans suggest that the rat may be a useful model to predict OAT-mediated DDIs in humans. If these trends hold for all 16 participants in this powered clinical study, results from the controlled rat study could be used to identify a panel of metabolites as OAT biomarkers, which in turn would normalize the inter-individual variability in one or more biomarkers.

This work was supported by NIH/NICHD R01HD081299.

References:

1. Shen et al., J Pharmacol Exper Therapeut, 368(1), 136-145.
2. Tang, J. et al., 2021. Drug Metab Dispos, 49(12), 1063-1069.

P191 - IDENTIFICATION OF PUTATIVE ORGANIC ANION TRANSPORTER 2 INHIBITORS: SCREENING, STRUCTURE-BASED ANALYSIS AND CLINICAL DRUG INTERACTION RISK ASSESSMENT

Sangwoo Ryu¹, Nathaniel Woody², and Manthena Varma¹
Pfizer, United States and ²Pfizer, Switzerland

Organic anion transporter 2 (OAT2 or SLC22A7), located primarily in the liver and kidney, play an important role in the hepatic uptake and renal secretion of several endogenous compounds and drugs. The goal of this work is to understand the structure activity of OAT2 inhibition and assess drug interaction risk at clinical doses. To this end, we initially employed a single-point *in vitro* screen to investigate the inhibition potential of about 150 drugs and drug-like compounds on OAT2-mediated cGMP transport. This single-point inhibition data was used to develop a quantitative structure-activity relationship (QSAR) model to predict OAT2 inhibition based on physicochemical properties and chemical structures. Inhibitors identified in the single-point screening assay were subsequently assessed to obtain inhibition potency (IC50) values. DDI risk potential to modulate hepatic and renal OAT2 transport were estimated based on static DDI models, and several drugs were identified as potential inhibitors at clinical doses. About half the compounds screened showed >50% inhibition at 300µM concentration; and for these 'inhibitors', concentration-dependent inhibition potency (IC50) was measured. Acids represented about 65% of all putative inhibitors, and the frequency of bases-plus-zwitterions almost doubled for 'non-inhibitors'. Interestingly, 9 of the 10 compounds with most potent inhibition (i.e., low IC50) are acids with pKa in the range of 3-5. In contrast, weakest inhibitors (non-inhibitors) possessed a basic amine with pKa in the range of 8-9. Additionally, inhibitors are significantly larger and lipophilic than non-inhibitors. *In silico* (binary) models were developed to identify inhibitors and non-inhibitors. Finally, *in vivo* OAT2 inhibition risk was assessed via static drug-drug interaction (DDI) models based on unbound maximum plasma concentration (Imax,u) or unbound maximum liver inlet concentration (lin,max,u) and IC50. Within the identified inhibitors, several compounds showed an Imax,u/IC50 ratio >0.1 and lin,max,u/IC50 >1.25 suggesting potential for *in vivo* renal and hepatic OAT2 inhibition, respectively, at clinical doses. In conclusion, this is the first study assessing global inhibition pattern of OAT2-ligand interactions and subsequently identifying potential *in vivo* inhibitors of OAT2.

P192 - EVALUATION OF THE TRANSWELL SYSTEM AS A NEW TOOL TO PREDICT ORGANIC CATION TRANSPORTER 2 (OCT2) AND MULTIDRUG AND TOXIN EXTRUSION PROTEINS (MATES) MEDIATED RENAL DDI

Leticia S. Vieira and Joanne Wang
University of Washington, United States

The renal organic cation (OC) secretion system is one of the major systems of xenobiotic renal transport, consisting of the Organic Cation Transporter 2 (OCT2) and Multidrug and Toxin Extrusion proteins (MATEs). OCT2 and MATEs are recognized by regulatory agencies as an important site for drug-drug interactions (DDIs), which can impact systemic and intrarenal exposure of drugs, potentially playing a role in nephrotoxicity of compounds [1]. Currently, predictions for transporter-mediated DDIs are often analyzed using maximum unbound inhibitor plasma concentration (Imax,u) and IC50/Ki values determined through *in vitro* uptake experiments in single transporter-transfected cell lines. However, while the methodology is simple and straightforward, emerging evidence suggests this approach frequently leads to false prediction of renal transporter-mediated DDIs, especially for the MATEs [2]. Previous studies from our laboratory have suggested that MATE inhibitors act on the transporter intracellularly under physiological conditions [3], and therefore inhibitor accessibility to intracellular space is an important factor that is rarely considered when estimating the inhibitory potential towards MATEs in single transporter-transfected system. We hypothesize that the transwell system using hOCT2/hMATE1 double-transfected MDCK cells represents a more physiologically relevant system to assess

hOCT2/hMATE1-mediated DDIs in comparison to single transporter-transfected cell lines. Although this system has been used to study transepithelial flux of hOCT2/hMATE1 substrates, its potential in quantitatively predicting renal drug DDIs still has to be explored. In this study, we have explored the use of a transwell system employing hOCT2/hMATE1 double-transfected MDCK cells as a tool to better understand the inhibition kinetics of the OC secretion system, while taking in account inhibitor accessibility to its site of interaction and the interplay between hOCT2 and hMATE1 transporters. Our data revealed that potent inhibition of hMATE1 seen *in vitro* using simple uptake experiments may not necessarily translate into inhibition in the transwell system. This corroborates the hypothesis that inhibitor accessibility to intracellular space is crucial for MATE inhibition. In addition, compared to predictions using IC₅₀ determined from single-transfected hOCT2 or hMATE1 cell lines, our results show that the apparent IC₅₀ values estimated from our transwell experiments were able to better predict the observed impact of classic MATE inhibitors in *in vivo* DDI studies. In summary, the study of inhibitors using hOCT2/hMATE1 double-transfected cell line in a transwell system represents a promising approach to investigate the inhibitory potential of compounds towards renal organic cation transporters and has the potential to improve the prediction of *in vivo* MATE-mediated renal DDIs.

References:

1. Yin J, Wang J. Renal drug transporters and their significance in drug-drug interactions. *Acta Pharm Sin B*. 2016 Sep;6(5):363-373. <https://doi.org/10.1016/j.apsb.2016.07.013>.
2. Krishnan S, Ramsden D, Ferguson D, Stahl SH, Wang J, McGinnity DF, Hariparsad N. Challenges and Opportunities for Improved Drug-Drug Interaction Predictions for Renal OCT2 and MATE1/2-K Transporters. *Clin Pharmacol Ther*. 2022 May 22. Epub ahead of print. <https://doi.org/10.1002/cpt.2666>.
3. Yin J, Duan H, Wang J. Impact of Substrate-Dependent Inhibition on Renal Organic Cation Transporters hOCT2 and hMATE1/2-K-Mediated Drug Transport and Intracellular Accumulation. *J Pharmacol Exp Ther*. 2016 Dec;359(3):401-410. <https://doi.org/10.1124/jpet.116.236158>.

P193 - DRUG-DRUG INTERACTION POTENTIAL OF PHARMACEUTICAL EXCIPIENTS ON UPTAKE AND EFFLUX TRANSPORTERS

Megan Graves¹, Acilegna Rodriguez¹, Yewei Du¹, Ilene Kaufman¹, Robert Taylor¹, Isabelle Ragueneau-Majlessi², Jingjing Yu², Joseph Polli³, and **Mark Warren**¹

¹BioIVT, United States, ²UW Drug Interaction Solutions, United States, and ³ViiV Healthcare, United States

Pharmaceutical excipients are often considered to be inert in oral drug formulations as they do not convey therapeutic properties or safety risks, and as such are not routinely required for drug-drug interaction (DDI) testing under current regulatory guidelines. However, these excipients may inhibit drug transporters expressed in the gastrointestinal tract where the highest concentrations of excipients will occur, which can alter the pharmacokinetics of the active pharmaceutical ingredients. Excipient-mediated inhibition of uptake transporters, such as OATP2B1, could potentially decrease drug absorption, limiting the oral bioavailability and efficacy of pharmaceuticals that are substrates of OATP2B1. In contrast, excipient-mediated inhibition of efflux transporters, such as BCRP and P-gp, could potentially increase the oral bioavailability of drugs that are substrates of these efflux transporters, increasing unwanted safety effects. This work investigated the effects of 46 common excipients, from various chemical classes, on these transporters, using concentrations consistent with the dosage allowed in oral formulations as described in the FDA's excipient database (<https://www.accessdata.fda.gov/scripts/cder/iig/index.cfm>). Inhibition assays were conducted in MDCK-II cells expressing OATP2B1, BCRP, or P-gp. DDI studies were conducted by incubating cells with a probe substrate and various concentrations (n=6 in triplicate) of the excipients and measuring inhibition of transporter-dependent uptake (for OATP2B1) or efflux (for BCRP and P-gp). To ensure that the effects on efflux transporters were due to excipient-mediated inhibition as opposed to cell monolayer disruption, cell monolayer integrity was also monitored using the paracellular permeability marker mannitol. Results showed that several excipients, such as capsaicin, glycerol monolinoleate, oleanolic acid, polyethylene glycol 300, and soybean lecithin, were found to selectively inhibit the efflux transporters with no or minimal inhibition of OATP2B1. For capsaicin, the IC₅₀ values were 12.0 µg/mL for P-gp and 12.8 µg/mL for BCRP, but no inhibition was seen for OATP2B1 even at the maximal concentration tested (30 µg/mL). Others, such as Kolliphor EL, Kolliphor RH-40, and polysorbate 40, were at least 10-fold more potent towards OATP2B1 (IC₅₀ values between 8.55 and 44.2 µg/mL) than towards BCRP or P-gp (IC₅₀ values between 81 and 1000 µg/mL). Excipients such as Acconon MC8-2 were found to be somewhat selective towards P-gp (IC₅₀ = 18.4 µg/mL), with minimal inhibition of BCRP and OATP2B1, while Acconon C-50 inhibited both P-gp (IC₅₀ = 26.3 µg/mL), and OATP2B1 (IC₅₀ = 9.96 µg/mL), with no inhibition of BCRP (IC₅₀ > 3000 µg/mL). These results confirm that common excipients can affect drug transporters in the GI tract and potentially impact plasma exposure of pharmaceuticals. Excipients that inhibit gastrointestinal uptake transporters may not only decrease drug efficacy but also potentially introduce safety issues if they block uptake of important dietary nutrients. Excipients that inhibit gastrointestinal efflux transporters while avoiding inhibition of uptake transporters could potentially be used to improve oral drug bioavailability.

P194 - BIOENGINEERING MICRORNAS TO MODULATE SOLUTE CARRIER TRANSPORTERS AND XENOBIOTIC TRANSPORT

Colleen Yi, Gavin Traber, Neelu Batra, Mei-Juan Tu, and Ai-Ming Yu
 UC Davis, United States

MicroRNA (miRNA) are genome-derived noncoding RNAs (ncRNAs) with crucial roles in the control of posttranscriptional gene regulation, including ADME genes underlying xenobiotic/drug metabolism and disposition [1, 2]. Solute carrier (SLC) transporters are a diverse family of facilitative or secondary active transporters responsible for the influx and efflux of a wide array of substrates, including essential nutrients and medications [3, 4]. Some miRNAs have been shown to directly regulate specific SLCs and influence xenobiotic disposition and drug efficacy or toxicity [5, 6]. In addition, there is rising interest in the development of ncRNA therapeutics, which has been substantiated by the US Food and Drug Administration approval of four siRNA medications [7, 8]. However, RNA research and drug development commonly uses chemically synthesized RNA mimics with extensive modifications that are not present in natural RNAs [9]. The Yu laboratory has established a novel method to produce bioengineered or recombinant RNA agents (BioRNAs) in *Escherichia coli* [10, 11]. In this study, we aimed to compare the efficacy of htRNAGly/pre-miR-34a and htRNALeu/pre-miR-34a carriers to produce BioRNAs and utilize novel BioRNAs to explore miRNA-controlled regulation of SLCs and xenobiotic transport. A set of 20 BioRNA/miRNAs were designed and overexpressed in *E. coli*, among them 10 were based on the htRNAGly/pre-miR-34a carrier and 10 paired miRNAs on the htRNALeu/pre-miR-34a carrier. Fast Protein Liquid Chromatography was then used to purify individual recombinant miRNAs. High Performance Liquid Chromatography and Endotoxin Assay Kit were used to determine purity and endotoxin level of each BioRNA. After confirming the release of target miR-148a-3p from model BioRNA in human cells by stem-loop reverse transcription real-time qPCR method, we further employed Western blots to determine the effectiveness of biologic miR-148a-3p in the regulation of glucose transporter SLC2A1 (GLUT1), a known target of miR-148 [12, 13], as compared with chemo-engineered miR-148a mimic. Consequently, BioRNA/miR-148a altered glucose uptake capacity and mitochondrial respiration. Our data demonstrate the robustness of tRNA/pre-miRNA-based recombinant miRNA platform technology and applications of bioengineered RNAs to general biomedical research.

Acknowledgements: This study is supported by the National Institute of General Medical Sciences (R35GM140835) and National Cancer Institute (R01CA253230), National Institutes of Health.

References:

1. Yu, A.M., et al., *MicroRNA Pharmacoeigenetics: Posttranscriptional Regulation Mechanisms behind Variable Drug Disposition and Strategy to Develop More Effective Therapy*. *Drug Metab Dispos*, 2016. **44**(3): p. 308-19.
2. Yokoi, T. and M. Nakajima, *microRNAs as mediators of drug toxicity*. *Annu Rev Pharmacol Toxicol*, 2013. **53**: p. 377-400.
3. Hediger, M.A., et al., *The ABCs of membrane transporters in health and disease (SLC series): introduction*. *Mol Aspects Med*, 2013. **34**(2-3): p. 95-107.
4. International Transporter, C., et al., *Membrane transporters in drug development*. *Nat Rev Drug Discov*, 2010. **9**(3): p. 215-36.
5. Dragomir, M.P., E. Knutsen, and G.A. Calin, *Classical and noncanonical functions of miRNAs in cancers*. *Trends Genet*, 2022. **38**(4): p. 379-394.
6. Yi, C. and A. Yu, *MicroRNAs in the regulation of solute carrier (SLC) proteins behind xenobiotic and nutrient transport in cells*. *Frontiers in Molecular Biosciences*, in press.
7. Mounne, L., A.C. Marie, and N. Crouvezier, *Oligonucleotide Therapeutics: From Discovery and Development to Patentability*. *Pharmaceutics*, 2022. **14**(2).
8. Yu, A.M. and M.J. Tu, *Deliver the promise: RNAs as a new class of molecular entities for therapy and vaccination*. *Pharmacol Ther*, 2022. **230**: p. 107967.
9. Yu, A.M., et al., *RNA therapy: Are we using the right molecules?* *Pharmacol Ther*, 2019. **196**: p. 91-104.
10. Tu, M.J., et al., *Expression and Purification of tRNA/ pre-miRNA-Based Recombinant Noncoding RNAs*. *Methods Mol Biol*, 2021. **2323**: p. 249-265.
11. Li, P.C., et al., *In vivo fermentation production of humanized noncoding RNAs carrying payload miRNAs for targeted anticancer therapy*. *Theranostics*, 2021. **11**(10): p. 4858-4871.
12. Wu, L., W. Qiu, and J. Sun, *Down regulation of miR-148a is related to enhanced pancreatic cancer pathogenesis through targeting GLUT1*. *Int J Clin Exp Pathol*, 2018. **11**(10): p. 4950-4956.
13. Tiemin, P., et al., *Dysregulation of the miR-148a-GLUT1 axis promotes the progression and chemoresistance of human intrahepatic cholangiocarcinoma*. *Oncogenesis*, 2020. **9**(2): p. 19.

P195 - IS THE PROTEIN-MEDIATED UPTAKE OF STATINS BY HEPATOCYTES AN EXPERIMENTAL ARTIFACT?Mengyue Yin¹, Jashvant Unadkat¹, Kazuya Ishida², Xiaomin Liang², and Yurong Lai²¹University of Washington, United States and ²Gilead Sciences Inc., United States

Background: Many investigators, including us, have found that IVIVE of hepatic clearance (CL_h) of OATP-transporter statins is improved by inclusion of plasma or plasma proteins (e.g. albumin) in the uptake studies (Kumar et al., 2021). This, so-called protein-mediated uptake effect (PMUE), is thought to be due to an interaction between the drug-protein complex and the cell membrane, which causes an increase in the unbound drug concentration at the cell surface and results in an increase in the apparent hepatic intrinsic uptake clearance (CL_{int,uptake}) of the drug (Miyachi et al., 2018). However, we have shown, that this “apparent” PMUE on statin uptake by OATP1B1-expressing cells, in the presence of human serum albumin (HSA), is mostly an artifact caused by non-specific binding (NSB) of the statin-albumin complex to cells, labware or both (Yin et al., 2022).

Objective: To determine if the PMUE on uptake of statins by hepatocytes is also an experimental artifact.

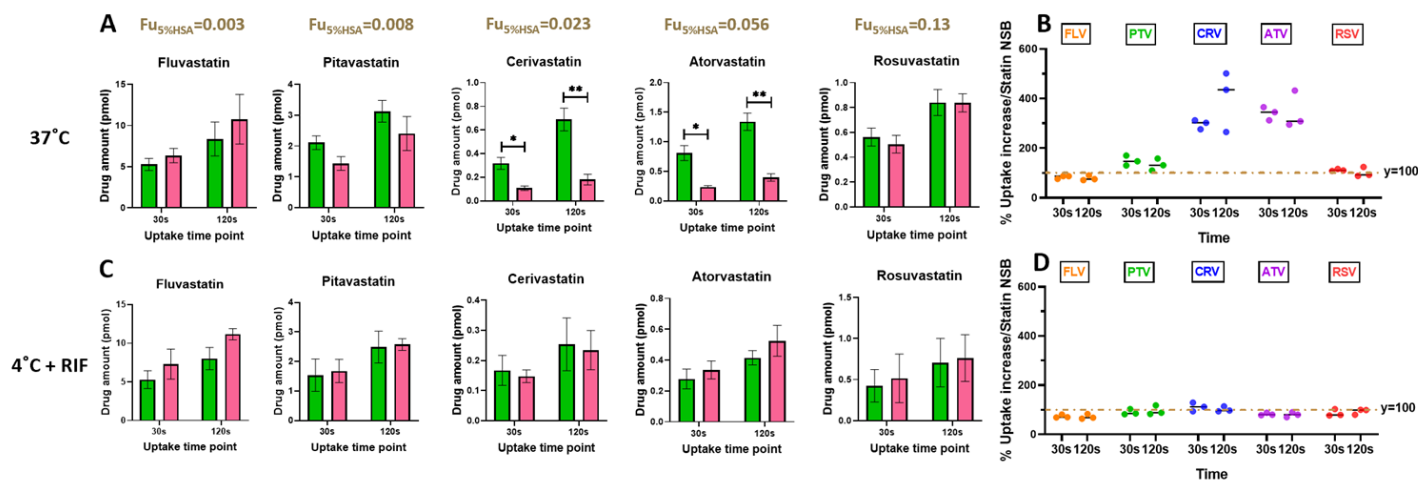
Methods: We studied the uptake of a cocktail of statins (atorvastatin, ATV, cerivastatin, CRV, fluvastatin, FLV, pitavastatin, PTV and rosuvastatin, RSV) by plated human hepatocytes (Lot: FEA, YTW and AOS) in the presence and absence of 5% HSA, at 37°C (active + passive uptake) and at 4°C+500 μM unbound rifampicin (RIF) (passive uptake). After terminating statin uptake by 3x washing with ice-cold buffer, we quantified the amount of HSA nonspecifically bound to the cells/labware by quantitative proteomics. Then, we estimated the amount of HSA-statin nonspecifically bound to the cells/labware using the fraction of statin bound to HSA which was measured at each time-point in each uptake study.

Results: The increase in passive uptake of all five statins, in the presence of 5% HSA, was completely explained by NSB of the stain-HSA complex (Figure C-D, only lot YTW shown). Except for ATV and CRV, this was also the case for the total uptake (37°C) of the other statins (Figure A-B, only lot YTW shown).

Conclusion: Our results suggest that the PMUE on the uptake of ATV or CRV by plated hepatocytes is a real phenomenon. However, due to its magnitude, incorporating this PMUE in IVIVE of CL_h is unlikely to bridge the underprediction of their *in vivo* CL_h (Kim et al., 2019). In addition, our results challenge the validity of the PMUE effect on the hepatocyte uptake of the other statins. If these results are replicated in suspended hepatocytes (studies ongoing), future research should be focused on delineating mechanism(s), other than PMUE, causing the underprediction of IVIVE of OATP-mediated CL_h.

Figure

Plated YTW Human Hepatocytes

**P196 - ABSTRACT WITHDRAWN**

- Abbasi, Armina, PS1.3
 Abudahab, Sara, P4
 Abu-Seini, Nama'a, P134
 Achour, Brahim, P142
 Adiwidjaja, Jeffry, A12
 Adusumalli, Sravani, P94
 Agrawal, Vaidehi, P167
 Ahire, Deepak, A6, A11, P31, P166
 Alade, Nathan, P83
 Alahmad, Saif, P134
 Albertolle, Matthew, SC1.1, P60
 Alberts, Jeffrey, P164
 Al-Eitan, Laith, P134
 Aleksunes, Lauren, PS2.1
 Aliwarga, Theresa, P114
 Al-majdoub, Zubida M., P84, P87, P142
 Aluri, Krishna, P65
 Alwadei, Nouf, P18
 Alwayn, Ian, P168
 Amaeze, Ogochukwu, P150
 Amory, John, P50
 Andrews-Jones, Lydia, P137
 Anselm, Viktoria In thai, P8
 Aravindhhan, Karpagam, P42
 Arian, Chrisopher, S4.4, P165
 Arnold, Sam, P167
 Artursson, Per, SC4.3, P71, P85, P86
 Åsberg, Anders, P72
 Authement, Aurora, P50

 Backes, Wayne, S2.2
 Backman, Janne T, P51
 Bae, Sungyeun, P5
 Bammler, Theo K., P93
 Bansal, Sumit, A7
 Bapiro, Tashinga, P117
 Barber, Jill, P142
 Barnabas, Ruanne, P167
 Barton, Eleanor, P104
 Basińska-Ziobroń, Agnieszka, P19
 Basit, Abdul, P166
 Bateman, Kevin, P125, P126
 Batra, Neelu, P120, P194
 Beers, Jessica, P73
 Bellaire, Susan, P43
 Bellamy, Francois, P41
 Benet, Leslie Z., K1
 Benzi, Jhohann Richard, A2
 Bergagnini-Kolev, Mackenzie, P151
 Berry, Shannon, P42
 Bershteyn, Anna, P167
 Bhoopathy, Sid, P15
 Bi, Yi-An, P176
 Birks, Vicky, P43
 Bjerregaard Stage, Tore, P1
 Blanchard, Stephanie, P44
 Blas-Y-Estrada, Florence, P70
 Bode, Chris, P15
 Bollini, Sangeetha, P2
 Bork Iversen, Ditte, A3, P1

 Broccatelli, Fabio, S1.3
 Bromek, Ewa, P19
 Brøsen, Kim, A3
 Brouwer, Kenneth, P92
 Brouwer, Kim, A12, P92, P147
 Brown, Colin, P91
 Bruel, Sandrine, P70
 Brzoska, Marie, P105
 Bujoso-Szekely, Virag, P10
 Bumpus, Namandjé, A5, P35, P100
 Burch, Peter, P184
 Burcham, Philip, P175
 Burris-Hiday, Sarah D., S2.4, P20
 Büsker, Sören, P146
 Byer-Alcorace, Alexander, P88, P107

 Cai, Lining, P180, P181
 Cannon, Joe, P128
 Capello, Astrid, P43
 Carney, Daniel, P139
 Carr, Cindy, P91
 Carvalho Padilha, Elias, P106
 Castro-Perez, Jose, P126
 Causon, Jason, P126
 Cech, Nadja, P165, P169
 Cerny, Matthew, A8, P21
 Ceylan, Merve, P85
 Chacko, Silvi, P128
 Chan, Chun Yip James, P154
 Chan, Eric Chun Yong, A1, P162
 Chan, James Chun Yip, P152, P155, P162
 Chan, Tom, S4.1, P88, P107
 Chandrashekar, Megha, P74
 CHAPA, REVATHI, P153
 Chau, Marvin, P16
 Chen, Eugene, P34
 Chen, Hong-bin, P112
 Chen, Kuan-Fu, P58
 Chen, Wei Yang, P101
 Chen, Weiqi, P108
 Chen, Weixuan, P23
 Cheng, Lisa, P82
 Cheong, Eleanor Jing Yi, P154, P162
 Cheong, Jonathan, P84, P87
 Cherrington, Nathan, P179
 Chevolleau-Mege, Sylvie, P70
 Chhonker, Yashpal, P167
 Chiang, Po-Chang, P82
 Chimalakonda, Anjaneya, P123
 Chin, Sheng Yuan, P152, P155, P162
 Cho, Hea-Young, P145, P149, P156
 Cho, Seok-jin, P145, P149, P156
 Cho, Sungjoon, P129
 Cho, Yong-Soon, P182
 Choi, Eunice, P94
 Chothe, Paresh, P185
 Christensen, James G., P116
 Christianson, Chad, P2
 Chung, Jae-Yong, P140
 Cilliers, Cornelius, P116

 Cirello, Amanda, P122
 Clarine, Jeff, P157
 Claw, Katrina, PS1.2
 Coe, Kevin, P23, P59
 Colombari, Julia, A2
 Cometa, Julianne Roi, P44
 Cooke, Ray, P39, P41, P104
 Coughlin, Laura, P143
 Creek, Darren, P92
 Croft, Marie, S5.1
 Czuba, Lindsay C., P144

 Dahl Steffensen, Karina, P1
 Dajani, Rana, P134
 Dalgård Dunvald, Ann-Cathrine, A4
 Dalio Bernardes da Silva, Gabriel, P109
 Dalvie, Deepak, SC2.1
 Damkier, Per, A3
 Daniel, Władysława, P19
 Dantonio, Alyssa, P171
 DaSilva, Ethan, P54
 Davis, John, P122
 Davis, Trisha, P25
 Davydov, Dmitri, S2.3
 De Bruyn, Tom, P84, P87
 de Ligt, Rianne, P39, P41
 De Lucca Thomaz, Matheus, A2
 Debrauwer, Laurent, P70
 Desai, Prashant, S1.2
 Deshmukh, Sujal, A6
 Devlin, Claire, P91
 Di, Li, SC2.2, P171
 Di Martino, Maria Letizia, P85, P86
 Diao, Xingxing, P130
 Dickinson, Gemma, P164
 Diermayr, Veronica, P44
 Ding, Xinxin, P22
 Dingemanse, Jasper, P24
 Donkers, Joanne, P168
 Dou, Tongyi, P177
 Drozdik, Marek, P6, P178
 Du, Yewei, P193
 Duarte, Geraldo, A2
 Dubbeld, Jeroen, P168
 Dulany, Chris, P75
 Dunvald, Ann-Cathrine, A3

 East, Lilly, P184
 Eberhard, Colten, P35
 Eisennagel, Stephen, P42
 Elk, Kevin, P138
 Endres, Chris, P170
 Eng, Heather, P171
 Engelhardt, Marc, P39
 Englund, Maria, P89
 Enogieru, Osatohanmwun, P185
 Enoru, Julius O., P90, P188
 Enquobahrie, Daniel A., P93
 Eriksson, Jens, P71, P85, P86
 Erpelinck, Steven, P69

- Ethirajulu, Kantharaj, P44
 Evans, Liam, P117
 Evers, Raymond, P84, P87, P185
- Fæste, Christiane, P110
 Fallon, John, A10
 Fan, Hao, A1
 Fehr, Michelle, P63
 Felici, Antonio, P139
 Feng, Mei, P78
 Ferguson, Nicholas, P14
 Ferrari, Livia, P139
 Ferron, Gianna, P137, P138
 Fischer, Sally, SC1.3
 Fontaine, Fabien, P124, P125, P126
 Fraczkiwicz, Grace, P55
 Fraczkiwicz, Grazyna, P153
 Fuhr, Uwe, P146
 Fullenwider, Cody, P45, P60
- Gaborik, Zsuzsanna, P10
 Galetin, Aleksandra, SC4.4, P84, P87, P189
 Gan, Sylvia Bong Hwa, P44
 Garceau, Dylan, P138
 Garriga, Albert, P124
 Gentles, Lucy, P91
 Georg, Gunda, P179
 Giménez, Pol, P124, P125
 Glass, Sarah, P23
 Gnerre, Carmela, P24
 Goosen, Theunis, P14, P54
 Graf, Wilhelm, P86
 Grater, Richard, P36
 Graves, Megan, P193
 Greene, Stephen, PS3.3
 Greenfield, Siannah, P171
 Gu, Chungang (Chuck), P173
 Gu, Xiaomei, P123
 Gunduz, Mithat, P122
 Guo, Jingjing, P84, P87
 Guo, Yukuang, P111
 Gupta, Meghna, S3.3
- Haag, Hannah, P8
 Hack, Michael, P59
 Haduch, Anna, P19
 Hahn, Robert G., P146
 Hakooz, Nancy, P134
 Hall, Michael, P43
 Hall, Stephen, P164
 Hammar, Rebekkah, P85, P86
 Hammer, Helen, A3, A4, A9, P29
 Han, Mei, SC1.2
 Handin, Niklas, P71, P72
 Hargis, Lauren, P116
 Hariparsad, Niresh, P65
 Harrelson, John, P52
 Harvey, Shalon, P73
 Hatley, Oliver, SC3.2
 Hattori, Yukiko, P112
- Hau, Raymond, P179
 Hayeshi, Rose, P27
 He, Kan, P180, P181
 He, Yi, P177
 Hebert, Mary F., P144
 Heerikhuisen, Margreet, P69
 Heinle, Lance, P78
 Heller, Kate, P167
 Henninot, Antoine, P139
 Herskind, Kamille, P1
 Heyward, Scott, A11, P166
 Hidalgo, Ismael, P15
 Higgins, James William, P59
 Higuchi, Yuichiro, P3, P32
 Hilgendorf, Constanze, P89
 Hillenweck, Anne, P70
 Hjelmesæth, Jøran, P72
 Ho, Ming-Chih, P68
 Hogan, Janita, P84
 Hogan, Janita, P87
 Hong, Young Bean, P145, P149
 Hoopmann, Michael, P25
 Hop, Cornelis, P163
 Hosaka, Takuomi, P62, P64
 Howlader, Saurav, P182
 Hsiao, Peng, P139
 Huang, Jiansheng, P173
 Hübscher, Michelle, P63
 Hunt, Peter, P115
 Hunter, Bridge, P184
 Hussner, Janine, P183
 Huynh, Christine, P24
 Hwang, Sejung, P140
- Ida-Tanaka, Miyuki, P3
 Iida, Yuichi, P3
 Imaoka, Tomoki, S4.3, P101, P114
 Ingelman-Sundberg, Magnus, S4.2, A9
 Ishida, Kazuya, P195
 Ishii, Yuji, S2.1, P112
 Isoherranen, Nina, P25, P50, P67, P118, P144, P150, P172
 Ito, Mamoru, P3
 Ito, Satoshi, P3
 Ivanova, Lada, P110
 Iyer, Ramaswamy, P108, P123
- Jackson, Klarissa, PL3, A10, P73
 Janefeldt, Annika, P89
 Jang, In-Jin, P140
 Jang, Ji-Hun, P38
 Jansson-Jansson-Löfmark, Rasmus, P72
 Järvinen, Erkka, A3, A4, A9
 Jaschob, Daniel, P25
 Jee, Alison, P81
 Jejurkar, Purvi, P90
 Jemnitz, Katalin, P10
 Jeong, Angela, P147
 Jeong, Seung-Hyun, P38
- Jespersen, Daniel, A3
 Jiang, Jiansen, P177
 Jindal, Rohit, P75
 Johnston, Christine, P167
 Jonasson, Elina, P85
 Jones, Alan Wayne, P146
 Jones, Barry, P13, P37, P76, P77
 Jones, Hannah, P58
 Jones, Robert, A11
 Jony, M. Rasheduzzaman, P182
 Joseph, Jeremiah, P139
 Joshi, Anand, P90
 Jung, Taeyoon, P17
 Jurva, Ulrik, P89
- Kaartinen, Taavi, P51
 Kaelin Aebi, Agnes, P39
 Kalgutkar, Amit, P171
 Kalina, Sara, P139
 Kalvass, John Cory, P12
 Kamimura, Hidetaka, P3
 Kamiyama, Yoshiteru, P7
 Kang, Dong Wook, P145, P149, P156
 Kanno, Yuichiro, P62, P64
 Kanta, Anne, P84, P87
 Karlinsey, Molly, P42
 Karlsson, Cecilia, P72
 Kathy Mosure, Kathy Mosure, P128
 Kaufman, Ilene, P193
 Kawai, Kenji, P3
 Kazuki, Yasuhiro, P3
 Keefer, Chrisopher, S1.1
 Kelly, Edward, SC2.4, P101, P105, P114
 Khan, Mostafa, P45, P49
 Khojasteh, Cyrus, A11, P34, P129
 Kilby, Greg, P119
 Kim, Daniel, P2
 Kim, Ju Hee, P145, P149, P156
 Kim, Kyoungyun, S6.3
 Kinong, Jennifer, P59
 Kinzi, Jonny, P183
 Kline, Zammany, P139
 Klotz, Ulrich, P146
 Knibbe, Catherijne, P168
 Kochansky, Christopher, P125, P126
 Koh, Andrew, P143
 Koh, Hor Cheng, P162
 Koleske, Megan, P161
 Korshøj Bergmann, Troels, P1
 Koudriakova, Tatiana, P59
 Kozminski, Kirk, P45
 Kralj, Thomas, P92
 Kroetz, Deanna, S3.1
 Krol, Ed, P109
 Krows, Meighan, P167
 Kruger, Laken, P93
 Kukla, David, P78
 Kulkarni, Priyanka, A11
 Kuninger, David, P75
 Kurzawski, Mateusz, P178

- Ladumor, Mayur K., P159, P185
- LaFrance, Jeffrey, P144
- Lai, Yurong, P161, P185, P187, P195
- Lanchote, Vera, A2
- Lapatto-Reiniluoto, Outi, P51
- Lapczuk-Romanska, Joanna, P6, P178
- Lapehn, Samantha, P93
- Lapham, Kimberly, P14
- Latli, Bachir, P107
- Lau, Yau Yi, P94
- Lauschke, Volker, P72
- LeBaron, Matthew, P127
- LeCluyse, Edward, P99
- Lee, Anthony, P170
- Lee, Dong-Hwan, P148
- Lee, Jonghwa, A10
- Lee, Kyeong-Ryoon, P160
- Lee, SeungHwan, P5, P140
- Lee, Yong-Bok, P38, P145, P156
- Leeder, Steven, A11
- Lekhooa, Makhoto, P27
- Leung, Perry, P59
- Li, Albert, P68, P95
- Li, Marina, SC1.4
- Li, Ren-shi, P112
- Li, Shaorong, P55
- Li, Wenyong, P108, P123
- Lian, Tengfei, P177
- Liang, Xiaomin, P161, P185, P187, P195
- Lim, Chiang Huay Freda, P154
- Lim, Nathan, P59
- Lin, Ching-yu, P135
- Lin, Jian, P54
- Lin, Jieying, P152, P155, P162
- Lin, Louis, P163
- Linehan, Stefan, P137, P138
- Litherland, Karine, P39
- Liu, Jinghan, S1.4, P28
- Liu, Miao, P55
- Liu, Pingrong, P107
- Lopes, Ana, P85, P86
- Lopez, Vanessa, P113
- Lu, Wei, P119
- Lukacova, Viera, SC3.1
- Lulla, Mukesh, P36
- Lundeen, Katherine, P49
- Lundquist, Patrik, P85, P86
- Ly, Justin, P131
- Lyu, Zhigang, P128
- Ma, Shuguang, P34, P129
- MacCoss, Michael, P25
- MacDonald, James, P93
- Mahadeo, Anish, P114
- Mahajan, Mukesh, P42
- Maier, Monica, P141
- Mair, Stuart, P41
- Manohar, Ravi, P117
- Marty, Sue, P127
- Marx, Matthew A., P116
- Mashego, Nicholas, P27
- Masterson, John, P137
- Matsumoto, Akihiro, P7
- Maw, Hlaing, P88
- Maw, Holly, P107
- Mayes, Ben, P49
- McCallister, Heather, P59
- McClymont, Lynn, P127
- McGinnity, Dermot, P11
- McNett, Debbie, P127
- Mehvar, Reza, P18
- Melli, Patricia, A2
- Metallides, Megan, P94
- Mettu, Vijaya Saradhi, P53, P166, P190
- Meyer, Alina, P71
- Meyer zu Schwabedissen, Henriette, P24, P63, P183
- Mezine, Igor, P15
- Migliorati, Julia, P47
- Misra, Bharat, P94
- Miura, Yoshie, P62
- Mizuno, Kunihiro, P84, P87
- Mizuno, Kuny, P45
- Mondick, John, PS3.4
- Monogue, Marguerite, P143
- Moretoni, Luca, P124
- Moritz, Robert, P25
- Morse, Bridget, SC3.3, P164
- Mortensen, Christina, P1
- Mozhui, Khyobeni, P93
- Mukashyaka, Marie Claire, P184
- Murayama, Norie, P32
- Murby, Susan, P189
- Murray, Bernard, A11
- Murry, Daryl, P167
- Na, Joo Young, P140
- Naboulsi, Wael, P8
- Nalaparaju, Anjaiah, P154
- Navarro, Uyen-Vy, P52
- Nellore, Ranjani, P44
- Neuhoff, Sibylle, SC4.2
- Nguyen, Aiden-Hung, P52
- Nguyen, James T., P165, P169, P190
- Nguyen, Natalie T., P66, P116, P157
- Nguyen, Phuoc Long, P182
- Nie, Ronnie, P137
- Nielsen, Flemming, A3
- Niemi, Mikko, P51
- Niosi, Mark, P14
- Nishiguchi, Hikaru, P64
- Niu, Congrong, P187
- Nooijen, Irene, P69
- Obach, R. Scott, P54, P69, P171
- Oberlies, Nicholas, P165, P169
- O'Brien, Tara, P2
- Öeren, Mario, P115
- Offei, Samuel, P28
- Ogungbenro, Kayode, P84, P87
- Ölander, Magnus, P72
- Orozco, Christine, P14
- Orsburn, Benjamin, A5, P100
- Oshimura, Mitsuo, P3
- Oste, Line, P43
- Ostrowski, Marek, P6
- Oswald, Stefan, P6, P178
- Paasche-Orlow, Michael, P167
- Pacsuta, Johanna, P10
- Paine, Mary F., A7, P165, P169, P190
- Pang, K. Sandy, K2
- Paquette, Alison, P93
- Parker, Cody, P97, P157
- Parsons, Cameron, P65
- Parvez, Md Masud, P188
- Pascual, Xavier, P124
- Pastor, Catherine, P147
- Patel, Mitesh, A6
- Patel, Yogesh, P184
- Patil, Kiran, PL2
- Pavek, Petr, P61
- Peckham, Gregory, P42
- Pendharkar, Vishal, P44
- Person, Elodie, P70
- Persson, Marie, P89
- Peters, Sheila Annie, P142
- Pham, Jennifer, P94
- Phipps, Richard, P117
- Piekos, Stephanie, P88, P99
- Pike, Andy, P11
- Pineda Garcia, Jorge Carlos, P112
- Pitcher, Annabell, P43
- Pitre, Franck, P41
- Planatscher, Hannes, P8, P29
- Poetz, Oliver, P8, P29
- Police, Anitha, P188
- Polli, Joseph, P193
- Poss, Michael, P128
- Pottegård, Anton, A4, P1
- Pötz, Oliver, A3, A4, A9
- Prasad, Bhagwat, A6, A11, P31, P53, P93, P166, P190
- Prativadibhayankara, Venkateshan Srirangam, P44
- Puklo, Renata, P19
- Qian, Emily, P180, P181
- Qin, Gengyao, P132
- Radchenko, Tatiana, P124
- Ragan, Tim, P137, P138
- Ragueneau-Majlessi, Isabelle, P56, P193
- Rahaoui, Hakim, P69
- Rahbaek, Lisa, P116, P157
- Rahighi, Simin, P18
- Ramsden, Diane, P60, P65
- Rashid, Mamunur, P18

- Ravikumar, Jeevapasath, P175
 Raymond, Klairynne, P79, P88, P107
 Reilly, Michael, P42
 Rettie, Allan, P83, P165, P169
 Ricklin, Daniel, P183
 Riddle, Ellen, P67
 Riffle, Michael, P25
 Rocha, Adriana, A2
 Rodino-Klapac, Louise R., P184
 Rodrigues, Marinelle, P143
 Rodriguez, Acilegna, P193
 Roethke, Theresa, P42
 Rostami-Hodjegan, Amin, P84, P87, P142, P189
 Rotter, Charles, P45
 Rowe, Joshua, P137
 Rozaini, Nurul Nazihah, P44
 Rubinow, Katya, P50
 Russell, Drake, P16, P17, P21
 Rysz, Marta, P63, P183
 Ryu, Sangwoo, P176, P191
- Sadighi, Armin, P188
 Sallam, Tamer, S6.4
 Salphati, Laurent, P34, P129
 Sandinge, Ann-Sofie, P89
 Santiago, Brandon, P42
 Sanvee, Gerda, P39
 Saran, Chitra, P92
 Sasaki, Takamitsu, P62, P64
 Sasner, Michael, P138
 Sathyanarayana, Sheela, P93
 Sato, Takumi, P62, P64
 Savoia, Paola, P139
 Sayama, Hiroyuki, PS3.1
 Scarfe, Graeme, P11
 Scaringella, Young-Sun, P107
 Schädeli, Julia, P63
 Schäfer, Anima, P63
 Schulz, Julia, P12
 Schuren, Frank, P69
 Schwab, Matthias, P146
 Schwardt, Oliver, P183
 Scotcher, Daniel, P189
 Scott, Brian, P59
 Scott, Emily, PL1, P20, P28
 Seeland, Swen, P24
 Segall, Matthew, P115
 Seguin, Ryan, P105
 Seibert, Isabell, P63, P183
 Sellin, Mikael E., P71, P85, P86
 Sernoskie, Samantha, P81
 Serrano Diaz, Erika, P143
 Shaffer, Christopher L., P173
 Shah, Abhi, P111
 Shah, Pranav, P46, P106
 Shanu-Wilson, Julia, P117
 Sharma, Ajay, P18
 Sharma, Sheena, P53, P166
 Shaw, Iain, P40, P41
 Shen, Jie, P137
- Shen, Kai, P55
 Shi, Qin, P180, P181
 Shi, Yuanyuan, A8
 Shin, Jae-Gook, P182
 Shizu, Ryota, P62, P64
 Shum, Sara, P144
 Sidharta, Patricia N., P24
 Sierra, Teresa, P94
 Simon, Keiann, P118
 Simonsen, Emma, P1
 Singh, Dilip Kumar, P31, P166
 Singh, Nand, P39
 Siramshetty, Vishal, P46
 Skaptason, Judith, P59
 Skogar, Martin, P85
 Skov Madsen, Jonna, P1
 Slavsky, Marina, P65
 Slobodchikova, Irina, P119
 Smith, Aaron, P11
 Smith, Bill, A11
 Smith, Phill, A10
 Soars, Matt, P128
 Sodhi, Jasleen K., P51
 Solhaug, Anita, P110
 Spindle, Tory R., A7
 Spires, Jessica, A12
 Spracklin, Douglas, S5.2
 Stage, Tore B., PS2.2, A3, A4, A9
 Stankiewicz Karita, Helen, P167
 Steele, Jonathan, P117
 Steinbronn, Claire, P167
 Steinhilber, Andreas, P8, P29
 Stevens, Lianne, P168
 Storelli, Flavia, P185
 Strelevitz, Timothy, P54
 Stresser, David, P12, P78, P90
 Stuart, Katie, P40
 Stüwe, Malin, P71
 Subash, Sandhya, A11
 Suemizu, Hiroshi, P3, P32
 Sugawara, Ayaka, P64
 Sun, Hao, P170
 Sun, Qin, PS1.1
 Sun, Shuyu, P55
 Sundbom, Magnus, P85
 Sydor, Jens, P42
 Sykes, Andrew, P117
- Takeda, Tomoki, P112
 Tam, Yuen, P23, P59
 Tan, Shawn Pei Feng, P152, P155, P162, P189
 Tan, Xiaofeng, P177
 Tanaka, Yoshitaka, P112
 Tang, Chongzhuang, P130
 Tang, Lloyd Wei Tat, A1
 Tania, Nussy, PS3.2
 Tanna, Rakshit, P165, P169
 Tao, Will, P45
 Tash, Joseph, P179
 Tashiro, Sari, P64
- Taub, Mitchell, P88, P99, P107
 Taubert, Max, P146
 Tawfik, Sherouk, P47
 Taylor, Jonathon, P52
 Taylor, Robert, P193
 Teitelbaum, Aaron, P107
 Templeton, Ian E., P170
 Thakur, Aarzo, P190
 Thummel, Kenneth E., P83, P165, P169
 Tian, Dan-Dan, P165
 Topletz-Erickson, Ariel, P170
 Toprak, Erdal, P143
 Tornio, Aleks, P51
 Totah, Rheem, A8, P16, P17
 Traber, Gavin, P120, P194
 Traeger, Sarah, P108
 Tran, Jonathan Q., P116
 Trapa, Parrick, P36
 Tritapoe, Julia, P75
 Tseng, Elaine, P54
 Tsykhotska, Olha, P70
 Tu, Mei-Juan, P120, P121, P194
- Uehara, Shotaro, P3, P32
 Uetrecht, Jack, P81
 Unadkat, Jashvant D., A7, P159, P185, P195
 Usta, Birol, P69
- Vaes, Wouter, P39, P69
 Vaes, Wouter H J, P41
 Valleix, Marine, P70
 van de Steeg, Evita, P69, P168
 van Duijn, Esther, P39
 van Groen, Bianca, S5.3
 Vance, Jennifer, P13, P37, P76, P77
 Vandrey, Ryan, A7
 Varma, Manthena, SC4.1, P176, P191
 Vary Jr., Jay C., P144
 Vasilogianni, Areti-Maria, P142
 Venkatapura Chandrashekar, Devaraj, P18
 Verheij, Elwin, P39
 Verma, Ravi Kumar, A1
 Vick, Andrew, P2
 Vieira, Leticia S., P192
 Vildhede, Anna, P89
 Volak, Laurie, P23, P59
 von Siebenthal, Franziska, P39
 Vora, Tarang, P55
 Vythilingam, Mirubagini, P183
- Walles, Markus, P122
 Wang, Bin, P129
 Wang, Jing, P34
 Wang, Joanne, PS2.3, P192
 Wang, Kai, P23
 Wang, Pengcheng, P122
 Wang, Shuai, P34

Wang, Ting, P79, P88, P107
Wang, Xiaoyu, P143
Wang, Yan, P56
Wang, Yi-Mei, P121
Wang, Yueting, P78
Warren, Mark, P193
Waxman, David J., S6.1
Weerts, Elise, A7
Wegerski, Chris, P116
Wegler, Christine, P72
Wei, Wan, A1
Wen, Bo, P48
Wener, Mark, P167
Wenzel, Christoph, P6, P178
West, Mark, P176
Westerhout, Joost, P168
Wheeler, Abigail, A5
Whitaker, Gareth, P40
Whitcher-Johnstone, Andrea, P107
Williams, Jordan, P106
Williams, Noelle, P143
Wilson, Joanne, P11
Wind, Mathias, P39
Wong, Harvey, P82, P163
Woody, Nathaniel, P191
Wright, Aaron, SC2.3
Wright, Matthew, P163
Wright, Stephen, P179
Wrigley, Stephen, P117
Wu, Xiangmeng, P22

Xie, Xiaodong, P187
Xu, Libin, P105
Xu, Xin, P46, P106

Yadav, Aprajita S., P144, P172
Yamaguchi, Emi, P176
Yamanaka, Yosuke, P7
Yamazaki, Hiroshi, P3, P32
Yang, Jade, P101, P105
Yao, Ming, P123
Yao, Yongjin, P90
Yeung, Catherine, P101, P114
Yi, Colleen, P120, P194
Yin, Mengyue, P195
Yoneda, Nao, P32
Yoshimoto, Francis, P28
Yoshinari, Kouichi, P62, P64
Young, Graeme, S5.4
Yu, Ai-Ming, P120, P121, P194
Yu, Jingjing, P56, P193
Yuan, Di, P72
Yuan, Yuting, P100
Yue, Guihua, P31, P93, P166

Zalko, Daniel, P70
Zamarripa, C. Austin, A7
Zamora, Ismael, P124, P125, P126
Zara, Nadia, P124
Zelter, Alex, P25, P67, P172
Zhang, Chenghong, P129
Zhang, Fagen, P127
Zhang, George, P57
Zhang, Haiying, P128
Zhang, Haoming, S3.2
Zhang, Lirong, S6.2
Zhang, Qing-Yu, P22
Zhang, Xinyuan, SC3.4
Zhang, Ying, P139
Zhao, Kaijing, P55
Zhao, Qi, P93
Zhao, Weiping, P129
Zhao, Yuqian, P144
Zhong, Guo, P25, P74
Zhong, Xiaobo, P47
Zhou, Mingyan, P55
Zhu, Linxi, P136
Zhu, Sean, P111
Zientek, Michael, A11, P49, P84, P87
Zubair, Faizan, P45, P49
Zuercher, Simone, P183

- 2-pyridine carboxaldehyde-tagging, P128
- ADME study, P173
- Adverse Drug Reactions, P81
- Adverse effects, P1
- Aging, P4
- All Ion Fragmentation, P128
- Analytical, P2
- Animal Models for PBPK, P3
- Antimicrobial, P139
- Aryl hydrocarbon receptor, P4
- Background Subtraction, P128
- Bioavailability, P5, P6, P193
- Biodistribution, P7
- Biomarkers, P1, P8
- Biopharmaceuticals, P2
- Cancer Biomarkers, P142
- Clearance Prediction, P10, P11, P12, P78, P168, P195
- Conjugation reactions and enzymes, P13, P14, P15, P16, P17, P32, P68, P69, P111
- Cyanide, P173
- Cytochrome P450, P3, P18, P19, P20, P21, P22, P23, P24, P25, P27, P28, P29, P31, P32, P59, P108, P109
- Derivatization, P173
- Differences in Metabolism (species, gender, age, diseases), P34, P104, P129, P166, P185
- Dioxin, P112
- Disposition, P35, P36, P37, P38, P39, P40, P41, P184
- DNA Methylation, P4
- Drug Discovery and Development, P42, P43, P44, P45, P46, P47, P48, P49, P57, P107, P120, P121, P123
- Drug Interaction, P27, P50, P51, P52, P53, P54, P55, P56, P57, P58, P62, P64, P94, P144, P151, P165, P169, P170, P177, P190, P191, P192
- Drug Stability, P118
- Drug Toxicity, P100
- Drug-Induced Organ Injury, P8
- Drug-Metabolism, P4
- Enzyme Induction, P29, P58, P59, P60, P61, P62, P63, P64, P65
- Enzyme inhibition/inactivation, P25, P28, P51, P54, P65, P66, P67, P97, P134
- Epigenetics, P4
- Excipients, P90
- Extrahepatic metabolism, P68, P69, P70, P85, P110
- Hepatic Uptake, P10, P53, P71, P75, P161, P183
- Hepatocytes, P60, P61, P72, P73, P74, P75, P76, P77, P78, P79, P95, P99, P101, P127, P176
- Heteroaromatic, P173
- High Resolution Mass Spectrometry, P132
- Immunotoxicology, P81
- In silico*, P46, P82, P115
- In vitro* ADME Assays, P90
- In vitro in vivo* Extrapolation (IVIVE), P11, P52, P83, P84, P85, P86, P87, P88, P89, P188
- In vitro* techniques, P14, P36, P73, P74, P79, P86, P90, P91, P92, P93, P94, P95, P97, P99, P100, P106, P122, P175, P179, P180, P181
- in vitro-in vivo* Metabolic Correlation, P132
- Kidney, P101
- Liver Cell Composition, P72
- Macrocyclic Peptide Metabolism, P128
- Mass Balance Study, P173
- Metabolic Soft Spot, P128
- Metabolism, P15, P16, P18, P20, P21, P24, P34, P39, P40, P41, P48, P70, P88, P104, P105, P106, P107, P108, P109, P110, P111, P112, P113, P114, P115, P116, P117, P118, P119, P120, P121, P122, P123, P124, P125, P126, P127, P128, P129, P132, P136, P145
- Microbiome, P113
- Nitrile, P173
- Non-P450 Phase 1 Enzymes, P31, P131
- Non-Specific Binding, P90
- Novel Metabolite, P173
- Oligonucleotide, P132
- Peptides, P89
- Personalized PBPK Model, P133
- Pharmacogenetics, P35, P134, P135, P136
- Pharmacokinetic Modeling, P145, P146, P147, P148, P149, P164, P167
- Pharmacokinetic Prediction, P84, P143, P148, P149, P163
- Pharmacokinetics and Pharmacodynamics, P184
- Pharmacokinetics and Pharmacodynamics, P6, P47, P49, P137, P138, P139, P140, P141, P142, P143, P144, P159
- Physiologically-based Pharmacokinetic (PBPK), P55, P87, P137, P138, P150, P151, P152, P153, P154, P155, P156, P157, P157, P159, P160, P161, P162, P163, P164, P165, P166, P167, P168, P169, P170
- Plasma Metabolite, P173
- Plasma Protein Binding, P43
- Product Ion Filtering, P128
- Protein Binding, P171
- Proteomics, P172
- Radiolabel, P173
- Remdesivir, P182
- Risk Assessment, P156
- Thiocyanate, P173
- Thiophene, P173
- Toxicity, P175
- Toxicology, P92, P114
- Transporters, P12, P42, P71, P91, P147, P152, P155, P162, P176, P177, P178, P179, P180, P181, P182, P183, P185, P187, P188, P189, P190, P191, P192, P193, P194, P195
- Unusual Metabolite, P173
- Venetoclax, P90